Synthesis and characterisation of permethylpentalene complexes and permethylpentalene derivatives

by

Samantha C. Binding

This thesis is submitted in partial fulfilment of the requirement for the degree of Doctor of Philosophy at the University of Oxford

Worcester College

Oxford

March 2015

The work described in this thesis was carried out in the Chemistry Research Laboratory, Mansfield Road, Oxford between October 2011 and March 2015 under the supervision of Professor Dermot O'Hare. All the work is my own unless stated to the contrary, and has not been previously submitted for any degree at this or any other university.

Samantha Carys Binding
Worcester College
March 2015

ABSTRACT

Synthesis and characterisation of permethylpentalene complexes and permethylpentalene derivatives

Samantha Carys Binding **D.Phil Thesis**

Worcester College **Hilary Term 2015**

This thesis expands the scope for using the permethylpentalene ligand and its precursors in the synthesis of organometallic complexes. **Chapter one** begins with a brief review of linked metallocenes, with which multimetallic compounds bridged by pentalene ligands have often been compared, followed by a comprehensive review of the routes used to make pentalenes and substituted pentalenes. Organometallic compounds of pentalenes are introduced, with a focus on bimetallic systems.

Chapter two explores the diversification of substituents added to the permethylpentalene (Pn*) precursor $WeissH_4$, to include ethyl and isopropyl groups. Low-symmetry mono-, di-, tri- and tetraalkylated products are formed, eight such organic molecules have been identified by NMR spectroscopy, and two characterised crystallographically. It has been demonstrated that subsequent hydrolysis and decarboxylation of two of these products produces low-symmetry alkylpentalene precursors. The chapter concludes with discussions on the selectivity exhibited in these reactions, and the assignment of stereochemistry.

Chapter three describes the synthesis of the first homoleptic double metallocene complex of iron. $Fe_2Pn^*_2$ has been characterised by X-ray diffraction, and cyclic voltammetry studies demonstrate four accessible oxidation states (-1, 0, +1, +2). Magnetic measurements in the solid and solution state reveal an unusual triplet configuration, and DFT calculations indicate the origin of a high magnetic moment likely resides in unquenched orbital angular momentum contributions from SOMOs which have metal *d* character. $Fe_2Pn^*_2$ is EPR silent at 5, 40, and 300 K both in solution and the solid state, suggesting a large zero-field splitting parameter. The reaction of the di-iron complex with carbon monoxide, ethylene and H_2 is reported; the bimetallic CO adduct, $Fe_2(\mu\text{-}\eta^5,\eta^3\text{-}Pn^*)(\mu\text{-}\eta^5,\eta^1\text{-}Pn^*)(CO)_2$, has been crystallographically characterised, and contains a highly distorted allylic bonding motif, which to the author's knowledge is believed to be unique among iron complexes.

Chapter four discusses the interaction of the bidentate Pn* ligand in *anti*-bimetallic fused metallocenes. A new ligand exchange route has been developed to access the complexes $(MCp)_2Pn^*$ (M = Co, Ni), and the isostructural complexes $(MCp^*)_2Pn^*$ have been made for M = Fe, Co, Ni by salt metathesis reactions. All five complexes have been characterised by single crystal X-ray crystallography, and have diamagnetic ground states in solution in common with their Pn bridged analogues. Variable temperature NMR studies reveal a spin-equilibrium between $S = 0$ and $S = 1$ in the dinickel complexes. DFT calculations reproduce the spin states found, and suggest the distortion towards η^3-coordination observed on crossing from Fe, to Co, to Ni, results from population of orbitals with M—bridgehead antibonding character. The electronic structures show it is important to draw comparisons between isoelectronic linked metallocenes. Electrochemical studies on the diiron, dicobalt, and $(NiCp)_2Pn^*$ complexes reveal at least three redox events for each.

Chapter five documents the successful synthesis and characterisation of monometallic complexes of iron and manganese with Pn*H ligands. The isostructural complexes $Fe(Pn^*H)_2$ and $Mn(Pn^*H)_2$ can have been characterised crystallographically, and are potential precursors for accessing heterometallic, and multimetallic complexes. $Mn(Pn^*H)_2$ is a rare example of a manganese sandwich compound and magnetic studies on a single isomer in the solution and solid states suggest it adopts intermediate spin states of $S = 2$ in solution, and $S = 3/2$ in the solid state.

Chapter six gives experimental details for all syntheses and studies described in the preceding chapters. **Chapter seven** provides characterising data for all new compounds. Fitting data for VT NMR and SQUID studies are provided in the **appendix** at the end of this thesis. Crystallographic data in the form of .cif files, DFT output files, and raw SQUID data, can be found in the **electronic appendix.**

ACKNOWLEDGEMENTS

First, I'd like to thank Dermot, for inviting me to stay on for a DPhil, (courtesy of SCG Chemicals) and creating a group where it's been incredibly fun to work. There are few places where I'd've had so much free reign to follow leads I found interesting, or had the opportunity to attend the scientific meetings in the company of such great friends, and for both these things I am grateful. Thanks must go to Professor Jenny Green, for taking an interest in this work, and the helpful discussions that have led me down tangents I thoroughly enjoyed.

Thanks to Sandy, Chris, and Duncan, who bore the brunt of the proof reading of this thesis, I owe you all many, many drinks; and also JC, Mark, Zoë, Yue, Gosh, and Jeorge, all of whom were supportive and constructive in their feedback. The advice from Dr Buffet has been greatly appreciated at keeping me on track when I really needed it. Also, the teaching and support from members of this department is second to none, and much of the work here could not have been undertaken without Drs Rees (NMR), Myers (EPR), Wiseman (SQUID), and Thompson (XRD), and Colin Myers (MS), who have been so generous with their time and advice.

The members of the O'Hare group have made the last four and a half years the most excellent place to be, there's not a time I didn't look forward to coming to labs. There are too many of you to name now, but a few really do need a mention. Special thanks to Hannah 'When in Rome' Buckley, and to Tom, it's been great to share the highs (and occasional lows) with these guys, and the dinners and holidays and house parties and waiting to be rescued from Ebbsfleet wouldn't've been the same without them. Mark "Master of Disaster" Chadwick and Coops, have both been excellent mentors and friends throughout, from keeping me on my toes as a part II, to pertinent work and life advice. Chris, Henry ('5 Pints'), Party Dave, Yue and Duncan, Saul, Anchalee, Joyce, and Charles, all made everyday extraordinary fun, from the T-time belly laughs to having the council turn up at our party, and the many nights that ended at the PT. To Hasna, for the initial organometallic and safety training; Andrew, for helping me understand where I was going wrong when I was hitting a wall, and not forgetting all the part IIs who've kept us entertained over the years.

I'd like to thank my Worcester friends, who've stayed supportive throughout my recent reclusiveness and made continuing in Oxford such great fun. The residents of Worcester House over the years have provided some of the best memories in my memory, from bonding over that shower curtain, to the dungeon discos. Claire and

Emma, I will always miss the penthouse massively, Stefano, Chris, Jason, Adam, I miss waking up on a Sunday to the braying of bruuunch. Tim, Eileen, and Charlotte, I hope you guys will be friends for life. Thanks too to Jason #1, for the late night curries and chats over tea that kept me sane, and to Fran, for the sequin covered surprises.

Lastly, and most importantly, I'd never have made it this far without the incredible love and support of my huge family. Mum and Dad thank you for never doubting me and sharing the rollercoasters of this work, even if I couldn't make you understand why it I love it so much. Gareth and Michael, I'm *so* proud of you both, and you won't know it but when nothing was working and I felt like giving up, you two are the reason I didn't.

For Gramps

CONTENTS

ELECTRONIC APPENDICES

X-ray crystallographic data for **2.1**

X-ray crystallographic data for **2.3**

X-ray crystallographic data for **3.1**

X-ray crystallographic data for **3.2**

X-ray crystallographic data for **4.1a**

X-ray crystallographic data for **4.2a**

X-ray crystallographic data for **4.2b**

X-ray crystallographic data for **4.3a**

X-ray crystallographic data for **4.3b**

X-ray crystallographic data for **5.1a**

X-ray crystallographic data for **5.3a**

Raw SQUID data for **3.1**

Raw SQUID data for **4.3a**

Raw SQUID data for **4.3b**

Raw SQUID data for **5.3a**

DFT output file for **4.1a**

DFT output file for **4.1b**

DFT output file for **4.2a**

DFT output file for **4.2b**

DFT output file for **4.3a**

DFT output file for **4.3b**

Kohn Sham orbitals for **4.1a**

Solid state structural comparison table for *anti*-bimetallics

ABBREVIATIONS AND COLLOQUIALISMS

3c2e	three centre two electron
Ac	acetyl, —$COCH_3$
acac	2,4-pentanedionato, 'acetylacetonate'
AM1	Austin model 1
bh	bridgehead
fulvalene	C_5H_4—C_5H_4
allyl	C_3H_5
CBC	Covalent Bond Classification
cent	centroid
CGC	constrained geometry catalyst
COD	cyclooctadiene
COSY	Correlation Spectroscopy
COT	1,3,5,7-cyclooctatetraene, C_8H_8
Cp	cyclopentadiene
Cp*	1,2,3,4,5-pentamethylcyclopentadiene
CSD	Cambridge Structural Database
CV	cyclic voltammetry
D_0	zero-field splitting
DCM	dichloromethane
DEPT	Distortionless Enhancement by Polarisation Transfer
DFT	Density Functional Theory
DME	dimethoxyethane
DMSO	dimethylsulfoxide
e.s.d.	estimated standard deviation
*ebo*Ind	edge-bridged open indenyl
E_{pa}	voltage at peak anodic current
E_{pc}	voltage at peak cathodic current
EPR	electron paramagnetic resonance
Et	ethyl, —CH_2CH_3
ET	electron transfer
Fc	ferrocene, $Fe(C_5H_5)_2$

Fp	$(\eta^5\text{-Cp})Fe(CO)_2$
FVP	flash vacuum pyrolysis
g	g-factor
GGP	Green, Green, and Parkin
HDVV	Heisenberg-Dirac-Van Vleck
HMBC	Heteronuclear Multiple-Bond Quantum Correlation
HOMO	highest occupied molecular orbital
HSQC	Heteronuclear Single Quantum Correlation
Ind	indenyl
Ind*	permethylindenyl, C_9Me_9
i_{pa}	peak anodic current
i_{pc}	peak cathodic current
^{i}Pr	isopropyl, $—CH(CH_3)_2$
IR	infra-red
LDA	lithium diisopropylamide
LSMP	least squares mean plane
LUMO	lowest unoccupied molecular orbital
Me	methyl, $—CH_3$
MM2	an ab-initio force field calculation method
MO	molecular orbital
^{n}Bu	n-butyl, $—CH_2(CH_2)_2CH_3$
NMR	nuclear magnetic resonance
NWT	non-wing-tip
*o*Ind	open indenyl
PM3	Parametric Method 3
Pn	pentalene, C_8H_8, bicycle[3.3.0]octa-1,3,4,6-tetraene
$Pn^{(1,4\text{-}Si^{i}Pr_3)}$	1,4-bis(triisopropylsilyl)pentalene, $C_8H_4(Si^{i}Pr_3)_2$
Pn*	hexamethylpentalene, $C_{14}H_{18}$
Pn^{*2-}	$[C_{14}H_{18}]^{2-}$
Pn*H	Permethylhydropentalene, $C_{14}H_{19}$
Pn_2	$(C_8H_6)_2$, [2+2] dimer
Pn^{2-}	$[C_8H_8]^{2-}$
ppb	parts per billion
ppm	parts per million
py	pyridine
R	chirality descriptor (Cahn-Ingold-Prelog rules)

R_p	planar chirality descriptor (Schlögl's rules)
S	total spin angular momentum quantum number; chirality descriptor (Cahn-Ingold-Prelog rules)
S_p	planar chirality descriptor (Schlögl's rules)
SCE	standard calomel electrode
SD	spin density
SOMO	singly occupied molecular orbital
SP	spin polarisation
SQUID	Superconducting Quantum Interference Device
THF	tetrahydrofuran
TLC	thin layer chromatography
TM	transition metal
TMEDA	*N,N,N',N'*-tetramethylethylene-1,2-diamine
TNE	total number of electrons
UV-vis	ultraviolet-visible light
VE	valence electron
$WeissH_4$	2,4,6,8-tetramethylcarboxylate-bicyclo[3.3.0]octa-3,7-dione
$WeissMe_4$	2,4,6,8-tetramethylcarboxylate-2,4,6,8-tetramethyl-bicyclo[3.3.0]octa-3,7-dione
WT	wing-tip
z_{eff}	effective nuclear charge
η^5,η^5-Pn_2	$(C_8H_6)_2$ single-bonded dimer
μ	magnetic moment
χ	magnetic susceptibility

Chapter 1 INTRODUCTION

1.1 General overview

In organometallic complexes containing multiple metal atoms, metal-metal interactions can take place either directly, or indirectly. In direct interactions, the two metals interact through space. Usually this occurs by the overlap of orbitals with metal-metal bonding character. In biological systems however, electrons can be relayed through molecular bridges and chains of redox cofactors, over distances reaching up to 2.5 nm, far exceeding the reach of orbital overlap.[1] These indirect M-M interactions occur when the metal atoms are remote from one another, and are facilitated by coordination to a mutual ligand. A change induced at one metal can affect properties and reactivity at the remote site, with implications in fields such as catalysis, sensing, and molecular electronics.

Recent advances in catalysis have seen multiple single-site catalysts tethered to a shared ligand outperform a mixture of the analogous untethered, monometallic, single-site catalysts. A review by Marks and coworkers highlights the high selectivity and activity that can be achieved in olefin polymerisation with the group IV homo- and heterobimetallic constrained geometry catalysts (CGCs),[2] while Bratko and Gómez have reviewed polymetallic complexes for functionalisation of organic molecules.[3] Researchers exploiting these enhanced selectivities and activities refer to "cooperative effects" in multimetallic systems. Cooperativity can have different roots. For example, in proximity bimetallics, the metals are too far apart to interact directly, but substituents can be introduced to one metal that take part in agostic bonding to the second centre, thereby influencing its reactivity.[4] Metal-substrate coordination can recognise functional groups and favour certain substrate geometries. The tethering of the second

site relieves entropic constraints (pre-organisation needed for the catalytic sites can be designed into the shared ligand, minimising loss of the substrate prior to a second process), thereby increasing the rate of reactions.[3] The role of the bridging ligand in these systems is largely to hold the active sites an optimal distance from each other, and the cooperative effect has a strong dependence on metal-metal distance.

Conjugated π systems of unsaturated bridging ligands facilitate indirect metal-metal interactions *via* overlap of π orbitals with metal orbitals of appropriate symmetry. Ligands with extensive delocalisation can form multimetallic complexes with very strong metal-metal interactions. That is to say, a perturbation of the electrons at one site can affect the remote site by influencing the character of electrons in molecular orbitals that overlap with both metal atoms.[5]

In ligands with conformational flexibility, efficient overlap can be reduced as steric interactions and entropic factors disrupt the conjugated pathway connecting two metals.

1.2 Scope

This thesis concerns the preparation of new organic molecules that are precursors to substituted pentalenes, and the preparation and characterisation of complexes in which derivatives of pentalene function as ligands for mono- and bimetallic complexes. This thesis restricts most discussions to systems that contain first row transition metal atoms coordinated to two five-membered aromatic ligands. Systems incorporating other π-conjugated ligands such as allyl, or benzene may be mentioned for the purpose of comparison where appropriate. For the most part, ligands such as indenyl, or indacene, containing one or more cyclopentadienyl groups annulated to other aromatic rings, are beyond the scope of this work.

1.3 Metallocenes

Ferrocene was first identified and published in 1951 simultaneously by Kealy and Pauson,[6] and by Miller *et al*.[7] The following year, Wilkinson, Rosenblum, Whiting, and Woodward proposed the eclipsing and staggered forms of the 'sandwich' structure that are now ubiquitous (Figure 1.1 b).[8] Independently, Fischer had collected unit cells for crystalline ferrocene, cobaltocene, and nickelocene,[9] confirming that Kealy and Miller's proposed linear connectivity – now termed monohapto- (Figure 1.1 a) – would not fit into the cell. The deduction that followed was a 'double cone', sandwich-type structure (Figure 1.1 c), confirming the hypothesis of Wilkinson *et al*.

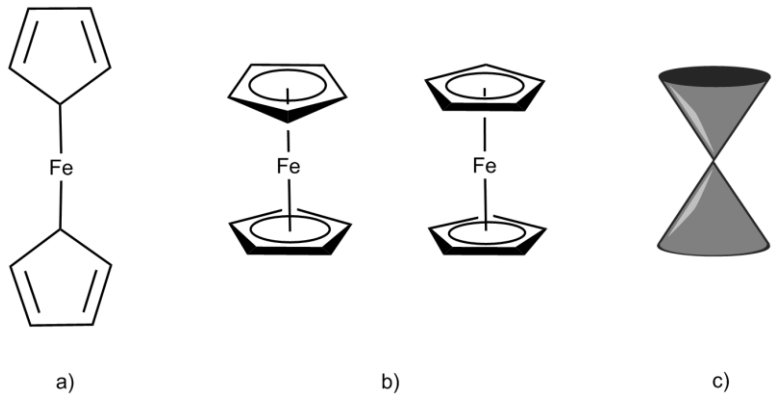

Figure 1.1 a) The structure of ferrocene initially proposed, b) and c) the 'sandwich' and double cone structures published simultaneously by Wilkinson *et al*. and Fischer.

The concept of metals being able to bond to carbon through overlap with π systems was revolutionary. Prior to the elucidation of the bonding in ferrocene, only coordinate and covalent bonds had been considered chemically possible.[10] Between 1952 and 1954, sandwich complexes of nearly all the transition metal elements were identified at an astonishing rate, mainly by the groups of Fischer, in Munich, and Wilkinson, in London. In awarding these two the 1973 Nobel Prize in Chemistry, the Nobel Prize Committee emphasised that their enormous contribution to the field had

"*widened the basic concepts of chemistry, and therefore also changed the structure of chemistry*".[11]

Sixty years later metallocene research is still flourishing. In 2013, an entire issue of Organometallics was dedicated to recent advances in the chemistry of ferrocenes,[12] including relatively new applications to anion detection,[13,14] and in boosting antitumor activity of cytotoxic molecules.[15,16] Only recently, the discovery of a way to make pentafluoroferrocene was published, incorporating for the first time the highly electron deficient pentafluorocyclopentadiene ligand into a first row transition metal metallocene.[17]

1.4 Linked metallocenes – fulvalene complexes and derivatives

Molecular organometallics containing multiple metal atoms have received extensive study as systems with useful and novel electronic and magnetic properties. As an example, polymeric nickel(II) species are predicted to display a 'Haldane [energy] gap' between their ground singlet and first excited triplet states, so below *ca.* 50 K the magnetism should approach zero, while for half-integer spin systems magnetic susceptibility reaches a limiting value at low T. This should limit conductivity below 50 K, making them attractive as materials for molecular switches or temperature dependent semiconductors. While this behaviour is realised by 1-dimensional chains of nickel cations bridged by heteroatoms,[18] the first example of a purely organometallic polynickelocene, $[\{C_5H_4\}Ni(C_5H_4C_3H_6)\}]_n$, is not a Haldane gap material, as the saturated linker between nickelocene units result in only weak antiferromagnetic intrachain interactions.[19] There is therefore still interest in synthesising model systems with bridging units that better facilitate extended overlap. Structures incorporating metallocene scaffolds are especially attractive because rational perturbations of their electrochemical behaviour can be achieved through systematic ring-substitution.[20] Multiferrocenyl linked metallocene complexes display robust, reversible Fe(II)/Fe(III)

redox couples, and have thus far found use in sensor technologies,[21–25] and molecular electronics.[20,26–37]

The metallocene unit, familiar as it now is, was not the target of Pauson's original research, which attempted to make the organic hydrocarbon fulvalene by a reaction analogous to that used to make biphenyl (oxidative coupling of cyclopentadienyl groups of CpMgBr using $FeCl_3$). Yet another serendipitous discovery was that the newly discovered ferrocene itself presented an access route to fulvalene complexes (Figure 1.2).[38] Coupling of ferrocenyllithiums in the presence of cobaltous chloride gives biferrocene and terferrocene.[39,40] Additionally the linked biferrocenyl (aka biferrocene), could be made in quantitative yield through an Ullmann coupling of iodoferrocenes over copper bronze.[41] This method can be adapted to make iron-fulvalene oligomers containing up to six ferrocenyl units,[42] and also of making the doubly linked bisfulvalenediiron, also known as 1,1'-biferrocenylene (Figure 1.2).[43,44]

Fulvalene, with a single bond between two Cp rings, is the simplest linked metallocene (a spiro system could not be aromatic). Cyclopentadienyl groups can also be joined through more than one vertex,[45] and linking groups can include heteroatoms, or hydrocarbon fragments which are aromatic, unsaturated, or saturated. A thorough review of metal-metal interactions in linked metallocenes pre-1995 has been published by Barlow and O'Hare.[45] A more recent review focussed on linked ferrocenes with

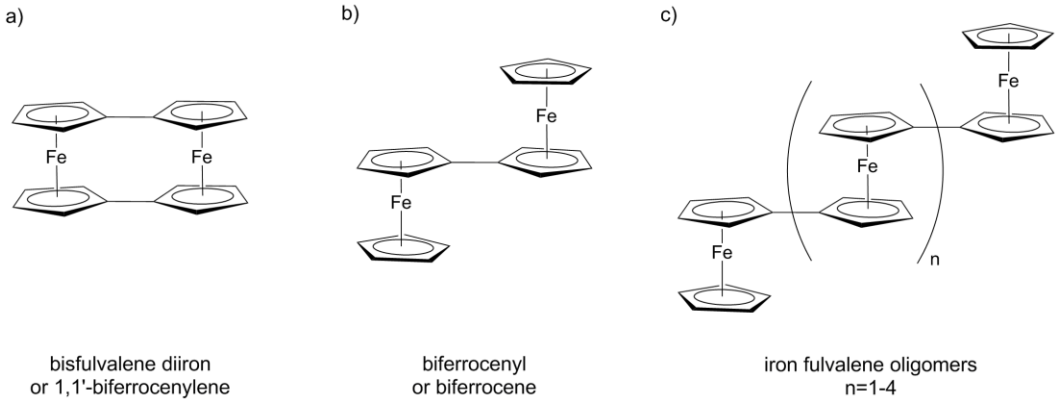

Figure 1.2 Multimetallic linked ferrocenes containing the fulvalene ligand.

unsaturated bridges (up to 2007) has been compiled by Debroy and Roy.[35]

The number of linked metallocenes containing iron significantly outweighs those of any other metal. This is unsurprising given the ease of funtionalisation of ferrocene, and its well-defined reversible redox couple.[46] Cobalt,[47,48] nickel,[49,50] and ruthenium[51–55] are also known components, with linked cobaltocenes often found as their cationic cobaltocenium salts. However, early transition metal analogues of titanium, vanadium[56,57] and chromium[58,59] are more scarce. The titanium(IV) metallocenes Cp_2TiCl_2 or Cp_2TiMe_2 readily undergo a reduction that results in two cyclopentadienyl ligands coupling together to give a fulvene ligand.[60–62] The two reduced titanium(III) centres coordinate to the same face of the ligand, with two M–H–M hydride bridges, formed with hydrogens abstracted from the cyclopentadienyl groups.[63,64]

1.4.1 Oligomers and polymers with metallocenes in the polymer chain

For molecular electronics, the study of linked ferrocenyl dendrimers has been popular,[21,22,31] and extended multimetallic systems of organometallic wires, capable of conducting electrical currents are desirable. A few examples exist of polyferrocenes with molecular weights of up to 7000;[65–70] however, in general, solubility decreases rapidly with increasing oligomerisation, and remains a synthetic challenge in extending systems beyond five or six metallocene units using conventional synthetic routes.

In the early 1990s, the group of Manners pioneered the ring-opening polymerisation of strained metallocenophanes (*ansa*-bridged metallocenes), revolutionising the field. The widely applicable route has since afforded organometallic polymers of iron,[71–77] cobalt,[78] ruthenium,[79,80] and very recently, nickel.[19] Although a handful of examples of polymetallocenes had been reported prior to its discovery, the ring-opening technique – which can be induced thermally, anionically, cationically, by donor solvent, or by transition metal catalysts – can incorporate a huge range of linking

groups, from saturated two-carbon bridges to *p*-block heteroatoms (Scheme 1.1).[72–74,81–91]

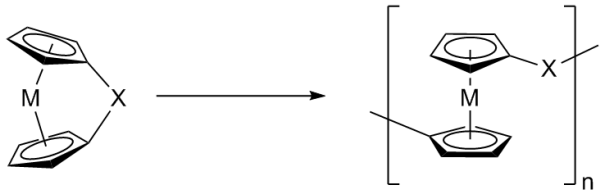

M = Fe ; X = C_2H_4, C_2Me_4, NMe_2, S, Se, GeR_2 (where R = Me, Et, Ph), $BN(SiMe_3)_2$, Sn^tBu_2, SiR'R" (where R' or R" = H, alkyl, aryl, alkoxide, aryloxide, 5-norboryl, Fc)
M = Ru ; X = C_2H_4
M = Co ; X = C_2H_4
M = Ni ; X = C_3H_6

Scheme 1.1 Ring opening polymerisation of strained metallocenophanes to make polymeric linked metallocenes.

1.5 Fused metallocenes – the pentalene ligand

Where the fulvalene ligand provides the simplest form of linked metallocene, with a single bond between cyclopentadienyl rings, fusion of two cyclopentadienyl groups gives the pentalene framework: an eight-carbon, bicyclic compound, with two fused five-carbon rings that share a common bond (Figure 1.3). While neutral fulvalene has 10π electrons, pentalene has eight, and is therefore Hückel anti-aromatic.

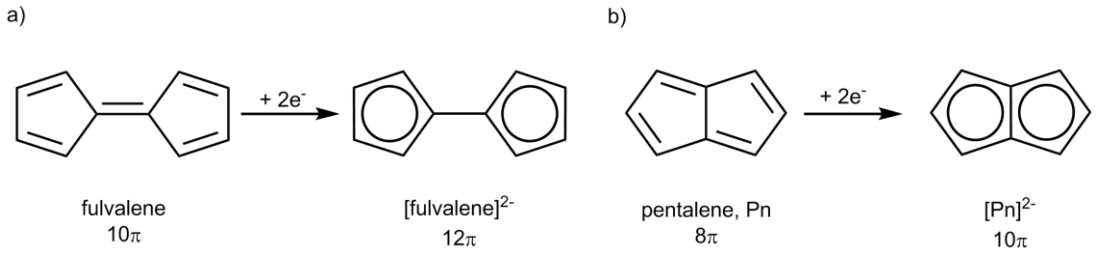

Figure 1.3 Neutral and dianionic forms of a) the fulvalene ligand, and b) the pentalene ligand.

Pentalene is isoelectronic with cyclooctatetraene, but the additional bond – across which the two C_5 rings are fused – forces the molecule to adopt a planar conformation. Unable to distort its geometry to relieve anti-aromaticity, pentalene and

the substituted 1-methylpentalene, 2-methylpentalene, and 1,3-dimethylpentalene, all dimerise rapidly at low temperatures to give [2+2] cycloaddition products.[92,93]

The first detection of monomeric pentalenes resulted from irradiation experiments on the unsubstituted,[93] 1-methyl,[92] 2-methyl and 1,3-dimethylpentalene[93] dimers. Photolysis of the dimers isolated in low temperature matrices was monitored by UV-vis spectroscopy, revealing that bands characteristic of the fulvene dimer diminish as two new bands grew in. It was proposed that the [2+2] cycloaddition was being reversed photolytically.

Bally *et al.* revisited this topic in 1997, performing a stepwise photolytic cleavage of the pentalene dimer Pn_2 (Figure 1.4).[94,95] The nature of the intermediate species was speculated to be a diradical, however could not be confirmed. The neutral tetraene isolated at 20 K did not recombine on warming to 30 K in an argon/dinitrogen matrix, but did when thawed in a Freon glass.[94]

Following the speculation by Armit and Robinson in 1922 on the existence of the pentalene molecule,[96] there ensued years of controversy among theoreticians over whether the molecule was better described as an aromatic hydrocarbon or a polyolefin.[97–100] By comparing electronic (UV-vis) and vibrational (IR) spectra of the monomer with electronic structures calculated using a wide variety of quantum chemical calculations, Bally and colleagues were able to confirm that the description of unsubstituted pentalene as anti-aromatic, with C_{2h} symmetry, and localised double

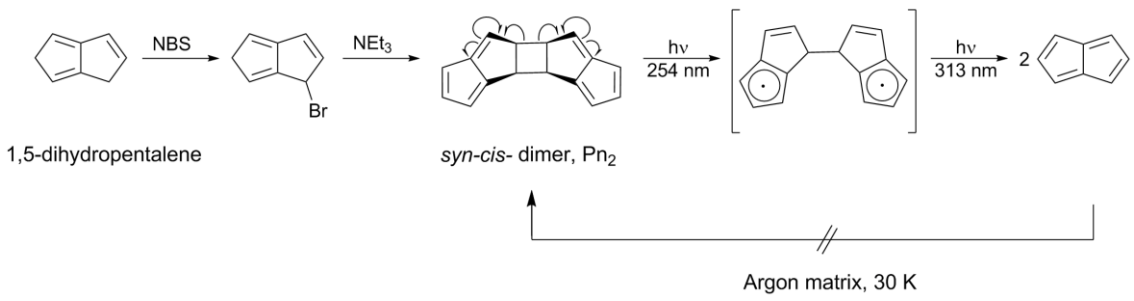

Figure 1.4 Stereoselective synthesis of the pentalene dimer Pn_2 and its photolytic cleavage to form monomeric pentalene.

bonds was most consistent with their experimental results.[94]

1.5.1 Nomenclature when describing pentalenes and complexes

Throughout this thesis, the carbon framework of pentalene and its derivatives are referred to by the numbering scheme shown in Figure 1.5. Carbon atoms 1, 3, 4, and 6 are at positions referred to at times as 'non-wing-tip' positions, carbons 2 and 5 as at 'wing-tip' positions, and atoms at positions 7 and 8 refer to 'bridgehead' carbons. Methyl groups attached to the carbon framework may be numbered C9 to C14, attached to C1 to C3 and C4 to C6 in ascending order. Note that in the numbering scheme for the protonated and deprotonated derivatives, the eight carbon skeleton is labelled differently, reflecting the 'substituted cyclopentadienyl' behaviour of the ligand in complexes. Pentalene and pentalenyl are used interchangeably in subsequent chapters to refer to the $[C_8H_6]^{2-}$ ligand and substituted derivatives.

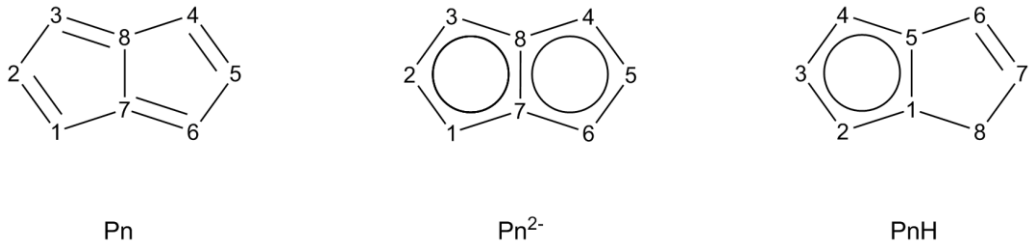

Figure 1.5 Numbering scheme for neutral (Pn) and dianionic (Pn^{2-}) pentalene rings, and hydropentalene (PnH).

The peralkylated derivative with six methyl groups is referred to interchangeably as hexamethypentalene or permethylpentalene, or by the abbreviation Pn*, and henceforth refers to the dianionic ligand, $[C_8Me_6]^{2-}$ unless specified otherwise.

1.5.2 Monomeric pentalenes

Dimerisation of pentalenes can be supressed either electronically, by adding groups that modify the reactivity of the π electrons and deter dimerisation, or sterically, by adding bulky substituents that prevent the electron rich π systems from overlapping

and reacting. An electronically and sterically stabilised derivative, containing 1,4-diphenylpentalene fused to two benzene rings had in fact been made in 1912 (Figure 1.6 a),[101] but only in the 1950s were further examples with fused groups explored.[102–105] Synthetic routes towards monomeric pentalene derivatives stabilised by annulation to one, or two aromatic (usually benzene) rings have recently been reviewed in detail by Saito,[106] and Hopf.[107] Surprisingly, the focus of research in this area has lain heavily in the area of organic synthesis. The first transition metal complex to incorporate a benzo-fused pentalene was only published in 2014; however, both Cp*Ru(II) coordinate to the six membered benzo- rings rather than the central pentalene unit.[108]

The first neutral pentalene monomer to be isolated that contained no fused rings was hexaphenylpentalene (Figure 1.6 b), which is air sensitive in solution, but stable to oxygen in its solid form. Published in 1962 by Le Goff, six phenyl groups provide both a steric barrier to dimerisation and inductive withdrawal of electron density from the four double bonds.[109] 1,3,5-tri-tertbutylpentalene is a sterically stabilised, monomeric

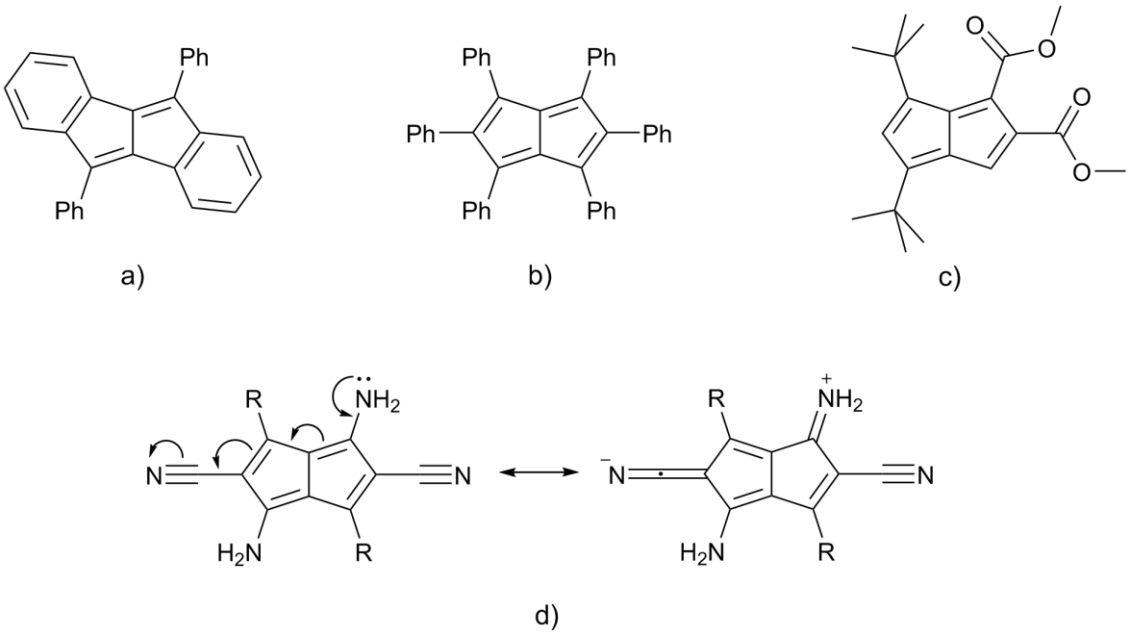

Figure 1.6 Bulky, monomeric neutral pentalenes. a) 1,4-diphenyl-dibenzopentalene, b) hexaphenylpentalene, c) 1,2-dicarboxymethyl-4,6-ditertbutylpentalene, d) 1,4-diamino-2,5-dinitrile-3,6-dialkylpentalene (R = Me, Et, C_5H_4).

pentalene,[110] and 1,2-dicarboxymethyl-4,6-ditertbutylpentalene is also monomeric (Figure 1.6 c), with both electronic and steric deactivation; both have crystal structures that show localised double bonds.[111] As is found for fulvalenes,[112] resonance stabilisation can be achieved by having electron donating groups in the 1- and 3-positions: 1,3-diaminopentalene resists dimerisation and is air stable at 20 °C for a number of hours.[113] Meanwhile, other than hexaphenylpentalene, the only per-substituted unfused pentalenes are the 1,4-diamino-2,5-dinitrile-3,6-dialkylpentalenes, where the strongly electron accepting nitrile group on one ring and the strongly electron donating amine group on the other ring work together, their "push-pull" effect lowering the energy of the flanked diene, and preventing dimerisation (Figure 1.6 d).[114]

1.6 Pentalenyl precursors

While efforts to isolate neutral pentalenes have proven challenging, it was recognised as early as the 1960s that reduction to the dianion would give a 10π aromatic ligand. As had recently been demonstrated for substituted butadienes,[115–118] and cyclooctatetraene,[119] coordination to metals could afford ways to isolate and study stable complexes containing highly reactive hydrocarbons, such as pentalene.

Nearly all sources of pentalenyl dianions start with the synthesis of a dihydropentalene, for which six isomers exist (Figure 1.7). Treatment of these with one or two equivalents of a strong base singly or doubly protonates the organic triene, and results in a pentalenyl mono- or dianion, usually as an alkali metal salt.

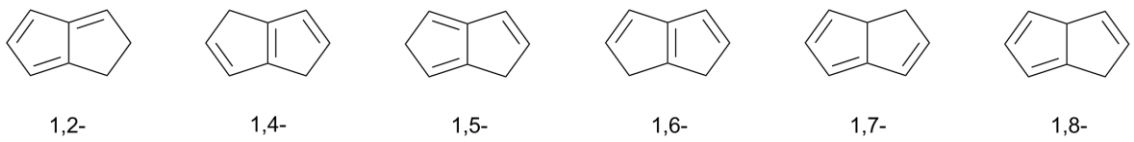

Figure 1.7 Six possible isomers of dihydropentalene.

1.6.1 Flash vacuum pyrolysis

Katz and Rosenberg reported the first synthesis of dilithium pentalene in 1962. In a technique known as flash vacuum pyrolysis (FVP), a reduced pressure nitrogen stream containing isocyclopentadiene was heated to 575 °C, resulting in isomerisation and subsequent cracking to form 1,5-dihydropentalene in 30% yield, which was deprotonated with ^{n}BuLi.[120,121] Crystallographic characterisation of the dimethoxyethane (DME) adduct, $Li_2Pn{\cdot}2DME$, reveals the $[Li{\cdot}DME]^+$ cations each coordinate to a five-carbon ring on opposite faces of the bridging ligand, and the 10π aromatic dianion is planar with D_{2h} symmetry.[122] It was later shown that FVP of cyclooctatetraene at 400 – 675 °C converts up to 90% to mixtures of dihydropentalene isomers, which can all be deprotonated with ^{n}BuLi·DME,[123,124] or ^{n}BuLi·TMEDA,[125] without the need for further separation. Recent work in the group of Cloke has optimised this technique, producing $Li_2Pn{\cdot}2DME$ on a 25 g scale in 87% yield.[126] Other sources of dihydropentalenes include the 5-cyclopentadienylidenemethyl-2-norborene and a methyl derivative, which undergo FVP at 520 °C, retrocleaving into cyclopentadiene, and 1,5-dihydropentalene or 1,5-dihydro-2-methylpentalene.[127]

Dihydropentalene isomers are susceptible to self-polymerisation, but this can be supressed by adding trace hydroquinone, whereupon a sample can be stored on dry ice for months. The dianion is precipitated as a white solid, and THF solutions are stable for months when stored at −70 °C.[121] Monodeprotonation of 1,5-dihydropentalene is achieved by thallous sulphate (Tl_2SO_4) in aqueous potassium hydroxide, precipitating the relatively air stable, yet highly toxic, organothallium(I) complex.[128–130] The base trimethylstannyldiethylamide ($SnMe_3(NEt)_2$) has been used stoichiometrically to deprotonated 1,5-dihydropentalene, forming trimethylstannylhydropentalene or bis(trimethylstannyl)pentalene.[131] In both cases, NMR studies show the molecules have fluxional behaviour, with stannyl moieties undergoing [1,5]-sigmatropic shifts around their respective C_5 rings. Bis(trimethylstannyl)pentalene forms as two isomers, with

stannyl groups on the same or opposite faces of the pentalene ligand in a 1:6 ratio. A fleeting mention was made of a tri- substituted, tris(trimethylstannyl)pentalene product, resulting from over-reaction, however no structure was proposed, and neither characterising information nor a mechanism for its formation were provided.[131]

Cloke and coworkers reacted the unsubstituted dianionic $Li_2Pn{\cdot}2DME$ with trimethylsilylchloride or triisopropylsilyltriflate electrophiles, resulting in formation of the 1,4-bistrialkylsilyl- substituted dihydropentalenes following work up and crystallisation. The isomers of 1,4-bistrimethylsilyl-1,4-dihydropentalene oligomerise above −20 °C, but the 1,4-bistriisopropylsilyl-1,4-dihydropentalene, for which only the a 'trans' arrangement of silyl groups forms, does not. Both can then be deprotonated readily with ^{n}BuLi in DME, or potassium amide respectively. Reaction of $Li_2Pn^{(1,4\text{-}SiMe_3)_2}$ with additional trimethylsilylchloride resulted in a single tetrasubstituted product; however, these additions also occurred at the 1- and 4- positions, meaning the degree of substitution could not be increased beyond two by this method.

Flash vacuum pyrolysis relies on highly specialised equipment, and fierce reaction conditions that must be painstakingly optimised for high yields. An example of the setup is shown in Figure 1.8. It also limits the availability of substituted isomers, thus far, to monomethylated dihydropentalenyls, and bistrialkylsilyl-pentalenes

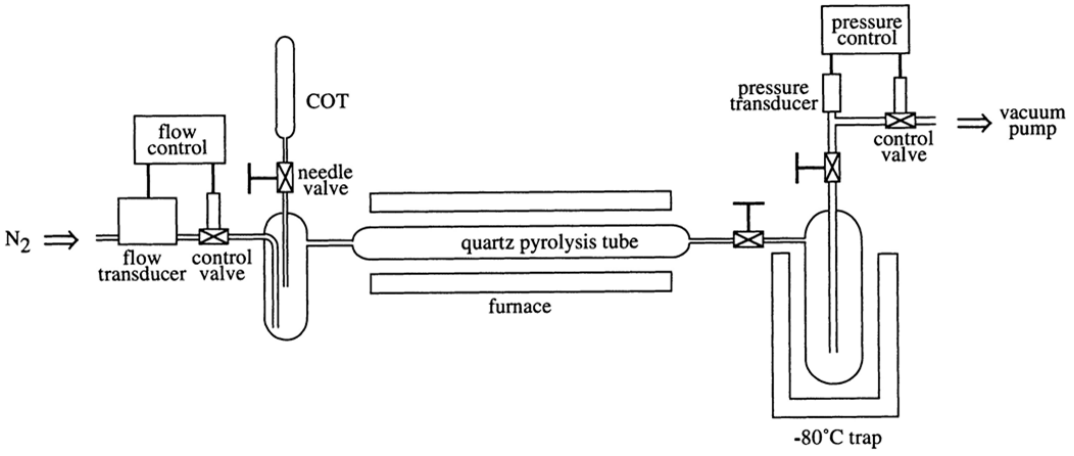

Figure 1.8 Schematic of the flash vacuum pyrolysis (FVP) apparatus used by Cloke and coworkers.[126]

obtained by subsequent reaction.

1.6.2 Non-pyrolytic routes to dihydropentalenes and pentalenes

1.6.2.1 Electrocyclisation

Gajewski and Cavender meanwhile demonstrated that cyclisation of a simple 6-vinylfulvene can be achieved at the relatively low temperature of 110 °C (Figure 1.9). Following a series of [1,5]-hydride shifts, the 1,5-dihydropentalene product was isolated, albeit in poor yield.[132]

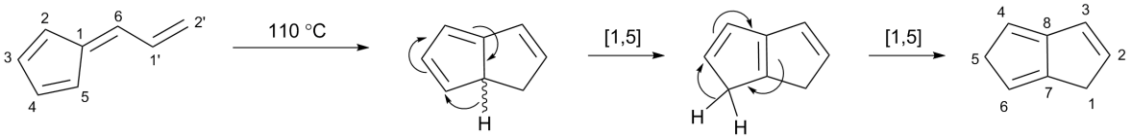

Figure 1.9 Electrocyclisation of 6-vinylfulvenes to make dihydropentalene and subsequent 1,5-hydride shifts.

Kaiser and Hafner further expanded the range of substituted dihydropentalenes that could be synthesised by reacting 6-(2'-aminovinyl)fulvenes in boiling piperidine to form 1-amino-2,3-dihydro-pentalenes.[133] The bicyclic ring thus formed undergoes base catalysed isomerisations to the more stable 3-amino-1,2-dihydro-pentalene, which contains a fulvene moiety. Nucleophilic hydride or alkyl addition to the 3-amino position of the 1,2-dihydro-pentalene, followed by hydrolysis and amine elimination, give 1,2-dihydropentalenes with substituents in the 1- and/or 3- positions. As one substituent is present in the vinylfulvene starting material, and another added following the ring closing cyclisation, it is therefore possible to add two different substituents, as demonstrated with combinations of methyl and phenyl groups.[133]

If 6-(2'-aminovinyl)fulvenes with substituents at both the 6 and 2' positions are used, reactions proceed below 20 °C (Figure 1.10).[112] Steric interactions between the two groups are relieved by rotation of the enamine out of the plane of the fulvene. This brings the C-N bond close to the fulvene ring, and electrocyclisation proceeds readily forming 1-amino-1,2-dihydropentalenes, again with substituents in the 1- and 3- positions. When there are alkyl or aryl substituents in only the 2' position of the starting fulvene, a reversible addition of piperidine follows the cyclisation. Elimination of the amine, results again in 3-amino-1,2-dihydropentalenes again, but this time with a substituent in the 2- position.[112]

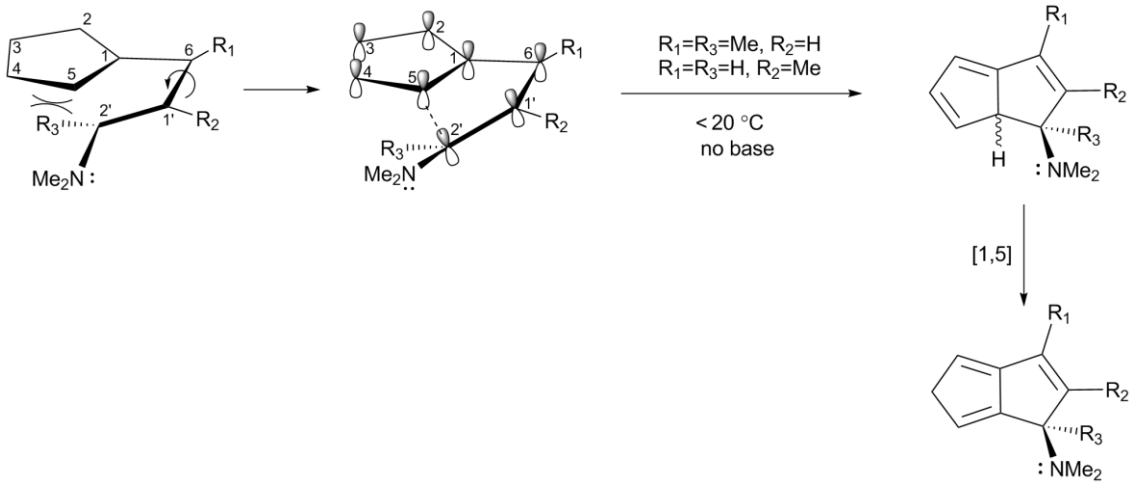

Figure 1.10 Facile cyclisation of substituted 6-(2'-amino)vinylfulvenes to make 1,3- and 2-alkyl substituted hydropentalenes.

1.6.2.2 Rearrangements

Reactions between 8,8-dibromobicyclo[5.1.0]oct-2-enes and octa-2,4-dienes with methyl lithium at low temperatures form tetrahydro- and dihydropentalenes respectively.[134] A labelling study confirmed that the mechanism is analogous to a Skattebøl rearrangement of vinyl-*gem*-dibromocyclopropanes to cyclopentenes.[135,136] With this knowledge, Jones *et al.* took the readily available 8,8-dibromobicyclo[5.1.0]octa-2,4-dienes (made from dibromocarbene and

cycloheptatriene), and by alkylation at the methylene position adjacent to the cyclopropane, were able to access dilithium salts of pentalene with methyl, ethyl and isopropyl substituents in the 1- position. Treatment of these dihydropentalens with ^{n}BuLi doubly deprotonated $Li_2Pn^{1\text{-}R}$, while the less basic thallium ethoxide exclusively mono deprotonates the rearrangement product, affording $Tl(Pn^{1\text{-}Me}H)$ and $Tl(Pn^{3\text{-}Me}H)$.[137]

1.6.2.3 Metal facilitated pentalene formation

A common method for isolating highly reactive organic moieties is to react them with excess $Fe(CO)_5$, thus stabilising the cyclic polyenes *via* coordination to iron carbonyls.[138–142] The reaction between iron carbonyl $Fe(CO)_5$ and 3-substituted 1,2-dihydropentalenes gave bimetallic complexes of 1-phenylpentalene,[143] and 1-(dimethylamino)pentalene.[144] For 1,5-dihydropentalenes however, this reaction is not viable: the dinuclear $Fe_2(CO)_9$ reacts with either 1,5-dihydropentalene,[145] or the Pn_2 dimer,[146] to furnish $[Fe(CO)_2]_2(\mu\text{-}CO)(\mu\text{-}Pn)$.

Reviews of the reactions between ruthenium carbonyls $Ru_x(CO)_y(L)_z$ (where L = $GeMe_3$, x,y,z = 1,4,2; 3,12,0; L = $SiMe_3$, x,y,z = 2,2,8) and cyclooctatetraenes or cyclooctatrienes are provided by Knox and Stone.[147,148] Dehydrogentation of the eight membered carbocycle is accompanied by formation of a transannular bond, and the resulting pentalenes are reduced and stabilised in *syn*-bi- or trimetallic complexes. Pentalenes formed in this way can be unsubstituted,[149,150] or have alkyl, phenyl, or silyl[151–153] substituents in up to three positions. The multimetallics thus formed are always *syn*-coordinated.

O'Hare *et al.* also showed that the bicyclic tetraene isomer of hexamethylpentalene can be reduced by $Fe_2(CO)_9$ or $Co_2(CO)_8$ to *syn*-bimetallic complexes which contain metal atoms in proximity, but do not feature metal-metal bonding.[154]

The tetramerisation of terminal acetylenes with $[(1,5\text{-COD})RhCl]_2$ results in an unprecedented selectivity for hydropentalenes.[155] Importantly, it is one of few routes available to construct tetrasubstituted pentalene precursors, with the isomer distributions shown in Scheme 1.2 being favoured over any other products.

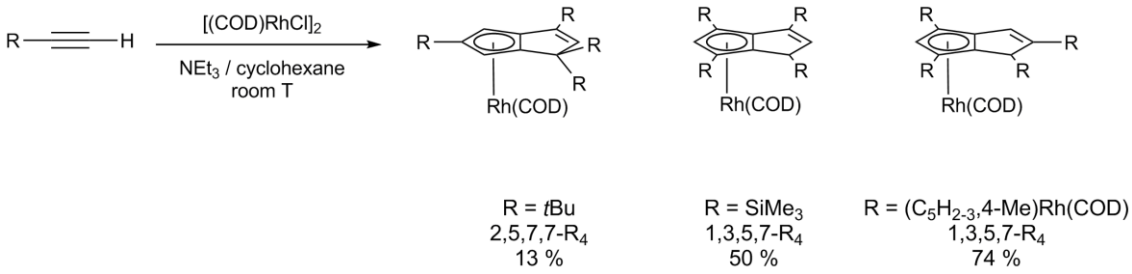

Scheme 1.2 Selective tetrametisation of acetylenes to give tetrasubstituted Rh(I)pentalene-cyclooctadiene complexes.

1.6.2.4 Permethylation

Attaining a high degree of substitution on the pentalene skeleton from the routes discussed above is limited, with only trisubstitution achieved in a straightforward manner. In 2007, O'Hare and coworkers tackled the limited routes available for making substituted pentalenes, removing the need for specialised lab equipment and reworking the synthesis to use only solution phase, common reactions, and easily obtainable reactants. The eight-carbon, bicyclic skeleton is formed by Aldol condensation reactions between two molecules of dimethyl-1,3-acetonedicarboxylate and one of glyoxal (ethanedial). The O'Hare method allows for functionalisation of the four 'non-wing-tip' positions adjacent to the bridgehead atoms (Scheme 1.3 a) by deprotonation followed

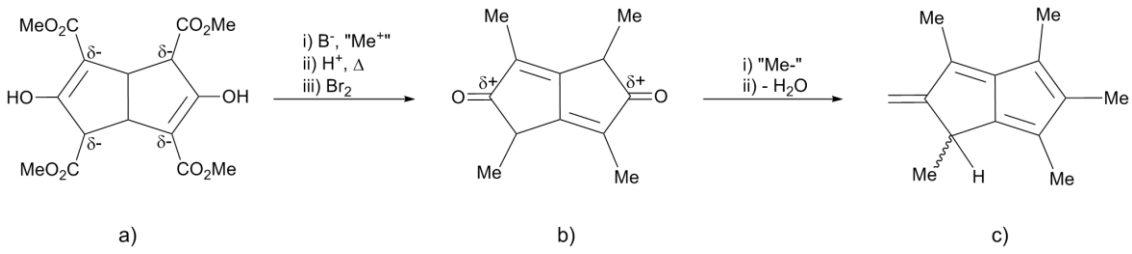

Scheme 1.3 Key intermediates in the synthesis of permethylpentalene (Pn*) that allow hexamethylation.

by addition of an electrophile, and of the two 'wing-tip' positions (Scheme 1.3 b) by nucleophilic attack on the ketone carbon. The pentalene precursor that results following dehydration is an isomer of the neutral tetraene, with substituents attached to all six positions (Scheme 1.3 c).[156]

It is well known that changes to the peripheral groups on cyclopentadienyl ligands can affect the reactivity of complexes in which they are coordinated, as well as stability, and solubility.[157] Specifically, methylation makes cyclopentadienyl ligands more electron rich, imparting improved stability to electron deficient complexes and enhanced reactivity to electron rich ones. Reduction of the hexamethylpentalene isomer (Scheme 1.3 c) to the monolithium salt requires use of the extremely strong hydride source *LS*-Selectride (lithium tri-secbutylborohydride), and the subsequent deprotonation can be achieved with ^{n}BuLi in ether, giving Li_2Pn^*.[158] It is worth emphasising that the permethylhydropentalenyl monoanion ($[Pn^*H]^-$) and pentalenyl dianion ($[Pn^*]^{2-}$) are formed under very different conditions to all other monoanion derivatives, so Li(Pn*H) provides access exclusively to hydropentalenyl derivatives, without resorting to stoichiometric control or very toxic thallium reagents. The mono and dianionic lithium salts can be reacted with Me_3SnCl to afford the softer stannyl sources of $[Pn^*]^{2-}$.

In summary, sources of pentalene used in forming organometallic compounds include dihydropentalene, the permethylpentalene isomer (Scheme 1.3 c), and the dimetallated lithium, potassium, thallium, and tin salts.

1.7 Fused metallocene complexes – pentalene as a bridging ligand

Pentalenes can coordinate to metal atoms through a plethora of multihaptic bonding modes, with between one and eight carbon atoms forming M—C bonds (Figure 1.11). The next section will review organometallic complexes of pentalenes, focussing on those containing a metallocene motif, with a short review of other binding modes afterwards. Comparisons are often made to the isoelectronic complexes of cyclooctatetraene.

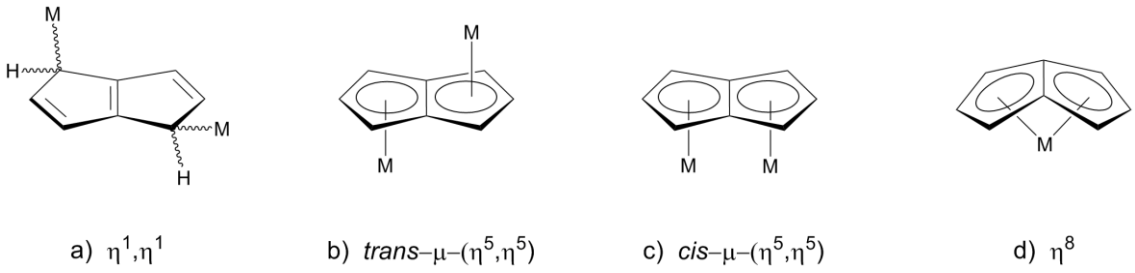

Figure 1.11 Variable hapticities of pentalene in coordination compounds.

1.7.1 Classification of M—L bonding interactions in pentalene bimetallics

In 2012, Green, Green, and Parkin developed a system to classify 3c2e bonds in molecular inorganic compounds according to how many electrons each atom contributes to the bond (Figure 1.12).[159] The GGP scheme extends the Covalent Bond Classification (CBC, 'LXZ') notation for 2c2e bonds,[160] to encompass both atomic and molecular bridging groups, and also bridging groups where the electrons are themselves contributed by a 2c2e bond. One of the major advantages of these extended CBC definitions is the accurate prediction of M—M bonding in complexes with 3c2e bonds, in agreement with the latest theoretical predictions.[159]

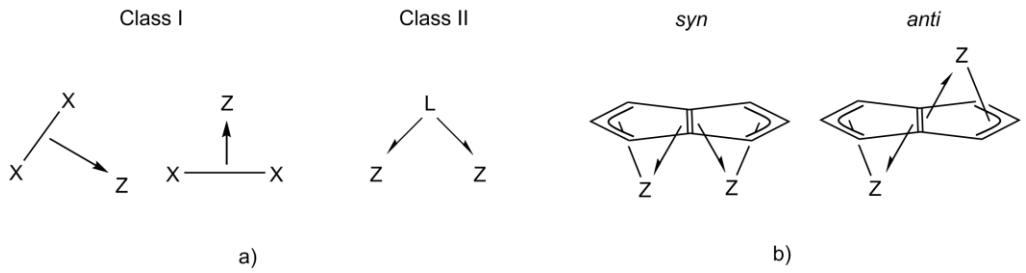

Figure 1.12 a) Classification of 3c2e bonds according to whether the electrons come from two atoms (Class I), or from a single atom (Class II); b) representation of Class II 3c2e bonds formed by pentalene in bimetallic complexes.

Pentalene forms Class II 3c2e bonds. This means that both electrons are contributed by the bridging ligand, independent of whether the ZLZ bond is linear, as in the case of *anti*-homobimetallics, or is acute or obtuse, as is the case for *syn*-bimetallics. Class II complexes are much less common than Class I complexes, where two of the three centres involved in the 3c2e bond each provide one electron.

Throughout this chapter, the neutral electron counting scheme is adhered to, in which ligands and metals are considered neutral components. Pentalene is therefore a neutral, eight π ligand in complexes, as represented in Figure 1.13 a. A useful way to consider this would be to localise the electrons into double bonds like in Figure 1.12 b. This resonance form of the pentalene ligand contains two allylic, $3e^-$ fragments, and a localised double bond across the bridgehead. According to GGP notation, each ring therefore contains one three-electron LX donor, while the two bridgehead π electrons can be donated to both metals, in a 3c2e bonding interaction, and thus is denoted a μ-L

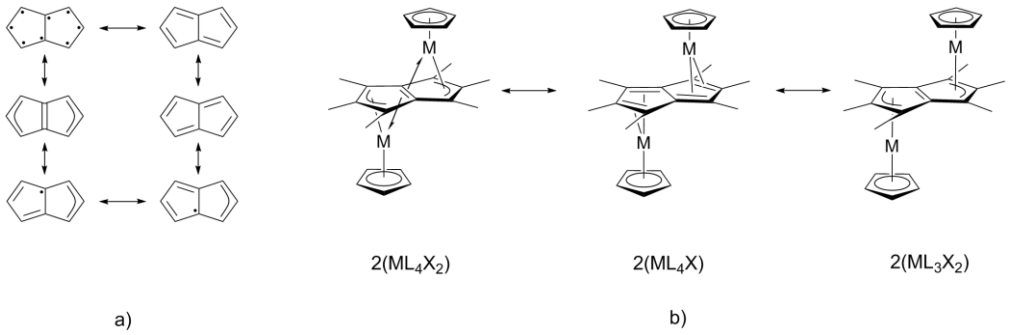

Figure 1.13 a) Some resonance forms of the neutral, 8π, pentalene molecule; b) GGP classification of metal environments in Pn* complexes with varying bonding contributions from the bridging ligand.

donor. In bimetallic compounds of pentalene, the bridging ligand would then be described as having an L_2X interaction with each metal fragment when all the ligand π electrons are in bonding molecular orbitals. The bonding contribution from the bridgehead π electrons can be denoted as in Figure 1.13 b, where the half arrows are used to indicate the 3c2e bond, and each represents a bonding interaction containing two electrons.

The "18 electron rule", used to predict the stability of transiton metal complexes, often fails to describe the physical characteristics of linked multimetallic complexes, so is best avoided, except when drawing comparisons with similar monometallic species. Saillard and co-workers classify bimetallic complexes of pentalene according to the Total Number of Electrons (TNE).[161] This method is useful for comparing isoelectronic complexes with different ligand subsets, and comparisons should be drawn between complexes that share a TNE. For example the TNE of the $[(CoCp)_2fulvalene]^{2+}$ cation is 36, making it isoelectronic with neutral biferrocene (Figure 1.2 b). It should be noted however that this method lacks information pertaining to the environment around the metal atoms, which is available from GGP classification.

1.7.2 Bis-pentalene complexes, M_2Pn_2

In the bimetallic "double metallocene" series, two M^{2+} cations are sandwiched between two pentalene ligands. The two pentalene ligands hold the two metal atoms close to each other, allowing direct metal-metal bonding, which can lead to unusual macroscopic properties. Only eight papers exist describing these fused analogues of the aforementioned linked bisfulvalene complexes. The first examples were the dinickel, and dicobalt double sandwiches of pentalene synthesised by Katz.[162,163] Unlike their paramagnetic linked metallocene analogues, both are diamagnetic, with Ni_2Pn_2 displaying a remarkable stability to water, requiring six hours in HCl solution to cause degradation, while Co_2Pn_2 solutions decompose rapidly in air. Cloke and coworkers have

formed group VI, VII and X examples of $M_2Pn^{(1,4\text{-}Si^iPr_3)}{}_2$ (M = Cr,[164] Mo,[165] Mn,[166] Rh, Pd[167]), while the O'Hare group have focussed on making the first row transition metal series $M_2Pn^*{}_2$ (M = V, Cr, Mn, Co, Ni) (Figure 1.14).[168]

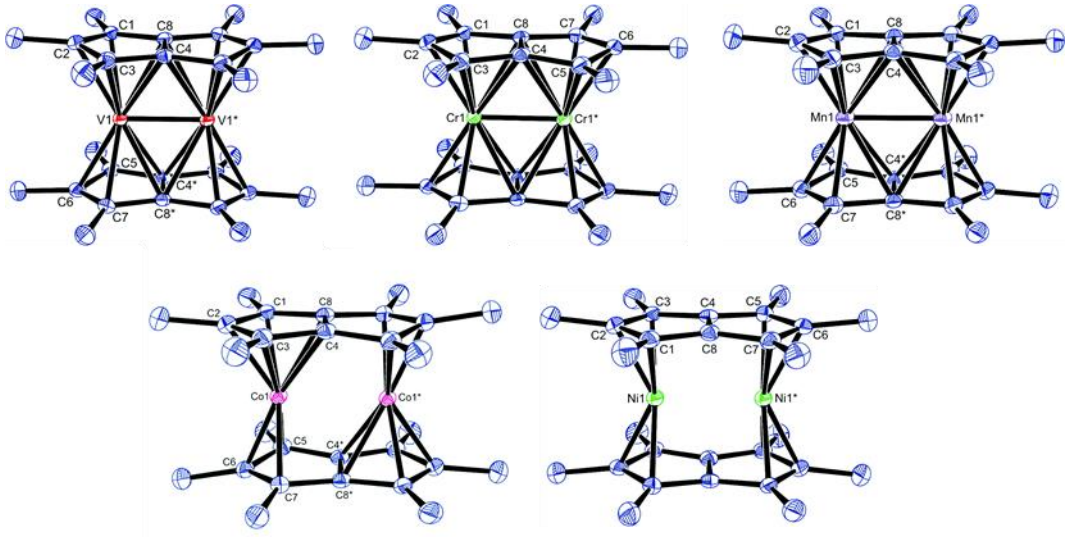

Figure 1.14 Crystal structures of the series $M_2Pn^*{}_2$ (M = V, Cr, Mn, Co, Ni).

These series of compounds have been of interest for the comparison of computational methods to predict bonding interactions accurately. For example the diamagnetic molecule $Mo_2Pn^{(1,4\text{-}Si^iPr_3)}{}_2$ has a bond length intermediate between double and quadruple bond, yet is best described as having a bond order of 2.[169] An "eighteen electron rule" style treatment of each metal atom in $V_2Pn^*{}_2$, would predict a quintuple bond. Despite the V—V bond length of 2.1689(5) Å being the shortest recorded for a pure organovanadium species at the time of publishing, DFT calculations showed the electrons associated with the bridgehead double bonds can be considered to act as 3c2e donors, like bridging hydrides,[159] resulting in a metal-metal interaction better described as a triple bond bridged by two 3c2e donors.[168]

Kilpatrick *et al.* recently published the first example of the unusual dititanium derivative, $Ti_2Pn^{(1,4\text{-}Si^iPr_3)}{}_2$,[170] containing a highly unusual, Ti(II)-Ti(II) doubly-bonded

core, as well as its reactions with CO_2 and CO: the first examples of small molecule activation by compounds with this structure.[171]

The ligands in $Mn_2Pn^{(1,4\text{-}Si^iPr_3)_2}$ display an extreme asymmetric form of coordination: one manganese is low spin and bound η^5,η^5-, while the other is high spin and coordinated η^1,η^1- to silylated ring positions (Figure 1.15 a). Applying different computational methods to analysis of the model system Mn_2Pn_2 result in predictions of a C_{2v} structure, or the C_2 asymmetry found experimentally for the silylated derivative (Figure 1.15 a).[161,166] On the other hand, for the dodecamethylated $Mn_2Pn^*_2$, X-ray analysis reveals a D_{2h} structure with both manganese atoms coordinated symmetrically. Theoretical studies predicting novel properties for pentalene complexes abound. These examples demonstrate the importance of expanding the small library of physical compounds, to be able to verify whether these many predictions are valid.

The chain structure adopted by $K_2Pn^{(1,4\text{-}Si^iPr_3)_2}$ in the solid state can also be considered a subset of this category. The ligands in the doubly anionic $[K_2Pn^{(1,4\text{-}Si^iPr_3)_2}]^{2-}$ units each bend away from the sandwiched metals, buckling out of their planar geometry to coordinate a potassium cation in an η^8- mode on the other side (Figure 1.15 b).[126]

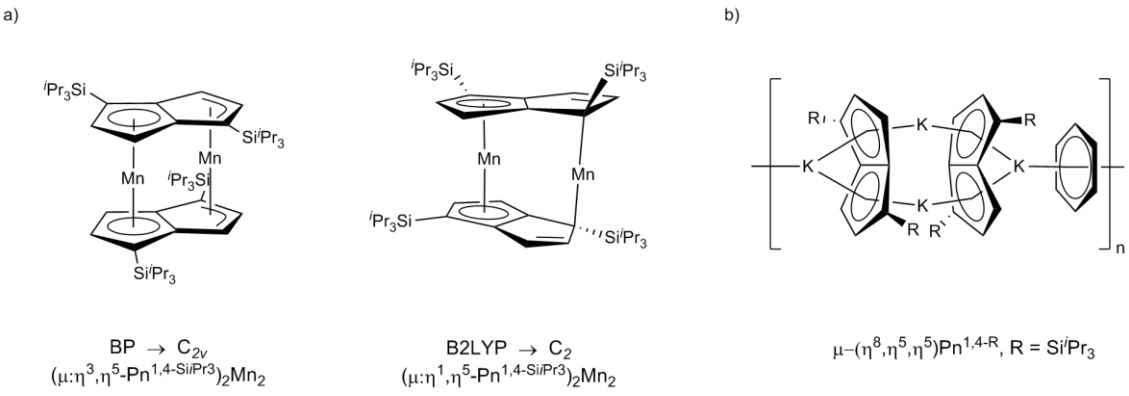

Figure 1.15 a) Structures for $Mn_2Pn^{(1,4\text{-}Si^iPr_3)_2}$ using different DFT functional levels – the C_2 structure has been crystallographically characterised, b) the chain structure of the benzene solvate of $K_2Pn^{(1,4\text{-}Si^iPr_3)_2}$ identified in the solid state.

1.7.3 Transition metal fused metallocenes, $(MCp)_2Pn$

Two metal fragments can coordinate to the two five-membered rings of pentalene in either a *syn*- or an *anti*- arrangement relative to the plane. When the metals are in the 2+ oxidation state and bonded to a cyclopentadiene ring, the resulting bimetallic complexes are the fused analogues of biferrocenes (Figure 1.16).

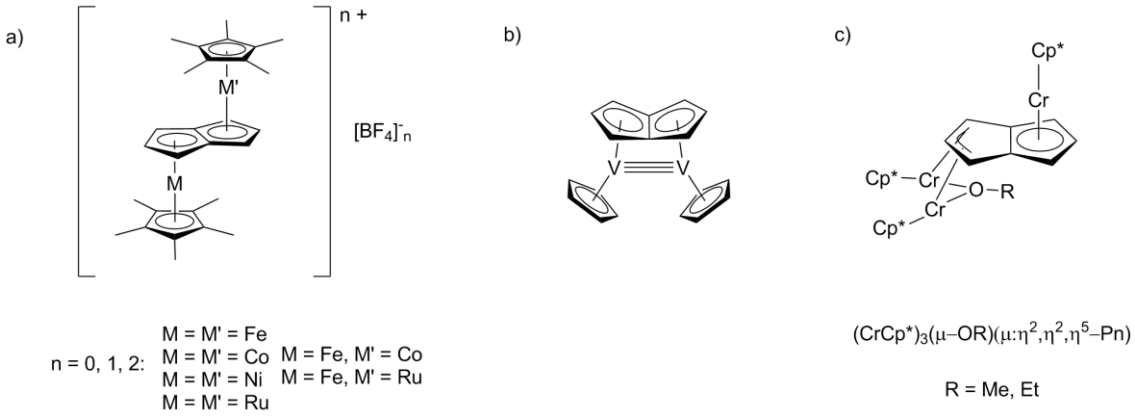

Figure 1.16 Homo and hetero-multimetallic complexes of pentalene: a) *anti*-(MCp)Pn(M'Cp), b) *syn*-$(MCp)_2$Pn, and c) trimetallic chromium complex with the η^2 coordination mode.

Homo and heterobimetallic complexes and salts of groups VIII-X have been made by the group of Manrìquez (Figure 1.16 a).[172,173] These demonstrate extensive delocalisation of electrons through the bridging ligand over both metals, with isolable complexes in two accessible two oxidation states reported. With the exception of the mixed FeRu monocation, magnetic behaviour in molecules that contain unpaired electrons is described by the Curie-Weiss law, with weak antiferromagnetic intermolecular ordering. The FeRu cation displays weakly ferromagnetic intermolecular interactions.

The only example of the unusual *cis*-fused geometry with Cp capping ligands is the triply bonded divanadium complex $(VCp)_2(\eta^5,\eta^5\text{-Pn})$, (Figure 1.16 b).[174] The pentalene ligand only slightly bends away from the vanadium atoms, such that they are 0.1 Å further apart than in the diamagnetic COT complex *syn*-$(VCp)_2(\eta^5,\eta^5\text{-COT})$. This results in a weaker antiferromagnetic interaction between the two unpaired electrons in

the pentalene complex, with a smaller HOMO-LUMO separation giving rise to weak paramagnetism, and a weaker M—M triple bond.

Interestingly, in attempts to make the *syn*- and *anti*- chromium complexes, $(MCp)_2COT$, when NaCp is replaced with LiCp* neither bimetallic is observed resulting only in the monometallic (η^8-COT)CrCp*.[175] This is mirrored in pentalene chemistry, whereby the reaction of $(CrCp^*Cl)_2$ with $Li_2Pn{\cdot}DME_2$ gave the trimetallic complex shown in Figure 1.16 c, which features the only case of η^2-coordination to pentalene ligands.

1.7.4 Lanthanide fused metallocenes, $(LnCp)_2Pn$

Bimetallic complexes similar to those of Manrìquez are seen for the lanthanide complexes $(LnCp^*THF)_2Pn^{(1,4\text{-}Si^iPr_3)}$ (Ln = Eu, Yb, Sm), and for which an *anti*-conformation of coordinated metal fragments is confirmed by crystal structural analysis.[176,177] The 'sandwich' structure is disrupted by incorporation of solvent to the coordination sphere of the large, 5d M^{2+} ions. Of particular interest is the comparison made with the isoelectronic COT counterparts, because unlike for vanadium and chromium *vide supra*, the planar bridging COT ligand coordinates to both lanthanide ions with an *anti*-η^8,η^8- hapticity (Figure 1.17 a).[176]

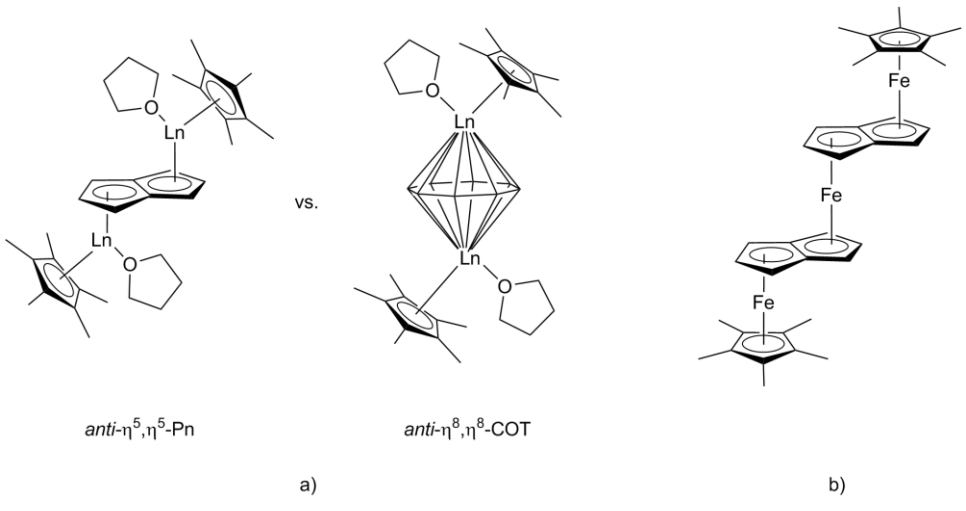

Figure 1.17 a) *anti*-$(LnCp^*)_2$ complexes of $Pn^{(1,4\text{-}Si^iPr_3)}$ and $COT^{(1,4\text{-}Si^iPr_3)}$ (Ln = Eu, Yb, Sm), Si^iPr_3 groups have been omitted for brevity, b) Manrìquez quadruple-decker triiron complex of pentalene.

1.7.5 Hydropentalenyl and multimetallic chain structures

The hydropentalene ligand contains one aromatic five-carbon ring, and one ring containing a localised double bond, and an sp^3-hybridised, protonated ring carbon, and behaves more like a substituted cyclopentadiene or an indenyl than the pentalenes we have considered thus far. Indeed, the first hydropentalenyl complex made was $Fe(PnH)_2$, by reaction of 1,2-dihydropentalene with 1.1 equivalents of ^{n}BuLi followed by reaction with $FeCl_2$.[178] Hydropentalenyl iron and ruthenium pentamethylcyclopentadienyl were similarly made by reaction with Cp*Fe(acac)[173] or $(Cp^*RuCl)_4$ respectively.[179]

These three complexes can all be deprotonated by ^{n}BuLi, and reacted onwards with Cp*Fe(acac), Cp*Co(acac) or $[(COD)RhCl]_2$, to furnish the *trans*-heterobimetallic complexes Cp*Fe(μ-Pn)ML where ML = CoCp*,[173] RuCp*,[173] or FeCp*,[173] and Cp*Ru(μ-Pn)Rh(COD),[180] as well as the trimetallic, quadruple decker complex Cp*Fe(μ-Pn)Fe(μ-Pn)FeCp* (Figure 1.17 b).[181]

1.7.6 Zwitterionic pentalene complexes

The elusive zwitterionic complexes, Cp*MPn (where M = Co, Cr, Rh), first described by Jonas and coworkers, have not been disclosed in peer reviewed journals, yet from the reports in which they are mentioned, their reactivity was clearly studied extensively.[182,183] In this unusual coordination mode, one ring of pentalene coordinates to a Cp*M(III) fragment, and the remaining ring is uncoordinated, but carries a negative charge (Figure 1.18 a). The anionic ring of the zwitterion can be doubly alkylated by successive reaction with alkyl iodides then KH, and the cobalt can be encouraged to migrate to the substituted ring allowing dialkylation of the other ring in overall high yield. Two reduction events accomplished by alkali metals in THF reduce the cobalt to an alkali metal complexed Co(I) zwitteranion. Abstraction of the Cp*Co(I) can be accomplished through reaction of the zwitterion with 1,5-COD, leaving the alkali metal salt of a 1,3,4,6-tetrasubstitutedpentalene.

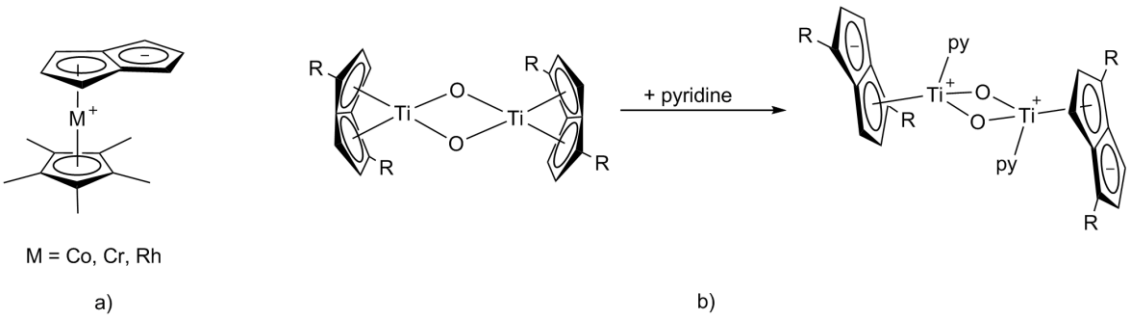

Figure 1.18 Zwitterionic pentalene complexes: a) Cp*MPn, and b) oxo-bridged double zwitterion of Kilpatrick *et al*.

This coordination mode is also seen for group IV metals. Kilpatrick *et al.* have demonstrated that addition of pyridine to the doubly oxo-bridged $(\eta^8\text{-Pn}^{(1,4\text{-Si}^i\text{Pr}_3)}\text{TiO})_2$ results in the doubly zwitterionic species shown in Figure 1.18 b.[171] The η^8 bound compound $ZrPn_2$ undergoes a similar opening, with methylation at the metal by methyl lithium resulting in two anionic, allylic pentalenes with two Li^+ countercations.[182] It is noteworthy that this particular example displays stability with respect to formation of a C—C single bond between the two allyl fragments, which fuels the discussion of whether the ring-localised negative charge should be considered allylic or C_5 aromatic.

1.8 Other pentalene coordination compounds

1.8.1 Multimetallic 'half-sandwich' fused complexes

'Half sandwich' complexes like that shown in Figure 1.18 b, in which each metal atom coordinates to one five-membered Pn ring and to ligands other than Cp are also known.

In bis(allylnickel)pentalene, an *anti*- coordination of two allylnickel fragments to an η^5,η^5 bridging pentalene forms a diamagnetic complex.[184] The authors report similar tetraallyldichromium and hexaallyldizirconium analogues, but fail to include any evidence for their formation save for saying elemental analysis results were correct.[185]

As well as the bi- and multimetallic carbonyls of Fe, Ru, Rh, and Co referenced in section 1.6.2.3, pentalene complexes with carbonyls of group VII Mn and Re have been

made by reaction of $Li_2Pn{\cdot}2DME$ with two equivalents of $Mn(CO)_2(py)Br$ and $[Re(CO)_3(THF)Br]_2$, respectively.[186] $Mn^I(CO)_3$ fragments coordinate η^5,η^5- to the bridging pentalene in an exclusively *anti*- manner, while the Re analogue can be formed in both the *syn*- and *anti*- configurations. Additionally, the dinulear group IX tetracarbonyls *syn*-$[M(CO)_2]_2Pn$ (M = Rh, Ir), can be made by reaction of the dimeric $[MCl(CO)_2]_2$ with the soft, stannyl source of permethylpentalene, *cis*-$(SnMe_3)_2Pn^*$.[187] A serendipitous isolation of crystals of the *anti*- rhodium isomer when pentane was used instead of THF could not be repeated, even when the *anti*-bisstannyl source of Pn* was employed.

1.8.2 Folded η^8 metallocenes

The final coordination mode common to pentalene complexes occurs when all eight carbon atoms coordinate to a single metal atom. Folding of the ligand, with the bridgehead bond acting as a hinge, allows stronger overlap of ligand *p*π orbitals with the metal d orbitals, which outweighs the unfavourable loss of aromaticity that comes from disrupting the planarity of the ligand. This mode of bonding is rare, with most examples coming from complexes of the group IV transition metals Ti, Zr, and Hf.[188–193] Very recently, Chadwick *et al.* reported the first examples of ethylene polymerisation catalysed by group IV complexes containing η^8 pentalenes. Their initial results found zirconium complexes exhibited very high activities (as defined according to the Gibson scale[194]). The η^8 coordination mode is also known for scandium,[177] for vanadium[195] and tantalum from group V,[196,197] the lanthanides cerium[198,199] Sm,[200] Tb, Dy, Ho, and Yb,[177] and for the actinides thorium and uranium.[201–204] The tantalum complex $(\eta^8\text{-}Pn^{(1,5\text{-}SiMe_3)})TaCl_3$, was serendipitously discovered in a transannular dehydrogenation reaction similar to those discussed in section 1.6.2.3, by protonolysis of $(COT^{(1,4\text{-}SiMe_3)})TaMe_3$ with 3 equivalents of $[NH^iPr_2Et]Cl$, followed by sublimation. The cerium complexes are particularly interesting in displaying somewhat ambiguous

oxidation states, and hence have been investigated by a number of theoretical studies similar to those applied to cerocenes.[205,206]

1.9 Aims of this thesis

The relative dearth of organometallic pentalene chemistry has made huge leaps forward since the late 1990s. This has coincided and indeed been caused by the development of sources of the ligand that can be made on a large scale, and have longevity, in particular the disilylated ligand 1,4-bis(triisopropylsilyl)pentalene, and hexamethylpentalene (Pn*). Employment of these two ligands has more than doubled the number of organometallic complexes of pentalene that exist.

This thesis aims to extend the reach of the permethylpentalene synthesis, to incorporate other alkyl groups and produce a range of substituted pentalene precursors. It also aims to investigate the synthesis, characterisation, and reactions of multimetallic complexes of the permethylpentalene ligand, producing a series of compounds that can be compared to permethylmetallocene and linked metallocene counterparts.

1.10 References

(1) Winkler, J. R.; Gray, H. B. *J. Am. Chem. Soc.* **2014**, *136*, 2930.
(2) McInnis, J. P.; Delferro, M.; Marks, T. J. *Acc. Chem. Res.* **2014**, *47*, 2545.
(3) Bratko, I.; Gómez, M. *Dalton Trans.* **2013**, *42*, 10664.
(4) Liu, S.; Motta, A.; Mouat, A. R.; Delferro, M.; Marks, T. J. *J. Am. Chem. Soc.* **2014**, *136*, 10460.
(5) Aguirre-Etcheverry, P.; O'Hare, D. *Chem. Rev.* **2010**, *110*, 4839.
(6) Kealy, T. J.; Pauson, P. L. *Nature* **1951**, *168*, 1039.
(7) Miller, S. A.; Tebboth, J. A.; Tremaine, J. F. *J. Chem. Soc.* **1952**, 632.
(8) Wilkinson, G.; Rosenblum, M.; Whiting, M. C.; Woodward, R. B. *J. Am. Chem. Soc.* **1952**, *74*, 2125.
(9) Pfab, W.; Fischer, E. O. *Zeitschrift für Anorg. und Allg. Chemie* **1953**, *274*, 316.
(10) Huheey, J. E.; Keiter, E. A.; Keiter, R. L. *Inorganic chemistry: principles of structure and reactivity*; 5th ed.; Addison Wesley, 2005; p. 1993.
(11) Werner, H. *Angew. Chem., Int. Ed.* **2012**, *51*, 6052.
(12) Heinze, K.; Lang, H. *Organometallics* **2013**, *32*, 5623.
(13) Romero, T.; Orenes, R. A.; Tárraga, A.; Molina, P. *Organometallics* **2013**, *32*, 5740.
(14) Kelly, M. J.; Tirfoin, R.; Gilbert, J.; Aldridge, S. *J. Organomet. Chem.* **2014**, *769*, 11.
(15) Braga, S. S.; Silva, A. M. S. *Organometallics* **2013**, *32*, 5626.

(16) Goitia, H.; Nieto, Y.; Villacampa, M. D.; Kasper, C.; Laguna, A.; Gimeno, M. C. *Organometallics* **2013**, *32*, 6069.
(17) Suenkel, K. *J. Am. Chem. Soc.* **2014**, *137*, 126.
(18) Yamashita, M.; Ishii, T.; Matsuzaka, H. *Coord. Chem. Rev.* **2000**, *198*, 347.
(19) Baljak, S.; Russell, A. D.; Binding, S. C.; Haddow, M. F.; O'Hare, D.; Manners, I. *J. Am. Chem. Soc.* **2014**, *136*, 5864.
(20) Connelly, N. G.; Geiger, W. E. *Chem. Rev.* **1996**, *96*, 877.
(21) Villena, C.; Losada, J.; García-Armada, P.; Casado, C. M.; Alonso, B. *Organometallics* **2012**, *31*, 3284.
(22) Ornelas, C.; Ruiz, J.; Belin, C.; Astruc, D. *J. Am. Chem. Soc.* **2009**, *131*, 590.
(23) Caballero, A.; García, R.; Espinosa, A.; Tárraga, A.; Molina, P. *J. Org. Chem.* **2007**, *72*, 1161.
(24) Caballero, A.; Tárraga, A.; Velasco, M. D.; Espinosa, A.; Molina, P. *Org. Lett.* **2005**, *7*, 3171.
(25) Dong, T.-Y.; Chang, C.-K.; Cheng, C.-H.; Lin, K.-J. *Organometallics* **1999**, *18*, 1911.
(26) Donoli, A.; Bisello, A.; Cardena, R.; Prinzivalli, C.; Santi, S. *Organometallics* **2013**, *32*, 1029.
(27) Akita, M. *Organometallics* **2011**, *30*, 43.
(28) Zhang, R.; Wang, Z.; Wu, Y.; Fu, H.; Yao, J. *Org. Lett.* **2008**, *10*, 3065.
(29) Jiao, J.; Long, G. J.; Rebbouh, L.; Grandjean, F.; Beatty, A. M.; Fehlner, T. P. *J. Am. Chem. Soc.* **2005**, *127*, 17819.
(30) Wenger, O. S. *Chem. Soc. Rev.* **2012**, *41*, 3772.
(31) Astruc, D.; Ornelas, C.; Ruiz Aranzaes, J. *J. Inorg. Organomet. Polym. Mater.* **2007**, *18*, 4.
(32) Santi, S.; Orian, L.; Donoli, A.; Bisello, A.; Scapinello, M.; Benetollo, F.; Ganis, P.; Ceccon, A. *Angew. Chem., Int. Ed.* **2008**, *47*, 5331.
(33) Wagner, M. *Angew. Chem., Int. Ed.* **2006**, *45*, 5916.
(34) Long, N. J. *Angew. Chem., Int. Ed.* **1995**, *34*, 21.
(35) Debroy, P.; Roy, S. *Coord. Chem. Rev.* **2007**, *251*, 203.
(36) Barlow, S.; Marder, S. R. *Chem. Commun.* **2000**, 1555.
(37) Breuer, R.; Schmittel, M. *Organometallics* **2012**, *31*, 1870.
(38) Goldberg, S. I.; Mayo, D. W. *Chem. Ind.* **1959**, 671.
(39) Hata, K.; Motoyama, I.; Watanabe, H. *Bull. Chem. Soc. Jpn.* **1964**, *37*, 1719.
(40) Watanabe, H.; Motoyama, I.; Hata, K. *Bull. Chem. Soc. Jpn.* **1966**, *39*, 790.
(41) Rausch, M. D. *J. Am. Chem. Soc.* **1960**, *82*, 2080.
(42) Rausch, M. D.; Roling, P. V.; Siegel, A. *J. Chem. Soc. D Chem. Commun.* **1970**, 502.
(43) Hedberg, F. L.; Rosenberg, H. *J. Am. Chem. Soc.* **1969**, *91*, 1258.
(44) Rausch, M. D.; Kovar, R. F.; Kraihanzel, C. S. *J. Am. Chem. Soc.* **1969**, *91*, 1259.
(45) Barlow, S.; O'Hare, D. *Chem. Rev.* **1997**, *97*, 637.
(46) Hudson, R. D. . *J. Organomet. Chem.* **2001**, *637-639*, 47.
(47) Davison, A.; Smart, J. C. *J. Organomet. Chem.* **1973**, *49*, C43.
(48) McManis, G. E.; Nielson, R. M.; Weaver, M. J. *Inorg. Chem.* **1988**, *27*, 1827.
(49) Sharp, P. R.; Raymond, K. N.; Smart, J. C.; McKinney, R. J. *J. Am. Chem. Soc.* **1981**, *103*, 753.
(50) Smart, J. C.; Pinsky, B. L. *J. Am. Chem. Soc.* **1977**, *99*, 956.
(51) Neuse, E. W.; Loonat, M. S. *Transit. Met. Chem.* **1981**, *6*, 260.
(52) Bednarik, L.; Neuse, E. W. *J. Org. Chem.* **1980**, *45*, 2032.
(53) Watanabe, M.; Motoyama, I.; Shimoi, M.; Iwamoto, T. *Inorg. Chem.* **1994**, *33*, 2518.
(54) Watanabe, M.; Kawata, S.; Sano, H.; Motoyama, I. *J. Organomet. Chem.* **1990**, *399*, 301.
(55) Legzdins, P.; Phillips, E. C.; Trotter, J.; Yee, V. C.; Einstein, F. W. B.; Jones, R. H. . *Organometallics* **1991**, *10*, 986.
(56) Smart, J. C.; Pinsky, B. L. *J. Am. Chem. Soc.* **1980**, *102*, 1009.
(57) Hudeczek, P.; Koehler, F. H. *Organometallics* **1992**, *11*, 1773.

(58) Köhler, F. H.; Doll, K. H.; Prößdorf, W.; Müller, J. *Angew. Chemie* **1982**, *94*, 154.
(59) Köhler, F. H.; Doll, K. H.; Prößdorf, W.; Müller, J. *Angew. Chem., Int. Ed.* **1982**, *21*, 283.
(60) Clauss, K.; Bestian, H. *Justus Liebigs Ann. Chem.* **1962**, *654*, 8.
(61) Watt, G. W.; Baye, L. J.; Drummond, F. O. *J. Am. Chem. Soc.* **1966**, *88*, 1138.
(62) Salzmann, J.-J.; Mosimann, P. *Helv. Chim. Acta* **1967**, *50*, 1831.
(63) Brintzinger, H.; Bercaw, J. E. *J. Am. Chem. Soc.* **1970**, *92*, 6182.
(64) Davison, A.; Wreford, S. S. *J. Am. Chem. Soc.* **1974**, *96*, 3017.
(65) Korshak, V. V.; Sosin, S. L.; Alekseeva, V. P. *Dokl. Akad. Nauk SSSR* **1960**, *132*, 360.
(66) Korshak, V. V.; Sosin, S. L.; Alekseeva, V. P. *Vysok. Soed.* **1961**, *2*, 1332.
(67) Nesmeyanov, A. N.; Korshak, V. V.; Voevodskii, V. V.; Kochetkova, N. S.; Sosin, S. L.; Materikova, R. B.; Bolonikova, T. N.; Chibrikin, V. M.; Bazhin, N. M. *Dokl. Akad. Nauk SSSR* **1961**, *137*, 1370.
(68) Rosenberg, H.; Neuse, E. W. *J. Organomet. Chem.* **1966**, *6*, 76.
(69) Spilners, I. J.; Pellegrini Jr., J. P. In *paper presented at 148th National Meeting, A.C.S., September*; 1964.
(70) Nguyen, P.; Gómez-Elipe, P.; Manners, I. *Chem. Rev.* **1999**, *99*, 1515.
(71) Musgrave, R. A.; Russell, A. D.; Manners, I. *Organometallics* **2013**, *32*, 5654.
(72) Foucher, D. A.; Tang, B. Z.; Manners, I. *J. Am. Chem. Soc.* **1992**, *114*, 6246.
(73) Manners, I. *J. Inorg. Organomet. Polym.* **1993**, *3*, 185.
(74) Finckh, W.; Tang, B. Z.; Foucher, D. A.; Zamble, D. B.; Ziembinski, R.; Lough, A.; Manners, I. *Organometallics* **1993**, *12*, 823.
(75) Manners, I. *Adv. Organomet. Chem.* **1995**, *37*, 131.
(76) Dagani, R. *Chem. Eng. News* **1993**, *71*, 22.
(77) Foucher, D. A.; Honeyman, C. H.; Nelson, J. M.; Tang, B. Z.; Manners, I. *Angew. Chem., Int. Ed.* **1993**, *32*, 1709.
(78) Mayer, U. F. J.; Gilroy, J. B.; O'Hare, D.; Manners, I. *J. Am. Chem. Soc.* **2009**, *131*, 10382.
(79) Nelson, J. M.; Lough, A. J.; Manners, I. *Organometallics* **1994**, *13*, 3703.
(80) Nelson, J. M.; Lough, A. J.; Manners, I. *Angew. Chem., Int. Ed.* **1994**, *33*, 989.
(81) Honeyman, C. H.; Foucher, D. A.; Dahmen, F. Y.; Rulkens, R.; Lough, A. J.; Manners, I. *Organometallics* **1995**, *14*, 5503.
(82) Baumgartner, T.; Jäkle, F.; Rulkens, R.; Zech, G.; Lough, A. J.; Manners, I. *J. Am. Chem. Soc.* **2002**, *124*, 10062.
(83) Jäkle, F.; Rulkens, R.; Zech, G.; Foucher, D. A.; Lough, A. J.; Manners, I. *Chem.—Eur. J.* **1998**, *4*, 2117.
(84) Foucher, D. A.; Edwards, M.; Burrow, R. A.; Lough, A. J.; Manners, I. *Organometallics* **1994**, *13*, 4959.
(85) Foucher, D.; Ziembinski, R.; Petersen, R.; Pudelski, J.; Edwards, M.; Ni, Y.; Massey, J.; Jaeger, C. R.; Vancso, G. J.; Manners, I. *Macromolecules* **1994**, *27*, 3992.
(86) Foucher, D. A.; Manners, I. *Die Makromol. Chemie, Rapid Commun.* **1993**, *14*, 63.
(87) Foucher, D. A.; Ziembinski, R.; Tang, B. Z.; Macdonald, P. M.; Massey, J.; Jaeger, C. R.; Vancso, G. J.; Manners, I. *Macromolecules* **1993**, *26*, 2878.
(88) Rulkens, R.; Gates, D. P.; Balaishis, D.; Pudelski, J. K.; McIntosh, D. F.; Lough, A. J.; Manners, I. *J. Am. Chem. Soc.* **1997**, *119*, 10976.
(89) Pudelski, J. K.; Gates, D. P.; Rulkens, R.; Lough, A. J.; Manners, I. *Angew. Chem., Int. Ed.* **1995**, *34*, 1506.
(90) Braunschweig, H.; Dirk, R.; Müller, M.; Nguyen, P.; Resendes, R.; Gates, D. P.; Manners, I. *Angew. Chem., Int. Ed.* **1997**, *36*, 2338.
(91) Russell, A. D.; Musgrave, R. A.; Stoll, L. K.; Choi, P.; Qiu, H.; Manners, I. *J. Organomet. Chem.* **2014**, *784*, 24.
(92) De Mayo, P.; Bloch, R.; Marty, R. A. *J. Am. Chem. Soc.* **1971**, *93*, 3071.
(93) Hafner, K.; Dönges, R.; Goedecke, E.; Kaiser, R. *Angew. Chem., Int. Ed.* **1973**, *12*, 337.

(94) Bally, T.; Chai, S.; Neuenschwander, M.; Zhu, Z. *J. Am. Chem. Soc.* **1997**, *119*, 1869.
(95) You, S.; Neuenschwander, M. *Chimia (Aarau).* **1996**, *50*, 24.
(96) Armit, J. W.; Robinson, R. *J. Chem. Soc.* **1922**, *121*, 827.
(97) Boehm, M. C.; Schuett, J. *J. Phys. Chem.* **1992**, *96*, 3674.
(98) Koyanagi, T.; Yamaguchi, H. *Bull. Chem. Soc. Jpn.* **1977**, *50*, 521.
(99) Nakajima, T. In *Structure and Transformations of Organic Molecules*; Fortschritte der Chemischen Forschung; Springer-Verlag: Berlin/Heidelberg, 1972; Vol. 32, pp. 1–42.
(100) Binsch, G.; Heilbronner, E.; Murrell, J. N. *Mol. Phys.* **1966**, *11*, 305.
(101) Brand, K. *Berichte der Dtsch. Chem. Gesellschaft* **1912**, *45*, 3071.
(102) Blood, C. T.; Linstead, R. P. *J. Chem. Soc.* **1952**, 2263.
(103) Chuen, C. C.; Fenton, S. W. *J. Org. Chem.* **1958**, *23*, 1538.
(104) Hafner, K.; Schneider, J. *Justus Liebigs Ann. Chem.* **1959**, *624*, 37.
(105) Le Goff, E. *J. Am. Chem. Soc.* **1962**, *84*, 1505.
(106) Saito, M. *Symmetry (Basel).* **2010**, *2*, 950.
(107) Hopf, H. *Angew. Chem., Int. Ed.* **2013**, *52*, 12224.
(108) Kuwabara, T.; Ishimura, K.; Sasamori, T.; Tokitoh, N.; Saito, M. *Chem.—Eur. J.* **2014**, *20*, 7571.
(109) Le Goff, E. *J. Am. Chem. Soc.* **1962**, *84*, 3975.
(110) Hafner, K.; Süss, H. U. *Angew. Chem., Int. Ed.* **1973**, *12*, 575.
(111) Kitschke, B.; Lindner, H. J. *Tetrahedron Lett.* **1977**, *18*, 2511.
(112) Kaiser, R.; Hafner, K. *Angew. Chem., Int. Ed.* **1973**, *12*, 335.
(113) Hafner, K.; Bangert, K. F.; Orfanos, V. *Angew. Chem., Int. Ed.* **1967**, *6*, 451.
(114) Hartke, K.; Matusch, R. *Angew. Chem., Int. Ed.* **1972**, *11*, 50.
(115) Criegee, R.; Schröder, G. *Angew. Chemie* **1959**, *71*, 70.
(116) Hübel, W.; Braye, E. H. *J. Inorg. Nucl. Chem.* **1959**, *10*, 250.
(117) Hübel, W.; Braye, E. H.; Clauss, A.; Weiss, E.; Krüerke, U.; Brown, D. A.; King, G. S. D.; Hoogzand, C. *J. Inorg. Nucl. Chem.* **1959**, *9*, 204.
(118) Freedman, H. H. *J. Am. Chem. Soc.* **1961**, *83*, 2194.
(119) Katz, T. J. *J. Am. Chem. Soc.* **1960**, *82*, 3784.
(120) Katz, T. J.; Rosenberger, M. *J. Am. Chem. Soc.* **1962**, *84*, 865.
(121) Katz, T. J.; Rosenberger, M.; O'Hara, R. K. *J. Am. Chem. Soc.* **1964**, *86*, 249.
(122) Stezowski, J. J.; Hoier, H.; Wilhelm, D.; Clark, T.; Schleyer, P. von R. *J. Chem. Soc. Chem. Commun.* **1985**, 1263.
(123) Jones, M.; Schwab, L. O. *J. Am. Chem. Soc.* **1968**, *90*, 6549.
(124) Meier, H.; Pauli, A.; Kolshorn, H.; Kochhan, P. *Chem. Ber.* **1987**, *120*, 1607.
(125) Wilhelm, D.; Courtneidge, J. L.; Clark, T.; Davies, A. G. *J. Chem. Soc. Chem. Commun.* **1984**, 810.
(126) Cloke, F. G. N.; Kuchta, M. C.; Harker, R. M.; Hitchcock, P. B.; Parry, J. S. *Organometallics* **2000**, *19*, 5795.
(127) Griesbeck, A. G. *Synthesis (Stuttg).* **1990**, *1990*, 144.
(128) Katz, T. J.; Mrowca, J. J. *J. Am. Chem. Soc.* **1967**, *89*, 1105.
(129) Fritz, H. P.; Köhler, F. H. *J. Organomet. Chem.* **1971**, *30*, 177.
(130) Janiak, C. *Coord. Chem. Rev.* **1997**, *163*, 107.
(131) Ustynyuk, Y. A.; Shestakova, A. K.; Chertkov, V. A.; Zemlyansky, N. N.; Borisova, I. V.; Gusev, A. I.; Tchuklanova, E. B.; Chernyshev, E. A. *J. Organomet. Chem.* **1987**, *335*, 43.
(132) Gajewski, J. J.; Cavender, C. J. *Tetrahedron Lett.* **1971**, *12*, 1057.
(133) Kaiser, R.; Hafner, K. *Angew. Chem., Int. Ed.* **1970**, *9*, 892.
(134) Baird, M. S.; Reese, C. B. *Tetrahedron Lett.* **1976**, *17*, 2895.
(135) Fleischhauer, I.; Brinker, U. H. *Chem. Ber.* **1987**, *120*, 501.
(136) Burger, U.; Bianco, B. *Helv. Chim. Acta* **1983**, *66*, 60.
(137) Jones, S. C.; Roussel, P.; Hascall, T.; O'Hare, D. *Organometallics* **2006**, *25*, 221.
(138) Emerson, G. F.; Watts, L.; Pettit, R. *J. Am. Chem. Soc.* **1965**, *87*, 131.

(139) Emerson, G. F.; Ehrlich, K.; Giering, W. P.; Lauterbur, P. C. *J. Am. Chem. Soc.* **1966**, *88*, 3172.
(140) Rodeheaver, G. T.; Farrant, G. C.; Hunt, D. F. *J. Organomet. Chem.* **1971**, *30*, C22.
(141) Ehntholt, D. J.; Kerber, R. C. *J. Chem. Soc. D Chem. Commun.* **1970**, 1451.
(142) Landesberg, J. M.; Sieczkowski, J. *J. Am. Chem. Soc.* **1968**, *90*, 1655.
(143) F. Hunt, D.; W. Russell, J. *J. Organomet. Chem.* **1972**, *46*, C22.
(144) Hunt, D. F.; Russell, J. W. *J. Am. Chem. Soc.* **1972**, *94*, 7198.
(145) Hunt, D. F.; Russell, J. W. *J. Organomet. Chem.* **1976**, *104*, 373.
(146) Weidemüller, W.; Hafner, K. *Angew. Chem., Int. Ed.* **1973**, *12*, 925.
(147) Knox, S. A. R.; Stone, F. G. A. *Acc. Chem. Res.* **1974**, *7*, 321.
(148) Knox, S. A. R.; McKinney, R. J.; Riera, V.; Stone, F. G. A.; Szary, A. C. *J. Chem. Soc. Dalton Trans.* **1979**, 1801.
(149) Brookes, A.; Howard, J.; Knox, S. A. R.; Stone, F. G. A.; Woodward, P. *J. Chem. Soc. Chem. Commun.* **1973**, 587.
(150) Howard, J. A. K.; Knox, S. A. R.; Riera, V.; Stone, F. G. A.; Woodward, P. *J. Chem. Soc. Chem. Commun.* **1974**, 452.
(151) Howard, J. A. K.; Knox, S. A. R.; Stone, F. G. A.; Szary, A. C.; Woodward, P. *J. Chem. Soc. Chem. Commun.* **1974**, 788.
(152) Howard, J. A. K.; Knox, S. A. R.; McKinney, R. J.; Stansfield, R. F. D.; Stone, F. G. A.; Woodward, P. *J. Chem. Soc. Chem. Commun.* **1976**, 557.
(153) Howard, J. A. K.; Stansfield, R. F. D.; Woodward, P. *J. Chem. Soc. Dalton Trans.* **1979**, 1812.
(154) Ashley, A. E.; Balázs, G.; Cowley, A. R.; Green, J. C.; O'Hare, D. *Organometallics* **2007**, *26*, 5517.
(155) Komatsu, H.; Suzuki, Y.; Yamazaki, H. *Chem. Lett.* **2001**, 998.
(156) Ashley, A. E. Permethylpentalene chemistry, DPhil Thesis, University of Oxford, 2006, pp. 200–204.
(157) Bruce King, R. *Coord. Chem. Rev.* **1976**, *20*, 155.
(158) Ashley, A. E.; Cowley, A. R.; O'Hare, D. *Chem. Commun.* **2007**, 1512.
(159) Green, J. C.; Green, M. L. H.; Parkin, G. *Chem. Commun.* **2012**, *48*, 11481.
(160) Green, M. L. H. *J. Organomet. Chem.* **1995**, *500*, 127.
(161) Bendjaballah, S.; Kahlal, S.; Costuas, K.; Bévillon, E.; Saillard, J.-Y. *Chem.—Eur. J.* **2006**, *12*, 2048.
(162) Katz, T. J.; Acton, N. *J. Am. Chem. Soc.* **1972**, *94*, 3281.
(163) Katz, T. J.; Acton, N.; McGinnis, J. *J. Am. Chem. Soc.* **1972**, *94*, 6205.
(164) Balazs, G.; Cloke, F. G. N.; Gagliardi, L.; Green, J. C.; Harrison, A.; Hitchcock, P. B.; Shahi, A. R. M.; Summerscales, O. T. *Organometallics* **2008**, *27*, 2013.
(165) Kuchta, M. C.; Cloke, F. G. N.; Hitchcock, P. B. *Organometallics* **1998**, *17*, 1934.
(166) Balazs, G.; Cloke, F. G. N.; Harrison, A.; Hitchcock, P. B.; Green, J.; Summerscales, O. T. *Chem. Commun.* **2007**, 873.
(167) Summerscales, O. T.; Rivers, C. J.; Taylor, M. J.; Hitchcock, P. B.; Green, J. C.; Cloke, F. G. N. *Organometallics*, **2012**, *31*, 8613.
(168) Ashley, A. E.; Cooper, R. T.; Wildgoose, G. G.; Green, J. C.; O'Hare, D. *J. Am. Chem. Soc.* **2008**, *130*, 15662.
(169) Cloke, F. G. N.; Green, J. C.; Jardine, C. N.; Kuchta, M. C. *Organometallics* **1999**, *18*, 1087.
(170) Kilpatrick, A. F. R.; Green, J. C.; Cloke, F. G. N.; Tsoureas, N. *Chem. Commun.* **2013**, *49*, 9434.
(171) Kilpatrick, A. F. R.; Cloke, F. G. N. *Chem. Commun.* **2014**, *50*, 2769.
(172) Bunel, E. E.; Valle, L.; Jones, N. L.; Carroll, P. J.; Barra, C.; Gonzalez, M.; Munoz, N.; Visconti, G.; Aizman, A.; Manriquez, J. M. *J. Am. Chem. Soc.* **1988**, *110*, 6596.
(173) Manriquez, J. M.; Ward, M. D.; Reiff, W. M.; Calabrese, J. C.; Jones, N. L.; Carroll, P. J.; Bunel, E. E.; Miller, J. S. *J. Am. Chem. Soc.* **1995**, *117*, 6182.
(174) Jones, S. C.; O'Hare, D. *Chem. Commun.* **2003**, 2208.

(175) Heck, J.; Rist, G. *J. Organomet. Chem.* **1988**, *342*, 45.
(176) Summerscales, O. T.; Jones, S. C.; Cloke, F. G. N.; Hitchcock, P. B. *Organometallics* **2009**, *28*, 5896.
(177) Kilpatrick, A. F. R. Bimetallic Complexes of d- and f-Block Metals with Pentalene Ligands, PhD Thesis, 2014.
(178) Katz, T. J.; Rosenberger, M. *J. Am. Chem. Soc.* **1963**, *85*, 2030.
(179) Burgos, F.; Arancibia, V.; Manriquez, J. M.; Chavez, I. *Bol. Soc. Chil. Quim.* **2000**, *45*, 621.
(180) Burgos, F.; Chávez, I.; Manriquez, J. M.; Valderrama, M.; Lago, E.; Molins, E.; Delpech, F.; Castel, A.; Rivière, P. *Organometallics* **2001**, *20*, 1287.
(181) Oelckers, B.; Chavez, I.; Manriquez, J. M.; Roman, E. *Organometallics* **1993**, *12*, 3396.
(182) Jonas, K. *Max-Planck-Institut für Kohlenforschung Report for the Period of January 2000 - December 2001*; 2002.
(183) Jonas, K.; Hannappel, M.; Nienhaus, U. *Mononuclear and Polynuclear Transition Metal Complexes with Pentalene and Related Polycycles as Ligands, in Max-Planck-Institut für Kohlenforschung Report for the Period of January 2002 - December 2004*; 2005; pp. 65–70.
(184) Kitano, Y.; Kashiwagi, M.; Kinoshita, Y. *Bull. Chem. Soc. Jpn.* **1973**, *46*, 723.
(185) Miyake, A.; Kanai, A. *Angew. Chem., Int. Ed.* **1971**, *10*, 801.
(186) Jones, S. C.; Hascall, T.; Barlow, S.; O'Hare, D. *J. Am. Chem. Soc.* **2002**, *124*, 11610.
(187) Bennett, L. A. Group IX Bimetallic Carbonyl Permethylpentalene Complexes, University of Oxford, 2008, pp. 17–34.
(188) Jonas, K.; Kolb, P.; Kollbach, G.; Gabor, B.; Mynott, R.; Angermund, K.; Heinemann, O.; Krüger, C. *Angew. Chem., Int. Ed.* **1997**, *36*, 1714.
(189) Cooper, R. T.; Chadwick, F. M.; Ashley, A. E.; O'Hare, D. *Organometallics* **2013**, *32*, 130319084431007.
(190) Li, H.; Feng, H.; Sun, W.; Xie, Y.; King, R. B.; Schaefer III, H. F. *New J. Chem.* **2011**, *35*, 1718.
(191) Gleiter, R.; Bethke, S.; Okubo, J.; Jonas, K. *Organometallics* **2001**, *20*, 4274.
(192) Chadwick, F. M.; Cooper, R. T.; Ashley, A. E.; Buffet, J.-C.; O'Hare, D. M. *Organometallics* **2014**, *33*, 3775.
(193) Gabor, B.; Jonas, K.; Mynott, R. *Inorganica Chim. Acta* **1998**, *270*, 555.
(194) Britovsek, G. J. P.; Gibson, V. C.; Wass, D. F. *Angew. Chemie Int. Ed.* **1999**, *38*, 428.
(195) Jonas, K.; Gabor, B.; Mynott, R.; Angermund, K.; Heinemann, O.; Krüger, C. *Angew. Chem., Int. Ed.* **1997**, *36*, 1712.
(196) Abbasali, Q. A.; Cloke, F. G. N.; Hitchcock, P. B.; Joseph, S. C. P. *Chem. Commun.* **1997**, 1541.
(197) Cloke, F. G. N.; Hitchcock, P. B.; Kuchta, M. C.; Morley-Smith, N. A. *Polyhedron* **2004**, *23*, 2625.
(198) Ashley, A.; Balazs, G.; Cowley, A.; Green, J.; Booth, C. H.; O'Hare, D. *Chem. Commun.* **2007**, 1515.
(199) Balazs, G.; Cloke, F. G. N.; Green, J. C.; Harker, R. M.; Harrison, A.; Hitchcock, P. B.; Jardine, C. N.; Walton, R. *Organometallics* **2007**, *26*, 3111.
(200) Summerscales, O. T.; Johnston, D. R.; Cloke, F. G. N.; Hitchcock, P. B. *Organometallics* **2008**, *27*, 5612.
(201) Cloke, F. G. N.; Hitchcock, P. B. *J. Am. Chem. Soc.* **1997**, *119*, 7899.
(202) Cloke, F. G. N.; Green, J. C.; Jardine, C. N. *Organometallics* **1999**, *18*, 1080.
(203) Chadwick, F. M.; Ashley, A.; Wildgoose, G.; Goicoechea, J. M.; Randall, S.; O'Hare, D. *Dalton Trans.* **2010**, *39*, 6789.
(204) Chadwick, F. M.; O'Hare, D. M. *Organometallics* **2014**, *33*, 3768.
(205) Kerridge, A.; Kaltsoyannis, N. *Comptes Rendus Chim.* **2010**, *13*, 853.
(206) Kerridge, A.; Coates, R.; Kaltsoyannis, N. *J. Phys. Chem. A* **2009**, *113*, 2896.

Chapter 2 NOVEL, LOW-SYMMETRY ALKYLPENTALENE PRECURSORS

2.1 Introduction

The parallels between the pentalene ligand and cyclopentadiene make it pertinent to investigate whether substitution of the peripheral positions with groups other than methyl is possible. In organometallic cyclopentadienyl complexes, changes to the substituted groups can have a dramatic effect on the species' properties,[1–3] and on reactivity.[4–6] Inductively electron releasing alkyl groups can stabilise electron deficient metal centres, and destabilise antibonding molecular orbitals of higher energy. For example manganocene changes from high to low spin at elevated temperatures,[7] while decamethylmanganocene exists purely in a low spin state due to a larger HOMO-LUMO gap.[8] In electrochemistry, the ferrocenium cation is a mild chemical oxidant for reactions in organic solvents, and is used as a standard to which most redox agents in organic solvents are compared.[9] Standard electrode potentials of ferrocenes can be systematically altered by substitution of the cyclopentadienyl ring positions, such that the redox couple can be tailored to range from −0.63 V with electron donating substitutents, to 0.64 V with electron withdrawing substituents.[9] In the field of catalysis, changes to the substitution pattern of the cyclopentadienyl ligands in group IV metallocene derivatives has marked changes on the activity and productivity of olefin polymerisation,[5,6] and can be used to introduce stereospecificity to the growing polymer chain.[4] Catalyst design can therefore allow control of the microstructure of a polymer, changing the physical properties of the polymers produced.[10]

As discussed in Chapter 1, alkylation of pentalenes was limited prior to the advent of hexamethylpentalene (Pn*). At most, three positions could be substituted, as demonstrated by Hafner and coworkers.[11,12] The O'Hare route to making highly substituted pentalenes allows for alternative alkyl groups to be introduced to the two 'wing-tip' and four 'non-wing-tip' ring positions. The introduction of multiple alkyl substituents using this route has thus far only been investigated with methylating reagents.[13]

The synthesis of highly substituted pentalene frameworks employs the bicyclic compound 2,4,6,8-tetramethylcarboxylate-bicyclo[3.3.0]octa-3,7-dione, **2.i**, (commonly known as WeissH_4). During step two of the synthesis (Scheme 2.1), electrophilic groups are introduced to the α- position of the four β-keto esters of **2.i**. During step five, an organocerium is prepared *in situ* from an organolithium and cerium trichloride, and this

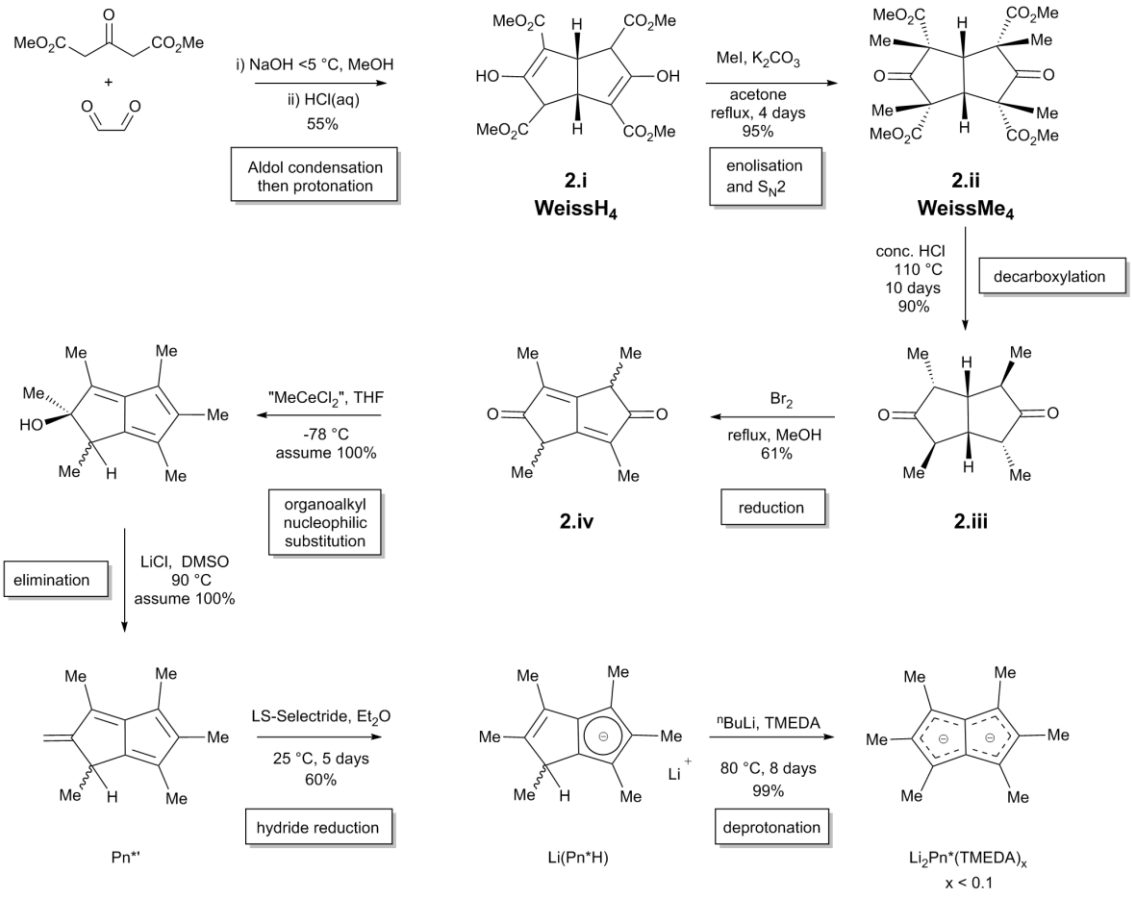

Scheme 2.1 Synthesis of $Li_2Pn^*TMEDA_x$.

is alkylated preferentially at the ketone carbons in the dienedione **2.iv**. The use of the organocerium reagent avoids Michael addition of alkyl groups at the 'bridgehead' carbon positions, which is known for alkyllithium reagents.[14]

2.1.1 Alkylation of WeissH$_4$, **2.i**

In step two of the Pn* synthesis (Scheme 2.1), the four non-wing-tip positions of **2.i** repeatedly undergo deprotonation by potassium carbonate in acetone. The enolates thus formed undergo nucleophilic attack on iodomethane, resulting in methylation of these four positions. For multiple alkylations to be possible, it is important that the deprotonating and alkylating reagents can coexist in the reaction mixture without reacting. The most acidic protons of **2.i** are at the α- positions of the β-ketoester, with a pK_a of around about 7.8.[15]

Optimisation of the reaction conditions determined that nine equivalents of potassium carbonate and iodomethane were initially necessary for each equivalent of **2.i**, with more iodomethane added periodically until complete tetramethylation was achieved. At lower concentrations of base, alkylation was incomplete.[13] The sole product is the tetramethylated 2,4,6,8-tetramethylcarboxylate-2,4,6,8-tetramethyl-bicyclo[3.3.0]octa-3,7-dione, WeissMe$_4$, **2.ii**, which exhibits an NMR spectrum with two very broad, hump-like resonances corresponding to the methylcarboxylate groups and those of the skeletal methyl groups. The breadth of the resonances is attributed to a fluxional structure in solution, which can be resolved upon cooling to 10 °C.

The crystal structure of WeissMe$_4$ reveals alkylation solely on one face of the bicycle.[13] Each successive methylation occurs on the exposed *exo*- face, which nucleophilically attacks MeI, in doing so forcing carboxylate groups to further hinder the *endo*- face. The tertiary bridgehead positions give the molecule a folded geometry, with an *exo*- face on the same side as the bridgehead hydrogen atoms, and an *endo*- face on the opposite side. As can be seen in the crystal structure of WeissMe$_4$, **2.ii**, with all four

ester groups occupying the *endo*- face of the molecule, this results in great strain in the molecule.

2.1.2 Alternative alkylations β-keto esters

Functionalisation of ring positions of WeissH$_4$ has been achieved by other research groups, often with the aim of forming natural and non-natural polyquinene products.[16] Direct alkylation of the disodium salt of WeissH$_4$ with allyl iodide results in mixtures of mono-, di- and tri- alkylated products. The desirable 2,6- and 2,8- double alkylation of the ring can be directed by first forming the bisenol ether using diazomethane, followed by treatment with potassium hydride or potassium tert-butoxide[17] and allyl iodide (Scheme 2.2). The 2,6- and 2,8- diallyl isomers are formed in 49 and 44% yield respectively.[18] Hydrolysis with acid then reforms the 3,7-dione from the enol ethers, and the molecule readily undergoes two decarboxylations. The same reaction and 2,6- and 2,8- selectivity can be achieved using tetrabutylammonium 2-oxopyrrolidin-1-ide to deprotonate, and iodomethane to alkylate.[19] Alternatively, a selective 4,8-decarboxylation of WeissH$_4$, **2.i**, can be achieved by treatment with sodium methoxide in refluxing DMSO.[20] The 2,4- and 4,6- decarboxymethylation products are not observed, and subsequent deprotonation and allylation with KH/allyl iodide[18] or methanolic NaOMe/CH_2CHX (X = CN, CO_2Me)[21]

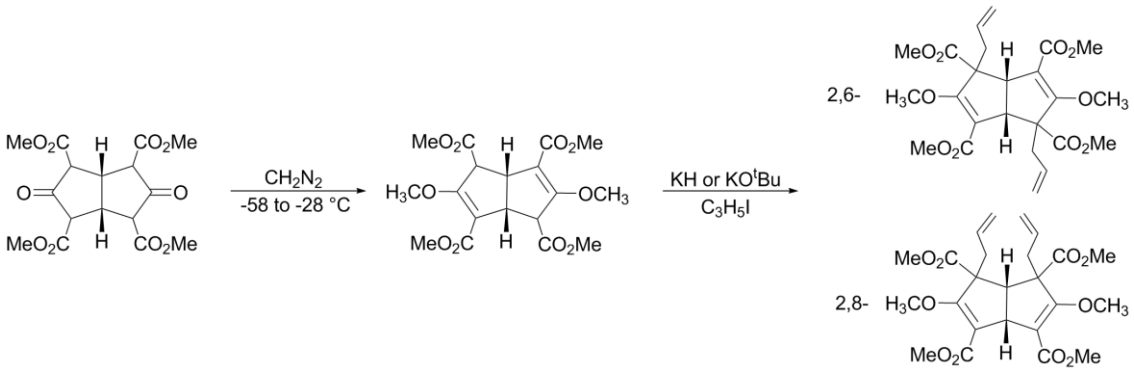

Scheme 2.2 Selective 2,6- and 2,8- diallylation of 2.i *via* the bisenolether

affords exclusively 2,6-dimethylcarboxylate-2,6-disubstituted diones. Treatment of **2.i** with KH and MeI or Me_2SO_4 resulted in multiple products which could not be elucidated.[22]

Dianions of β-keto esters can be formed in a variety of ways,[23] however, selective alkylation typically proceeds in poor yield.[24,25] Alkylation of the γ- position of β-keto esters was first reported in the 1970s by Weiler.[26,27] Double deprotonation at 0 °C, once at the acidic α- position by sodium hydride, and once at the γ- position by one equivalent of ^{n}BuLi, methyl lithium, or two equivalents of lithium diisopropylamide (LDA), gave a dianion that reacted with alkyl halides to form exclusively the γ-substituted product. The use of the metal salt (NaH) to form the initial enolate protects the carbonyl from alkylation by the alkyl lithiums used as bases for the second deprotonation.[27,28] Following alkylation of the γ-position with MeI, EtBr, ^{i}PrI, and ^{n}BuBr however, the resulting mono-anionic sodioenolate (70-99% yield) undergoes no further alkylation with alkylhalides. Conversely, Brieger *et al*. demonstrated that treatment of the same substrate with two equivalents of ^{n}BuLi followed by refluxing resulted exclusively in addition to the ester, and subsequent cleavage of the ester—α-carbon bond to form ketones.[28] The limited reactivity of the sodioenolates makes NaH an unsuitable base for achieving multiple alkylations of **2.i**, and the reaction at and cleavage of the ester rules out the use of ^{n}BuLi as a deprotonating agent.

Optically active sulphonium salts have been employed – in combination with potassium carbonate – to alkylate β-keto esters under enantiomeric control, producing a range of alkylation products from reaction at the α-carbon positions and the β-keto-enolate oxygen.[29] In fact, the generation of chiral all-carbon quaternary centres from ketone enolates is possible using a range of stoichiometric or catalytic reactions.[30–33] With the bicyclic tetraester **2.i** however, such a specific approach is unnecessary as alkylation proceeds under steric control, only on the exposed *exo*-face of the bicyclic

octadione.[22,34] This is of great benefit as we will see later in the chapter, because it limits the range of epimers that can form.

2.2 Synthesis and characterisation of alkylation products

2.2.1 Alkylation of **2.i**

Boiling of an acetone solution containing 2,4,6,8-tetramethylcarboxylate-bicyclo[3.3.0]octa-3,7-dione, **2.i**, with nine equivalents of potassium carbonate (*i.e.* a 125% excess) resulted in a creamy precipitate. Following the addition of 18 equivalents of RI (R = Et, ^{i}Pr) and refluxing for 2 days, the solution turned yellow when R = Et, or very pale yellow when R = ^{i}Pr, and NMR spectra of aliquots revealed mixtures of alkylated isomers (Scheme 2.3). Addition of further alkyl iodide did not result in further reaction; however, if fewer than 18 equivalents were initially employed, additional alkyl iodide did result in further reaction, until the product distribution seen with 18 equivalents of RI was reached. After quenching and extraction of the organic products into pentane, the removal of the solvent resulted in pale yellow oils, which were separated into fractions by column chromatography (2:1 diethyl ether/hexane solutions through silica). Eluents trialled include combinations of ethyl acetate, hexane, diethyl ether, toluene, and ethanol. Increasing the polarity of the mixture caused severe smearing of product spots, while reducing the polarity caused more overlapping of products spots. This is evidenced later where some fractions contained mixtures of

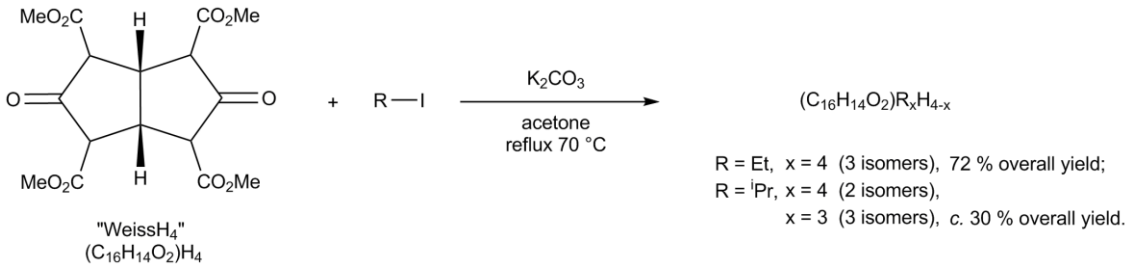

Scheme 2.3 Synthesis of low-symmetry alkyl derivatives of 2,4,6,8-tetraesterbicyclo[3.3.0]octa-3,7-dione.

products that could not be separated.

NB throughout this chapter, all structures with C_s or C_2 symmetry can form enantiomers. Where structures are discussed or drawn showing one enantiomer, they represent a racemic mixture of enantiomers, and are used interchangably. Reaction conditions involve no chiral synthons and are assumed to proceed without enantiomeric enrichment.

2.2.2 Synthesis and characterisation of ethylation products

A mixture of tetraethylated species could be recovered as a yellow oil in 72% overall yield. Thin layer chromatography revealed three major components, with some minor shadows that ran very close to these spots and which could not be separated further. After chromatographic separation, pure samples of **2.1**, **2.2**, and **2.3** (Figure 2.1) were isolated in yields of 8%, 4% and 24% respectively. All three are structural isomers of "WeissEt$_4$" and all mass spectra contain molecular ion peaks at *m/z* 483.2, corresponding to the chemically ionised $[M+H]^+$, and 505.2 corresponding to $[M+Na]^+$. Compounds **2.1**, **2.2**, and **2.3** were each identified and characterised by NMR and IR spectroscopy. Additionally, **2.1** and **2.3** were characterised by single crystal X-ray diffraction. During separation, a large quantity of **2.3** (over 36%) was lost in mixed fractions containing multiple products with retention times too close to be separated.

As noted in the original synthesis, the reaction requires a polar, aprotic solvent.[22]

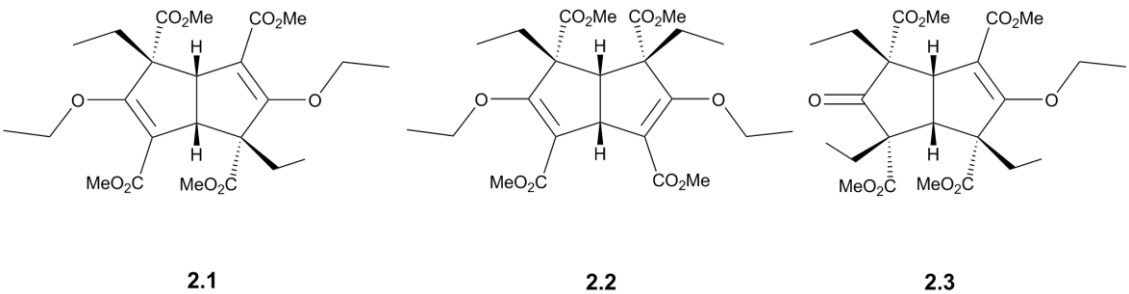

Figure 2.1 Three tetraethylated products.

With that in mind it was decided to used dimethylsulfoxide (DMSO) instead of acetone, to see if this would alter the product distribution. Immediate consumption of starting material resulted in an intensely dark reaction mixture, which following work up yielded a very small amount of an intensely red oil. The complicated NMR spectrum for this contained four carboxylate resonances at 3.59, 3.67, 2.92, and 2.99 ppm, and a single quartet at 4.10 ppm characterisitic of *O*-alkylation. The low chemical shift (δ) of two of the methylcarboxylate groups could suggest a product with C_2 or C_v symmetry containing two alkylations of carboxylate oxygens. No resonances were attributable to ring alkylated positions.

2.2.2.1 NMR Characterisation of **2.1**

The first fraction to elute contained 2,4,6,8-tetramethylcarboxylate-3,7-diethoxy-2,6-*exo*-diethyl-bicyclo[3.3.0]octa-3,7-diene, **2.1**, a tetraethylated isomer of WeissEt$_4$ with C_2 symmetry, in which two ethyl groups have attached at opposite 'corners' of the bicycle, and there are two *O*-alkylations at the ketone positions of the starting material. The rotational axis which runs normal to the centre of the bridgehead double bond results in identical bridgehead protons, one aliphatic ethyl environment, one ethoxy environment, and two ester environments: one attached to a vinylic sp^2-hybridised carbon of the bicyclic skeleton, and one attached to an sp^3-hybridised carbon.

The two methylene protons in the ethoxy group are inequivalent as they cannot be related by a plane of symmetry in the C_2 structure; this results in two doublets of quartets. The geminal protons have a $^2J_{HH}$ coupling of −9.9 Hz to each other and both have a $^3J_{HH}$ of 7.0 Hz to the terminal methyl group. Typical values for gem coupling at acyclic sp^3 positions or in unstrained rings range from −10 to −13 Hz.[35] The similarity of the protons in this AA' system results in a roofing effect, with the two quartets in each

doublet of quartets having unequal intensities. The protons of the aliphatic ethyl groups appear as a triplet and quartet, with a mutual $^{3}J_{HH}$ coupling constant of 7.3 Hz.

The methylene protons in the aliphatic ethyl groups should also be inequivalent. However, on first inspection only one doublet of quartets is apparent at 1.95 ppm. The 7.3 Hz coupling constant of this resonance is consistent with vicinal coupling to methyl protons, however, the 1.1 Hz *J*-value is very small for geminally coupled methylene protons. Close inspection of the HMBC spectrum shows the carbonyl carbon (172.8 ppm) of the nearest ester group couples only to a proton at 1.948 ppm, while the vinylic ring proton at the ethoxylated position (168.3 ppm) couples only to a proton at 1.951 ppm. These cross peaks represent through space coupling interactions. The two methylene protons are indeed inequivalent, but each appears as a quartet at essentially the same chemical shift (separated by 0.003 ppm, or 1.1 Hz), and they show no geminal coupling (the spin-spin transition is symmetry forbidden for species with the same δ).

2.2.2.2 XRD Characterisation of **2.1**

Compound **2.1** crystallises in the $Pna2_1$ space group. The four identical molecules in the unit cell are related to each other through transformations around 2-fold screw axes parallel to the *c*-axis, and through glide planes along the *ac* and *bc* directions. This is not a chiral space group and it contains a racemic mixture of molecules related to each other through the glide planes.

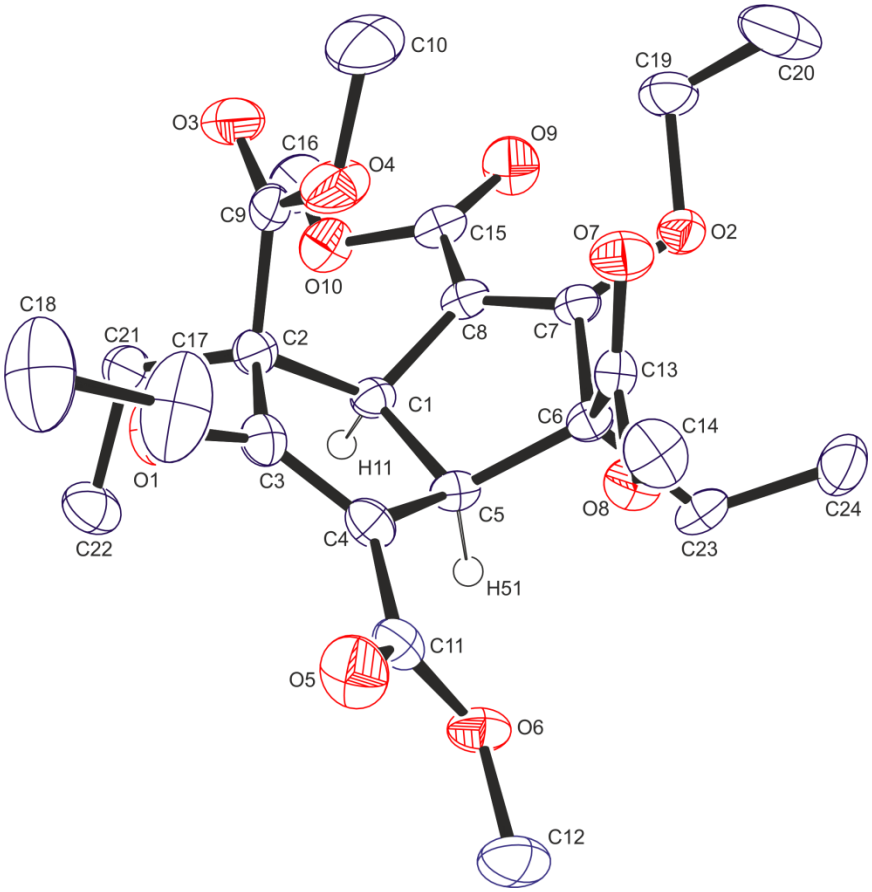

Figure 2.2 Molecular structure of 2.1. Displacement ellipsoids drawn at the 50% probability level. Carbon atoms are shown in blue, oxygen atoms are red, selected hydrogen atoms have been omitted for clarity. Selected bond lengths (in Å): C1—H11 0.993; C5—H51 1.004; C1—C5 1.553(4); C1—C2 1.572(3); C2—C3 1.520(3); C3—C4 1.348(4); C4—C5 1.512(3); C5—C6 1.575(4); C6—C7 1.523(3); C7—C8 1.351(4); C8—C1 1.506(3); C3—O1 1.350(3); C7—O2 1.334(3); C2—C9 1.522(4); C6—C13 1.527(3); C4—C11 1.473(4); C8—C15 1.473(4); C2—C21 1.540(4); C6—C23 1.556(4).

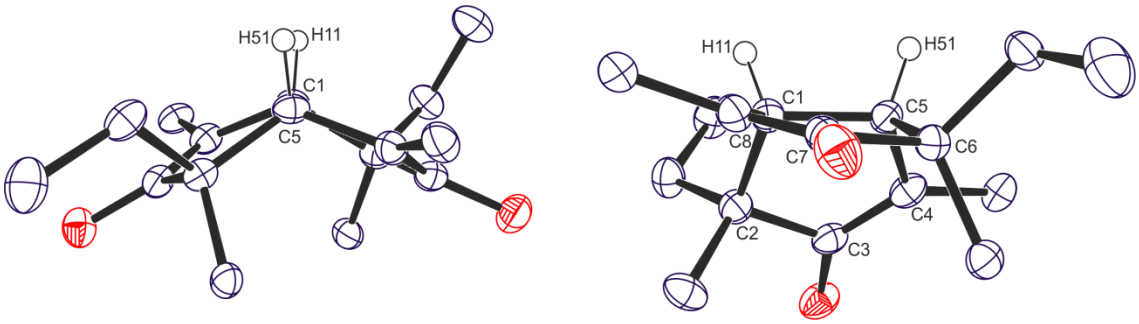

Figure 2.3 Views along the bridgehead bond of 2.1 showing the torsion angle between H11 and H51 (left), and along the O2—C7 bond showing the twisted half-chair conformation of rings (right). Displacement ellipsoids drawn at the 50% probability level.

As deduced from the NMR data, the crystal structure confirms that both ethylations have occurred on the *exo*- face of the bicyclic ring (Figure 2.2). The molecules in the solid state lack the C_2 symmetry observed for this structure in solution. The two sp^3-hybridised ring carbons bear the same substituents in differing conformations: one *exo*- ethyl group points away from the bridgehead while one is angled to point over the five-carbon ring to which it is attached; one *endo*- methyl carboxylate group has a ketone pointing in, towards the concave face, while the other has a methoxy group angled inwards. This contrasts with the structure of **2.i**, where the molecule displays pseudo C_2 symmetry in the solid state.[13] Interestingly, the carbonyls of the two sp^2 ester groups point away from the bridgehead, with dihedral angles of −23.28° and 2.44° for C3-C4-C11-O15 and C7-C8-C15-O9 respectively. This contrasts with molecular mechanical data deduced for the monoanionic charged intermediates (Section 2.3.2), which consistently demonstrates lower energy structures when the carbonyls are oriented parallel to the conjugated enol ether double bond.

Each five-membered ring contains two sp^2-hybridised carbons and three sp^3-hybridised atoms, and adopts a cyclopentene twist conformation (rather than an envelope conformation) as can be seen by the view along the C7—O2 bond shown in Figure 2.3. The bridgehead C—C bond is 1.553(4) Å long and there is a torsional angle (H11-C1-C5-H51) of 10.3° between the *cis*- methine protons. The fold angle, defined as the angle between the lines that join the bridgehead centroid to the two wing-tip carbon atoms is 123.91°. Other than $WeissMe_4$, **2.ii**, literature compounds for comparison either contain four ester groups but no ring substitution, or contain two ring substitutions in the 2- and 6- positions but only two ester groups, also in the 2- and 6- positions. The tetramethylester dienols (**2.vi**, see Section 2.3.1) with the same C_2 symmetry as **2.1** crystallise in a range of polymorphic packing sequences,[36] with bridgehead torsion angles varying between 6.6 and 11.2°. In the tetramethylester dienol methyl ether (**2.vii**, Section 2.3.1) this dihedral angle is larger than in **2.1** at 14.70°, and the molecule is less

folded than **2.1** with a fold angle of 115.1°. Bridgehead C—C bonds in these molecules typically fall in the range 1.545 - 1.570 Å, as is seen here.

The large deviation in carbon-carbon single bond lengths around the edges of the two rings of **2.1**, from 1.503(3) Å to 1.575(4) Å with a mean C—C single bond length of 1.535 Å, gives an indication of the intense strain in the structure. To measure this puckering from planarity, the shortest distance of deviation of the non-wing-tip ring carbons from the plane defined by C1, C5 and C3 is measured. Atom C2 lies 0.147 Å above this plane and C4 lies 0.158 Å below. For the plane defined by C1, C5 and C7, the shortest distance of deviation from the plane by C6 is 0.154 Å and by C8 is 0.170 Å (depicted on the right in Figure 2.3). By comparison, in **2.i** which has a saturated rings each with only one sp^2 carbon, the corresponding deviations from the plane by the four sp^3-hybridised non-wing-tip atoms are 0.317, 0.320, 0.512, and 0.546 Å. The greater twist between the fused rings of **2.i** gives the larger torsion angle of 34.5°, with a bridgehead bond of 1.568(2) Å and a mean carbon-carbon single bond length of 1.548 Å.

2.2.2.3 IR Characterisation of **2.1**

Two carbonyl bands are apparent at 1708 and 1734 cm^{-1}, corresponding to the two ester environments in the C_v structure. Two bands at 1613 and 1622 cm^{-1} are characteristic of the enol-ether C=C stretches. A very strong feature at 1203 cm^{-1} is assigned to the C-O-C stretching band of the vinyl ether, while medium bands at 1231 and 1250 cm^{-1} correspond to the C-O-C stretching bands of the two esters.

2.2.2.4 NMR Characterisation of **2.2**

2,4,6,8-tetramethylcarboxylate-3,7-diethoxy-2,8-*exo*-diethyl-bicyclo[3.3.0]octa-3,6-diene, **2.2**, is the second isomer separated and also results from two *O*-alkylations. This time however, a plane of symmetry runs along the bridgehead bond, resulting in a structure with C_s symmetry (Figure 2.1). Two sets of resonances of equal intensity are seen in ^1H and ^{13}C NMR spectra corresponding to the two ester groups: the methyl

protons appearing as singlets at 3.67 ppm for the sp^2 attached ester, and 3.57 ppm for the sp^3 attached group. The two bridgehead methine protons form an AB system, with one occuring as a doublet at 2.74 ppm, and the other located using COSY at 4.15 ppm, underneath the ethoxyl doublet of quartets. As with **2.1**, the ethoxyl methylene protons are inequivalent in **2.2**. Unlike **2.1**, the magnetic inequivalence of the aliphatic ethylene protons is clear in the 1D ^{1}H NMR spectrum; two doublets of quartets at 1.82 and 1.95 ppm have a geminal coupling of −14.5 Hz, and the same roofing effect of intensites commented on previously for AA' systems and seen for ethoxyl protons in **2.1**.

2.2.2.5 NMR Characterisation of **2.3**

Four large ester singlets in the ^{1}H NMR spectrum at 3.42, 3.57, 3.62, and 3.73 ppm, each with equal intensity indicated a structure with C_1 symmetry. The presence of the now characteristic doublet of quartets splitting pattern for ethoxyl groups, centred at 4.26 ppm, had a total intensity of one third relative to an ester resonance, indicating only one ethoxyl group. With the assumption that alkylation only occurs on the *exo*- face, as no evidence to the contrary has been found, only one tetraethylated structural isomer fits this description, with three ethyl ring substituents, one ketone, one double bond, and one ethoxide. The 2D and ^{13}C NMR spectra are consistent with this assignment, with the bridgehead methine protons appearing as doublets at 2.89 and 3.68 ppm.

2.2.2.6 XRD Characterisation of **2.3**

Compound **2.3** crystallises as a racemic mixture in the *P*-1 space group. The two molecules per unit cell are related to each other by an inversion centre. The bridgehead bond is 1.560(2) Å long, with a H11-C1-C5-H51 dihedral angle of 17.0°, and each five membered ring has a twisted, half-chair conformation. The deviation by non-wing-tip ring carbons from the plane defined by the two bridgehead atoms and the wing-tip atom can be used as an indication of the twistedness. In the ring with a ketone

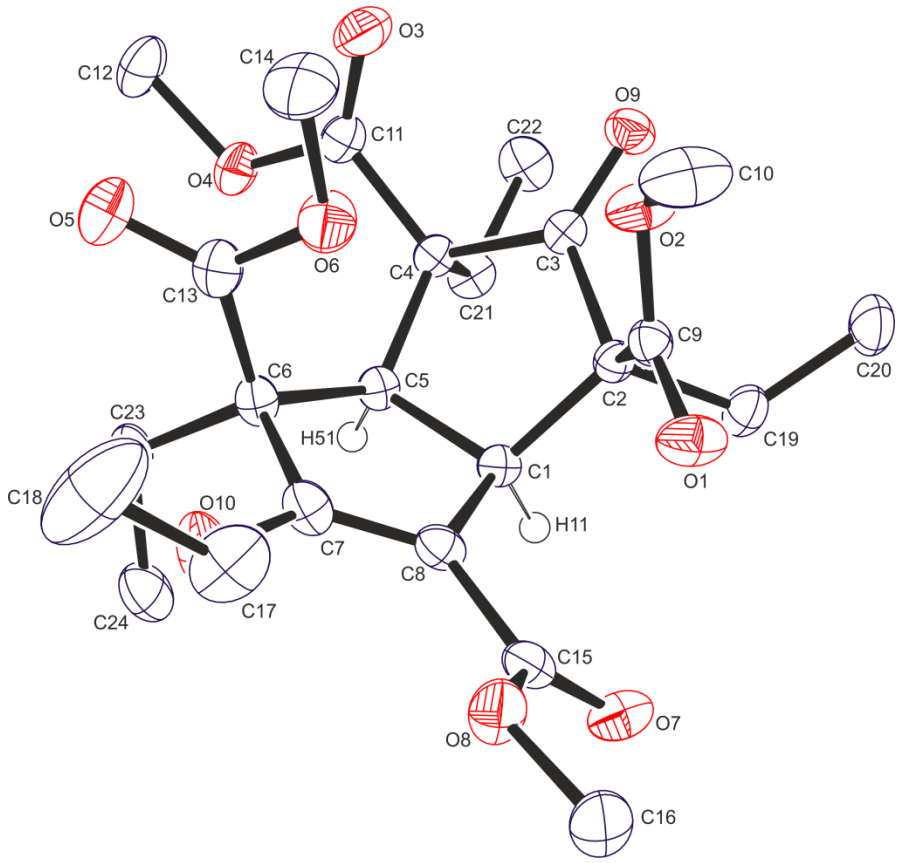

Figure 2.4 Molecular structure of 2.3. Displacement ellipsoids drawn at the 50% probability level. Carbon atoms are shown in blue, oxygen atoms are red, selected hydrogen atoms have been omitted for clarity. Selected bond lengths (in Å): C1—C5 1.560(2); C1—H11 1.006; C5—H51 0.985; C1—C2 1.563(1); C2—C3 1.538(2); C3—C4 1.530(1); C4—C5 1.552(2); C5—C6 1.566(2); C6—C7 1.527(2); C7—C8 1.341(2); C8—C1 1.506(2); C3—O9 1.207(1); C7—C10 1.347(2); C8—C15 1.482(2); C2—C9 1.528(2); C4—C11 1.522(2); C6—C13 1.529(2); C2—C19 1.558(2); C4—C21 1.566(2); C6—C23 1.547(1).

at the 3- position, C2 and C4 are 0.172 and 0.322 Å below and above the (C1,C3,C5) plane respectively. The ring containing two sp^2-hybridised carbon atoms is flatter as expected, and C6 and C8 lie below and above the (C1,C7,C5) plane by 0.161 and 0.137 Å respectively, which is more similar to the values in **2.1**. The skewedness in $WeissMe_4$, **2.ii**, is very large when measured in this way with deviations of 0.317-0.564 Å and a fold angle (as defined in section 2.2.2.2) of 122.6°. The fold angle in **2.3** is 126.37°, larger than both **2.1** and **2.ii**.

In contrast to **2.1**, the ketone of the sp^2 ester group in **2.3** adopts an orientation more parallel to the enolate C=C bond, with a C7-C8-C15-O7 dihedral angle of 152.24°. The range of ring C—C single bond lengths from 1.506(2) to 1.566(2) Å, is slightly

smaller than in **2.1**, with a similar mean length of 1.540 Å (*cf.* 1.535 Å), and an enolate double bond length of 1.341(2) Å (*cf.* 1.348, 1.351 Å in **2.1**). The *endo*- ester groups in the 2- and 6- positions have ketones pointing away from the concave cavity of the folded molecule, while the C=O bond of the 4-*endo*- ester points towards the cavity. The 2- and 4- ethyl substituents point away from the bridgehead, while the 6- ethyl group points over the five-membered ring to which it is attached.

Interestingly, the ester groups attached to C4 and C6 adopt an antiparallel arrangement (Figure 2.5). The C13—C11 separation of 2.849(2) Å, and distances between keto carbons (C11 and C13) and oxygens in the neighbouring ester of 3.063(2) to 3.255(2) Å are all significantly less than the 3.6 Å distance over which attractive carbonyl-carbonyl interactions are recognised.[37] The attractive energy between antiparallel carbonyls with C···O distances in the range 2.92–3.32 Å is greater than −20 kJ mol^{-1}, *i.e.* comparable to medium strength hydrogen bonds.[37] Van der Waals

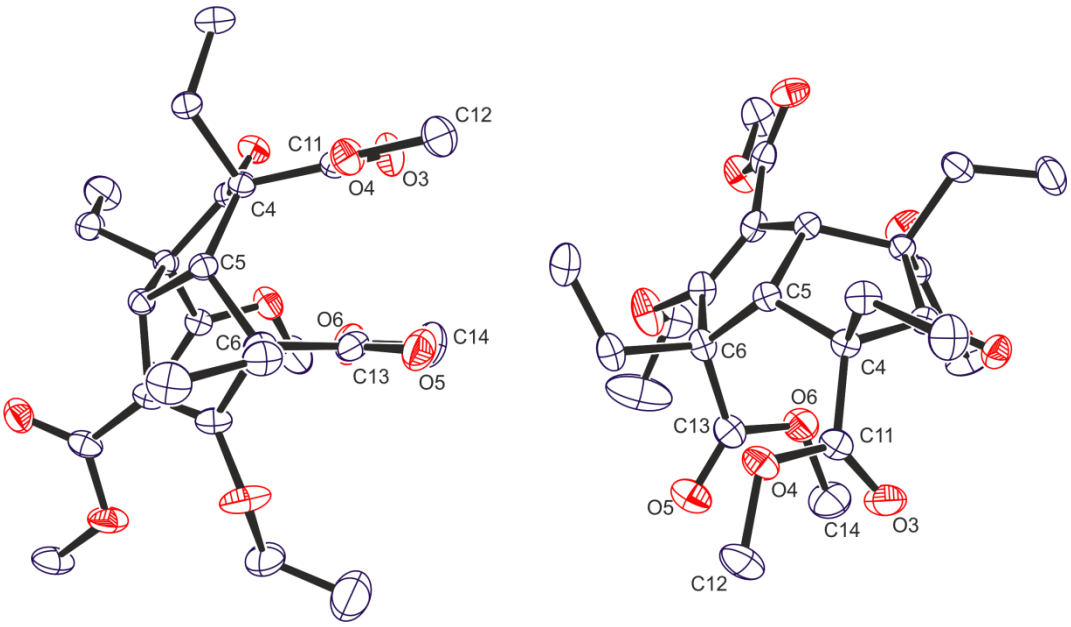

Figure 2.5 Molecular structures of 2.3 showing the almost parallel orientation of methylcarboxylate groups in the 4- and 6- positions (left) and dipole-dipole interactions (right). Displacement ellipsoids drawn at the 50% probability level. Carbon atoms are shown in blue, oxygen atoms are red, hydrogen atoms have been omitted for clarity. Angle between mean plane least squares planes of ester groups is 13.40°. Selected intramolecular distances (in Å): C11—C13 2.849(2); C11—O5 3.255(2); C11—O6 3.063(2); C13—O4 3.092(2); C13—O3 3.240(2); O3—C14 3.274(2); O5—C12 3.329(2).

forces between opposing dipole moments are primarily responsible for this favourable interaction,[38] which can clearly be seen on the right in Figure 2.5.

In addition, the stacked arrangement in **2.3** brings each methyl group close to the neighbouring keto oxygen. In 1,3-dimethyluracil, the methyl substituents prevent crystal packing of molecules being dictated by the formation of NH···O hydrogen bonds.[39] Dimers still exist however, in which intermolecular distances between the methyl carbons and neighbouring oxygen atoms of 3.29 Å are significantly shorter than the 3.4 Å expected based on the sum of Van der Waals radii. Similarly, in **2.3** a shortening of C14—O3 to 3.274(2) Å and C12—O5 to 3.329(2) Å can be taken as evidence of an intramolecular CH···O hydrogen bonding interaction,[40] rather than purely a crystal packing feature.

2.2.2.7 IR Characterisation of **2.3**

The carbonyl region contains strong overlapping bands, four of which can be resolved at 1693, 1722 (br), 1738, and 1765 cm^{-1}. This complicated overlapping of multiple carbonyl resonances is typical for these type of compounds,[41] while the vinylic enol ether stretch is characteristic, appearing at 1633 cm^{-1}. The β-keto group in **2.3** is located between two esters, which doubles the inductively withdrawing effect experienced by the ketone, strengthening the bond. The carbonyl stretches of β-keto esters typically occur at 1748 and 1710 cm^{-1},[27] so the ketone stretching frequency in **2.3** is shifted to even higher wavenumber and can tentatively be assigned to the highest C=O band at 1765 cm^{-1}.

2.2.3 Synthesis and characterisation of isopropylation products

The alkylation reaction conducted with 2-iodopropane as the alkylating agent produces a wide range of products, most of which (**2.4 — 2.10**) could be fully assigned using 1D and 2D NMR spectroscopy (Figure 2.6). The overall yield of alkylated products

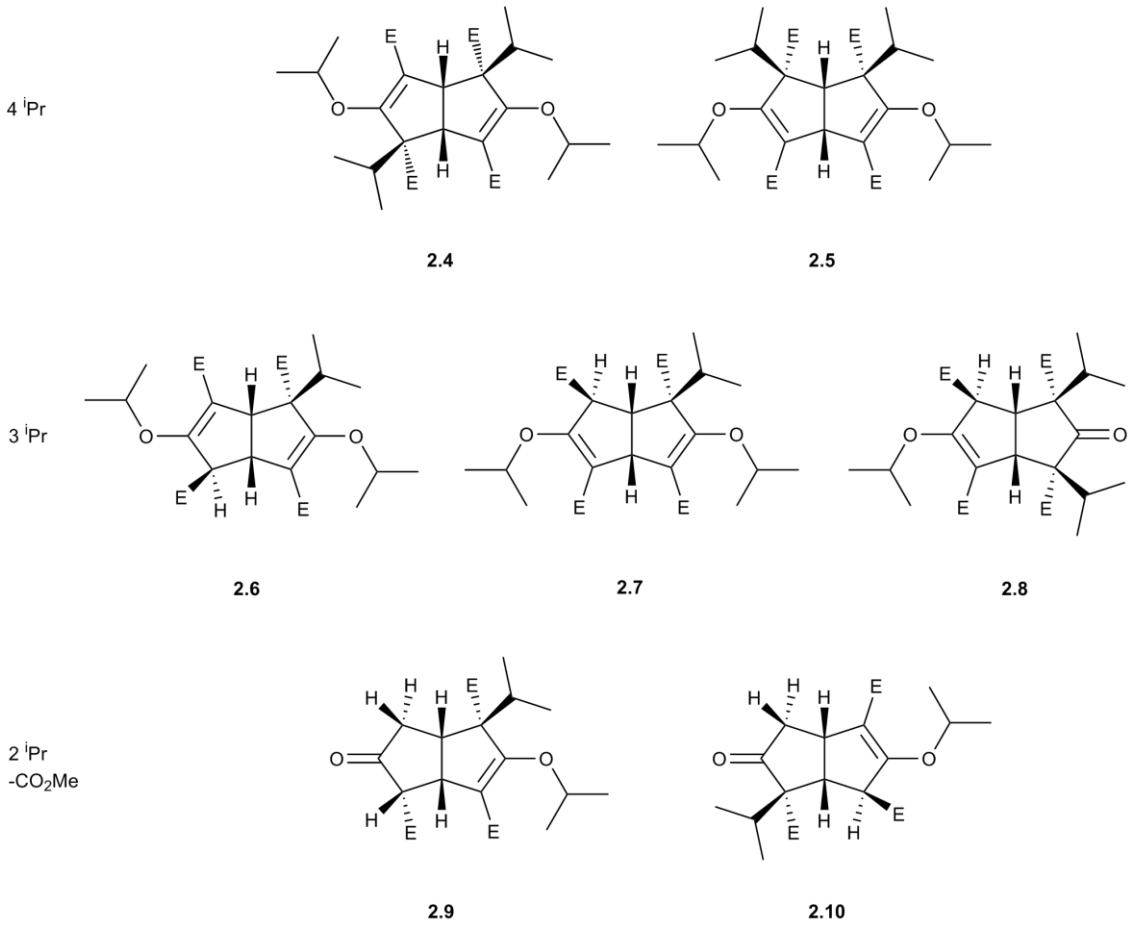

Figure 2.6 Tetraisopropylated reaction products.

was 2.78 g after starting with 6.93 g of **2.i**. As the alkylated products contained a mixture of products with differing RMM, this could only be converted into a rough overall yield of 30%.

2.2.3.1 NMR Characterisation of **2.4** and **2.5**

Two products, each containing four isopropyl groups, were produced by the reaction with 2-iodopropane. The dienol ethers 2,4,6,8-tetramethylcarboxylate-3,7-diisopropoxy-2,6-*exo*-diisopropyl-bicyclo[3.3.0]octa-3,7-diene (**2.4**), and 2,4,6,8-tetramethylcarboxylate-3,7-diisopropoxy-2,8-*exo*-diisopropoxy-bicyclo[3.3.0]octa-3,6-diene (**2.5**), both contain two *O*-alkylated wing-tip positions, and two unique methylcarboxylate environments. **2.4** has C_2 symmetry with ring alkylation at the 2- and 6- positions, and double bonds at positions 3- and 7-. **2.5** is

alkylated at the 2- and 8- positions, with double bonds at the 3- and 6- positions, giving the molecule C_s symmetry. The bridgehead protons of **2.4** are therefore equivalent, and appear as a singlet at 3.50 ppm. The bridgehead protons of **2.5** occupy two very different environments: one aliphatic and one allylic, so appear as two doublets at 2.65 and 4.20 ppm respectively. The bridgehead protons are not affected by the deprotonation or nucleophilic substitution reactions that form these products, so remain locked in a *cis* conformation relative to each other, as in the starting material. The junction between the two fused cyclopentene rings is best described by a half-chair conformation, with a $^3J_{HH}$ value of 8.35 Hz in **2.5**. Products **2.4** and **2.5** are analogous to the structures **2.1** and **2.2** respectively.

In these and all other isopropylated compounds in this chapter, the two methyl groups in each isopropyl or isopropoxide unit are diastereotopic because they cannot be related to each other by a plane of symmetry of the molecule. Therefore, each isopropyl or isopropoxide group is characterised by three ^{1}H resonances, and three ^{13}C resonances. In ^{1}H NMR spectra, the two sets of methyl protons are each split into a doublet by vicinal coupling to the central methine proton. The equal $^3J_{HH}$ coupling of the isopropyl methine to both sets of methyl protons results in an overlapping quartet of quartets, that invariably appear as a binomial septet.

2.2.3.2 NMR Characterisation of **2.6**

The triisopropylated dienol ether 2,4,6,7-tetramethylcarboxylate-3,7-diisopropyl-2-*exo*-isopropyl-bicyclo[3.3.0]octa-3,7-diene (**2.6**), was isolated in 6% yield. After storing the colourless oil in air for a number of weeks, a white, amorphous solid nucleated, which gave a correct elemental analysis for the assigned structure.

The ^{1}H NMR spectrum of **2.6** (Figure 2.7) contains six doublets and three septets corresponding to three ^{i}Pr environments. The septets occur with equal intensity at 2.37, 4.56, and 5.24 ppm, indicating the molecule contains one isopropyl and two isopropoxide groups. Four different ester environments result in four methyl singlets of equal intensity at 3.49, 3.59, 3.60 and 3.69 ppm, and three doublets of doublets account for the three ring protons. Couplings of 9.2 and 5.5 Hz experienced by the proton at 3.84 ppm are more consistent with vicinal *J* values, while the smallest coupling constant of 2.6 Hz, between protons at 3.61 and 3.72 ppm suggests a longer coupling pathway, over four bonds (see Figure 2.7 inset). The two bridgehead methine protons are known to be fixed in a *cis*- conformation, faithful to the starting material, and by comparison with coupling constants in other compounds in this chapter, the 9.2 Hz coupling can be assigned to the $^{3}J_{HH}$ coupling across the bridgehead. The 5.5 Hz coupling is smaller

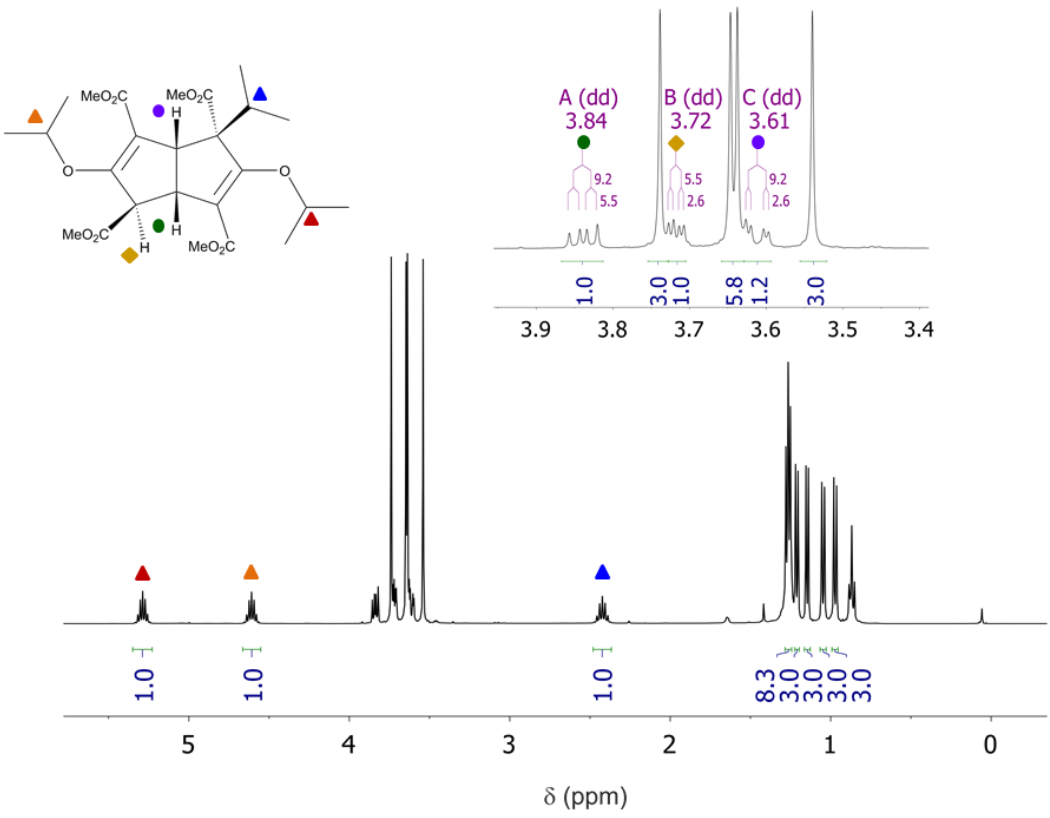

Figure 2.7 ^{1}H NMR spectrum of 2.6 showing assignment of selected resonances, with inset showing the bridgehead and ring methine multiplets.

because a greater dihedral angle is possible between the middle proton and the sp^3 hybridised non-bridgehead ring proton. This assignment is confirmed by HMBC correlations. The ring proton that is not attached to the bridgehead exhibits cross coupling to both sp^2 ring carbon resonances with similar intensity, as expected for $^3J_{HC}$ couplings, so cannot be used to distinguish between these vinylic positions. However, each bridgehead proton experiences one $^2J_{HC}$ cross coupling (to the vinylic carbon on the same side of the bridgehead bond as it), and one $^3J_{HC}$ cross coupling (to the vinylic carbon on the opposite side of the bridgehead bond), resulting in one stronger correlation peak and one weaker in 2D HMBC spectrum, for each bridgehead proton. This can be used to complete the full assignment of **2.6**.

2.2.3.3 NMR Characterisation of **2.7**

2,4,6,8-tetramethylcarboxylate-3,7-diisopropoxy-2-*exo*-isopropoxy-bicyclo[3.3.0] octa-3,6-diene, **2.7**, was identified as the major component in a mixed fraction that also contained its isomers **2.6**, and **2.8**. As seen with **2.6**, the spectra of **2.7** also show a structure with C_1 symmetry, with two isopropoxide, one isopropyl, and four methylcarboxylate environments, and three protonated ring positions. The methine doublet of doublets at 3.02 ppm exhibited strong cross peak correlations in COSY NMR spectra with the doublet of doublets at 4.25 ppm, and with a proton at 3.66 ppm which was obscured by carboxylate singlets in the 1D spectrum. Correlations between the 3.66 ppm resonance and its directly bonded carbon were also seen in HSQC spectra, and cross peaks in the HMBC spectrum show coupling to two vinylic carbons, at 160.9 and 111.8 ppm, allowing a full assignment of this compound. The proton at 4.25 ppm couples symmetrically to all ring carbons in the HMBC spectrum, so is assigned to the vinylic bridgehead methine.

2.2.3.4 NMR Characterisation of **2.8**

The ^{1}H and ^{13}C NMR spectra of the final fractions isolated from this reaction clearly depict a mixture of two species with C_1 symmetry in a 1:2 ratio. 2,4,6,8-tetramethylcarboxylate-3-keto-7-isopropoxy-2,4-*exo*-diisopropyl-bicyclo[3.3.0]-oct-6-ene, **2.8**, contains three isopropyl groups: one *O*-alkylation, and two isopropyl substituted positions. Of the three possible isomers for this compound (see Figures 2.13 and 2.14 in Section 2.3.2), only the one in which both alkylated positions are on the same ring can account for the cross peak in HMBC spectra that couples both isopropyl methine protons to the carbonyl carbon resonance at 208.7 ppm. As with compounds seen previously, two doublets of doublets are observed at 3.43 and 4.10 ppm, and correlation peaks show the third ring methine proton occurs at 3.66 ppm, and is obscured in 1D spectra by the methylcarboxylate peaks. The doublet of doublets at 3.43 ppm belongs to the bridgehead proton between the two non-bridgehead methine protons, and very similar $^{3}J_{HH}$ coupling constants to the adjacent protons of 8.9 and 9.1 Hz, causes it to appear as a triplet.

2.2.3.5 NMR Characterisation of **2.9**

The minor species isolated in a 1:2 mixture with **2.8** was 2,4,6-trimethylcarboxylate-7-keto-3-isopropoxyl-2-*exo*-isopropyl-bicyclo[3.3.0]oct-3-ene, **2.9**. The starting material, 2,4,6,8-tetramethylcarboxylate-bicyclo[3.3.0]octa-3,7-dione, **2.i**, has undergone two alkylations and loss of an ester group to form **2.9**. The compound contains one isopropoxide group, one isopropyl group and three ester environments, and a ketone carbon in the ^{13}C NMR spectrum at 211.4 ppm. A coupling network between protons indicates a linear arrangement of five protons. HSQC correlation shows two of the protons have $^{1}J_{CH}$ coupling to the same carbon atom, and together with the large, -19.2 Hz, $^{2}J_{HH}$ geminal coupling between these two protons, indicates the path terminates at one end in a methylene group. HSQC is

used to identify the four carbon atoms along this pathway, and 135-DEPT to confirm inversion of the CH_2 methylene resonance at 42.7 ppm. Four structures can be proposed that contain the aforementioned features (**a**–**d** in Figure 2.8). NB It is assumed that tautomerisation of esters at methine ring positions occurs. Assignment of non-bridgehead methine stereochemistry is discussed in Section 2.3.1.

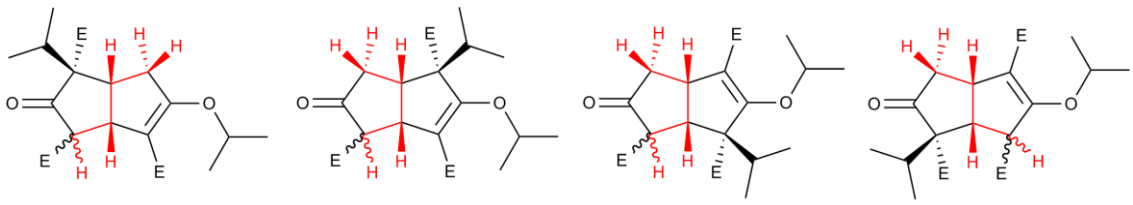

Figure 2.8 Four stereoisomers possible for structure 2.9.

The methine proton of the isopropyl group couples over three bonds to the bridgehead carbon which is adjacent to the methylene protons. The isopropyl group is therefore on the same side of the bridgehead as the methylene group. This rules out structures **c** and **d** in Figure 2.8. The geminal methylene protons couple to both sp^3-hybridised non-bridgehead ring carbons. In structure **a**, these cross peaks would represent one three-bond and one four-bond H-C coupling, while in structure **b**, both peaks could be caused by H-C couplings across three bonds. Structure **b** is therefore more likely, and confirmation of this comes from coupling of the three non-bridgehead protons to the carbonyl resonance at 211.4 ppm. The mechanism of formation of **2.9** is discussed in Section 2.3.3 of this chapter.

2.2.3.6 Mixtures containing partially characterised species

A mixed fraction contained tetraalkylated **2.5**, and trialkylated **2.6**. After accounting for resonances attributed to these, all remaining features in the NMR spectrum could be interpreted, but not fully assigned. Intensities tentatively suggested two further molecules, however, the resolution of 2D NMR spectra was not fine enough

to fully assign connectivity. One product contains three ester environments, and one contains four ester groups. A total of three aliphatic ^{i}Pr groups are characterised by septets in the region 2.2–2.7 ppm, six isopropoxide groups can be assigned to six septets in the region 4.77–5.02 ppm, and finally six doublets, or doublets of doublets, occur at resonances appropriate to ring protons, with COSY cross peaks demonstrating mutual coupling between these.

The mixed fraction containing **2.6** and **2.7** also contained a third molecule. The three products had very similar solubilities and retention times, and could not be isolated from each other chromatographically or by crystallisation. While not fully assignable, the clean mixture of three products and good resolution of the 1D and 2D spectra, coupled with observation that loss of an ester group can occur, means a number of deductions regarding the structure of this third species, **2.10**, can be drawn.

2.2.3.7 Partial assignment of **2.10** by NMR spectroscopy

The ^{13}C NMR spectrum contains a single resonance at 213.1 ppm unaccounted for by **2.6** or **2.7**, and can only be ascribed to a ketone. Two septets in an approximately 1:1 ratio occur at 4.74 and 2.26 ppm, indicate one isopropoxide environment and one isopropyl environment respectively.

A very clear coupling network is observed in COSY, where the five remaining multiplets are connected. Two doublets of doublets couple to each other, and to a multiplet at 3.59 ppm that is obscured by CO_2Me signals. The two doublets share a first coupling constant of −19.7 Hz, characteristic of $^{2}J_{HH}$ geminal coupling of methylene protons. Their second coupling constants of 7.0 and 9.3 Hz indicate differing three-bond vicinal couplings, as would be expected for differing dihedral angles formed between the two methylene protons and C—H bond on the adjacent carbon. The obscured proton at 3.59 ppm which couples to the methylene protons has a strong cross peak indicating coupling to a doublet of doublets at 3.26 ppm ($^{3}J_{HH1}$ 8.5 Hz, $^{3}J_{HH2}$ 5.7 Hz). This doublet of

doublets then couples to a final doublet of doublets at 3.86 ppm ($^3J_{HH}$ 5.7 Hz, $^4J_{HH}$ 1.8 Hz). Coupling constants of 8.5, and 5.7 Hz are consistent with two three-bond couplings, and the much smaller 1.8 Hz with a $^4J_{HH}$ coupling network. For that reason, **2.10** contains the proton network in Figure 2.9.

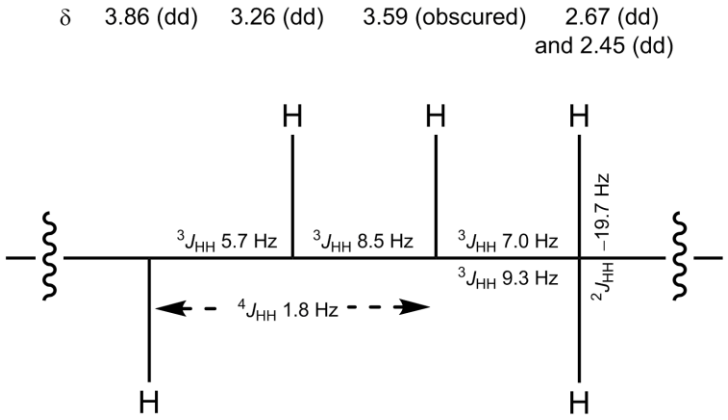

Figure 2.9 Coupling network for ring protons in 2.10.

The features of **2.10** are very similar to **2.9**, and the range of possible structures for **2.10** are again given by Figure 2.8 (**2.9** has structure **b**). Cross peaks are seen between the isopropyl carbon of **2.10** and both the 3.26 ppm bridgehead and 3.86 ppm ring protons. The isopropyl group is therefore on the opposite side of the bridgehead to the methylene protons, eliminating structure **a** (Figure 2.8). The methylene protons do not couple to the ^{13}C resonance at 163.0 ppm, however, the methine proton at the opposite end of the network does. This shift is characteristic of the sp^2 ring-carbon with the isopropoxide group attached. The methine group must therefore occur adjacent to the enol ether, while the methylene group is on the other five-membered ring. **2.10** must have structure **d**. Therefore, **2.10** is 2,4,6-trimethylcarboxylate-7-keto-3-isopropoxyl-6-*exo*-isopropyl-bicyclo[3.3.0]oct-2-ene (Figure 2.6).

2.2.4 Hydrolysis and decarboxylation of **2.3**

Cook and coworkers demonstrated the formation of alkylated 2,4,6,8-tetramethylcarboxylate-3,7-ethoxy-bicyclo[3.3.0]octa-1,5-dienes, which have one[42] or two[43] ring-bound alkyl substituents. These compounds, with either hydrogen or methyl groups at the bridgehead positions, are analogous to **2.1**, **2.2**, **2.4**, **2.5**, **2.6** and **2.7**. Enol ethers at positions 3- and 7- of the bicyclic ring can be converted back into ketones by protonolysis with glacial acetic acid in HCl.[43] Decarboxylation was achieved at the same time in a one-pot reaction, by refluxing for 2 hours in a 1:1 mixture of glacial acetic acid and 1 M HCl.[42]

This procedure was followed using a sample of **2.3**. Heating at reflux for 24 hours yielded a single, clean reaction product, where the allylic ethoxide had been converted back to the ketone. The triply ring-alkylated triester 2,4,6-trimethylcarboxylate-2,4,6-*exo*-triethyl-bicyclo[3.3.0]octa-3,7-dione, **2.11**, was formed (Scheme 2.4), with no indication of further decarboxylation or hydrolysis of the ester groups under the conditions employed. The reaction was worked up, yielding **2.11**, as a yellow oil in 98% yield.

Using COSY, HSQC, and HMBC, the ^{1}H and ^{13}C NMR spectra could be fully assigned, and the only species present in the mass spectrum were $[M+H]^+$ and $[M+Na]^+$ and a fragment resulting from loss of an ester group. The five carbonyl stretches overlapped in the IR spectrum, while three equal intensity bands at 1218, 1239, and

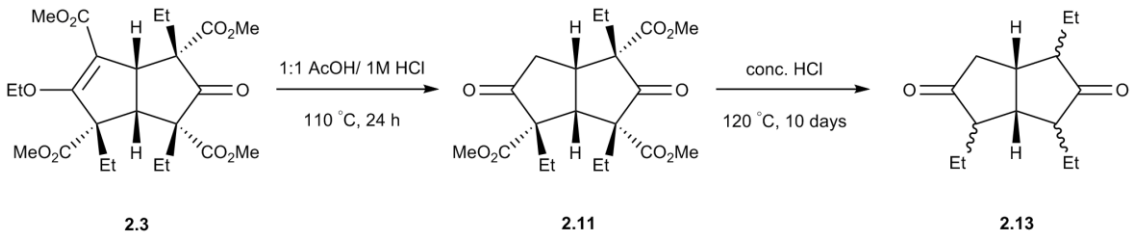

Scheme 2.4 Hydrolysis and decarboxylation of 2.3.

1259 cm^{-1} can be assigned to the three ester C-O-C asymmetric stretching vibrations.

A similar decarboxylation was achieved with a sample of **2.6**, resulting in the formation of the monocarboxylate, monopropyl dione **2.12** (Scheme 2.5). The monomethyl analogue of **2.12** is known, and can be decarboxylated by refluxing with sodium chloride in DMSO to yield a mixture of *endo* and *exo*-methylated isomers.[44]

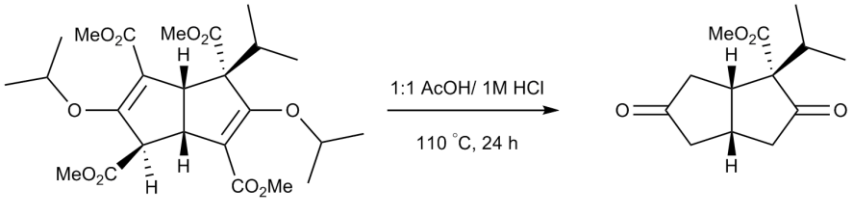

2.6 **2.12**

Scheme 2.5 Hydrolysis of 2.6.

The loss of methylcarboxylate groups only from unalkylated ring positions is not surprising. The same selectivity is observed upon exposure of 2,4,6,8-tetramethylcarboxylate-2,6-diallyl-bicyclo[3.3.0]octa-3,7-dione to these conditions.[18] Indeed, for 2,4,6,8-tetramethylcarboxylate-2,4,6,8-tetramethyl-bicyclo[3.3.0]octa-3,7-dione, **2.ii**, while the initial decarboxylations occur swiftly in hot concentrated HCl, presumably greatly relieving intense strain in the folded molecule, removal of the final carboxylate groups requires refluxing for extended reaction times of up to 10 days.[13] The limiting step must be hydrolysis of the ester to the carboxylic acid, as 2,4,6,8-tetra-*tert*butylcarboxylate-2,6-diallyl-bicyclo[3.3.0]octa-3,7-dione readily undergoes elimination of all four carboxylate groups under similar conditions.[18]

2.11 was therefore dispersed in 2 mL concentrated HCl and heated at reflux. Aliquots taken over the course of nine days revealed a steady decrease in the relative intensity of the methylcarboxylate resonances until they were completely absent and a single product remained. The persistence of these methyl resonances confirms that the methylcarboxylate groups are highly resistant to hydrolysis in refluxing hydrochloric acid. Following work up, 2,4,6-triethyl-bicyclo[3.3.0]octa-3,7-dione, **2.12**, was isolated

as a yellow oil in 20% yield, thus demonstrating that species of lower symmetry than **2.ii** that are substituted with bulkier alkyl groups can form analogues of dione **2.iii**.

The product of the decarboxylation reaction can undergo acid-catalysed keto-enol tautomerisation between stereoisomers. The equilibrium mixture of the monosubstituted allyl product favours an *exo*- over an *endo*- form in a 3:1 ratio,[45] while the tetramethylated product **2.iii** on the other hand forms as a single isomer, with 2,6-*exo*-4,8-*endo*- stereochemistry.[13] Unlike the monosubstituted allyl product, which only has two possible isomers, or **2.iii** which simplifies to C_2 symmetry, all eight stereoisomers of **2.12** are C_1 symmetric. However, a single stereoisomer of **2.12** is clearly present in the NMR spectrum. Fourteen lines appear in the ^{13}C NMR spectrum as expected, two occuring at 219.8 and 221.4 ppm are characteristic of two ketone environments, and four lines invert during DEPT135 NMR experiments, indicating four CH_2 environments (three ethyl and one on the ring). Overlapping, almost coincident ethyl C$\underline{H}_2$ and C$\underline{H}_3$ resonances in the ^{1}H NMR spectrum have complex multiplet structures, and five ring protons can be paired with the carbon atom to which they are bonded using HSQC. The multiplicities of the ring protons are unclear, and preclude further inference of the structure of **2.12**. During the course of subsequent reactions in the synthesis of alkylpentalenes by the method of O'Hare *et al.*,[13] the stereochemistry of this species is not pertinent so efforts were not made to identify it at this time.

2.3 Discussion

2.3.1 Assignment of structures **2.6**–**2.10** using $^3J_{HH}$ coupling constants

Conformational analysis of cyclopentanes using vicinal coupling constants should be approached with caution,[46] as *J* values are sensitive to substituent effects, and cyclopentanes can adopt a variety of puckered conformations which are similar in energy, and for which coupling constants can be equal for *cis* and *trans* related ring

protons. For our purposes, analysis is simplified by some restrictions imposed by the fused ring system of the starting material **2.i**, and by the reaction mechanism. The *cis* conformation of bridgehead protons in the starting material is unaltered under the alkylation conditions, and alkylation occurs solely on the *exo*- face of the molecule, as discussed previously. While the conformation of the bridgehead and alkylated ring positions can therefore be rationalised, assignment of the conformation of protonated sp^3 non-bridgehead ring positions is more difficult.

The Karplus equation describes the relationship between dihedral angle, ϕ, and vicinal coupling constants, ${}^3J$, in Hz:

$$^3J = J_0 \cos^2 \phi - 0.28$$

where the initial values J_0 = 8.5 when 0° ≤ ϕ ≤ 90° and 9.5 when 90° ≤ ϕ ≤ 180°, yield a first approximation of vicinal coupling values.[47] In practise, J_0 can vary from 5.7 to 14.7 Hz, depending on the particular system under study. Precise values are best determined empirically, using experimental data for molecules with similar conformation and substitution patterns as the system of interest. Abrahams *et al.* demonstrated that for systems with two *cis*-fused five membered rings, values of J_0 = 9.3 when 0° ≤ ϕ ≤ 90°, and J_0 = 10.4 when 90° ≤ ϕ ≤ 180°, give ${}^3J$ coupling constants that better reflect experimental data.[48] Using Abraham's values, the ϕ angle predicted for the *cis* fused bridgehead protons in complexes **2.3**, **2.6**, **2.8,** and **2.9** would give nonsense values (with $2\phi > 1$).

The ester functionalities common to compounds studied here have quite different electronegative influences than the systems studied by Abrahams. As can be seen in Figure 2.10, the fused five-membered rings of **2.1** and **2.3** have almost planar geometries, with a very slight twist to a half-chair conformation, rather than the fused envelope-twist structures for which the J_0 values above were calculated. The availability of crystal structural data therefore makes it sensible to determine a value for J_0 empirically.

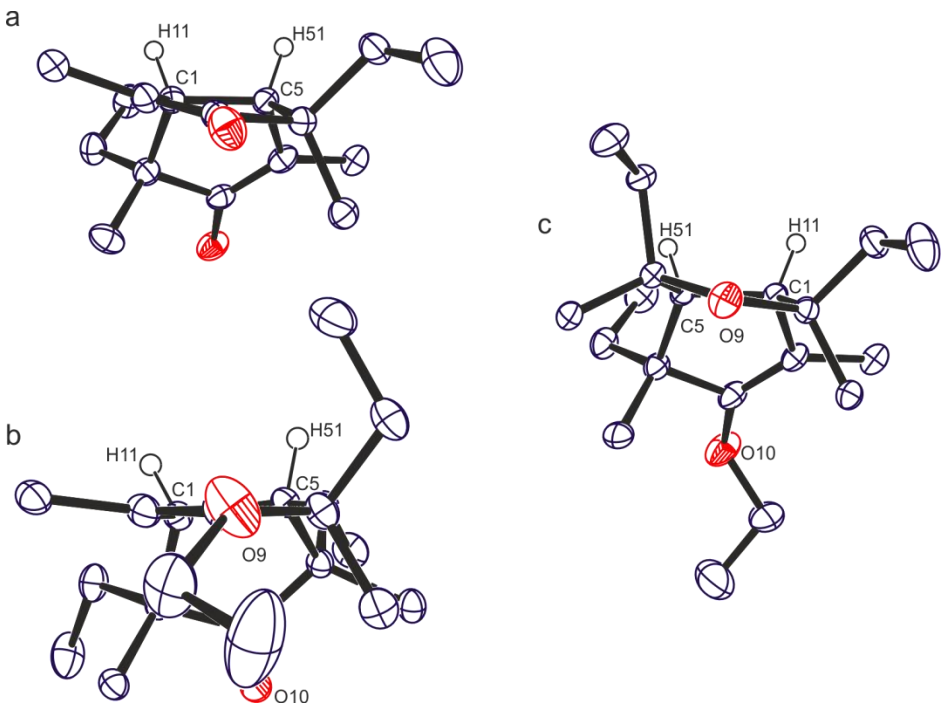

Figure 2.10 Views along the O2—C7 bond of 2.1 (a), the O9—C3 bond of 2.3 (b), and the O10—C7 bond of 2.3 (c), showing nearly planar carbocyclic rings. Displacement ellipsoids drawn at the 50% probability level. Carbon atoms are shown in blue, oxygen atoms are red, hydrogen atoms and selected ester atoms have been omitted for clarity.

Few examples exist where both torsional angles (from crystal structures) and $^3J_{HH}$ coupling constants are provided. In Vossen's Red Salt,[49] (**2.v** in Figure 2.11) the H_a-C-C-H_b torsion angles in the solid state of 159.6° and 142.2° would suggest $^3J_{HH}$ coupling constants of 8 or 6 Hz respectively, and these are in excellent agreement with the value of 7.9 Hz recorded in solution. The C_2 symmetric tetraester dienol, **2.vi**, also has ester groups *cis* to the bridgehead protons, and various polymorphs can be isolated.[36] Torsion angles range from 130.0° to 136.5° when solvent is incorporated into the single crystals, or 114.0 to 119.2° or 138.4° to 140.1° in its absence. The coupling constant between protons H_a and H_b is 2.7 Hz in solution, *i.e.* much smaller.

Similarly in both 2,4,6,8-tetramethylcarboxylate-3,7-diethoxy-bicyclo[3.3.0]octa-2,6-diene, **2.viii**, and in 2,4,6,8-tetraethylcarboxylate-3,7-diol-bicyclo[3.3.0]octa-2,6-diene, **2.ix**, the $^3J_{HH}$ coupling constants of 1.8 Hz,[18] and 2.7 Hz respectively are interpreted to mean the protons reside on opposite sides of the bicyclic

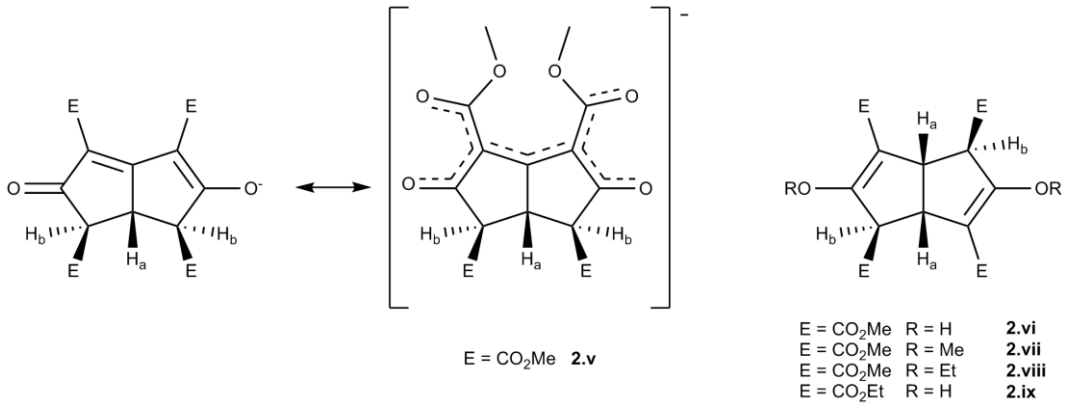

Figure 2.11 Bicyclo[3.3.0]octadiene tetraester complexes for comparison.

ring.[50] These values, summarised in Table 2.1, are much smaller than the analogous coupling constants found in complexes **2.6 — 2.10**.

Table 2.1 Compilation of $^3J_{HH}$ torsion angles (from crystal structures) and coupling constants for bicycle[3.3.0]octadiene structures.

	Point group	Bridgehead torsion angle (°)	$^3J_{HH}$, bh–bh (Hz)	Bridgehead–methine torsion angle (°)	$^3J_{HH}$, bh-methine (Hz)	Ref
2.v	C_s	-	-	142.2, 159.6	7.9	49
2.vi	C_2	7.5-10.1[a] (6.6 or 11.2)[b]	-	130.0-136.5[a] (114.0, 119.2 or 138.4, 140.1)[b]	2.7	36*a* (36,51)*b*
2.vii	C_2	14.7	-	106.8, 108.2	†	51
2.viii	C_2	†	-	†	1.8	18
2.ix	C_2	†	-	†	2.7	50
2.1	C_2	10.3	-	-	-	*c*
2.2	C_s	†	7.35	-	-	*c*
2.3	C_1	17.0	9.4	-	-	*c*
2.4	C_2	†	-	-	-	*c*
2.5	C_s	†	8.35	-	-	*c*
2.6	C_1	†	9.2	†	5.5	*c*
2.7	C_1	†	7.8	†	5.4	*c*
2.8	C_1	†	9.1	†	8.9	*c*
2.9	C_1	†	9.7	†	7.7	*c*
2.10	C_1	†	8.5	†	5.7	*c*

bh = bridgehead, *i.e.* the bond along which the bicyclic structure is fused, [a] Polymorph I, [b] Polymorphs II and III, [c] this work, † not available

Fortunately, two pairs of values are available that allow J_0 to be solved in the acute and obtuse regions. Assuming dihedral angles in solution do not deviate hugely

from those in crystal structures, **2.3** has a ^3J of 9.4 Hz with ϕ = 17, yielding J_0 = 10.6 when 0° ≤ ϕ ≤ 90°. Similarly, using the obtuse angle available in **2.v**, a ^3J of 7.9 Hz when the mean ϕ = 150.9°, yields J_0 = 10.7 when 90° ≤ ϕ ≤ 180°. In the five-membered rings containing sp^2 hybridised carbons, the roughly planar conformation means adjacent substituents can be fully eclipsing. Torsional strain is maximised, causing puckering, but less so than in the fused systems studied by Abraham. As such, fully eclipsing geometries offer even higher vicinal couplings.

Dihedral angles for bridgehead protons can therefore be predicted to range from 10° (for **2.9**) to strongly distorted 61° (for **2.2**). The ^3J values of 5.5–7.7 Hz for coupling of bridgehead protons to methine protons could be achieved either by acute dihedral angles of 41–43° and *exo*- methine protons, or by obtuse angles of 137–138° and *endo*-methine protons. The latter range is far more feasibly accommodated in existing crystal structures,[22,36,49,51] so by extrapolation, these coupling constants can be used to assign *endo*- methine protons, *i.e*. *exo*- ester groups in structures **2.6**, **2.7**, and **2.10**. The coupling constants of 7.7 and 8.9 Hz could be achieved with either 31° or 21° acute ϕ between protons, or a 150° or 158° trans arrangement in **2.8** and **2.9** respectively. For **2.8**, both of these values fall 10° outside the range of torsion angles observed in crystal structures, so assignment of the epimers formed cannot be made based on ^3J coupling constants. For **2.9**, the acute angle is identical to a dihedral angle found in **2.3**, while the value of 158° would require a significantly distorted structure, indicating **2.9** has an *exo*- methine proton, and a preference for a structure with an *endo*- ester.

2.3.1.1 Assignment of structure based on chemical shift

It has been shown that for esters with the bicycle[3.3.0]octane structure and an acidic proton at the α- position, a range of epimers can exist. For **2.ix**, only the 2,6-*exo*- epimer is observed in solution.[50] The disodium salt of **2.vi** can be isolated as either the kinetic 2-*exo*-6-*endo*-, or thermodynamic 2,6-*exo*- product. The

exo,endo- epimer is converted to the *exo,exo*- epimer upon refluxing in basic methanol solution, or to the protonated *exo,exo*-dienol by acid.[52] A molecular mechanic study showed that for **2.x** (an analogue of **2.vi** where bridgehead protons have been replaced by a 1-ethyl and a 5-methyl group), the 2,6-*exo*- stereoisomer had the lowest energy of formation, but the 2-*exo*-6-*endo*- and 2-*endo*-6-*exo*- stereoisomers lie only 2.91 and 2.77 kcal mol^{-1} higher in energy respectively (the 2,6-*endo*- isomer was 7.82 kcal mol^{-1} higher in energy).[53]

It may therefore be relevant to compare the chemical shifts of non-bridgehead methine protons in **2.6**–**2.10** with chemical shifts of methine protons in **2.x**. In 2,6-*exo*-**2.x**, the two *endo*- methine proton environments have chemical shifts of 3.88 and 4.06 ppm, while in 2-*exo*-6-*endo*-**2.x**, the *endo*- methine has a shift of 3.98 ppm and the *exo*- methine 3.57 ppm. **2.8** has a very large methine chemical shift of 4.10 ppm, in agreement with the *endo*- configuration assigned to it based on the $^3J_{HH}$ coupling constant. **2.10** also has a very large methine chemical shift of 3.86 ppm, indicating an *endo*- configuration, and an *exo*- ester group. **2.9** has a very low chemical shift of 3.38 ppm, and by this argument, would be assigned an *exo*- methine hydrogen, and *endo*- ester. AM1 and PM3 calculations of the relative heats of formation for the two epimers of **2.9** reveals that the *exo*-ester epimer is indeed higher in energy than the *endo*-ester epimer by 3-4 kcal mol^{-1}. MM2 geometry optimisation suggests this is due to a significant dipole/dipole repulsion between two esters on one side of the molecule, which is relieved when the ester is *endo*-. All other contributors to the molecules total energy are similar.

2.3.2 Rationalising the regio-chemistry of reactions

In contrast to methylation which forms $WeissMe_4$, **2.ii**, a single product, alkylation of **2.i** with ethyl or isopropyl iodides produces multiple products of *C*- and *O*-alkylation. In examples from literature where **2.i** is subjected to similar conditions,

formation of only a handful of the many possible isomers is observed.[22,53] This is the first time such a wide variety of products of ring alkylation have been formed. Helpfully, while **2.ii** exhibits fluxionality in solution, ethylated and isopropylated products have well-defined NMR spectra at ambient temperature.

In general, the range of alkylation products observed increases with the bulkiness of the alkylating agent, in the order Me < Et < ^{i}Pr. In addition, *O*-alkylation is observed for the bulkier EtI and ^{i}PrI electrophiles, but is completely absent for smaller MeI. Enolates of β-keto esters can undergo reaction at either the α-carbon, or the enolate oxygen.[54,55] Our results are in accord with the known trend that the ratio of *O*-/*C*-alkylation of enolates increases with the increasing size of the electrophile,[55–58] and is based on steric arguments, *i.e.* the oxygen atom is less hindered than the α-C, which is bonded to three other atoms, and this becomes more pertinent with increasing size of the alkyl substituent being introduced. The desirable ring alkylated products of **2.i** result from S_N2 attack by the α-carbon ring position on an alkyl iodide molecule.

The *O*-/*C*-alkylation ratio of enolates of β-keto esters with alkyl halides also increases with solvent polarity.[59] DMSO (polarity index, P' = 7.2)[60] is in fact the most polar solvent other than water (P' 10),[60] explaining the complete absence of ring alkylation products observed in DMSO. Therefore, greater ring alkylation may be favoured by employing a solvent that is less polar than acetone (P' 5.1).[60] The pK_a of α-protons in **2.i** is around 7.8,[15] of the conjugate acid of K_2CO_3 is 10.25, and of acetone is 19.3,[15] therefore **2.i** will be deprotonated by potassium carbonate, but acetone will not. Ethyl acetate (P' 4.4,[60] pK_a 25),[15] methyl ethyl ketone (P' 4.7, pK_a ≈19.8),[61] methyl *n*-propyl ketone (P' 4.5, pK_a ≈20),[61] or methyl amyl ketone (P' 4.4, pK_a ≈20.5)[61] may therefore improve the product distribution in favour of ring-alkylation products. The *O*-/*C*- alkylation ratio in dipolar aprotic solvents is also sensitive to the leaving group used increasing in the order $I^- < Br^- < Cl^- < (RO)_2SO_2^-$.[56,62]

It is of interest to see whether there was any regioselectivity to the ring alkylation reactions observed. It has already been noted previously that dimethylation of **2.vi** forms only the 2,6- and 2,8- dienol ether isomers.[19] The full range of products possible from *C*- and *O*- alkylation reactions of monoalkylated **2.i** are shown in Figures 2.12–2.14.

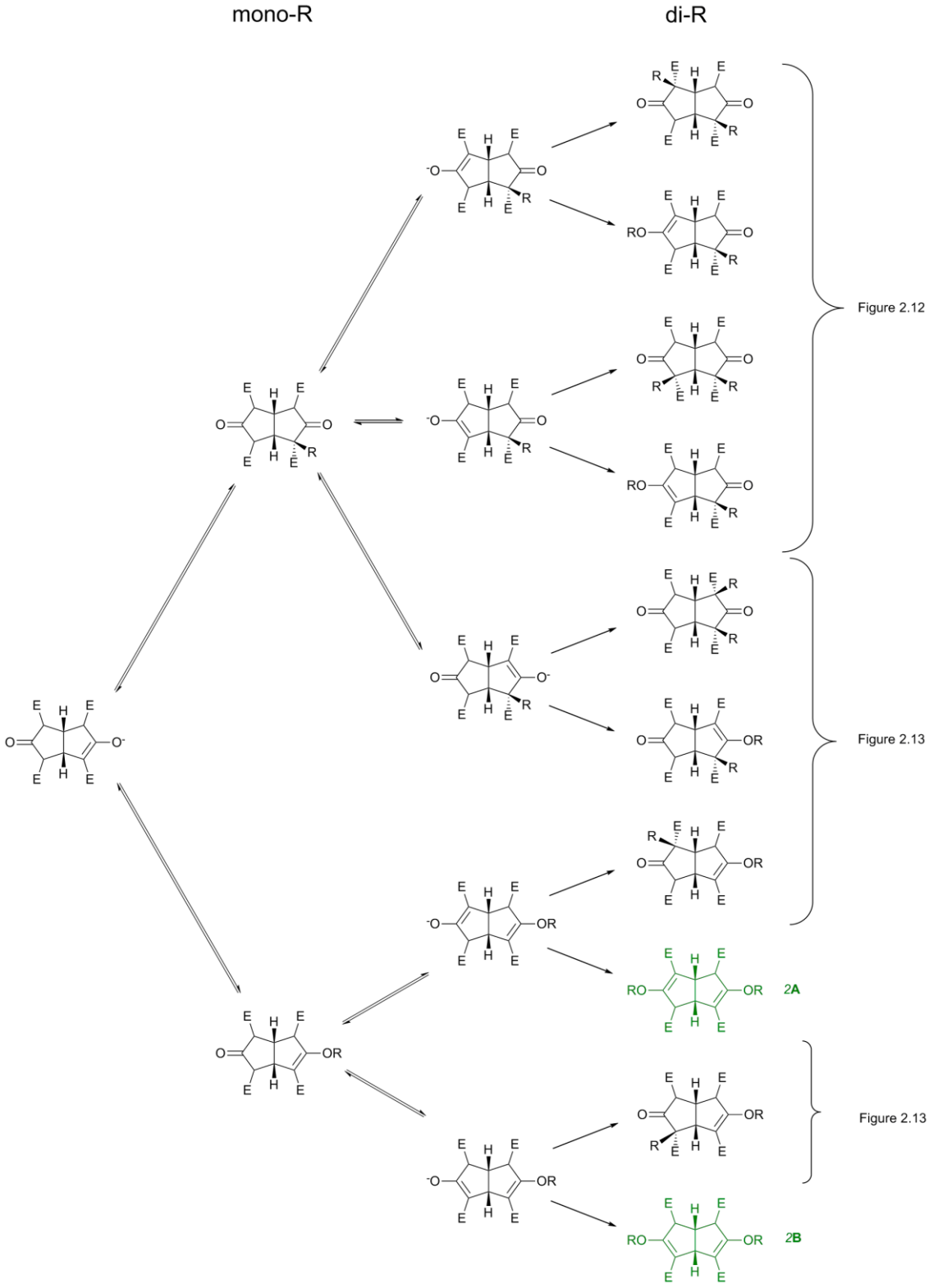

Figure 2.12 Scheme showing the mono and di-substituted stereoisomers formed upon alkylation of WeissH$_4$, 2.i.

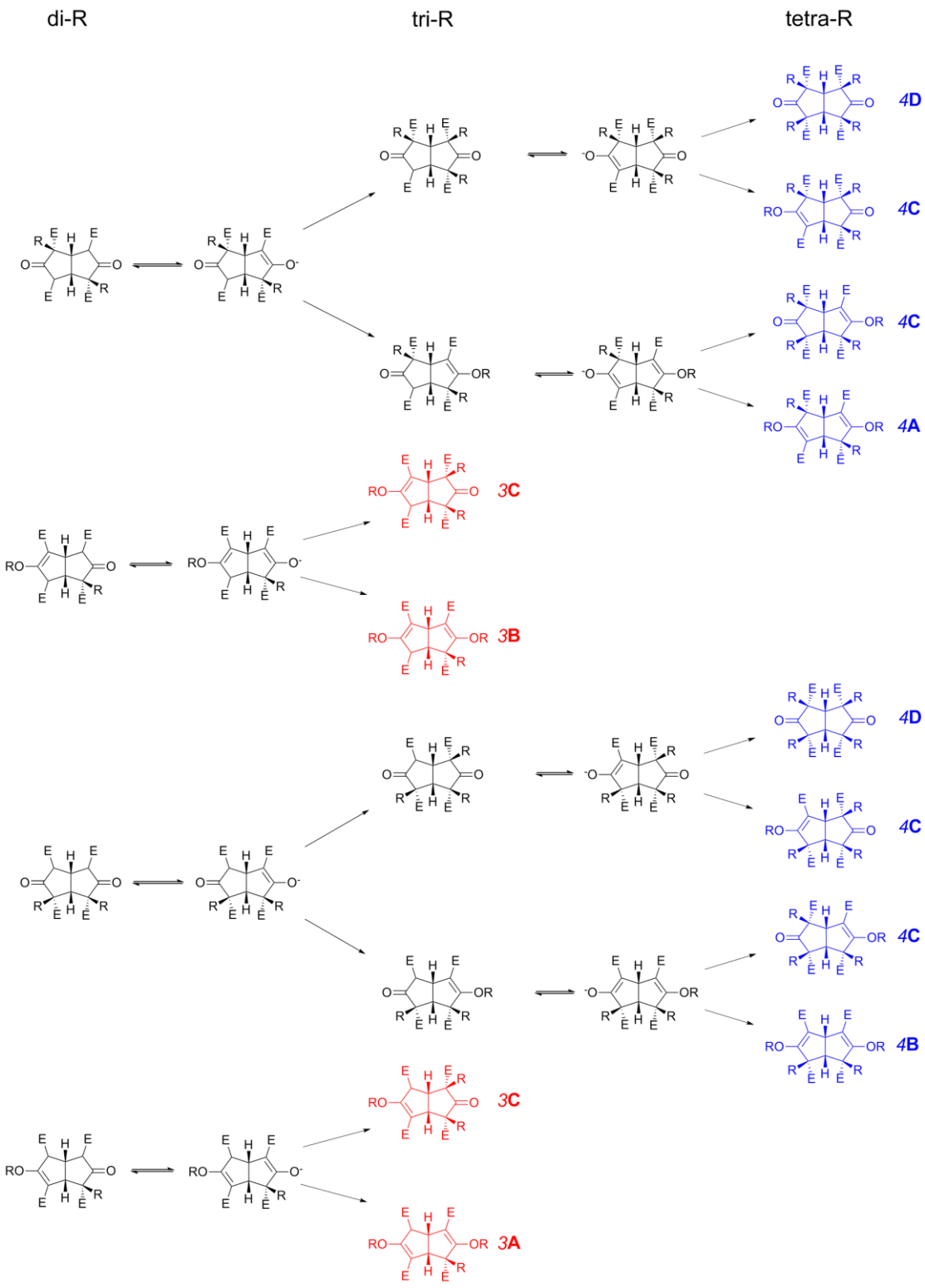

Figure 2.13 Scheme showing the tri- and tetra-substituted stereoisomers formed upon alkylation of products shown in Figure 2.12.

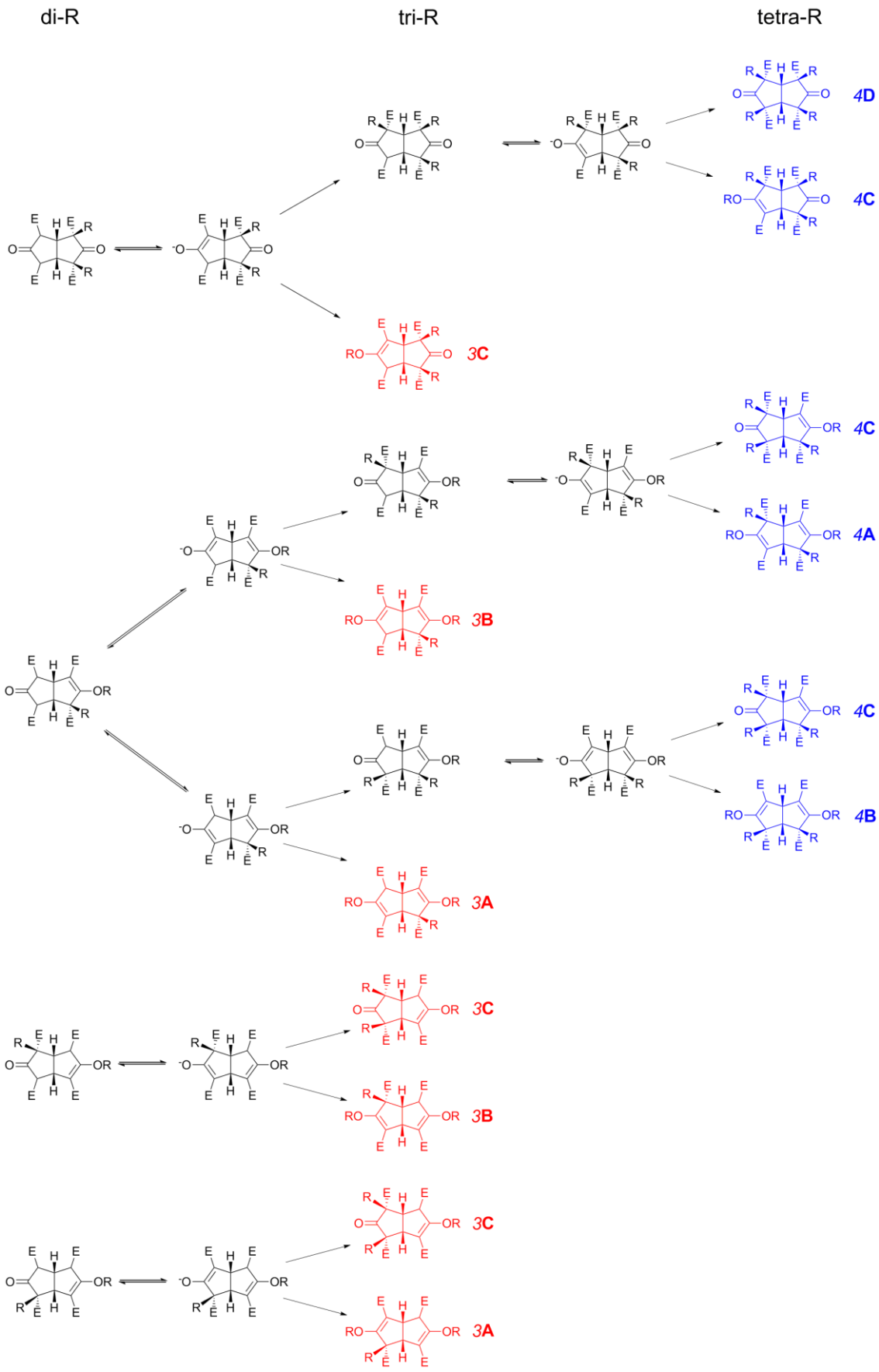

Figure 2.14 Scheme showing the tri- and tetra-substituted stereoisomers formed upon alkylation of products shown in Figure 2.12.

Figures 2.12–2.14 demonstrate that for molecules that undergo reaction until further alkylation is blocked, four tetraalkylated stereoisomers, three trialkylated stereoisomers, and two dialkylated stereoisomers are possible. These account for all of the products, **2.1**–**2.8**. (Only in **2.9** is further alkylation possible, and this molecule has undergone loss of an ester group.)

Of the four tetraalkylated isomers, statistically, *4***A**, *4***B**, *4***C,** and *4***D** occur in a 2:2:7:3 ratio. *4***A**, *4***B**, and *4***C** have the structures of the three tetraethylated products **2.1**, **2.2**, and **2.3** respectively. The total yield of mixed tetraethylated products from the reaction was 72% and of this **2.1**, **2.2**, and **2.3** were isolated in a 1.8 : 1 : 13.6 ratio, indicating that there was almost no regioselectivity to this reaction. In the isopropylation reaction, structures *4***A** and *4***B** are identified in **2.4**, and **2.5** respectively. The complete absence of products with structure *4***D** could be due to a steric barrier to formation from folding all four ester groups into the *endo*- face of the molecule, although this can occur in the methylation reaction. In both cases, the absence of products with structure *4***D** is more likely due to competing *O*-alkylation when using the bulkier alkyls under the conditions employed (*vide supra*), and hence to it being formed in very small amounts (< 0.5%) and hidden in mixed fractions so not being identified.

The ratio of trialkylated terminal products to tetraalkylated terminal products is 11 : 14. The three trialkylated stereoisomers, *3***A**, *3***B**, and *3***C,** form in a 3 : 3 : 5 ratio. The three trialkylated products isolated from the isopropylation reaction, **2.6**, **2.7**, and **2.8**, have structures *3***A**, *3***B**, and *3***C** respectively. The most abundant product was **2.6** (*3***A**, 6% isolated yield), followed by **2.5** (*4***B**, 2%), then **2.7** and **2.8** (*3***B** and *3***C**, both < 1%).

Overall, no regiochemistry is shown for ring-alkylation. With increasing size of electrophile, deactivating *O*-alkylations become more favoured over desirable *C*-alkylation.

2.3.3 Mechanism of deesterification

The products **2.9**, and **2.10**, which bear a methylene non-wing-tip position, have undergone elimination of an ester group. This de-esterification is desired at a later stage. During the alkylation step however, it deactivates the position from undergoing further reactions. The base-catalysed condensation of dimethylcarbonate with ketones to make β-keto esters is well known,[63] and the reverse process present here proceeds with loss of propylmethylcarbonate.

This ester cleavage is known to occur in methanolic sodium ethoxide solutions.[64,65] Indeed the tetraethylester version of Vosser's Red Salt, **2.v**, can be made in this way,[41] and **2.i** undergoes selective elimination of dimethylcarbonate from the 2,6- positions.[20] Addition of a nucleophile directly to the ester requires one of the three groups attached to this carbon to be eliminated (Figure 2.15). Expulsion of the bicyclic ring is made favourable by formation of an enolate. Base-catalysed transesterification does not appear to be significant as no isopropyl esters are detected, indicating elimination of the enolate is favoured over elimination of methoxide. While the initial nucleophilic addition is reversible, the expulsion of propylmethylcarbonate is irreversible once protonation follows. The decarboxylation product can then undergo base-catalysed keto-enol tautomerisation between epimers.

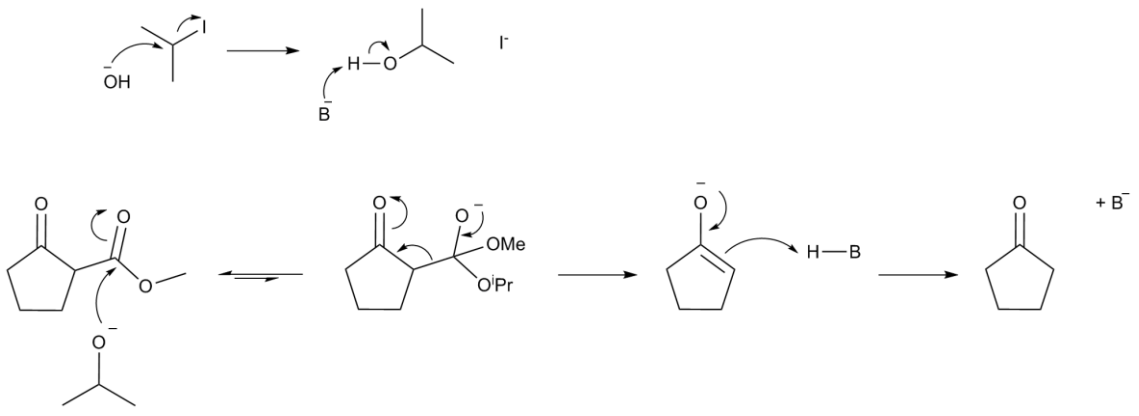

Figure 2.15 Mechanism of de-esterification that takes place to form 2.9 and 2.10.

The source of nucleophile in the reaction of **2.i** with isopropoxyl groups must be either the alkyl halide, or the solvent. The reagents and solvents used in this step were not subjected to drying procedures, so there may be hydroxide ions that can substitute the iodide in ^{i}PrI, which is deprotonated in the presence of the 2.25-fold excess of base.

Protonation must occur faster than the S_N2 reaction with a molecule of alkyl iodide, otherwise one of the protons in the ring methylene group would be replaced by an alkyl group. The pK_{aH} of a keto-enolate is 25.8,[66] *i.e.* a stronger base than anything else in the reaction mixture, so the solvent (acetone, pK_a 19), **2.i** (pK_a 7.8), or intermediate species can all act as proton sources.

2.4 Conclusions

Replacing iodomethane in step two of the permethylpentalene synthesis with RI where R = Et or ^{i}Pr results in formation of a range of products with one, two, or three alkylated ring positions. Eight of these novel products were identified and fully assigned by NMR spectroscopy. The product distribution is solvent dependent, and intermediate alkylated species undergo *O*-alkylation of the enolate, which deactivates the molecule from further reaction. Tetraalkylation of the bicyclic ring is not observed in any of the products when R = Et or ^{i}Pr. In addition, when R = ^{i}Pr, it was found that decarboxylation can occur under the basic reaction conditions used, resulting in a further two novel alkylated species that have been identified and characterised. Subsequent acid hydrolysis of the 2,4,6-triethyl substituted product **2.3**, followed by decarboxylation was effective in producing a 2,4,6-triethyl substituted dione. The intermediate triester-triethyl-dione and decarboxylated product have been characterised. Thus, we have demonstrated that the alkylation reaction employed by O'Hare and coworkers can be used to afford di- and triethylated, and mono-, di- and triisopropylated pentalene precursors.

2.5 References

(1) Cozak, D.; Gauvin, F. *Organometallics* **1987**, *6*, 1912.
(2) Robbins, J. L.; Edelstein, N.; Spencer, B.; Smart, J. C. *J. Am. Chem. Soc.* **1982**, *104*, 1882.
(3) Breuer, R.; Schmittel, M. *Organometallics* **2012**, *31*, 1870.
(4) Alt, H. G.; Köppl, A. *Chem. Rev.* **2000**, *100*, 1205.
(5) Möhring, P. C.; Coville, N. J. *J. Organomet. Chem.* **1994**, *479*, 1.
(6) Möhring, P. C.; Coville, N. J. *Coord. Chem. Rev.* **2006**, *250*, 18.
(7) Wilkinson, G.; Cotton, F. A.; Birmingham, J. M. *J. Inorg. Nucl. Chem.* **1956**, *2*, 95.
(8) Smart, J. C.; Robbins, J. L. *J. Am. Chem. Soc.* **1978**, *100*, 3936.
(9) Connelly, N. G.; Geiger, W. E. *Chem. Rev.* **1996**, *96*, 877.
(10) Gahleitner, M.; Severn, J. R. In *Tailor-Made Polymers*; Severn, J. R.; Chadwick, J. C., Eds.; Wiley-VCH Verlag GmbH & Co. KGaA, 2008; pp. 1–42.
(11) Kaiser, R.; Hafner, K. *Angew. Chem., Int. Ed.* **1970**, *9*, 892.
(12) Kaiser, R.; Hafner, K. *Angew. Chem., Int. Ed.* **1973**, *12*, 335.
(13) Ashley, A. E.; Cowley, A. R.; O'Hare, D. *Eur. J. Org. Chem.* **2007**, *2007*, 2239.
(14) Imamoto, T.; Sugiura, Y.; Takiyama, N. *Tetrahedron Lett.* **1984**, *25*, 4233.
(15) Jencks, W. P.; Regenstein, J. In *Handbook of Biochemistry and Molecular Biology*; Fasman, G. D., Ed.; CRC Press, Cleveland, 1976; pp. 305–351.
(16) Gupta, A. K.; Fu, X.; Snyder, J. P.; Cook, J. M. *Tetrahedron* **1991**, *47*, 3665.
(17) Gupta, A. K.; Sambasivarao, K.; Opansky, B.; Cook, J. M. *J. Org. Chem.* **1990**, *55*, 4480.
(18) Lannoye, G.; Sambasivarao, K.; Wehrli, S.; Cook, J. M.; Weiss, U. *J. Org. Chem.* **1988**, *53*, 2327.
(19) Sieburth, S. M.; Elena Doval, S. *Tetrahedron Lett.* **1994**, *35*, 8127.
(20) Bhatnagar, S. P.; Weiss, U.; Highet, R. J. *J. Org. Chem.* **1977**, *42*, 3089.
(21) Dehmlow, E. V.; Breyholz, H.-J.; Neumann, B.; Stammler, A.; Stammler, H.-G. *Eur. J. Org. Chem.* **2001**, *2001*, 1413.
(22) Ashley, A. E. Permethylpentalene chemistry, DPhil Thesis, University of Oxford, 2006, pp. 200–204.
(23) Mao, C.-L.; Hauser, C. R.; Miles, M. L. *J. Am. Chem. Soc.* **1967**, *89*, 5303.
(24) Wolfe, J. F.; Harris, T. M.; Hauser, C. R. *J. Org. Chem.* **1964**, *29*, 3249.
(25) Sugiyama, N.; Yamamoto, M.; Takano, T.; Kashima, C. *Bull. Chem. Soc. Jpn.* **1967**, *40*, 2909.
(26) Weiler, L. *J. Am. Chem. Soc.* **1970**, *92*, 6702.
(27) Huckin, S. N.; Weiler, L. *J. Am. Chem. Soc.* **1974**, *96*, 1082.
(28) Brieger, G.; Spencer, D. G. *Tetrahedron Lett.* **1971**, *12*, 4585.
(29) Umemura, K.; Matsuyama, H.; Watanabe, N.; Kobayashi, M.; Kamigata, N. *J. Org. Chem.* **1989**, *54*, 2374.
(30) Reeves, C. M.; Stoltz, B. M. In *Asymmetric Synthesis: More Methods and Applications*; Christmann, M.; Bräse, S., Eds.; Wiley-VCH Verlag GmbH & Co. KGaA, 2012; pp. 1–10.
(31) Dolling, U. H.; Davis, P.; Grabowski, E. J. J. *J. Am. Chem. Soc.* **1984**, *106*, 446.
(32) Yamashita, Y.; Odashima, K.; Koga, K. *Tetrahedron Lett.* **1999**, *40*, 2803.
(33) Doyle, A. G.; Jacobsen, E. N. *J. Am. Chem. Soc.* **2005**, *127*, 62.
(34) Balkenhohl, F.; Bohnenpoll, M.; Winterfeldt, E. *Chem. Ber.* **1989**, *122*, 797.
(35) Hore, P. J. In *Nuclear Magnetic Resonance*; Oxford University Press, 1995; p. 38.
(36) Gao, J.; Bhadbhade, M. M.; Bishop, R. *CrystEngComm* **2012**, *14*, 138.
(37) Allen, F. H.; Baalham, C. A.; Lommerse, J. P. M.; Raithby, P. R. *Acta Crystallogr. Sect. B Struct. Sci.* **1998**, *54*, 320.
(38) Le Fèvre, R. J. W.; Radford, D. V.; Stiles, P. J. *J. Chem. Soc. B Phys. Org.* **1968**, 1297.

(39) Banerjee, A.; Dattagupta, J. K.; Saenger, W.; Rabczenko, A. *Acta Crystallogr. Sect. B Struct. Crystallogr. Cryst. Chem.* **1977**, *33*, 90.
(40) Sutor, D. J. *J. Chem. Soc.* **1963**, 1105.
(41) Tanaka, S. *J. Am. Chem. Soc.* **1958**, *80*, 5264.
(42) Sambasivarao, K.; Kubiak, G.; Lannoye, G.; Cook, J. M. *J. Org. Chem.* **1988**, *53*, 5173.
(43) Lannoye, G.; Cook, J. M. *Tetrahedron Lett.* **1987**, *28*, 4821.
(44) Knölker, H.-J.; Winterfeldt, E. *Liebigs Ann. der Chemie* **1986**, *1986*, 465.
(45) Bertz, S. H.; Lannoye, G.; Cook, J. M. *Tetrahedron Lett.* **1985**, *26*, 4695.
(46) Karplus, M. *J. Am. Chem. Soc.* **1963**, *85*, 2870.
(47) Karplus, M. *J. Chem. Phys.* **1959**, *30*, 11.
(48) Abraham, R. J.; Hall, L. D.; Hough, L.; McLauchlan, K. A. *J. Chem. Soc.* **1962**, 3699.
(49) Djaidi, D.; Bishop, R.; Craig, D. C.; Scudder, M. L. *New J. Chem.* **2002**, *26*, 614.
(50) Camps, P. *Tetrahedron Lett.* **1974**, *15*, 4067.
(51) Vega, A.; Donoso-Tauda, O.; Ibañez, A.; Escobar, C. A. *Acta Crystallogr. Sect. C Cryst. Struct. Commun.* **2008**, *64*, o199.
(52) Bertz, S. H.; Rihs, G.; Woodward, R. B. *Tetrahedron* **1982**, *38*, 63.
(53) Vaughan Williams, R.; Gadgil, V. R.; Vij, A.; Cook, J. M.; Kubiak, G.; Huang, Q. *J. Chem. Soc. Perkin Trans. 1* **1997**, 1425.
(54) Rhoads, S. J.; W. Hasbrouck, R.; Pryde, C.; Holder, R. W. *Tetrahedron Lett.* **1963**, *4*, 669.
(55) Yoffe, S. T.; Vatsuro, K. V.; Kugutcheva, E. E.; Kabachnik, M. I. *Tetrahedron Lett.* **1965**, *6*, 593.
(56) Brieger, G.; Pelletier, W. M. *Tetrahedron Lett.* **1965**, *6*, 3555.
(57) Kurz, A. L.; Beletskaya, I. P.; Macías, A.; Reutov, O. A. *Tetrahedron Lett.* **1968**, *9*, 3679.
(58) Le Noble, W. J.; Morris, H. F. *J. Org. Chem.* **1969**, *34*, 1969.
(59) House, H. O. *Modern Synthetic Reactions*; Benjamin, W. A., Ed.; 2nd ed.; W.A. Benjamin: Menlo Park, CA, 1972; pp. 492–628.
(60) Snyder, L. R. *J. Chromatogr.* **1978**, *92*, 223.
(61) Smith, M. B. In *Organic Chemistry: An Acid-Base Approach*; CRC Press, 2011; pp. 1119–1192.
(62) Kurts, A. L.; Genkina, N. K.; Macias, A.; Beletskaya, L. P.; Reutov, O. A. *Tetrahedron* **1971**, *27*, 4777.
(63) Wallingford, V. H.; Homeyer, A. H.; Jones, D. M. *J. Am. Chem. Soc.* **1941**, *63*, 2252.
(64) Cope, A. C.; McElvain, S. M. *J. Am. Chem. Soc.* **1932**, *54*, 4319.
(65) Connor, R. *J. Am. Chem. Soc.* **1933**, *55*, 4597.
(66) Bordwell, F. G.; Fried, H. E. *J. Org. Chem.* **1991**, *56*, 4218.

Chapter 3 SYNTHESIS, STRUCTURE, MAGNETIC STUDIES AND REACTIVITY OF AN ELUSIVE DIIRON COMPOUND

3.1 Introduction

As described in Chapter 1, linked ferrocenes, the simplest of which are bisfulvalene diiron and biferrocene, have found many applications.

King's original report on decamethylferrocene alludes to "several failures" in attempts to obtain $FeCp^*_2$ from ferrous chloride ($FeCl_2$) and LiCp*.[1] The reported procedure involves boiling ferric chloride ($FeCl_3$) and iron in THF to make the $FeCl_2$ before reaction with LiCp*. The linked diiron complex bisfulvalene diiron can similarly be made by reaction of the fulvalene dianion with $FeCl_2$.[2]

In an η^5-haptic bonding mode, pentalene can donate up to five electrons to each coordinated metal (NB neutral counting scheme employed throughout). Intuitively therefore, it may be expected that the bimetallic compounds Fe_2Pn_2 and $Fe_2Pn^*_2$ would be stable bis-18 valence electron (VE) complexes, achieving two ferrocene-like configurations. Katz *et al.* employed a reaction analogous to King's, combining ferrous chloride with dilithium pentalenide (Li_2Pn) in search of the species Fe_2Pn_2. However, this yielded only the monometallic compound Fe(η^5,η^5-Pn_2), in which two Pn ligands have formed an *ansa* bridge, with a new C–C bond between pentalene ligands (Scheme 3.1 a).[3,4] O'Hare and co-workers reported similar attempts to make the permethylated analogue, $Fe_2Pn^*_2$. Reactions between $FeCl_2$ solvates and Li_2Pn^*, or with the softer $(SnMe_3)_2Pn^*$ reagent, resulted in the isolation of metallic iron, and intractable solids containing the permethylpentalene dimer, Pn^*_2 (Scheme 3.1 b).

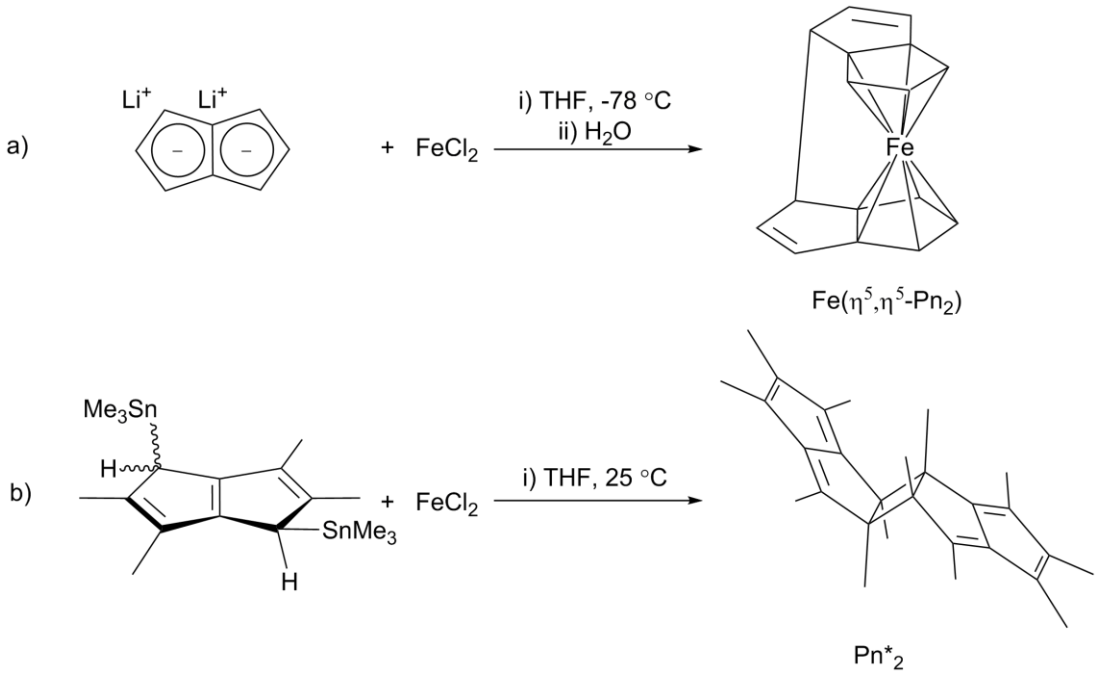

Scheme 3.1 Synthesis of a) the mono-iron compound Fe(Pn$_2$) and b) dimer Pn*$_2$.

In Katz's monometallic Fe(η^5,η^5-Pn$_2$) there is significant tilting of the ligands, with a centroid–Fe–centroid angle of 161.7(3)°.[4] It was postulated that the methyl groups of Pn* would be able to preclude formation of a single C–C bond, and stabilisation of the unstable 'diradical' Fe(Pn*)$_2$ might still be achieved by coordination to a second iron(II) cation. O'Hare and co-workers studied the supposed intermediates for formation of a Pn* analogue of Katz's Fe(η^5,η^5-Pn$_2$), and found the sterically forced parallel arrangement of the ligands prevents close contact between the ring carbon atoms of the Pn* skeleton. The closest approach between carbon atoms in the C_2 chiral structure Fe(Pn*)$_2$ was calculated to be 3.61 Å, *i.e.* much longer than the 1.59 Å C–C bond in Fe(Pn$_2$). The HOMO calculated for Fe(Pn*)$_2$ is concentrated on both the iron atom and on the uncoordinated ring in the correct positions to form an *ansa*-bridge, however, the large separation ultimately precludes this C–C bond formation. Unable to form a C–C bond, it is postulated that the (unobserved) Fe(Pn*)$_2$ would therefore exist transiently as an unstable diradical, with a propensity to reduce iron(II) to iron(0), leaving two neutral Pn* molecules. Following the elimination of neutral iron, the neutral Pn* molecules can approach more closely and dimerise in a [2+2] cycloaddition.

The hypothetical Fe_2Pn_2 complex has a total number of electrons (TNE) count of 32.[5] The only known bisfulvalene dimetal complex that falls into this class is bisfulvalene dichromium.[6–8] The 34 TNE manganese equivalent has not been reported, nor its 32 TNE dication, and the fused 32 TNE metallocene *anti*-$(MnCp)_2Pn$ not known. The *syn*-facially coordinated sandwich complexes $Mn_2Pn^*_2$ and $Co_2Pn^*_2$ do exist, but in electrochemical studies, neither the 32 TNE dianion $[Mn_2Pn^*_2]^{2-}$ nor the dicationic $[Co_2Pn^*_2]^{2+}$ were found to form within the solvent window.[9] Similarly, while *anti*-coordinated $(FeCp^*)_2Pn$ is known, the dication $[(FeCp^*)_2Pn]^{2+}$ has not been reported.[10] These absences offer some insight to the elusiveness of a diiron bispentalene molecule thus far.

3.2 Synthesis of $Fe_2Pn^*_2$, **3.1**

A red-orange solution of $Fe(acac)_2$ in THF was reacted with Li_2Pn^* at room temperature, with an immediate colour change to black. After removal of the solvent and drying overnight, a purple-brown solution was extracted from the crude black residue with benzene. A purple-black microcrystalline powder was recrystallised in 23% yield from a saturated benzene solution stored at 9 °C, and gave a satisfactory elemental analysis for $Fe_2Pn^*_2$, **3.1** (Scheme 3.2). This modest yield is much higher than those reported by Katz *et al.* in the synthesis of Ni_2Pn_2 and Co_2Pn_2,[3,11] and similar to the yields for other first row $M_2Pn^*_2$ complexes (7 – 55%).[9]

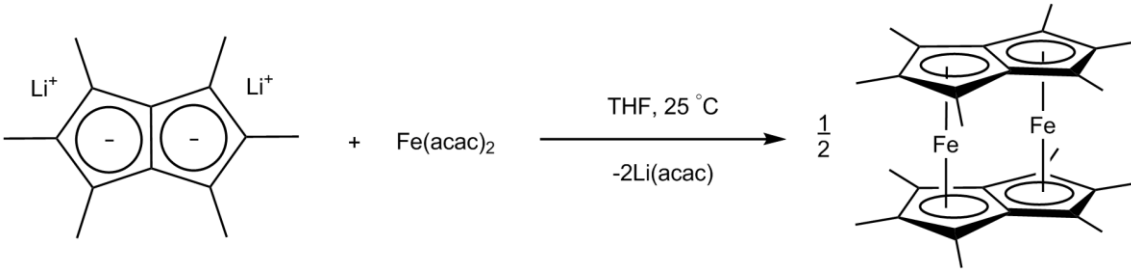

Scheme 3.2 Synthesis of $Fe_2Pn^*_2$, 3.1

3.2.1 Optimisation

The reaction proceeds cleanly to produce a single product, and very pure samples of $Fe_2Pn^*_2$ gave lilac solutions. However, the high solubility of the Li(acac) byproduct in organic solvents hampered isolation of the uncontaminated product in high yields. Attempts to purify batches by sublimation at 10^{-2} mbar and temperatures of 120 °C (the conditions used to isolate $FeCp^*_2$[1]), resulted in collection of a red crystalline powder that contained no **3.1**. To avoid this product degradation, the dried crude residue was subjected to a 10^{-7} mbar vacuum in an attempt to separate either the product, or the lithium acetylacetonate byproduct (m.p. 250 °C, 1 atm), however neither sublimed at temperatures between 20 and 60 °C.

It was found that **3.1** precipitates from toluene solutions at −35 °C as a dark red solid that is subsequently extremely insoluble in toluene, even at elevated temperatures. Concentration of solutions in hexane results in a small amount of decomposition, with observation of a thin metal film on the glass, and it was concluded that extraction into hot benzene (rather than boiling toluene or hexane) resulted in higher isolated yields, free from contamination by Li(acac) (as assessed by ^{7}Li NMR spectroscopy) and metallic iron impurities (assessed by the absence of hysteresis during isothermal field sweeps measuring magnetic susceptibility). Lithium acetylacetonate coprecipitates from toluene or hexane solutions at −35 °C; however, crystallisation from concentrated benzene at 9 °C gave clean batches of **3.1** (23% yield).

3.3 NMR characterisation of $Fe_2Pn^*_2$

Two broad resonances indicate D_{2h} symmetry in solution. The resonances could be assigned to the wing-tip methyl protons (−89.10 ppm in toluene-d_8), and non-wing-tip methyl protons (12.04 ppm) based on their relative intensities. Despite wide ranging ^{13}C NMR scans and 2D experiments employing a variety of acquisition times and recovery delays, only one of five expected ^{13}C resonances could be located, at

–199.7 ppm, and the assignment of this resonance is therefore ambiguous. Large contact shifts are common for paramagnetic metallocenes and decamethylmetallocenes.[12]

3.4 Crystallographic characterisation of $Fe_2Pn^*_2$

Intensely red crystals of $Fe_2Pn^*_2$ were grown from a slowly evaporated THF solution. The molecules crystallise in the triclinic $P\bar{1}$ space group, with one bimetallic molecule in the unit cell (Figure 3.1). An inversion centre is located between the two iron atoms, and the true molecular symmetry of each molecule in the solid state is C_i (lower than the D_{2h} or C_{2v} probed by DFT), resulting from slightly differing coordination to each of the two five-carbon rings.

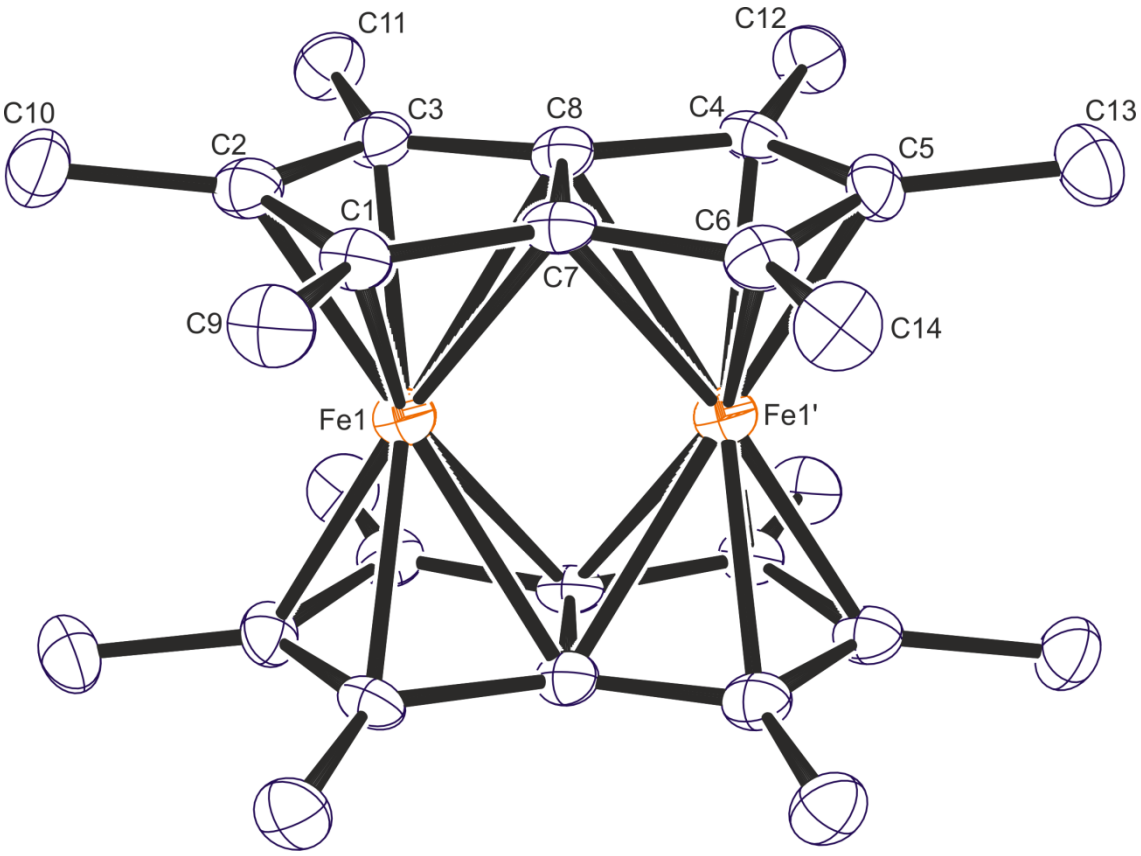

Figure 3.1 Molecular structure of $Fe_2Pn^*_2$, 3.1. Ellipsoids shown at the 50% probability level. Carbon atoms are shown in blue, and iron atoms in orange. Hydrogen atoms have been omitted for clarity.

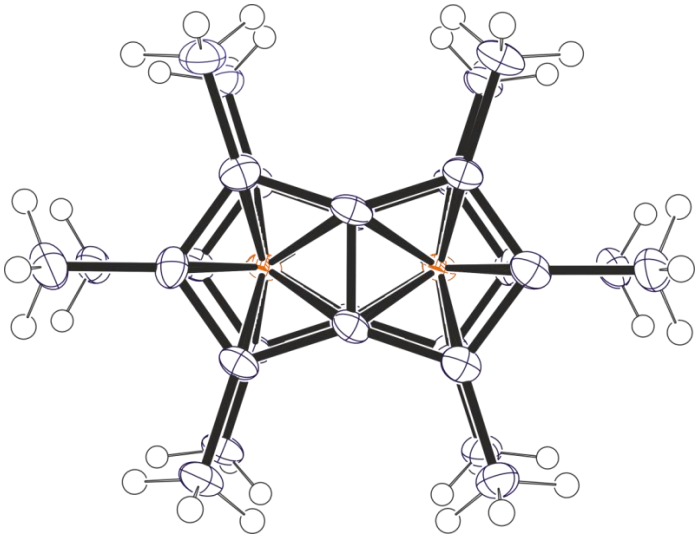

Figure 3.2 Plan view of $Fe_2Pn^*_2$, 3.1.

Table 3.1 Selected bond lengths, distances, and angles for $Fe_2Pn^*_2$, 3.1. Structural parameters calculated with D_{2h} symmetry are shown in *italics*.

Bond lengths and distances (Å)		
Fe1–Fe1'	2.3175(9)	*2.36*
Fe1–Pn^*_{cent}	1.737(2), 1.736(2)	*1.76*
Fe1–C1	2.070(4)	*2.09*
Fe1–C2	2.057(4)	*2.07*
Fe1–C3	2.078(5)	
Fe1–C4	2.083(5)	
Fe1–C5	2.041(4)	
Fe1–C6	2.067(4)	
Fe1–C7	2.210(4), 2.217(4)	
Fe1–C8	2.215(4), 2.222(5)	
C1–C2	1.451(8)	*1.45*
C2–C3	1.445(6)	
C3–C8	1.438(7)	
C4–C5	1.442(8)	
C5–C6	1.439(6)	
C6–C7	1.456(7)	
C7–C8	1.438(7)	*1.45*
C1–C7	1.446(5)	*1.46*

Angles (°)		
Pn^*_{cent}-Fe1-Pn^*_{cent}	168.99(10)	
Hinge angle	5.87, 6.96	*1.54*
Fold angle	0.8(3)	*1.53*

Hinge angle = mean angle between least square mean planes of C1,7,8,3 and C1,2,3, and of C6,7,8,4 and C4,5,6; Fold angle = angle between mean planes of C1,2,3,8,7 and C4,5,6,7,8.

Ring slippage (Å)	
Fe1-C1,2,3,7,8	0.173
Fe1-C4,5,6,7,8	0.186
δ (%)	8.07

$\delta(\%) = \frac{[(M-C4)-(M-C2)]}{(M-C2)} \times 100$

The distances between the iron atoms and the centroid of the five-membered rings of Pn* (*i.e.* Fe—Pn^{*}_{cent}) of 1.736(2) and 1.737(2) Å, are intermediate between the 1.78 Å M—centroid distance found in the 16 VE monometallic $CrCp^{*}_{2}$,[13] and the 1.66 Å in $FeCp^{*}_{2}$.[14] Iron–carbon bond lengths ranging from 2.041(4) Å to 2.083(5) Å are more similar to the Fe—$\underline{C}_5H_5$ distances than to the Fe—$\underline{C}_5F_5$ distances in pentafluoroferrocene (mean values of 2.05 and 2.00 Å respectively).[15]

The two C_8 ligand planes lie parallel to each other (fold angle 0.8(3)°), as has been found for all other M_2Pn_2 complexes except $Ti_2Pn^{(1,4\text{-}Si^{i}Pr_3)}{}_2$.[9] Within each C_5 ring however, deviation from planarity is seen in the hinge angles (Figure 3.3). When complexes undergo ring-slippage, this may or may not be accompanied by a folding of the ring of the C_5 ligand.[16] In pentalene complexes, the hinge angle is defined as the mean angle between the least squares mean plane (LSMP) of the bridgehead and non-wing-tip carbons and the LSMP of the non-wing-tip and wing-tip carbons (see Figure 3.3) and in **3.1** has values of 6.96° and 5.87°. These are larger than the 1.54° hinge angle predicted by DFT geometry optimisation, and consistent with a trend observed on crossing the symmetrically substituted $M_2Pn^{*}_{2}$ series: decreasing from 9.30 and 9.11° for $Cr_2Pn^{*}_{2}$, to 8.21 and 7.85° for $Mn_2Pn^{*}_{2}$, to those observed for **3.1**, then to 3.25 and 3.68° in the dinickel complex $Ni_2Pn^{*}_{2}$. The cobalt complex has mixed η^3 and η^5 coordination modes and thus anomalous hinge angles. The shift towards η^3 coordination meanwhile of 8.07% for $Fe_2Pn^{*}_{2}$ is very close to the 9% predicted for Fe_2Pn_2.[5]

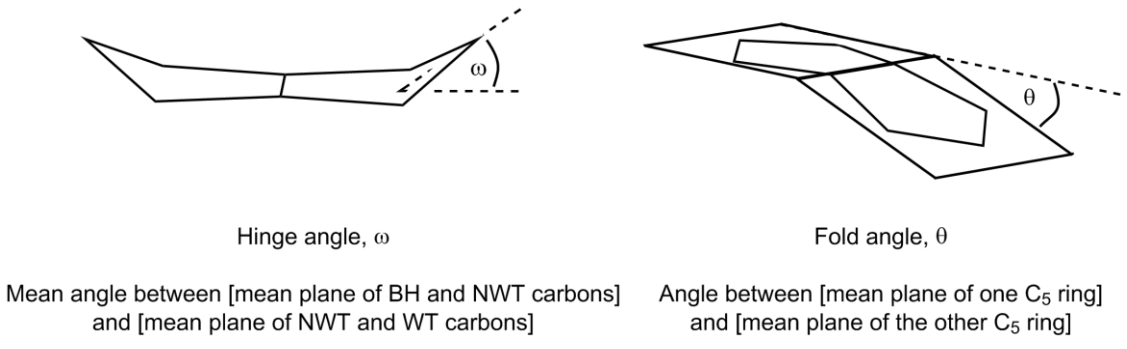

Figure 3.3 Definitions of hinge and fold angles in pentalene complexes.

Table 3.2 M—M bond distances in first row M_2Pn_2 complexes.

M	M—M bond length (Å)	Bond order (exp/*pred*)	Ref
$Ti_2Pn^{(1,4\text{-}Si^iPr_3)}{}_2$	2.399(2)	2	17
$V_2Pn^*{}_2$	2.169(1)	3 *2.83*	9
$Cr_2Pn^*{}_2$	2.150(1)	2 *1.98*	9
$Mn_2Pn^*{}_2$	2.277(1)	1 *1.13*	9
$Fe_2Pn^*{}_2$	2.3175(9)	0 *0.26*	*This work*
$Co_2Pn^*{}_2$	2.491(2)	0 *–0.59*	9
$Ni_2Pn^*{}_2$	2.569(1)	0 *0.03*	9

As each Pn* ligand donates two fewer electrons than a fulvalene ligand, the isoelectronic linked metallocene analogue is bisfulvalene dichromium, which has not been structurally characterised. Bisfulvalene diiron however has an Fe—Fe distance of 3.984(4) Å,[18] while in **3.1** the metal-metal distance of 2.3175(9) Å is lower than the sum of radii in metallic iron (2.52 Å in a 12-coordinate environment),[19] and thus within the range for metal-metal bonding. A diiron bond was reported over the much longer distance of 2.686(1) Å for the *syn*-coordinated diiron complex $[Fe_2(\mu\text{-}X)(CO)_4(\mu\text{-}\eta^5,\eta^5\text{-}C_8H_8)]$, (X = C(OR)Ar or CAr 'carbyne');[20] however, the rigid structure of the Pn* ligands forces *syn*-sandwiched metal atoms to be held in proximity, and hence the metal–metal distance is not a good indicator of bond formation. A fragment analysis was conducted as part of DFT calculations,[21,22] affording a decomposition of the bonding in terms of the population of MOs of the Fe_2 dimer and the Pn* ligand and enabling an estimation of the Fe–Fe bond order. The result was an order of 0.26 implying a weak, net favourable interaction between the two Fe atoms.

3.5 Magnetic characterisation

When two or more unpaired spins within a system interact with each other, they are said to be 'exchange coupled' to one another. To model this exchange coupling, we can use the Heisenberg-Dirac-Van Vleck (HDVV) Hamiltonian,[23] which defines the exchange interaction between spin *i* and spin *j*:

$$\hat{\mathrm{H}}_{ij} = -2J_{ij}\hat{\mathrm{S}}_i \cdot \hat{\mathrm{S}}_j$$

The spin angular momentum operators indicate that the exchange interaction results from the coupling between two electron spin angular momentums. The expectation value of $\hat{\mathrm{H}}_{ij}$ gives the energies, E_{ij}, of the various coupled states that can result from two interacting spins. The magnitude of the difference in energies between states of different multiplicity, ΔE, depend on the exchange parameter, J_{ij}, *i.e.* on the strength of the interaction between unpaired spins.

Two spins that couple ferromagnetically (*i.e.* $S_{tot} = 1$), result in a triplet state with $E_{ij} = -J_{ij}/2$, while if spins couple antiferromagnetically (*i.e.* a singlet), $S_{tot} = 0$, and $E_{ij} = 3J_{ij}/2$. The singlet-triplet gap between the singlet and the triplet states is given by $E_{singlet} - E_{triplet} = \Delta E = 2J_{ij}$, so when $J_{ij} > 0$, the singlet state is higher in energy than the triplet, when $J_{ij} < 0$, the singlet state is lower in energy than the triplet (Figure 3.4).

It is important to note the sign of J_{ij} as defined in the Hamiltonian. For a system described by the HDVV equation above, when $J_{ij} > 0$, the coupling between spin i and spin j is, by definition, ferromagnetic. Conversely when $J_{ij} < 0$, the coupling between

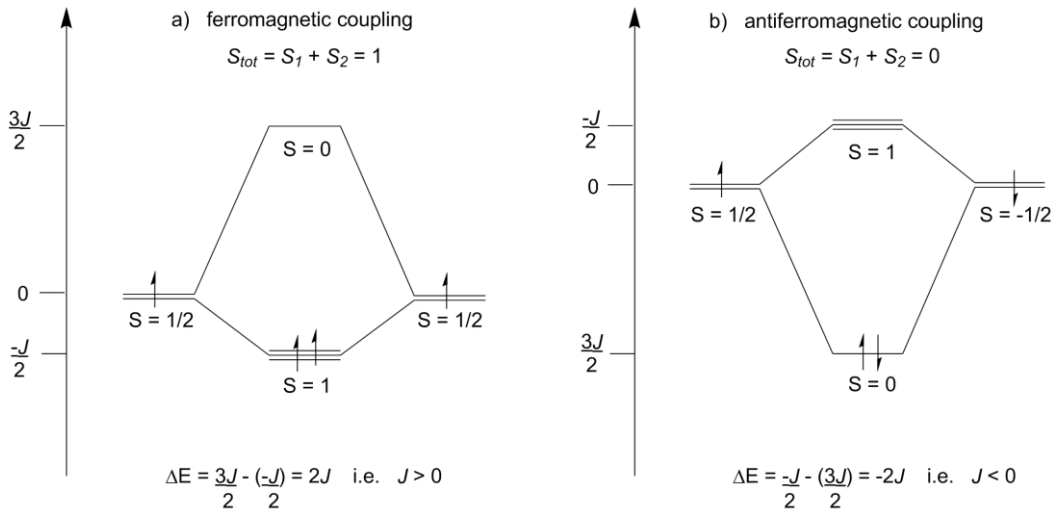

Figure 3.4 a) Ferromagnetic and b) antiferromagnetic coupling of unpaired electrons, as defined by the Heisenberg-Dirac-Van Vleck equation.

spin *i* and spin *j* is antiferromagnetic.

3.5.1 Solution studies

The bulk magnetic susceptibility of a 12 mM solution of **3.1** in toluene was measured on a 500 MHz spectrometer at 353 K using the Evans' method,[24] and resulted in an effective magnetic moment of 3.4 μ_B per molecule. This is higher than the spin-only value of 2.83 μ_B expected for a triplet, and the 2.44 μ_B for two spin-only non-interacting doublets, indicating that unquenched orbital angular momentum contributes to the magnetic moment of $Fe_2Pn^*_2$.

A variable temperature ^{1}H NMR study revealed a temperature dependence for the methyl ^{1}H resonances between −70 °C and 50 °C (Figure 3.5). The resonance for the wing-tip methyl protons underwent a very large change in shift of over 50 ppm in magnitude and opposite in sign to the non-wing-tip methyl group, which varied by only 19 ppm over the same range.

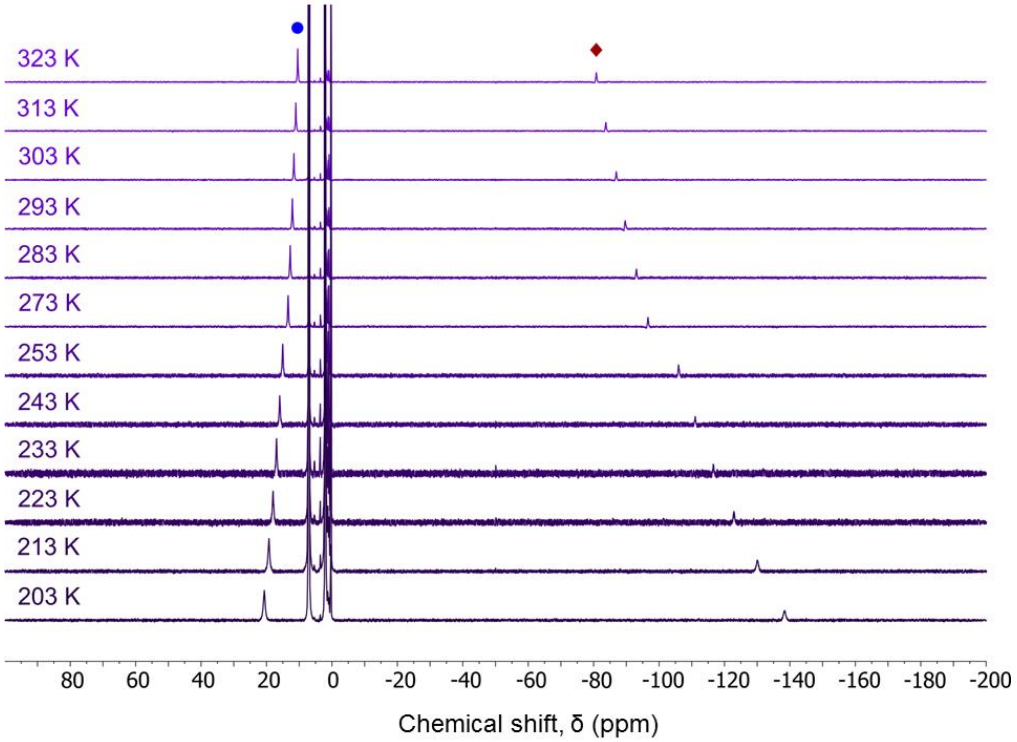

Figure 3.5 Variable temperature ^{1}H NMR stack plot for paramagnetic $Fe_2Pn^*_2$, 3.1, in toluene-d_8. ● indicates the resonance attributed to the non-wing-tip (NWT) methyl protons, and ◆ to the wing-tip (WT) methyl protons.

A plot of shift *vs* T^{-1} demonstrates a linear relationship (Figure 3.6), signifying simple Curie magnetism between 203 and 323 K. The linear fit can be described by the equation:

$$\delta(T) = \delta_0 + \delta_P \cdot m(T)$$

where $\delta(T)$ is the chemical shift at temperature T, δ_0 gives the chemical shift of each proton in the high temperature limit, $m(T)$ describes the temperature dependence of the magnetic susceptibility, and δ_p is a constant that relates this behaviour to the effect it has on a given chemical shift.[25] For a Curie paramagnet, the magnetisation, $m(T)$, is proportional to T^{-1}, as increasing temperature causes thermal motion, which disrupts the coupling between the moments of solvated molecules and an applied field, which in turn causes the magnetisation measured to decrease.[26] The Curie model assumes there is no intermolecular coupling present.[26]

Fermi contact shifts in metallocenes are generally much larger than pseudo-contact shifts.[27,28] However, chromocenes and ferrocenium cations have orbitally degenerate ground states and large g-anisotropy ($g_{\parallel} = 4.35$ and $g_{\perp} = 1.26$ for

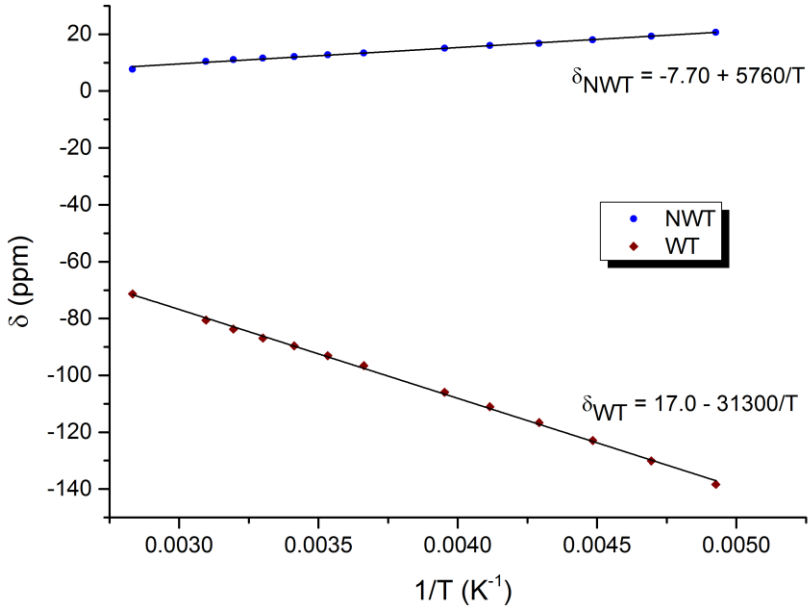

Figure 3.6 Plot of chemical shift against inverse temperature for 3.1 in toluene-d_8 solution.

$[FeCp_2]^+$),[29] and it has been postulated that for these, the isotropic shift may be solely pseudo-contact in origin.[29,30] The parameter δ_p has values of 5,760 for the NWT methyl protons of **3.1**, and −31,300 for the WT protons. The difference in magnitude and sign indicate the isotropic shifts have very different temperature dependencies in the two different methyl environments, and is discussed in more depth in Chapter 4.

3.5.2 Solid state studies

The temperature dependence of the magnetic susceptibility of **3.1** in the solid state was measured between 5 and 300 K. Mass magnetic susceptibilities were field corrected and multiplied by the relative molecular mass of $Fe_2Pn^*_2$, before correcting for the underlying diamagnetism of the sample using Pascal's constants.[31] This results in a magnetic susceptibility and effective magnetic moment calculated per mole of $Fe_2Pn^*_2$ molecules (which contains two moles of iron atoms).

Magnetic susceptibility data sets measured for a zero-field cooled and field cooled sample of $Fe_2Pn^*_2$ coincide exactly, indicating the absence of long-range interactions between spins. A plot of χ_{mol}^{-1} *vs* T gives a straight line (Figure 3.7), with

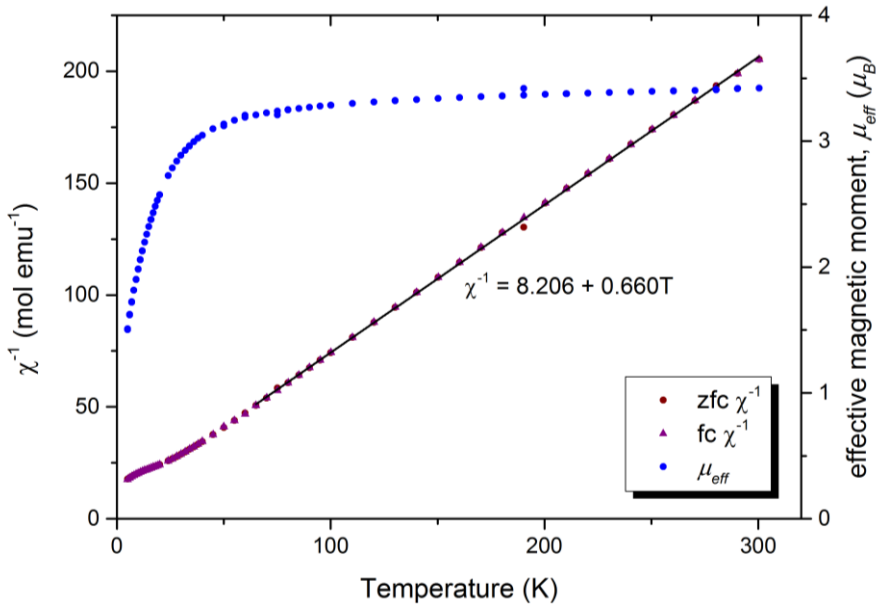

Figure 3.7 Plot of effective magnetic moment and inverse magnetic susceptibility for $Fe_2Pn^*_2$, 3.1, between 5 and 300 K.

small deviation below 32 K. $Fe_2Pn^*_2$ therefore displays Curie paramagnetism above *circa* 60 K in the solid state, and can be fit to the inverted Curie-Weiss Law:

$$\chi^{-1} = \frac{T - \theta}{C}$$

The small, negative Weiss temperature (θ) of −12.3 K indicates a weak, antiferromagnetic intermolecular interaction between molecules at low temperature. The gradient of the line fitted between 65 and 300 K gives a Curie constant (C) of 1.51, which is related to the effective magnetic moment by the following equation:

$$C = \chi_{mol}T = \frac{N_{Av}g^2S(S+1)\mu_B^2}{3k} = \frac{N_{Av}\mu_{eff}^2}{3k}$$

yielding the effective magnetic moment:

$$\mu_{eff} = g\sqrt{S(S+1)}\mu_B = \sqrt{8\chi_{mol}T}$$

Using the gradient of the plot in Figure 3.7, the effective magnetic moment calculated for **3.1** at 298 K is 3.48 μ_B. This is in good agreement with plotted μ_{eff} (Figure 3.7). The small increase from 3.19 μ_B at 60 K to 3.42 μ_B at 300 K is due to the smaller influence of the θ value at higher temperature. These values are also in good agreement with the μ_{eff} obtained from solution studies (Section 3.5.1).

Bimetallic iron complexes with a triplet ground state are relatively rare,[32] and the ground state paramagnetism exhibited by 32 TNE $Fe_2Pn^*_2$ contrasts with the linked metallocene analogue bisfulvalene dichromium, which is diamagnetic.[33] All the neutral *syn*-diiron complexes of cyclooctatetraene, $[Fe_2(\mu\text{-}C(OR)R)(CO)_4(C_8H_8)]$, also contain longer Fe—Fe distances but Fe—Fe bonds, and are diamagnetic.[20,34,35]

3.6 DFT study

Quantum chemical calculations were performed by Professor J. C. Green using the Amsterdam Density Functional package using density functional methods with a BP functional and triple-zeta Slater type basis orbitals.[36–38] The geometry of **3.1** was optimised with singlet, triplet and quintet spin states, the lowest energy confirming a

triplet ground state. No symmetry was used in the optimisation but the result was a structure of D_{2h} symmetry, confirmed as a minimum by a frequency calculation. The Fe—Fe distance calculated using this method is 2.357 Å, *i.e.* longer than the 2.3175(9) Å found experimentally.

Calculated structural parameters for the D_{2h} structure are given in Table 3.1, alongside the corresponding crystallographically determined values. Overall the calculated values are in reasonable agreement with the experimental results. The C—C distances of the rings are all very similar, reflecting the fact that bonding to the iron atoms does not disrupt the aromaticity of the ligand. Thus the shift of the metal atoms towards the wing-tip hydrogens is not well described by an allylic coordination. The metals are bonded to the bridging carbons and there is no double bond localised across the bridgehead of the Pn* ligand.

The first excited singlet state is calculated to lie 0.48 eV above the triplet state. This is consistent with the 0.51 eV gap predicted for Fe_2Pn_2.[5] An energy difference of 0.48 eV corresponds to a 3.2 ppb population of the excited state at 298 K, therefore population of this level is not significant enough to affect the magnetic susceptibility of $Fe_2Pn^*_2$. This energy gap is very large, and corresponds to a 2*J* splitting of 3870 cm^{-1}, or 46 kJ mol^{-1}. Population of thermally accessibly excited states would be expected if energy differences were on the order of magnitude of the thermal energy, *kT*, *i.e.* 210 cm^{-1} at 298 K (*i.e.* 0.026 eV, or 2.5 kJ mol^{-1}). Energy differences on this order of magnitude would be expected for exchange coupled systems containing unpaired spins that interact, suggesting that in $Fe_2Pn^*_2$ the two spins are strongly coupled. It was found that the lowest lying quintet configuration is 0.73 eV higher in energy than the triplet.

The molecular orbital diagram for $Fe_2Pn^*_2$ was first published in 2008,[9] and is reproduced in Figure 3.8 along with the principle levels involved in bonding and key orbitals. The two highest occupied orbitals are the half populated, metal based $12b_{2g}$ and $10b_{3g}$ levels, displaying d_{yz} and d_{xz} character respectively (when the *xz* plane reflects one

Pn* ligand onto the other, and contains both iron atoms, the line between which defines the *z* direction). These two orbitals are effectively degenerate.

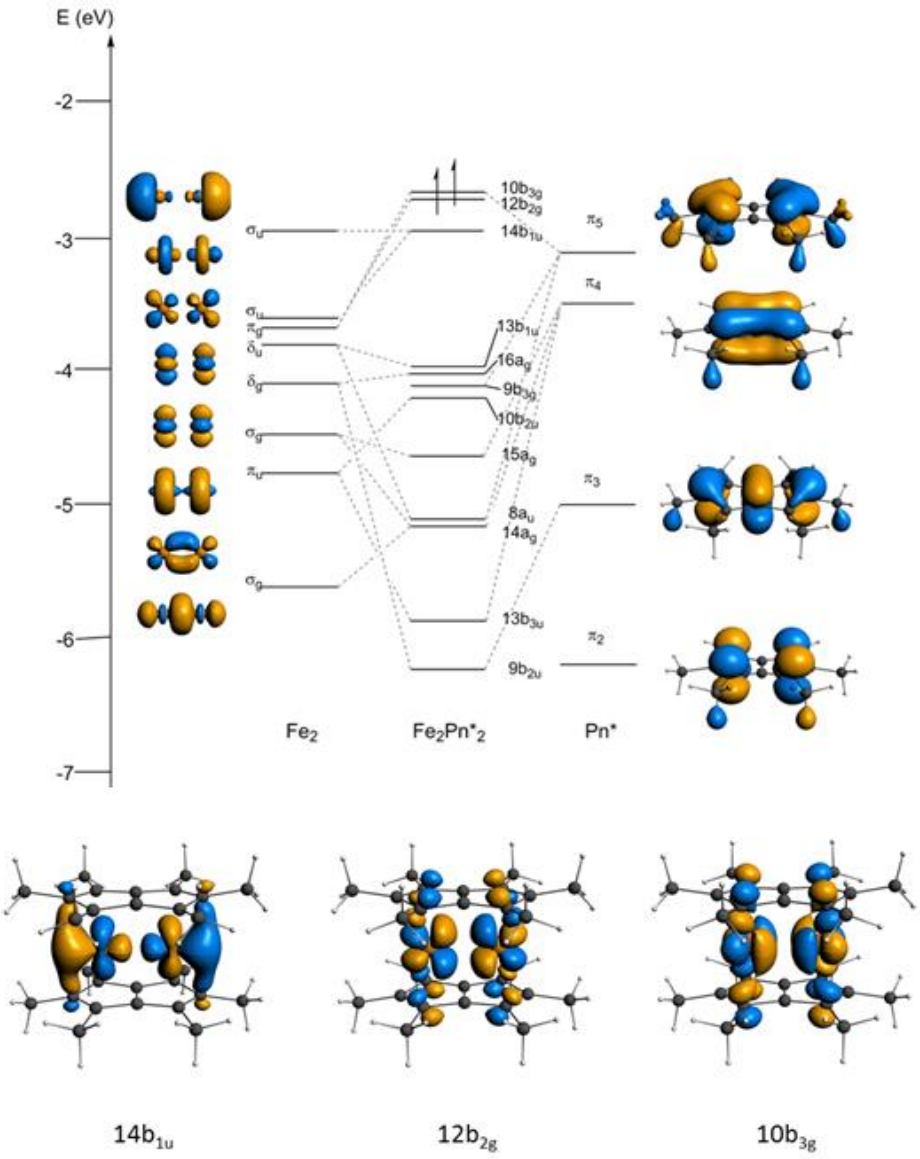

Figure 3.8 MO scheme for $Fe_2Pn^*_2$, 3.1 (D_{2h} symmetry) showing the principle levels involved in M-L bonding with the two SOMOs indicated (top); selected Kohn-Sham orbitals (bottom).

The two singly occupied molecular orbitals (SOMOs, $12b_{2g}$ and $10b_{3g}$) and the highest fully occupied orbital ($14b_{1u}$), depicted in Figure 3.8, all have Fe–Fe antibonding character.

The magnetic data indicates an orbital contribution to the magnetic moment, and this is supported by the MO analysis which indicate the SOMOs have metal-*d* character,

and therefore the orbital angular momentum of electrons in these orbitals is significantly unquenched, and hence μ_{eff} is greater than the spin-only predicted value.

Table 3.3 Calculated spin densities for $Fe_2Pn^*_2$ by Mulliken population analysis.

	Metal	Ring C	Methyl C	Methyl H	Mean H
Fe	1.1				
Non-wing-tip		0.0143	−0.0005	0.0017	0.0001
				−0.001	
				−0.0005	
Wing-tip		−0.046	0.0047	−0.0004	-0.0017
				−0.0004	
				−0.0043	
Bridgehead		−0.0328			

The spin densities calculated for the atoms are shown in Table 3.3. Both the singly occupied orbitals have positive spin density at the non-wing-tip ring positions of Pn*, reflecting their contribution to the $10b_{3g}$ and $12b_{2g}$ levels. However spin polarisation around the ring results in greater absolute spin density on the wing-tip carbons of opposite sign. The net spin density transmitted to the attached methyl hydrogens is of the same direction as the ring carbons. Thus, if the observed isotropic NMR shifts are dominated by the contact interaction,[27,28,39] the fact that the wing-tip protons experience an upfield shift that is greater than the downfield shift of the non-wing-tip hydrogens is in agreement with the calculation.

The calculated μ_{eff} of 3.4 μ_B for **3.1** is high for a triplet, and consistent with the absence of an Fe—Fe bond. The two SOMOs of the triplet state both possess significant Fe *d* contributions, and this could be the source of large, unquenched orbital contributions to the magnetic moment in solution. In a system with two unpaired spins, it may be expected they interact through an exchange interaction, as discussed for the systems $(NiCp^*)_2Pn^*$ and $(NiCp)_2Pn^*$ in Chapter 4. Exchange interactions typically give

rise to thermally accessible excited states, yet there are no significantly populated excited states in this molecule over the temperature ranges studied. Two reasons for this are possible: either (1) the two unpaired electron spins in **3.1** have no interaction at all, or (2) they have an incredibly strong ferromagnetic interaction, such that $|2J| \gg kT$, and the ground state is a triplet. The latter is more likely, as the SOMOs with b_{2g} and b_{3g} symmetry both have a *z*-component, so have appropriate symmetry to mix with each other.

A large zero-field splitting could therefore account for the deviation from the Curie Law at low T. This would cause depopulation of the highest energy *J*-states of the triplet at very low temperatures.

3.7 EPR

EPR spectra recorded at 300, 40, 15, and 5 K at varying powers on a glassy toluene sample reveal no signal for the triplet species **3.1**. The spectra collected at room temperature reveal the presence of a rhombic species and a broad feature at high field corresponding to a *g*-value of around 4, which are believed to be from an Fe(III) impurity. At 5 K, the rhombic species is absent and the high field feature resolves into two broad lumps, only one of which is present in a background scan of the resonator chamber. Measurements at 300, 40, and 7 K on a solid sample of 1% **3.1** doped in isostructural, diamagnetic $Co_2Pn^*_2$, revealed no features that could be modelled, and little similarity with the solution sample.

DFT calculations predict **3.1** would have a rhombic spectrum with $g_x = 2.045$, $g_y = 2.030$, g_z 2.006, *i.e.* $\langle g \rangle = 2.027$. The absence of any signal for **3.1** is reminiscent of early experiments on nickelocene, which similarly has a triplet ground state and fails to give an EPR signal due to the large zero-field splitting, $D_o = 33.6\ cm^{-1}$, of the ground triplet state.[40,41] This is suggested by the curve of the χ^{-1} *vs T* plot in Figure 3.7 at low

temperatures, but is not so explicit as in $NiCp_2$ and hence a D_o value cannot be reliably calculated using the data presently available.

3.8 Electrochemical study of **3.1**

Cyclic voltammetry was conducted on solutions of **3.1** in THF with a tetrabutylammonium hexafluorophosphate electrolyte. Full scans of the accessible solvent window at 0.01 and 0.1 V s^{-1} reveal **3.1** undergoes four quasi-reversible redox events (I, II, III, and IV) (Figure 3.9 a). In Figure 3.9 b, the wave corresponding to process IV has been cut off by the edge of the scan window due to reference electrode drift, but it is clearly defined in many scans, e.g. Figure 3.10 b.

The isoelectronic 32 TNE complex bisfulvalene dichromium undergoes two one-electron oxidations in acetonitrile, at −1.29 V (0⇌+1) and −0.63 V (+1→+2) *vs* $Fc^{0/+}$,[33,42] and hence waves II and III are assigned to the $[\mathbf{3.1}]^{0/+}$ and $[\mathbf{3.1}]^{+/2+}$ couples respectively. Complex **3.1** requires slightly more anodic potentials to effect these transfers, which may be a result of the higher effective nuclear charge of Fe compared to Cr.[43] The wave I then corresponds to the reduction **3.1**→$[\mathbf{3.1}]^{-}$. It is notable that a similar quasi-reversible feature is observed in all voltammograms of permethylpentalene complexes,

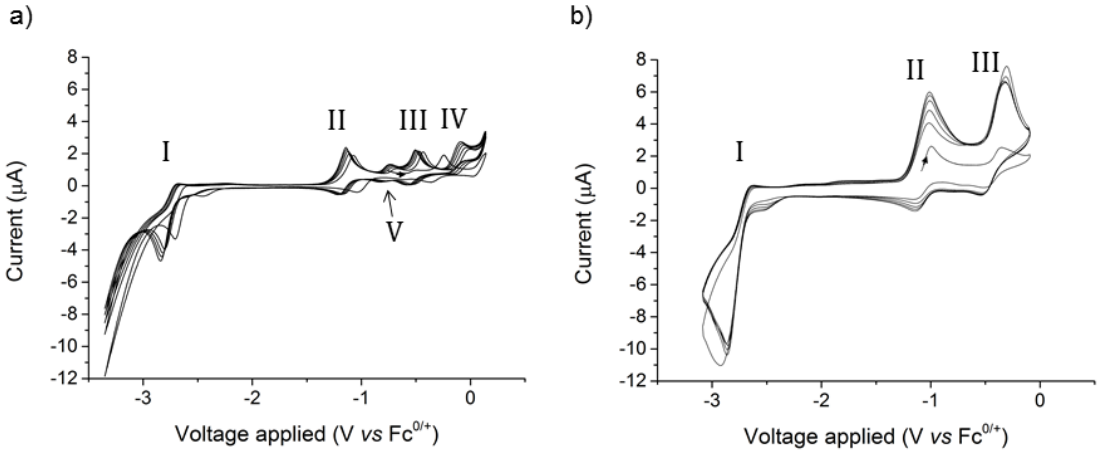

Figure 3.9 Overlaid full survey cyclic voltammograms (5 cycles) obtained by scanning a 0.1 mM solution of 3.1 in THF containing 0.1 M $[NBu_4][PF_6]$ at scan rates of a) 0.01 V s^{-1}, and b) 0.1 V s^{-1}.

at potentials of –4 to –2.5 V *vs* $Fc^{0/+}$ (see also Chapter 4),[9,44] and have been consistently attributed to a –1⇌0 couple.

Table 3.4 Electrochemical data for processes I to IV from cyclic voltammograms of 3.1 vs $Fc^{0/+}$.

M_2	$[M_2]^{-/0}$ (I)	$[M_2]^{0/+}$ (II)	$[M_2]^{+/2+}$ (III)	$[M_2]^{2+/3+}$ (IV)	$\Delta E_{½}{}^{0/2}$	$K_c{}^{0/2}$
$Fe_2Pn^*_2$ (**3.1**)	–2.84[a]	–1.15	–0.51	0.09	–0.60	1.4×10^{10}
$Cr_2(C_{10}H_8)_2$ [b]	–	–1.29	–0.63 [c]	–	–0.66	1.5×10^{11}

Potentials in volts, using $E_{½} = (E_{pa}+E_{pc})/2$. [a] E_{pc}. [b] Approximate: measured in 0.5 M $[NEt_4][ClO_4]$ acetonitrile solution *vs* a SCE reference or $Ag/AgNO_3$ quasi-reference electrode; reported *vs* SCE;[33] corrected using $Fc^{0/+}$ = 0.38 V *vs* SCE in 0.1 M $[NBu_4][ClO_4]$ in acetonitrile.[42] [c] E_{pa}

Voltammograms were collected over the central region at scan rates ranging from 0.1 to 1 V s^{-1}. The anodic and cathodic peak currents do not vary linearly with the square root of the scan rate (Figure 3.10 a), and the difference in peak potentials ($E_{pa} - E_{pc}$) for features II and III were found to be *c.* 240 and 520 mV respectively (*cf* 57 mV for a fully reversible single-electron transfer event at 298 K). Both of these results indicate processes II and III occur quasi-reversibly.

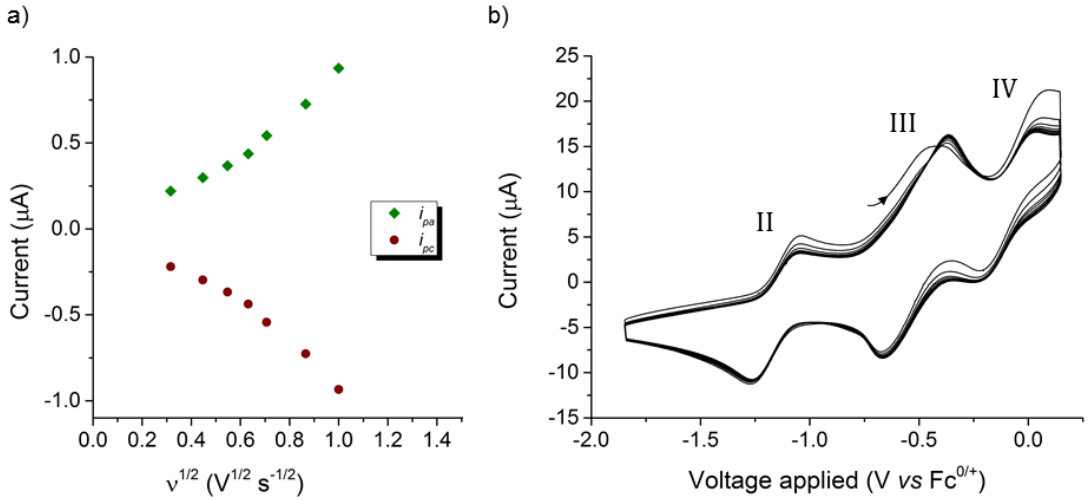

Figure 3.10 a) Variation of peak anodic and cathodic currents with the square root of the scan rate for the peak corresponding to process I, [3.1]⇌[3.1]$^+$, at scan rates of 0.1 to 1 V s^{-1}; b) Overlaid cyclic voltammograms (10 cycles) obtained by scanning a 0.1 mM solution of 3.1 in THF containing 0.1 M $[NBu_4][PF_6]$ at a scan rate of 1 V s^{-1}.

Wave II is centred at a mid-peak potential more negative than the corresponding $FeCp^*_2{}^{0/1+}$ $E_{½}$ of −0.44 V,[45] indicating it is easier to oxidise **3.1**, and harder to reduce [**3.1**]$^+$. The isostructural complexes $Mn_2Pn^*_2$ and $Co_2Pn^*_2$ each exhibit only one reduction and one oxidation couple within the solvent window.[9] A second quasi-reversible oxidation potential has only been observed for $Ni_2Pn^*_2$. The 32 TNE complex $[(C_{10}H_8)_2V_2(CO)_2]^{2+}$, by comparison, exhibits only a single, irreversible oxidation, corresponding to formation of the monoanion.[33]

In homobimetallic complexes of a symmetrically substituted bridging ligand, the comproportionation constant, $K_c = e^{\Delta E_{½}^{0/2} F/RT}$, for the reaction $[A]^{n+1} + [A]^{n-1} \rightarrow 2\,[A]^n$ offers an indication of electron delocalisation between the metal centres in a molecule.[46] In symmetrically substituted, dinuclear complexes with no delocalisation, redox waves for two one-electron transfer events would occur at the same potential for both metal centres, and the difference in half potentials for the two events ($\Delta E_{½}^{0/2}$) would be equal to zero. Delocalisation of electrons from one metal to another *via* the bridging ligand can stabilise or destabilise the ion formed, and make the second electron transfer (ET) event easier or more difficult to achieve. The peak potentials no longer coincide, and are observed separately, with $\Delta E_{½}^{0/2}$ given by $E_{½}(n+1 \rightleftharpoons n) - E_{½}(n \rightleftharpoons n-1)$. The K_c value of [**3.1**]$^+$ is greater than 10^6 (Table 3.4), so according to the Robin-Day classification of mixed-valence compounds, [**3.1**]$^+$ is stabilised by charge delocalisation, and can be described as a fractionally valent species.[47] K_c is similar in magnitude to bisfulvalene dichromium,[33] but smaller than the 1.2×10^{17} reported for $Ni_2Pn^*_2$.[9] Nuclear reorganisation is likely to be similar for the isostructural complexes, which share structural similarity with metallocenes,[48] so the large difference in K_c between them could be accounted for by the symmetries of orbital involved in ET processes, which have been found to cause significant differences the self-exchange rates in metallocenes and linked metallocenes. [48–50] In **3.1** one SOMO has π and one δ symmetry with respect

to ligand overlap, while in $Ni_2Pn^*_2$ the HOMO has π bonding character and a greater ligand-component,[9] so can facilitate stronger delocalisation in the mixed-valence species.[49]

At scan rates of 1 V s^{-1}, event IV was consistently observed with anodic peak potentials of 0.03 V *vs* $Fc^{0/+}$, and cathodic waves at −0.22 V (Figure 3.10 b), with peak-to-peak separations ranging from 150 mV (at 0.1 V s^{-1}) to 270 mV (at 1 V s^{-1}) indicating quasi-reversibility. $[FeCp_2]^+$ and $[FeCp^*_2]^+$ have been reported to undergo one-electron oxidations at 0.94 V and 0.52 V *vs* $Fc^{0/+}$ respectively in liquid sulphur dioxide at low temperatures.[51] The first and second oxidation waves occur at significantly lower potential than $Fc^{0/+}$, and it is possible event IV may therefore correspond to the unusual formation of a stable trication, $[\mathbf{3.1}]^{3+}$, and feature V in the scan at 0.01 V s^{-1}, which is not observed at any other scan rate, should thus be attributed to an electrochemical reaction of the product of oxidation IV. However, this assignment is tentative as oxidation potentials for monometallic metallocenes should correlate reasonably well with the ionisation potentials,[52] but for **3.1**, this is not the case. This could be due to the close proximity of the second metal atom.

3.9 Small molecule reactivity of $Fe_2Pn^*_2$

While metallocene derivatives have found many applications, as briefly mentioned in the introduction, the reactivity of pentalene complexes has been sparsely reported to date, such that it can be summarised quite succinctly herein.

The η^8-uranium(III) complex $UCp^*Pn^{(1,4\text{-}Si^iPr_3)}$ has been used to coordinate dinitrogen and the phosphaalkyne ^{t}BuC≡P, and can be used to effect their reduction,[53,54] while the uranium(III)Pn* chlorides of Chadwick and O'Hare undergo salt metathesis reactions.[55] A trimethyl tantalum pentalene complex undergoes sequential protonations to release methane,[56] and zirconium and hafnium mono and dicyclopentadienyl complexes have been tested as homogeneous polymerisation catalysts, with the

zirconium complexes demonstrating particularly high activities.[57] Other pentalene-containing zirconium complexes have also shown high rates of ethylene and α-olefin polymerisation activity, but in these only one ring of the pentalene coordinates to the metal with the other forming part of an ansa-bridge.[58]

For bimetallic complexes (aside from the formation of salts), the dititanium(II) sandwich compound $Ti_2Pn^{(1,4\text{-}Si^iPr_3)_2}$ can reductively cleave carbon dioxide to form a dititanium(II) dicarbonyl and a dimeric oxo-bridged Ti(III) species.[59] By contrast the molybdenum double sandwich complex $Mo_2Pn^{(1,4\text{-}Si^iPr_3)_2}$ resists coordination by CO, PMe_3, or H_2O.[60] The mixed rhodium(I)-ruthenium(II) heterobimetallic complex, Cp*RuPn*RhCOD, undergoes ancilliary ligand exchange with carbon monoxide (CO) and catalyses the hydrosilylation of styrene,[61] while the divanadium complex *syn*-$(VCp)_2Pn$ was mentioned to react with carbon monoxide in preliminary studies that were not elaborated upon.[62]

The 32 TNE bimetallic, $Fe_2Pn^*_2$, is classed as electron deficient,[5] and thus should result in enhanced reactivity compared to electronically saturated, monometallic ferrocene. Reactivity of 32 TNE bisfulvalene dichromium has not been reported. However, monometallic 16 VE chromocene coordinates CO,[63,64] and has found extensive use industrially as a homogenous ethylene oligomerisation catalyst and in the Union Carbide catalyst system.[65,66] The 16 VE Fp^+ cation (where Fp = $[(\eta^5\text{-Cp})Fe(CO)_2]$), as well as Cp* and indenyl analogues, have received attention as catalysts for the homogeneous conversion of syngas (CO and H_2) under mild conditions,[67,68] and readily coordinate CO which can then be reduced by borohydrides.

3.9.1 Synthesis and characterisation of $Fe_2Pn^*_2(CO)_2$, **3.2**

Exposure of a solution of **3.1** in aromatic solvents to CO causes the purple solution to turn orange upon mixing, as the bimetallic compound coordinates two molecules of CO (Scheme 3.3). Both molecules coordinate to the same iron atom,

forming bispermethylpentalenyldiiron dicarbonyl, **3.2**, which contains a unique example of a stable, coordinatively unsaturated derivative of bis(allyl)iron dicarbonyl. Bis(allyl)iron, $(C_3H_5)Fe$, is unknown, although the bulky silylated analogue $[(1,3\text{-}SiMe_3)_2C_3H_3]_2Fe$ has recently been isolated, and upon exposure to CO coordinates two molecules to the iron atom to form $[(1,3\text{-}SiMe_3)_2C_3H_3]_2Fe(CO)_2$.[69]

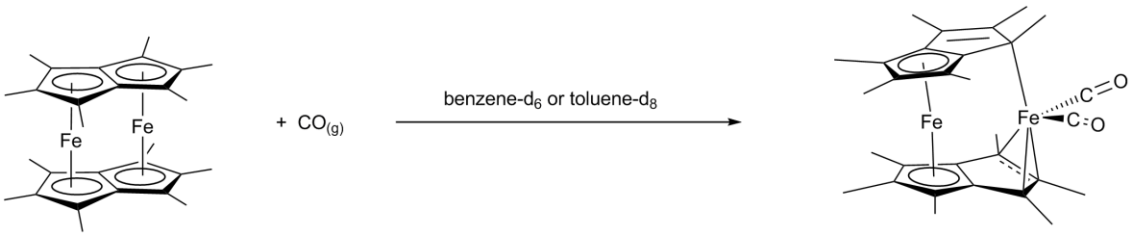

Scheme 3.3 Synthesis of $Fe_2Pn^*_2(CO)_2$, 3.2.

That **3.1** reacts with CO is unusual in itself. Electron deficient 24 TNE $Ti_2Pn^{(1,4\text{-}Si^iPr_3)}{}_2$ coordinates two molecules of CO in a symmetrical manner, one to each metal, and the two pentalenyl ligands tilt towards each other.[59] Yet, while it has been established that pentalene ligands can satisfy the electron count of multimetallics by donation of five electrons to both metal centres,[5,70] clearly here there is still a thermodynamic drive towards the formation of one 18 VE ferrocene moiety.

Resonance structures can be drawn for **3.1** that contain a ferrocene unit and a 14 VE bis(allyl)iron fragment (d in Figure 3.11). Other resonance structures include two electronically saturated ML_4X_2 ferrocene moieties (Figure 3.11 c), or the ML_4 structure that contains two '16 VE' units isoelectronic with chromocene (Figure 3.11 b). The coordination of two CO molecules resembles the reaction between 14 VE $Ti^{II}Cp_2$ and CO,[71,72] which forms $Cp_2Ti(CO)_2$, rather than the 1:1 adduct that forms when 16 VE Cp_2Cr^{II} is exposed to carbon monoxide,[63] suggesting therefore that resonance structure d in Figure 3.11 is a better descriptor of **3.1** than structure b or c.

The IR spectrum of **3.2** contains two CO stretching bands at 1888 and 1942 cm^{-1}, assigned to the antisymmetric and symmetric stretches of the dicarbonyl species, as well

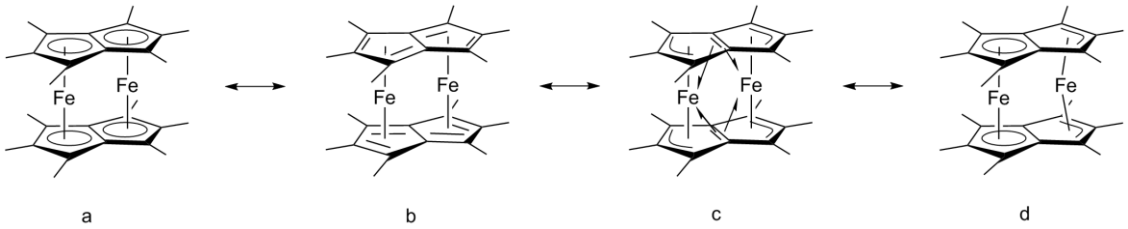

Figure 3.11 Some resonance structures for $Fe_2Pn^*_2$, 3.1.

as bands very similar to the parent **3.1**. The high wavenumbers (free υ_{CO} = 2143 cm^{-1}) indicate the carbonyls are terminally coordinated, rather than bridging. The carbonyl stretching bands of $Cp(C_3H_5)Fe(CO)_2$ are found at 1961 and 2010 cm^{-1},[73] similar to $(C_3H_5)_2Fe(CO)_2$ (1965 and 2020 cm^{-1}),[74] while the bulky bisallyl analogue $[(1,3\text{-}SiMe_3)_2C_3H_3]Fe(CO)_2$ is more electron rich, with asymmetric and symmetric bands at 1931 and 1986 cm^{-1} respectively.[69] The corresponding values obtained for **3.2** are 43 and 44 cm^{-1} lower than the bulky silylated species, indicating the iron atom in **3.2** is more electron rich than in any of these species, and that permethylpentalene is a stronger net electron donor.

The π-allyl complex **3.2** decomposes when subjected to electron bombardment, leading to the absence of a molecular ion peak in mass spectra. Molecular ion peaks are insignificant or completely absent in the series $(RC_3H_4)Fe(CO)_3X$ (where X = NO_3, Cl, Br; R = alkyl) and Fe—CO bond rupture was observed to increase with monoalkylation of the allyl ligand.[75] As noted above from IR data, Pn* is a much stronger net electron donor to iron than unsubstituted allyl ligands, and hence it may be expected that the Fe—CO bond is weaker so ruptures even more readily.

Single crystals of **3.2** were isolated from slow evaporation of the solvent from a benzene solution, and solved in the *P*–1 space group with two molecules in the unit cell. The C_1 structure revealed contains two carbonyls terminally coordinated to one iron atom (Figure 3.12). This coordination of both CO molecules to the same metal atom is accommodated by an unprecedented distortion of the permethylpentalene ligands, such

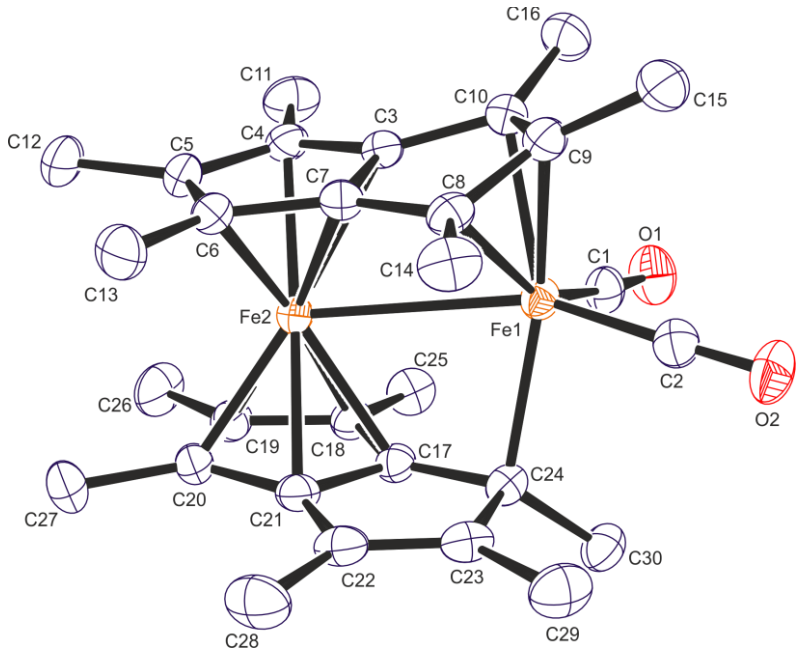

Figure 3.12 Molecular structure of $Fe_2(\mu\text{-}\eta^5,\eta^3\text{-}Pn^*)(\mu\text{-}\eta^5,\eta^1\text{-}Pn^*)(CO)_2$, 3.2. Ellipsoids are shown at 50% probability. Carbon atoms are in blue, iron atoms are in orange, and oxygen atoms are in red. Hydrogen atoms have been omitted for clarity.

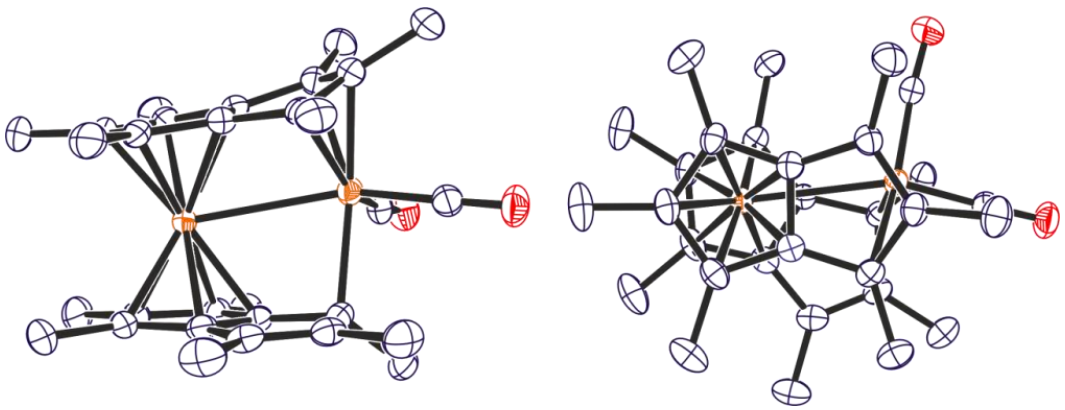

Figure 3.13 Side and plan views of the molecular structure of $Fe_2Pn^*_2(CO)_2$, 3.2, showing the twisted permethylpentalene ligand (left) and the staggered ferrocene unit and asymmetric coordination of the second iron atom (right). Ellipsoids are shown at 50% probability. Carbon atoms are in blue, iron atoms are in orange, and oxygen atoms are in red. Hydrogen atoms have been omitted for clarity.

that **3.2** incorporates one ferrocene moiety, and one η^1:η^3 coordinate iron(II) dicarbonyl. The result is an η^1-Pn* ring with an isolated double bond, while the remaining Pn* ligand, containing an allylic fragment, is heavily distorted towards η^2-coordination, as clearly depicted in the top down view shown in Figure 3.13.

Table 3.5 Selected bond lengths, distances, and angles for $Fe_2Pn^*_2(CO)_2$, 3.2.

Bond lengths (Å)	
Fe1—Fe2	2.8610(6)
Fe1—C1	1.767(3)
Fe1—C2	1.738(3)
C1—O1	1.159(4)
C2—O2	1.157(4)
Fe1—C3	2.471(3)
Fe1—C7	2.614(3)
Fe1—C8	2.209(3)
Fe1—C9	2.066(3)
Fe1—C10	2.111(3)
Fe1—C24	2.144(3)
Fe2—C3	2.152(2)
Fe2—C4	2.076(3)
Fe2—C5	2.042(4)
Fe2—C6	2.067(3)
Fe2—C7	2.084(3)
Fe2—C17	2.083(3)
Fe2—C18	2.082(3)
Fe2—C19	2.053(3)
Fe2—C20	2.068(3)
Fe2—C21	2.087(3)

Distances (Å)	
Fe2—Pn^*_{cent}(C3-C7)	1.6904(13)
Fe2—Pn^*_{cent}(C17-C21)	1.6783(14)
Ring slippage Fe2(C3-C7)	0.083
Ring slippage Fe2(C17-C21)	0.030
Fe1—C17	2.667(2)
Fe1—C21	3.488(3)
Fe1—C22	3.666(3)
Fe1—C23	2.986(2)

Ring slippage = difference between perpendicular projection of atom onto the plane of the ring, and the ring centroid

Angles (°)	
Fe1—C1—O1	171.8(3)
Fe1—C2—O2	178.0(3)
C1—Fe—C2	92.5(1)
C1—Fe1—C24	93.4(1)
C2—Fe1—C24	84.8(1)
Fe1—C24—C17	93.1(2)
Fe1—C24—C23	108.8(2)
Fe1—C24—C30	113.8(2)
Pn^*_{cent}–Fe2–Pn^*_{cent}	173.70(7)
Tilt angle (C3—C7)—(C17—C21)	9.28(17)
$(C3-C7)_{cent}$–C9–C15	166.13

The Fe1—Fe2 distance of 2.8610(6) Å in **3.2** is over 0.54 Å longer than in $Fe_2Pn^*_2$ (2.3175(9) Å). The two η^5-coordinated rings are staggered and tilted, so the η^3 and η^1 coordinated Pn* rings are offset from each other, and the perpendicular projection of Fe1 onto the (C17,C21-C24) plane falls outside the ring, 1.869 Å from the centroid. The

first example of an η^1-cyclopentadienyl iron compound to be crystallographically characterised, Fp(η^1-Cp), where Fp = (η^5-Cp)Fe(CO)$_2$, has an Fe—C single bond length of 2.11 Å to the η^1-Cp, slightly shorter than the Fe1—C24 bond in **3.2** (2.14 Å). The Fe(CO)$_2$ fragment in **3.2** contains a C1—Fe—C2 angle of 92.5(1)°, and both Fe—CO bonds are tilted towards the η^1-coordinated Pn* ligand. Bis(allyl)iron dicarbonyl complexes have thus far been isolated only as oils,[69,74,76] precluding structural comparison. However, this angle is more compressed than the corresponding 96° and 98.4° angles in the 18 VE complexes Fp(η^1-Cp) and Fp$_2$(μ-SnCl$_2$) respectively. One of the Fe—C—O units is almost linear, while the other is bent at an angle of 171.8(3)°. The single Fe—C1 bond (which has the more bent Fe—C—O angle), is slightly longer at 1.767(3) Å than the more linearly coordinated carbonyl, where the Fe1—C2 bond length is 1.738(3) Å. These are all longer than the (linear) 1.72 and 1.68 Å Fe—CO bonds in Fp(η^1-Cp).[77] The carbonyl C=O bond lengths in **3.2** are the same within error, and the same as those found in Fp(η^1-Cp) (all 1.16 Å);[77] these C=O bonds are over 0.62 Å shorter than in 18 VE FpI (1.78 Å),[78] indicating increased π back-donation from the Fe^{II} in the latter.

The ring atoms (C17 to C24) of the Pn* ligand that is η^1 coordinated to Fe1 are coplanar, with deviations from the Cremer & Pople plane[79] of +0.031 to −0.051 Å. The methyl groups of this ligand also lie in the same plane, except for C30. The C24—C30 bond points out of the plane, with an Fe1—C24—C30 angle of 133.8(2)°. Atoms C3—C7 are also coplanar, however the [C3,C7—C10] ring is best described as having an envelope conformation[79] where the C8 atom points inwards, towards the metal. The C—C bond lengths of the two aromatic rings demonstrate the delocalisation of electrons, while the short C23—C22 bond length of 1.361(4) Å clearly identifies this as an isolated double bond between tertiary carbons (Figure 3.14).[80] Similarly, the C17—C24 and C23—C24 bond lengths, at 1.474(4) and 1.499(4) Å respectively, are consistent with the 1.46 Å standard single bond between tertiary carbons.[80]

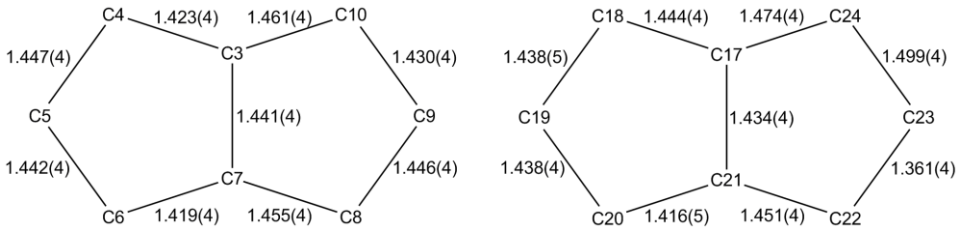

Figure 3.14 C—C bond lengths for Pn* ligands in $Fe_2Pn^*_2(CO)_2$, 3.2.

Exposure of a benzene-d_6 solution of **3.1** to a CO atmosphere for 10 seconds, without any freeze-thaw degas cycles, results in a clean NMR spectrum showing a mixture of **3.1** and a second, diamagnetic species, characterised by five singlet resonances. Following a freeze-thaw degas cycle and admission of CO, the NMR spectrum at 298 K indicates **3.1** has been consumed; the five resonances attributed to the new species have changed in intensity, and broad resonances are clearly present. The ^{13}C NMR spectrum at 298 K contains a total of 16 resonances; the two resonances at 213.7 and 226.2 ppm correspond to the coordinated carbonyls, and indicate a structure with two magnetically inequivalent carbonyl environments and two equivalent Pn* ligands. This spectrum remains unchanged upon removal of the CO atmosphere, and on heating the orange solution under a partial vacuum at temperatures of up to 60 °C. No decomposition occurred, with no loss of CO observed, so the carbonyl addition is concluded to be irreversible. This contrasts with the instability of unsubstituted $(C_3H_5)_2Fe(CO)_2$, which despite being an 18 VE complex, requires storage at low temperature under an inert atmosphere to prevent the coupling of allyl ligands and evolution of 1,5-hexadiene.[74]

3.9.2 Fluxional structure dynamics in solution

A variable temperature NMR study on **3.2** established a stereochemical lability in solution. The timescale of the fluxional process at ambient temperature is comparable

to the NMR timescale, such that 298 K corresponds to the coalescence point of the process, and results in a room temperature NMR spectrum that contains only one decipherable feature (Figure 3.15).

Below 298 K, the ^{1}H NMR spectrum in toluene-d_8 resolves to reveal ten resonances between 0.33 and 2.58 ppm, corresponding to a molecule with C_1 symmetry, as seen in the crystal structure. The CO resonances could not be located at 243 K in toluene-d_8, but in benzene-d_6 they are observed at 213.7 and 226.2 ppm at 298 K. A spectrum recorded in benzene-d_6 solution could be reconciled with the isothermal toluene-d_8 spectrum, confirming the presence of additional, overlapping resonances underneath the residual protio toluene peak at 2.09 ppm. A 2D HSQC experiment carried out at 243 K, where all visible proton signals are well resolved, clearly indicates that two additional resonances are obscured by the residual toluene signal (Figure 3.16). The solvent also partially obscures one resonance at high temperature.

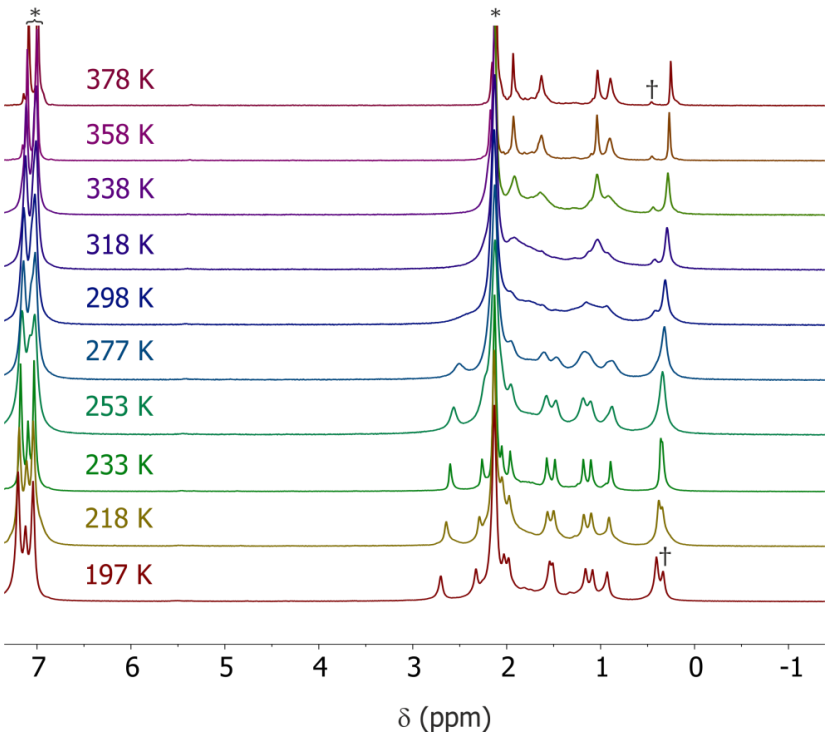

Figure 3.15 Variable temperature ^{1}H NMR stack plot for 3.2 in toluene-d_8 showing coalescent at 298 K. * indicates the overlapping residual protio solvent. † denotes a resonance attributed to silicone grease.

The HMBC spectrum can be used to assign the proton and Pn* carbon resonances at 243 K to a C_1 structure consistent with that seen in the solid state. The connectivity splits the resonances into two sets for the two Pn* moieties, and it is clear which ligand contains the NWT carbon atom with sp^3 hybridisation, because this atom has an unusually low tertiary ^{13}C chemical shift of 38.0 ppm. The two vinylic carbon resonances on this Pn* ligand have chemical shifts of 113.2 and 145.6 ppm, and all other tertiary ^{13}C resonances are found between 56.8 and 101.7 ppm. The diamagnetic spectrum indicates that the Pn* ligand that appears η^2-coordinated in the solid state must in fact be an allylic donor, to make **3.2** a closed shell, 18/16 VE bimetallic.

The twelve proton resonances broaden as temperature increases, and above 338 K six resonances emerge, which narrow exponentially and integrate with equal

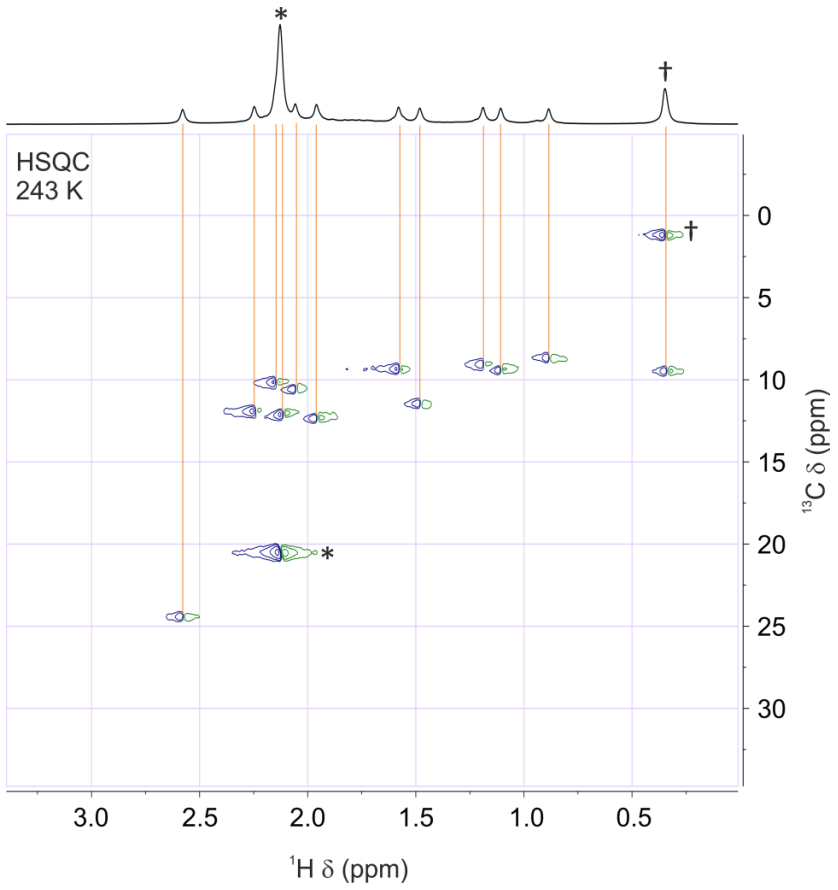

Figure 3.16 HSQC experiment on a solution of 3.2 in toluene-d_8 at 243 K showing the presence of twelve cross-peaks, the protons signals for two of which are obscured by the protio solvent peak (*). † labels a 1D methyl resonance that overlaps with silicone grease; the 2D cross peak for the silicone grease is indicated.

intensity (Figure 3.15). These can be correlated with six ^{13}C methyl resonances at 378 K, but the tertiary Pn* carbons and carbonyl resonances cannot be located in 1D or 2D experiments in the high temperature regime; presumably the signals are too broad to resolve. Fluxionality in bis(allyl)iron dicarbonyl complexes involves rotation of the allyl ligands above 14 °C.[81] However, this is prevented in **3.2** by the ferrocene moiety which bridges the structure and limits rotation of the ligands. The chemical shifts of the six resonances in the high temperature regime do not correspond to mean shifts of processes at low temperature however; for example, at 243 K the resonance at the lowest chemical shift of 0.34 ppm (integrating to three protons), moves to 0.26 ppm at 378 K, and has an integral of six. This means a structure emerges in which the two Pn* ligands are equivalent. The chemical shifts at high temperature do not correspond to the mean shifts of low temperature resonances however, indicating the absolute shifts vary with temperature.

Five of the ^{1}H and ^{13}C resonances at high temperature have shifts of 0.89 to 2.10 ppm and 9.54 to 12.38 ppm respectively, as expected for methyl groups at sp^2-hybridised ring positions. The remaining resonance, with a low ^{1}H shift of 0.24 ppm, and corresponding ^{13}C resonance at 1.56 ppm is tentatively assigned to the methyl at an sp^3-hybridised position. It should be noted, however, that in the low temperature regime, the sp^3 methyl resonance had chemical shifts in its ^{1}H and ^{13}C NMR spectra higher than the sp^2 methyl resonances (of 2.58 and 24.4 ppm respectively).

In considering the symmetry of the NMR spectra observed during fast exchange, there are three mirror planes and a rotation axis that would result in additional symmetry (Figure 3.17).

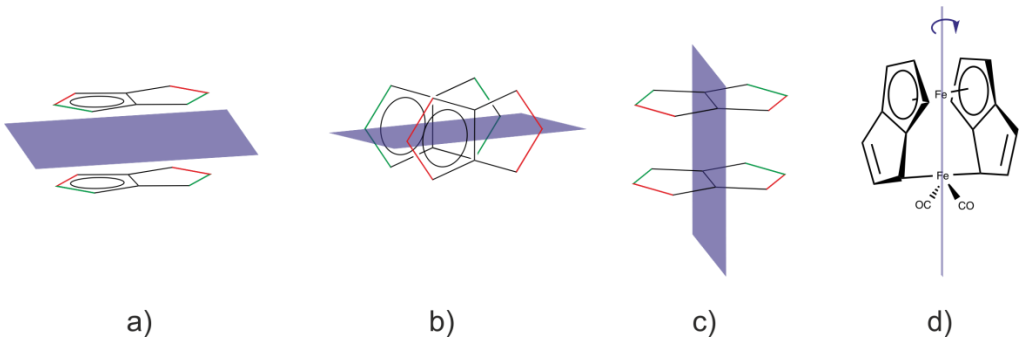

Figure 3.17 Planes of symmetry in a simplified schematic of the structure of 3.2, that could account for the observation of additional symmetry in the coalesced spectrum. Red and green colours are used to differentiate between non-equivalent environments.

If the $Fe(CO)_2$ fragment swivels between pointing towards one NWT, then to the other NWT, passing through an η^3-coordinated mid-point, then in the coalesced spectra the molecule would have four NWT proton environments, and four different wing-tip environments (Figure 3.17 b), *i.e*. more than are observed by ^1H NMR. There is no sign that the carbonyl ligands migrate between metal atoms, as the IR spectra (a fast technique compared to the NMR timescale) recorded at high temperature feature one symmetric and one antisymmetric carbonyl band, both with stretching frequencies indicating terminal coordination. This is consistent with the observed stability of **3.2** with respect to loss of CO, and rules out the structure with equivalent metal centres indicated in Figure 3.17 c.

Of the two remaining options for the fluxional process, a wagging motion in which the carbonyls point towards the η^1-coordinated Pn* ligand, then point towards the other Pn* ligand, with accompanying "$\eta^1 \rightarrow \eta^3$" and "$\eta^3 \rightarrow \eta^1$" switches of hapticity for the two Pn* ligands (Figure 3.18), would presumably have a lower activation barrier than the significant rotation necessary to achieve the C_2 symmetry (Figure 3.17 d). DFT probing of the intermediate bis-allylic C_{2v} transition state for the fluxionality in Figure 3.17 d confirm it lies >1 eV higher in energy than the ground state, and is thus not a viable path. On this basis, it is postulated the $Fe(CO)_2$ wagging motion is the fluxionality observed at high temperature.

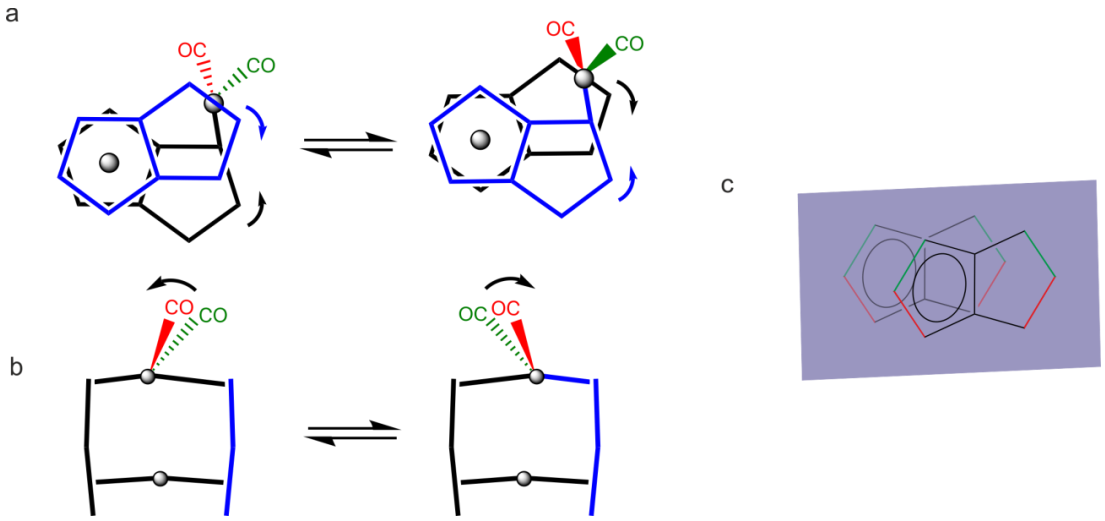

Figure 3.18 Schematics showing wagging motion of $Fe(CO)_2$ fragment a) plan view showing η^1-Pn*A-η^3-Pn*B to η^3-Pn*A-η^1-Pn*B switch, b) side view showing side-to-side wagging of $Fe(CO)_2$; c) resulting symmetry observed in the fast exchange regime.

The low temperature form of the dicarbonyl moiety in **3.2** contains an unusual combination of η^1 and distorted η^3 coordination, so is electron deficient compared to 18 VE Fp(η^1-Cp) and $(C_3H_5)_2Fe(CO)_2$ derivatives. The half-open-indenyl and edge-bridged half-open-indenyl metallocenes undergo an $\eta^5 \rightarrow \eta^3$ hapticity change of the open-indenyl ligand, allowing a single CO molecule to coordinate, again making 18VE complexes.[82,83] This $\eta^5 \rightarrow \eta^3$ ring slippage is a slow process in the Fe(II) half open sandwich complexes, taking from a few hours to days to coordinate CO.[83] By contrast, the reaction of **3.1** in solutions is immediate upon mixing, so it was surprising that no reaction was observed with the sigma donor PEt_3, with ethylene, or with dihydrogen. The *in situ* reactions between $FeCl_2$·THF, $Mg(C_3H_5)Br$, and phosphines form $(C_3H_5)_2Fe(PR_3)_2$ adducts.[76] Presumably, the absence of a reaction for **3.2** with PEt_3 and C_2H_4 is the result of a steric interaction between the incoming nucleophile and the methyl groups of Pn*.

3.10 Conclusions

A symmetrically coordinated diiron compound of a hexaalkylated pentalene derivative has been reported and fully characterised for the first time. Its 'double

sandwich' structure is in accord with those predicted for the unsubstituted parent pentelene, and crystallographic characterisation has confirmed the ligands adopt a parallel conformation. $Fe_2Pn^*_2$, **3.1**, possesses an unusual triplet ground state which obeys the Curie Law, and DFT simulations have indicated the two unpaired spins reside in metal based orbitals that are orthogonal, with a net favourable interaction between the two iron atoms, although not single bond formation. **3.1** has a large magnetic moment in solution and the solid state, which is not predicted by DFT calculations. The zero-field splitting of the triplet is likely to be large, hence no EPR signal is observed. $Fe_2Pn^*_2$ displays four accessible redox states (−1, 0, +1, +2).

A unique reactivity has been demonstrated for the diiron compound whereby irreversible coordination of two carbon monoxide moieties to one metal atom results in a C_1 structure that contains a ferrocene moiety, and one η^1- coordinated and one heavily distorted η^3-allyl Pn* ring in a highly unusual 16 VE bis(allyl)iron dicarbonyl unit. The coordination geometry of **3.2** is fluxional in solution, and in the low temperature limit is in agreement with the molecular structure derived crystallographically.

3.11 References

(1) King, R. B.; Bisnette, M. B. *J. Organomet. Chem.* **1967**, *8*, 287.
(2) LeVanda, C.; Bechgaard, K.; Cowan, D. O.; Mueller-Westerhoff, U. T.; Eilbracht, P.; Candela, G. A.; Collins, R. L. *J. Am. Chem. Soc.* **1976**, *98*, 3181.
(3) Katz, T. J.; Acton, N.; McGinnis, J. *J. Am. Chem. Soc.* **1972**, *94*, 6205.
(4) Churchill, M. R.; Lin, K. K. G. *Inorg. Chem.* **1973**, *12*, 2274.
(5) Bendjaballah, S.; Kahlal, S.; Costuas, K.; Bévillon, E.; Saillard, J.-Y. *Chem.—Eur. J.* **2006**, *12*, 2048.
(6) Elschenbroich, C.; Heck, J.; Massa, W.; Schmidt, R. *Angew. Chemie* **1983**, *95*, 319.
(7) Bachmann, B.; Hahn, F.; Heck, J.; Wuensch, M. *Organometallics* **1989**, *8*, 2523.
(8) Elschenbroich, C.; Heck, J.; Massa, W.; Nun, E.; Schmidt, R. *J. Am. Chem. Soc.* **1983**, *105*, 2905.
(9) Ashley, A. E.; Cooper, R. T.; Wildgoose, G. G.; Green, J. C.; O'Hare, D. *J. Am. Chem. Soc.* **2008**, *130*, 15662.
(10) Manriquez, J. M.; Ward, M. D.; Reiff, W. M.; Calabrese, J. C.; Jones, N. L.; Carroll, P. J.; Bunel, E. E.; Miller, J. S. *J. Am. Chem. Soc.* **1995**, *117*, 6182.
(11) Katz, T. J.; Acton, N. *J. Am. Chem. Soc.* **1972**, *94*, 3281.
(12) Hebendanz, N.; Köhler, F. H.; Scherbaum, F.; Schlesinger, B. *Magn. Reson. Chem.* **1989**, *27*, 798.
(13) Blümel, J.; Herker, M.; Hiller, W.; Köhler, F. H. *Organometallics* **1996**, *15*, 3474.

(14) Freyberg, D. P.; Robbins, J. L.; Raymond, K. N.; Smart, J. C. *J. Am. Chem. Soc.* **1979**, *101*, 892.
(15) Suenkel, K. *J. Am. Chem. Soc.* **2014**, *137*, 126.
(16) O'Connor, J. M.; Casey, C. P. *Chem. Rev.* **1987**, *87*, 307.
(17) Kilpatrick, A. F. R.; Green, J. C.; Cloke, F. G. N.; Tsoureas, N. *Chem. Commun.* **2013**, *49*, 9434.
(18) Churchill, M. R.; Wormald, J. *Inorg. Chem.* **1969**, *8*, 1970.
(19) Wells, A. F. *Structural Inorganic Chemistry*; 5th ed.; Clarendon Press: Oxford, 1984; p. 1288.
(20) Chen, J.; Li, D.; Yu, Y.; Jin, Z.; Zhou, Q.; Wei, G. *Organometallics* **1993**, *12*, 3885.
(21) Kuchta, M. C.; Cloke, F. G. N.; Hitchcock, P. B. *Organometallics* **1998**, *17*, 1934.
(22) Cloke, F. G. N.; Green, J. C.; Jardine, C. N.; Kuchta, M. C. *Organometallics* **1999**, *18*, 1087.
(23) Van Vleck, J. H. *The Theory of Electric and Magnetic Susceptibilities*; Oxford University Press, 1932.
(24) Schubert, E. M. *J. Chem. Educ.* **1992**, *69*, 62.
(25) Pfirrmann, S.; Limberg, C.; Herwig, C.; Knispel, C.; Braun, B.; Bill, E.; Stösser, R. *J. Am. Chem. Soc.* **2010**, *132*, 13684.
(26) Carlin, R. L. In *Magnetochemistry*; Springer-Verlag, 1986; pp. 19–35.
(27) Rettig, M. F.; Drago, R. S. *Chem. Commun.* **1966**, 891.
(28) Rettig, M. F.; Drago, R. S. *J. Am. Chem. Soc.* **1969**, *91*, 1361.
(29) Prins, R. *Mol. Phys.* **1970**, *19*, 603.
(30) Rettig, M. F. In *NMR of Paramagnetic Molecules: Principles and Applications*; La Mar, G. N.; Horrocks Jr., W. D.; Holm, R. H., Eds.; Academic Press Inc., 1973; pp. 218–241.
(31) Bain, G. A.; Berry, J. F. *J. Chem. Educ.* **2008**, *85*, 532.
(32) Tobita, H.; Izumi, H.; Ohnuki, S.; Ellerby, M. C.; Kikuchi, M.; Inomata, S.; Ogino, H. *J. Am. Chem. Soc.* **1995**, *117*, 7013.
(33) Smart, J. C.; Pinsky, B. L. *J. Am. Chem. Soc.* **1980**, *102*, 1009.
(34) Zhang, S.; Xu, Q.; Sun, J.; Chen, J. *Organometallics* **2002**, *21*, 4572.
(35) Zhang, S.; Xu, Q.; Sun, J.; Chen, J. *Chem.—Eur. J.* **2003**, *9*, 5111.
(36) ADF, 2010.
(37) Becke, A. D. *Phys. Rev. A* **1988**, *38*, 3098.
(38) Perdew, J. P.; Yue, W. *Phys. Rev. B* **1986**, *33*, 8800.
(39) Schachtschneider, J. H.; Prins, R.; Ros, P. *Inorganica Chim. Acta* **1967**, *1*, 462.
(40) Prins, R.; van Voorst, J. D. W.; Schinkel, C. J. *Chem. Phys. Lett.* **1967**, *1*, 54.
(41) Baltzer, P.; Furrer, A.; Hulliger, J.; Stebler, A. *Inorg. Chem.* **1988**, *27*, 1543.
(42) Connelly, N. G.; Geiger, W. E. *Chem. Rev.* **1996**, *96*, 877.
(43) Sanello, P. *Inorganic Electrochemistry: Theory, Practice and Applications*; Royal Society of Chemistry, 2003.
(44) Kilpatrick, A. F. R. Bimetallic Complexes of d- and f-Block Metals with Pentalene Ligands, PhD Thesis, 2014.
(45) Aranzaes, J. R.; Daniel, M.-C.; Astruc, D. *Can. J. Chem.* **2006**, *84*, 288.
(46) Aguirre-Etcheverry, P.; O'Hare, D. *Chem. Rev.* **2010**, *110*, 4839.
(47) Robin, M. B.; Day, P. *Adv. Inorg. Chem. Radiochem.* **1968**, *10*, 247.
(48) Nielson, R. M.; Golovin, M. N.; McManis, G. E.; Weaver, M. J. *J. Am. Chem. Soc.* **1988**, *110*, 1745.
(49) McManis, G. E.; Nielson, R. M.; Weaver, M. J. *Inorg. Chem.* **1988**, *27*, 1827.
(50) Gennett, T.; Milner, D. F.; Weaver, M. J. *J. Phys. Chem.* **1985**, *89*, 2787.
(51) Sharp, P. R.; Bard, A. J. *Inorg. Chem.* **1983**, *22*, 2689.
(52) Bard, A. J.; Garcia, E.; Kukharenko, S.; Strelets, V. V. *Inorg. Chem.* **1993**, *32*, 3528.
(53) Cloke, F. G. N.; Hitchcock, P. B. *J. Am. Chem. Soc.* **2002**, *124*, 9352.
(54) Tsoureas, N.; Kilpatrick, A. F. R.; Summerscales, O. T.; Nixon, J. F.; Cloke, F. G. N.; Hitchcock, P. B. *Eur. J. Inorg. Chem.* **2013**, *2013*, 4085.

(55) Chadwick, F. M.; O'Hare, D. M. *Organometallics* **2014**, *33*, 3768.
(56) Cloke, F. G. N.; Hitchcock, P. B.; Kuchta, M. C.; Morley-Smith, N. A. *Polyhedron* **2004**, *23*, 2625.
(57) Chadwick, F. M.; Cooper, R. T.; Ashley, A. E.; Buffet, J.-C.; O'Hare, D. M. *Organometallics* **2014**, *33*, 3775.
(58) Kaminsky, W.; Sperber, O.; Werner, R. *Coord. Chem. Rev.* **2006**, *250*, 110.
(59) Kilpatrick, A. F. R.; Cloke, F. G. N. *Chem. Commun.* **2014**, *50*, 2769.
(60) Summerscales, O. T.; Cloke, F. G. N. *Coord. Chem. Rev.* **2006**, *250*, 1122.
(61) Burgos, F.; Chávez, I.; Manriquez, J. M.; Valderrama, M.; Lago, E.; Molins, E.; Delpech, F.; Castel, A.; Rivière, P. *Organometallics* **2001**, *20*, 1287.
(62) Jones, S. C.; O'Hare, D. *Chem. Commun.* **2003**, 2208.
(63) Wong, K. L. T.; Brintzinger, H. H. *J. Am. Chem. Soc.* **1975**, *97*, 5143.
(64) Brintzinger, H. H.; Lohr, L. L.; Wong, K. L. T. *J. Am. Chem. Soc.* **1975**, *97*, 5146.
(65) Agapie, T. *Coord. Chem. Rev.* **2011**, *255*, 861.
(66) Theopold, K. H. *Eur. J. Inorg. Chem.* **1998**, *1998*, 15.
(67) Cutler, A. R.; Hanna, P. K.; Vites, J. C. *Chem. Rev.* **1988**, *88*, 1363.
(68) West, N. M.; Miller, A. J. M.; Labinger, J. A.; Bercaw, J. E. *Coord. Chem. Rev.* **2011**, *255*, 881.
(69) Rightmire, N. R.; Quisenberry, K. T.; Hanusa, T. P. *Organometallics* **2014**, *33*, 5678.
(70) Green, J. C.; Green, M. L. H.; Parkin, G. *Chem. Commun.* **2012**, *48*, 11481.
(71) Murray, J. G. *J. Am. Chem. Soc.* **1961**, *83*, 1287.
(72) Fachinetti, G.; Floriani, C. *J. Chem. Soc. Chem. Commun.* **1972**, 654.
(73) Pannell, K. H.; Lappert, M. F.; Stanley, K. *J. Organomet. Chem.* **1976**, *112*, 37.
(74) Nesmeyanov, A. N.; Kritskaya, I. I. *J. Organomet. Chem.* **1968**, *14*, 387.
(75) Nesmeyanov, A. N.; Nekrasov, Y. S.; Avakyan, N. P.; Kritskaya, I. I. *J. Organomet. Chem.* **1971**, *33*, 375.
(76) Gabor, B.; Holle, S.; Jolly, P. W.; Mynott, R. *J. Organomet. Chem.* **1994**, *466*, 201.
(77) Bennett, M. J.; Cotton, F. A.; Davison, A.; Faller, J. W.; Lippard, S. J.; Morehouse, S. M. *J. Am. Chem. Soc.* **1966**, *88*, 4371.
(78) Zeller, M.; Lazich, E.; Hunter, A. D. *Acta Crystallogr. Sect. E Struct. Reports Online* **2003**, *59*, m914.
(79) Cremer, D.; Pople, J. A. *J. Am. Chem. Soc.* **1975**, *97*, 1354.
(80) Ladd, M. F. C.Palmer, R. A. *Structure Determniation by X-Ray Crystallography*; 1985.
(81) Nesmeyanov, A. N.; Ustynyuk, Y. A.; Kritskaya, I. I.; Shchembelov, G. A. *J. Organomet. Chem.* **1968**, *14*, 395.
(82) Glöckner, A.; Bannenberg, T.; Ibrom, K.; Daniliuc, C. G.; Freytag, M.; Jones, P. G.; Walter, M. D.; Tamm, M. *Organometallics* **2012**, *31*, 4480.
(83) Volbeda, J.; Daniliuc, C. G.; Jones, P. G.; Tamm, M. *Organometallics* **2013**, *32*, 5918.

Chapter 4 SYNTHESIS, CHARACTERISATION, AND REDOX PROPERTIES OF BIMETALLIC COMPOUNDS OF PERMETHYLPENTALENE

4.1 Introduction

The pentalene ligand can coordinate to metals with a variety of hapticities, and the η^5 and η^8 bonding modes are prevalent in existing complexes. For aromatic five-membered rings, one of the most interesting features of the η^5 bonding mode is an ability to distort towards an η^3 hapticity, and accomodate an additional coordination site.[1] Cyclopentadienyl (Cp) and indenyl (Ind) complexes exhibit an η^5 to η^3 'ring slippage' which can either be accommodated with a planar geometry, or result in large hinge angles between the planes of the allylic fragment and the double bond or benzene ring (Figure 4.1).[2,3] This flexibility, coupled with the formation 3c2e bonds (Chapter 1.7.1), makes pentalene complexes ideal for a systematic study of how the bonding description varies with changes to the metal and the ligand.

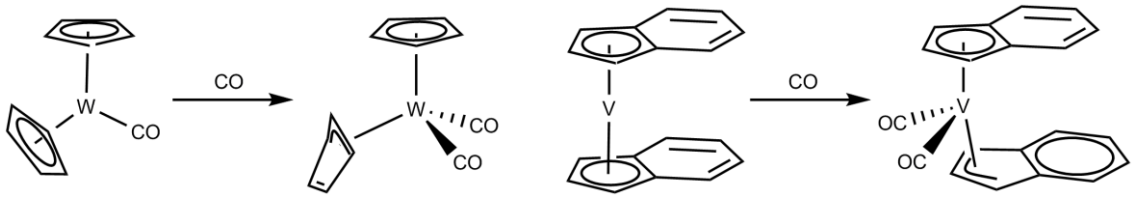

Figure 4.1 Examples of $\eta^5 \rightarrow \eta^3$ ring slippage in complexes with cyclopentadienyl (left) and indenyl (right) ligands.

For metallocenes, some striking differences in structure and chemistry arise when replacing unsubstituted Cp ligands with peralkylated ones.[4] A similar variation of properties may be expected across series of fused metallocenes, where electrons can be delocalised across both fused rings, in orbitals that overlap with both coordinated metal atoms. Compounds of the type Cp*M(μ-Pn)M'Cp* have been studied theoretically as

molecular electronic and magnetic materials.[5–10] However, an extensive study of the effect of ligand peralkylation has only become possible since development of a synthetic route for permethylpentalene (Pn*).[11,12] This chapter addresses the synthesis and characterisation of homobimetallic compounds that incorporate a Pn* bridging ligand. Comparisons with isostructural complexes with an unsubstituted bridging pentalene, and with fulvalene bridging ligands will be drawn, in the context of control of the HOMO-LUMO gap.

4.2 Synthesis of *anti*-bimetallics

4.2.1 Salt elimination reactions

Salt elimination reactions between $[MCp^*]^+$ transfer agents of iron, cobalt, or nickel, and the dilithium salt of permethylpentalene, $Li_2Pn^*TMEDA_x$ ('Li_2Pn^*'), result in the formation of bis(pentamethylcyclopentadienyliron)permethylpentalene, **4.1a**, bis(pentamethylcyclopentadienylcobalt)permethylpentalene, **4.2a**, and bis(pentamethylcyclopentadienylnickel)permethylpentalene, **4.3a**, respectively (Scheme 4.1). Compounds **4.1a** – **4.3a** were isolated as intensely dark brown-black crystals in moderate yield (35 – 43%).

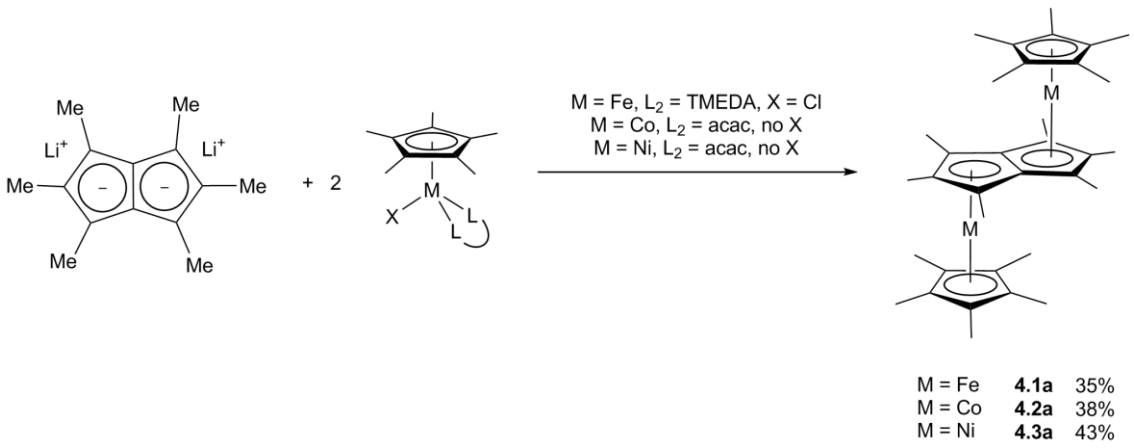

Scheme 4.1 General scheme for the synthesis of *anti*-$(MCp^*)_2Pn^*$.

In general, reactants were solvated in THF and added together at −78 °C. Following warming to room temperature and stirring for an hour, the precipitation of LiCl or Li(acac) was observed, and the desired bimetallics were extracted from the crude residue into a non-polar solvent. Compounds **4.1a** – **4.3a** typically had good solubility in THF and benzene, but limited solubility in toluene and aliphatics. The air-sensitive compounds degraded quickly (cobalt complexes) or gradually over a few hours (nickel and iron complexes) in chloroform.

4.2.1.1 Synthesis of $(FeCp^*)_2Pn^*$, **4.1a**

Addition of Li_2Pn^* to a lime green solution of Cp*FeCl·TMEDA caused instant darkening of the mixture. Concentration of a hexane extraction and storage at −78 °C yielded **4.1a**, in 35% yield.

Brown solutions of **4.1a** decompose in air to a red solution that contains the known decomposition product Pn^*_2 (by NMR spectroscopy). In the solid state, **4.1a** undergoes a thermal decomposition above 60 °C, which will be discussed in Chapter 5.

Upon changing the solvent to benzene, no bimetallic **4.1a** was observed, and the major products identified were $FeCp^*_2$, unreacted Cp*FeCl·TMEDA, and an unidentified paramagnetic species. Use of the softer bis(trimethylstannyl) source of the Pn* ligand, $(SnMe_3)_2Pn^*$, resulted in no reaction unless vigorous heating was employed, and in the latter case, **4.1a** was identified only in trace amounts by ^1H NMR spectroscopy. Attempts were made to employ the Cp*Fe(acac) reagent, prepared according to the method of Manrìquez, but repeatedly resulted in isolation of $Fe_2Pn^*_2$, **3.1**, instead of **4.1a**.

4.2.1.2 Synthesis of $(CoCp^*)_2Pn^*$, **4.2a**

The $[Cp^*Co]^+$ source Cp*Co(acac) was added to a slurry of Li_2Pn^*. On warming above −10 °C, precipitation of a black solid was observed, and the dicobalt complex, **4.2a**, was purified by repeated recrystallisation from hexane at −78 °C, in 38% yield.

Complex mixtures of paramagnetic products were observed by NMR spectroscopy of the reaction, and parallels can be drawn with the reaction between MCp^*_n (M = Li, Na, n = 1; M = Mg, n = 2) and anhydrous CoX_2 (X = Cl, Br, OAc) in THF,[4] which also gives a complex mixture of products.

4.2.1.3 Synthesis of $(NiCp^*)_2Pn^*$, **4.3a**

The room temperature reaction of Cp*Ni(acac) and Li_2Pn^* in toluene yielded **4.3a**, in 43% yield following work up and recrystallisation from benzene. Yields were not improved by conducting the reaction at lower temperatures. Crystallisation from toluene afforded an analytically pure sample of **4.3a**, however, once isolated, these crystals were poorly soluble in aliphatic solvents, and only sparingly soluble in benzene and toluene, with some crystals remaining insoluble in THF despite heating.

The salt metathesis routes to **4.1a** – **4.3a** resemble those used in the synthesis of decamethylmetallocenes,[4] for which yields were found to be sensitive to the choice of solvent, and of alkali metal Cp* salt employed (LiCp* producing lower yields of the sandwich complexes than NaCp*). More recently, Volbeda *et al.* have reported that with the Cp*FeI transfer reagent, selectivity is sensitive to the exact nature of the alkali metal ligand source in the synthesis of half-open and edge-bridged half-open metallocenes; stoichiometric reaction of $FeI_2{\cdot}2THF$ and LiCp* with the potassium salt of the "open indenyl" ligand, *o*Ind^{Me}, affords Cp*Fe(*o*Ind^{Me}) selectively,[13] while the potassium salt of the edge-bridged open indenyl ligand, *ebo*Ind^{Me}, forms significant amounts of decamethylferrocene alongside the desired Cp*Fe(*ebo*Ind^{Me}).[14] Similar sensitivity to the use of Li_2Pn^* *vs* Li_2Pn is likely here,[8] and may explain the modest yields.

In previous work, it has been noted that the Pn^*_2 dimer forms through an oxidative coupling of two Pn^{*2-} ligands in the presence of the iron salt $FeCl_2{\cdot}THF_{1.5}$.[15] It is notable that this byproduct was not identified in these reactions, reflecting the fact

that the metallocene reagents used and byproducts formed are mild to strong reducing agents,[16] rather than oxidising agents.[17]

4.2.2 Metallocene ligand substitution

There is precedent for metallocenes with a formal valence electron count (VE) of more than 18 to undergo ligand substitution reactions, in order to lower the electron count at the metal,[18] and this was exploited in an novel synthetic route to *anti*-bimetallic complexes with Cp capping groups. Mixing solutions of $CoCp_2$ or $NiCp_2$ with a Li_2Pn^* slurry results in exchange of one Cp ligand for a five-carbon ring of Pn*, and formation of the bimetallic compounds bis(cyclopentadienylcobalt)permethylpentalene, **4.2b**, and bis(cyclopentadienylnickel)permethylpentalene, **4.3b** (Scheme 4.2). The equivalent diiron complex could not be made *via* this route since $FeCp_2$, with 18 VE, is substitutionally inert.

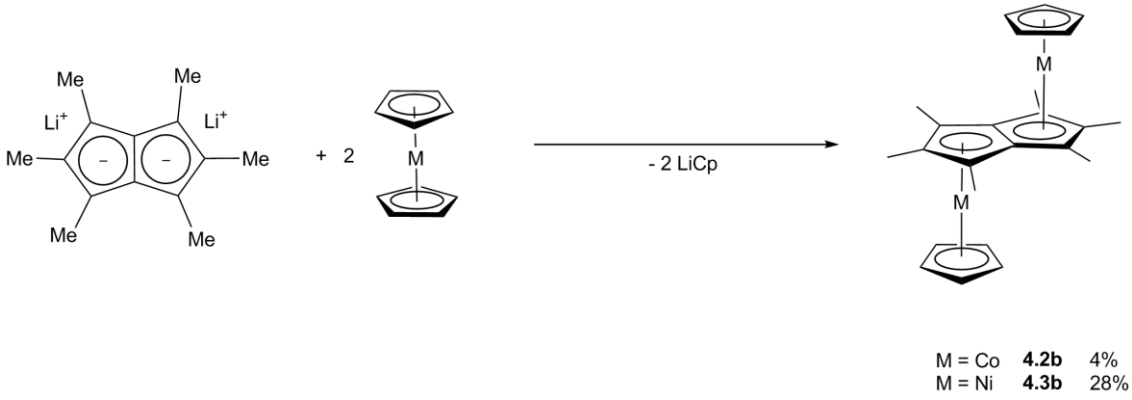

Scheme 4.2 General scheme for the synthesis of *anti*-$(MCp)_2Pn^*$.

4.2.2.1 Synthesis of $(CoCp)_2Pn^*$, **4.2b**

The reaction forming **4.2b** requires an excess of Li_2Pn^* to consume the cobaltocene, and proceeds slowly in THF. Recrystallisation from a minimum volume benzene solution at 6 °C afforded an analytically pure sample of **4.2b** in 4% yield.

In THF, an unidentified side-product forms, and is characterised by two broad resonances at −9.5 and −16.5 ppm with intensities in a 18:5 ratio. Following extraction of both this and **4.2b** from the crude residue with boiling hexanes, the desired dicobalt compound **4.2b** could be isolated by fractional crystallisation from hexanes at −78 °C. On conducting the reaction in benzene, the aforementioned side-product is not observed at all, and the reaction proceeds more cleanly overall, but requires heating at 65 °C to reach completion. A previously unobserved impurity appears in the diamagnetic region of the ^{1}H NMR spectrum, characterised by three sharp singlets of equal intensity at 4.02, 4.34, and 4.76 ppm. Compound **4.3b** could not be separated from this impurity by sublimation as both species co-sublimed (50 °C, 10^{-2} mbar).

In the synthesis of $(CoCp)_2$fulvalene (fulvalene = μ-η^5,η^5-$C_{10}H_8$), addition of excess cobaltocene causes oxidation of the bimetallic to the monocation,[19] and although **4.3b** has a lower formal valence electron count than the fulvalene bridged species, it is postulated that an analogous oxidation reaction is a possible explanation for the low isolated yield.

4.2.2.2 Synthesis of $(NiCp)_2Pn^*$, **4.3b**

Reaction of two equivalents of nickelocene with Li_2Pn^* proceeds cleanly in benzene at room temperature to form the dinickel compound, **4.3b**, which was isolated in 28% yield following crystallisation.

Katz and Acton found the reaction of Li_2Pn and nickelocene in a 1:1 stoichiometry made the sandwich compound Ni_2Pn_2.[20] However, when only one equivalent of $NiCp_2$ is reacted with Li_2Pn^*, neither **4.3b** nor the sandwich compound $Ni_2Pn^*_2$ is formed. With the 2:1 stoichiometry, dinickel complex **4.3b** is favoured over other products of ligand exchange, which contrasts with the findings of Hilbig *et al.*, who synthesised $(NiCp)_2$fulvalene from $Tl_2(C_{10}H_8)$ and LiCp and found the di- and trimetallic product mixtures were unstable with respect to ligand redistribution into $NiCp_2$ and

bisfulvalene dinickel in solution.[21] Davison and Smart have similarly reported that the relative distribution of $Co_2(C_{10}H_8)_2$, and $(CoCp)_2(C_{10}H_8)$ is sensitive to the NaCp stoichiometry employed during synthsis.[22]

4.3 Attempted syntheses

4.3.1 Attempted synthesis of $(CrCp^*)_2Pn^*$ and $(MnCp^*)_2Pn^*$ by salt elimination

In 2003, Jones *et al.* demonstrated that the reaction between $Li_2Pn{\cdot}2C_2H_4(OR)_2$ (R = Me, Et) and $[Cp^*Cr(\mu\text{-}Cl)]_2$ resulted in the novel, trinuclear complex $(Cp^*Cr)(\mu{:}\eta^5,\eta^2,\eta^2\text{-}Pn)[(CrCp^*)_2(\mu\text{-}OR)]$ (Scheme 4.3 a).[23] Additionally, Miyake and Kanai synthesised bis(allylnickel)pentalene and claim to have made the chromium analogue in "similar reactions", presumably by combining Li_2Pn with bis(allyl)chromium chloride; however no details or supporting evidence were provided.[24] It was envisaged therefore that the complex $(CrCp^*)_2Pn^*$ may be accessible using an analogous route. Addition of intensely dark blue THF solutions of $[Cp^*Cr(\mu\text{-}Cl)]_2$ to Li_2Pn^* at −78 °C resulted in dark, black coloured reaction mixtures. Grey-black solutions extracted from the crude residue gave molecular ion peaks in EI mass spectra consistent with the formulation Cp^*CrPn^* (Scheme 4.3 b) and protonated derivatives of this; however any products were NMR silent and could not be isolated or characterised further. Evidence for the formation of multimetallic species was not observed.

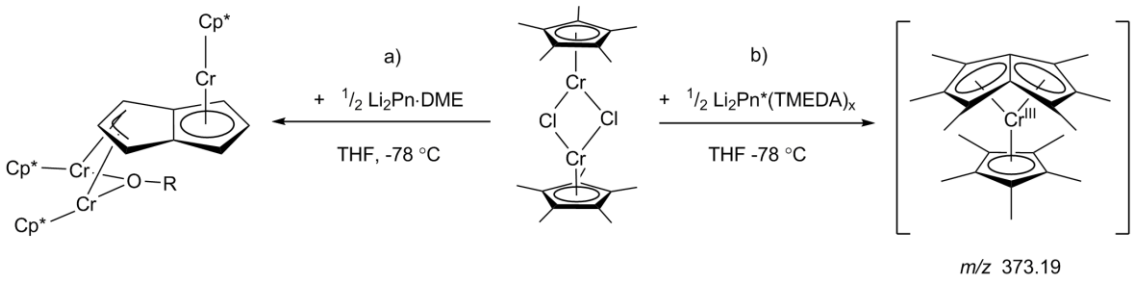

Scheme 4.3 Reactions of $[Cp^*Cr(\mu\text{-}Cl)]_2$ a) with Li_2Pn, and b) attempted reactions with Li_2Pn^*.

Half-sandwich complexes of manganese are rare, typically being constructed by photochemical replacement of the three carbonyl ligands of cymantrene ($CpMn(CO)_3$) with a six-electron donor,[25,26] and hence formally contain manganese(I). Soon after the publication of $MnCp_2$ by Cotton and Wilkinson,[27] the manganese(II) half-sandwich compound, methylcyclopentadienyl manganese chloride was employed by Coffield *et al.* to make aromatic sandwich compounds with mixed ligand sets; the preference for half *vs* full sandwich formation being achieved through stoichiometric control of the reaction between $NaCp^{Me}$ and $MnCl_2$ in tetrahydrofuran.[28]

In attempts to make a manganese bimetallic complex using the salt metathesis method, the previously unreported MnCp*(acac) reagent was pursued. Reacting $Mn(acac)_2$ with either LiCp* or $MgCp^*_2$ yielded bright orange solutions containing only the symmetrically substituted decamethylmanganocene. A milder transfer reagent for the Cp* group was sought, however, Cp^*SiMe_3 did not react with $MnCl_2$·THF or $Mn(acac)_2$.[29]

4.3.2 Attempted synthesis of $(CrCp)_2Pn^*$ and $(MnCp)_2Pn^*$ by ligand substitution

The bimetallic complex $(VCp)_2Pn$ was synthesised by Jones *et al.* and contains *syn*-coordinated vanadium units with a V—V triple bond.[30] Theoretical studies on the model chromium and manganese analogues have indicated that they are also electron deficient, and may exist with a *syn*-conformation that allows M—M bond formation.[31] It was therefore decided to attempt formation of the methylated derivatives using metallocene ligand substitution routes developed above.

Preliminary reactions of chromocene and Li_2Pn^* showed two major resonances by ^1H NMR spectroscopy, one attributed to LiCp and one to $CrCp_2$, as well as paramagnetically shifted resonances, however, complete consumption of the chromocene could not be achieved. Mass spectra showed parent ion peaks consistent

with the formulations CrCpPn*H and $CrPn^*_2H$, and fragmentation patterns thereof, but no multimetallic products.

Addition of a pale yellow THF solution of $MnCp_2$ to half an equivalent of solid Li_2Pn^* at room temperature resulted in immediate formation of intensely black brown solution, with large amounts of a black precipitate. NMR spectra of the crude mixture indicated a complex product distribution, with large amounts of unreacted $MnCp_2$ characterised by a very broad resonance at 21.17 ppm. The product distribution observed by NMR was not changed by use of a 4-fold excess of manganocene. Mass spectrometry indicated the presence of the *m/z* peaks for $Mn_2Cp_2Pn^*$ and fragmentations similar to those observed for $(MCp)_2Pn^*$ (M= Co, Ni); however, no bimetallic products could be isolated or identified.

4.4 Characterisation of *anti*-bimetallics **4.1a**, **4.2a**, **4.2b**, **4.3a**, and **4.3b**

4.4.1 Absorption spectra

IR spectra of all five compounds are superimposable (Figure 4.2), as expected when the ligand components are the same. The Cp capping groups in **4.2b** and **4.3b** cause an additional, broad C–H stretching band at 3098 cm^{-1}, and "oop" bending bands at 782 and 767 cm^{-1} respectively. A very small feature appears at 1211 cm^{-1} for the two nickel complexes, with a corresponding band at 1180 cm^{-1} for the iron and cobalt compounds.

The UV-vis spectra for the complexes each exhibit four discernible features, and spectra are similar for isoelectronic compounds. Like the decamethylmetallocenes,[4] peaks occur at lower wavelength for the Cp* capped **4.3a** compared to **4.3b**, but the λ_{max} values of both dicobalt complexes are very similar.

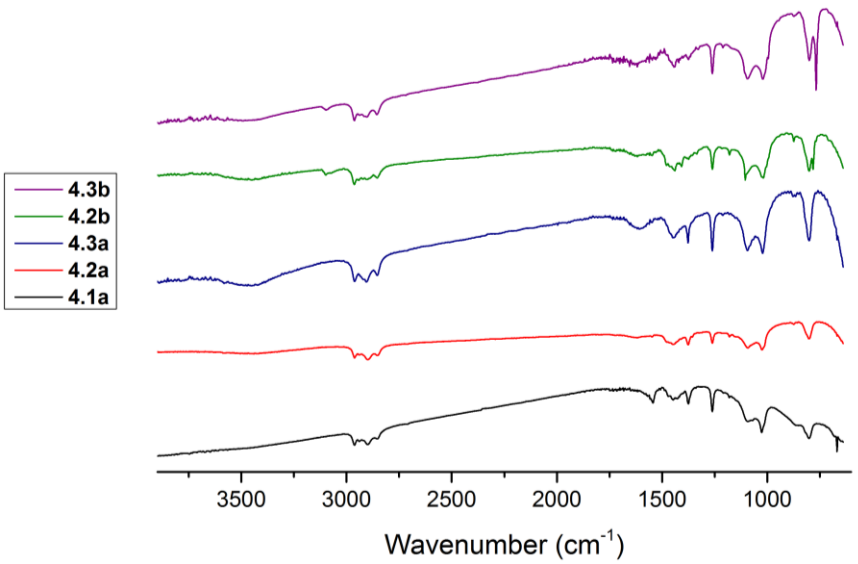

Figure 4.2 IR spectra of bimetallic complexes with a Pn* bridging ligand.

4.4.2 Crystallographic characterisation

The molecular structures of all five bimetallic compounds **4.1a** – **4.3b** were elucidated crystallographically, revealing the metal fragments to reside on opposite faces of the bridging Pn* ligand. In the three compounds **4.1a**, **4.2a**, and **4.3a**, the Cp* ligands adopt a staggered conformation with respect to the Pn* rings, while in the cyclopentadienyl complexes **4.2b** and **4.3b**, the Cp ring carbons eclipse the Pn* ring carbons. Structural data for all crystallographically characterised complexes of the type $(C_5R_5M)_2(Pn^R)$ can be found in the Appendix.

4.4.2.1 Crystallographic characterisation of **4.1a**

Black needles of $(FeCp^*)_2Pn^*$ (**4.1a**) crystallise in the monoclinic space group $P2_1/n$ with two molecules in the unit cell. There is an inversion centre in the middle of the bridgehead C—C bond, such that both iron atoms have identical sandwich structures (Figure 4.3).

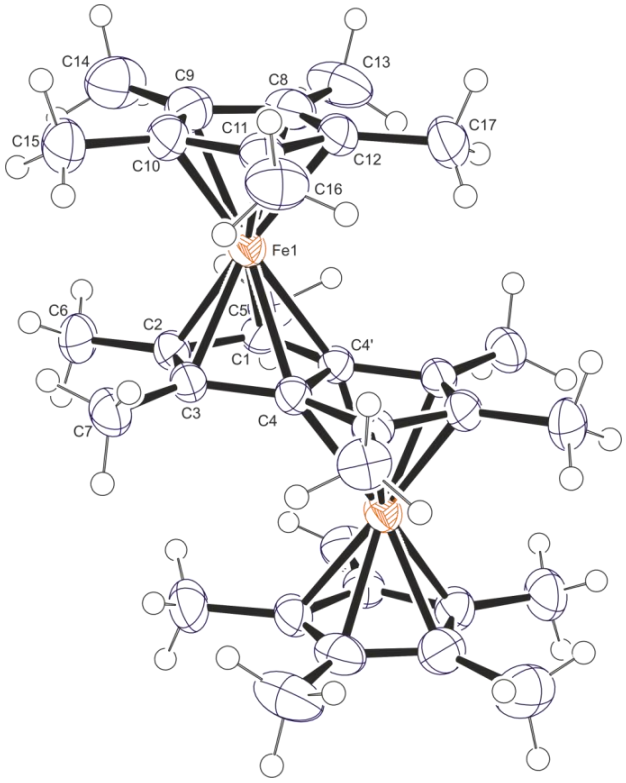

Figure 4.3 Molecular structure of $(FeCp^*)_2Pn^*$, 4.1a. Ellipsoids are shown at 50% probability. Carbon atoms are shown in blue, iron atoms in orange, and hydrogen atoms in black.

Table 4.1 Selected bond lengths, angles and distances for $(FeCp^*)_2Pn^*$, 4.1a.

Bond lengths (Å)	
Fe1—C1	2.050(3)
Fe1—C2	2.018(3)
Fe1—C3	2.050(3)
Fe1—C4	2.185(2)
Fe1—C4'	2.185(3)
Fe1—C8	2.065(3)
Fe1—C9	2.073(3)
Fe1—C10	2.056(3)
Fe1—C11	2.060(3)
Fe1—C12	2.071(3)
C4—C4'	1.453(3)

Distances (Å) and angles (°)	
Fe1—Pn^*_{cent}	1.7031(13)
Fe1—Cp^*_{cent}	1.6727(15)
Fe1—Fe1'	4.1208(7)
Cp^*_{cent}–Fe1–Pn^*_{cent}	176.52
Tilt angle	2.3(2)
Hinge angle	6.20
$(C4-C4')_{cent}$–C2–C6	175.64
δ (%)	8.2

Tilt angle = angle between mean planes of C1,2,3,4,4' and C8,9,10,11,12; Hinge angle = angle between mean planes of C1,3,4,4' and C1,2,3; $\delta(\%) = \frac{[(M-C4)-(M-C2)]}{(M-C2)} \times 100$

The mean planes of the C_5 rings of the Cp* and Pn* ligand are parallel (tilt angle 2.39°), with Fe—centroid distances to these of 1.6731(13) and 1.7027(15) Å

respectively. The five Cp* methyl carbons lie in the same plane as the five ring carbons. The distances between the iron atoms and the bridgehead carbons are on average 0.067 Å longer in **4.1a** than in $(FeCp^*)_2Pn$, with a similar Fe1—C2 distance,[7] resulting in a longer Fe—Fe separation and a delta (δ) value 3.1% larger, *i.e.* a greater distortion away from ideal η^5 coordination.

The C—C bond lengths within the Pn* ligand do not show a significant alternation effect within the estimated standard deviation (Figure 4.4), and are almost identical to those calculated for the dianionic Pn^{2-} in D_{2h} symmetry,[31] indicating extensive delocalisation in the bridging ligand. The bridgehead C4—C4' bond of 1.453(3) Å in **4.1a** is comparable to the 1.464(5) Å in $(FeCp^*)_2Pn$. In the Cp* ligands, the C8—C9, C9—C10, and C11—C12 bond lengths are shorter than the flanking C8—C12 and C10—C11 bonds. Similar π electron localisation has been demonstrated in the ML_4X species $Cp^*Co(CO)_2$,[32] and Cp*Co(acac),[33] and in the bisallyl bridged complex $(CpNi)_2(\mu{:}\eta^3,\eta^3\text{-}C_3H_5{-}C_3H_5)$,[34] and is quite common in half-sandwiches that lack cylindrical symmetry.[35]

Figure 4.4 C—C bond length variation in $(FeCp^*)_2Pn^*$, 4.1a.

4.4.2.2 Crystallographic characterisation of **4.2a** and **4.2b**

Single crystals of **4.2a** $(CoCp^*)_2Pn^*$ were grown by slow evaporation of a THF-d_8 solution, crystallising in the monoclinic, centrosymmetric $C2/c$ space group (Figure 4.5). The Co—Cp^*_{cent} distance of 1.6911(14) Å, and Co—Pn^*_{cent} distance of 1.7447(12) Å are the same (within 3 e.s.d.) to the corresponding lengths in $(CoCp^*)_2Pn$ (1.684 and 1.742 Å respectively),[8] suggesting that stronger L→M donation resulting from permethylation of

the bridging ligand is offset by increased steric repulsion between the alkyl groups. This contrasts with $CoCp^*_2$, which has a longer $Co—Cp^*_{cent}$ distance (1.714 Å) due to greater steric repulsion.[36] Surprisingly, there are few examples of cobaltocene structures with mixed cyclopentadienyl ligand sets in the CSD database, precluding further comparison.

Slow evaporation of a benzene-d_6 solution yielded single crystals of **4.2b** suitable for X-ray diffraction. With the structurally less bulky Cp capping groups, a contracted $Co—Pn^*_{cent}$ distance of 1.7388(11) Å, and elongated $Co—Cp_{cent}$ distance to the capping ligand of 1.7103(12) Å reflect the relief of steric interactions between the Pn* methyl groups and the ring substituents. The M—centroid distances for both **4.2a** and **4.2b** are considerably longer than corresponding values in the 18 VE mixed Co(I) sandwich compounds $(C_4R_4)Co(C_5H_4R')$ (R = Ph, R'= $C(O)(CH_2)_3OH$, $C(O)(CH_2)_3OC(O)C_2H_3$), which have a bulky cyclobutadiene ring, and $Co—Cp_{cent}$ distances of 1.700 and 1.704 Å

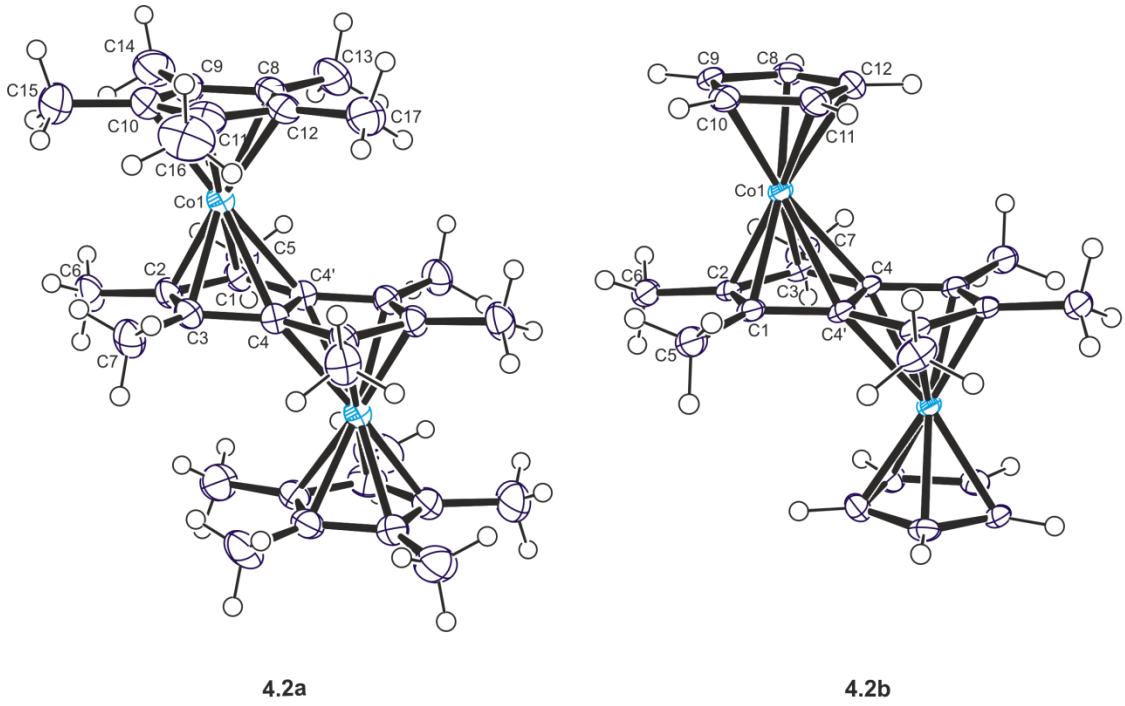

Figure 4.5 Molecular structure of $(CoCp^*)_2Pn^*$, 4.2a, and $(CoCp)_2Pn^*$, 4.2b. Ellipsoids are shown at 50% probability. Carbon atoms are shown in blue, cobalt atoms in turquoise, and hydrogen atoms in black.

respectively, with Co—$C_{4\,cent}$ distances 1.688 and 1.691 Å respectively.[37] Even with the bulky cyclobutadiene group (classed as an L_2 donor),[38] these ML_4X complexes show shorter Co—C distances, indicating that a description of Pn* as two L_2 donors is not a good representation of the bonding in solid **4.2a** or **4.2b**.

Table 4.2 Selected bond lengths, angles and distances for $(CoCp^*)_2Pn^*$, 4.2a, and $(CoCp)_2Pn^*$, 4.2b.

Bond lengths and distances in 4.2a (Å)		**Bond lengths and distances in 4.2b (Å)**	
Co1—C1	2.059(3)	Co1—C1	2.055(2)
Co1—C2	1.991(3)	Co1—C2	2.008(3)
Co1—C3	2.055(2)	Co1—C3	2.052(3)
Co1—C4	2.265(2)	Co1—C4	2.249(2)
Co1—C4’	2.267(2)	Co1—C4’	2.251(2)
Co1—C8	2.056(3)	Co1—C8	2.081(1)
Co1—C9	2.103(3)	Co1—C9	2.144(2)
Co1—C10	2.092(3)	Co1—C10	2.097(3)
Co1—C11	2.065(3)	Co1—C11	2.070(3)
Co1—C12	2.082(3)	Co1—C12	2.076(2)
C4—C4’	1.422(4)	C4—C4’	1.425(3)
Co1—Pn^*_{cent}	1.7447(12)	Co1—Pn^*_{cent}	1.7388(11)
Co1—Cp^*_{cent}	1.6911(14)	Co1—Cp_{cent}	1.7103(12)
Co1—Co1’	4.3032(5)	Co1—Co1’	4.2697(4)

Angles in 4.2a (°)		**Angles in 4.2b (°)**	
Cp^*_{cent}–Co1–Pn^*_{cent}	172.48	Cp_{cent}–Co1–Pn^*_{cent}	171.42
Tilt angle	1.06(17)	Tilt angle	2.15(15)
Hinge angle	6.84	Hinge angle	7.33
$(C4-C4')_{cent}$–C2–C6	173.38	$(C4-C4')_{cent}$–C2–C6	174.41
δ (%)	13.8	δ (%)	12.1

In **4.2a** and **4.2b**, neither bridging ligand shows any localisation of bonds around the edges of the two rings, but the bridgehead bonds are short, at 1.422(4) and 1.425(3) Å in **4.2a** and **4.2b** respectively. The Cp* and Cp ligands both show a similar alternation effect in C—C lengths to **4.1a**.

4.4.2.3 Crystallographic characterisation of **4.3a**, and **4.3b**.

Compound **4.3a** crystallises in the space group $P2_1/n$. Bond lengths between nickel and the bridging Pn* ring carbons range from 1.996(3) to 2.353(3) Å, resulting in a predominantly allylic coordination of Pn* (Figure 4.6, Table 4.3).

Complex **4.3b** crystallises from hexane in the *P*-1 space group. The Ni—C distances to the capping group are longer in **4.3b** than in **4.3a**, consistent with weaker L→M bonding when the Cp ring is less electron-rich.

The Ni—C2 distances are both slightly shorter and the metal–bridgehead distances are over 0.12 Å longer than in bis(allylnickel)pentalene, where the nickel is η^5 coordinated to the bridging Pn ligand.[39] This results in Ni—Pn^*_{cent} distances in **4.3a** and **4.3b** (of 1.8300(14) and 1.8505(15) Å respectively) much longer than the 1.72 Å Ni—Pn_{cent} distance in bis(allylnickel)pentalene, or 1.77 Å Ni—indacene$^*_{cent}$ distances in $(NiCp^*)_2$(*s*-indacene).[8] The distortion away from a symmetrical η^5-hapticity is therefore much more significant in **4.3a** and **4.3b**, and the δ values are the largest reported to date

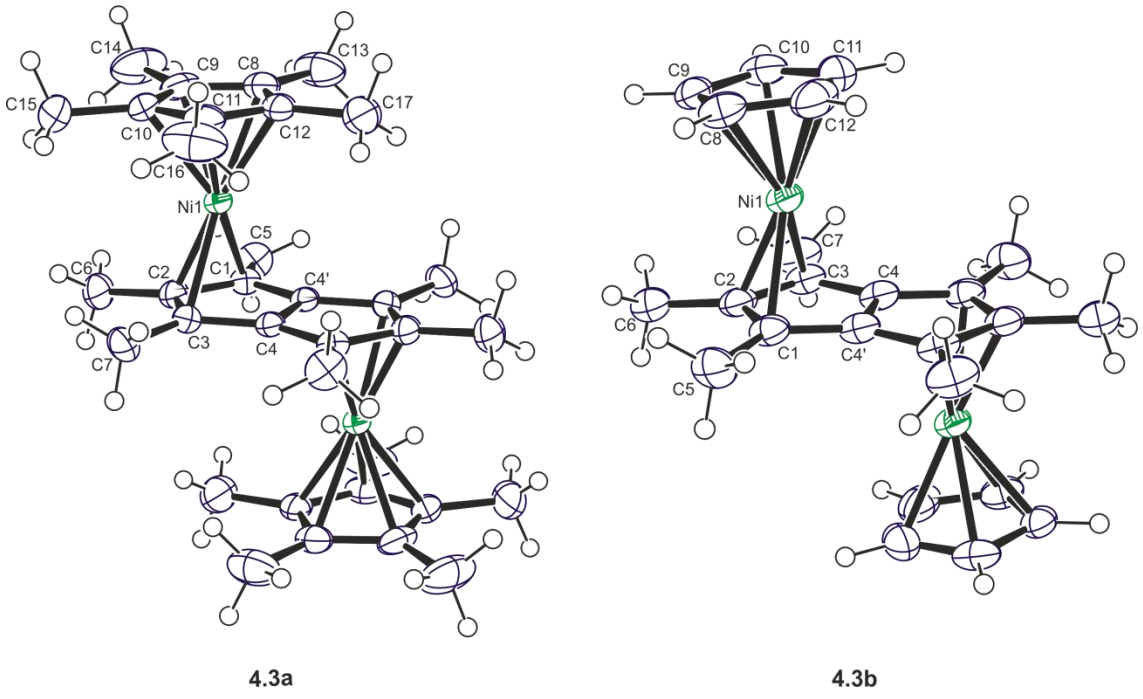

4.3a **4.3b**

Figure 4.6 Molecular structure of $(NiCp^*)_2Pn^*$, 4.3a, and $(NiCp)_2Pn^*$, 4.3b. Ellipsoids are shown at 50% probability. Carbon atoms are shown in blue, nickel atoms in green, and hydrogen atoms in black.

for coordination of nickel to a pentalene derivative.

Table 4.3 Selected bond lengths, angles, and distances for $(NiCp^*)_2Pn^*$, 4.3a, and $(NiCp)_2Pn^*$, 4.3b.

Bond lengths and distances in 4.3a (Å)		**Bond lengths and distances in 4.3b (Å)**	
Ni1—C1	2.131(3)	Ni1—C1	2.142(4)
Ni1—C2	1.996(3)	Ni1—C2	1.998(3)
Ni1—C3	2.147(3)	Ni1—C3	2.145(3)
Ni1—C4	2.353(3)	Ni1—C4	2.390(3)
Ni1—C4'	2.360(2)	Ni1—C4'	2.392(3)
Ni1—C8	2.141(3)	Ni1—C8	2.182(4)
Ni1—C9	2.145(3)	Ni1—C9	2.185(3)
Ni1—C10	2.151(3)	Ni1—C10	2.181(4)
Ni1—C11	2.146(3)	Ni1—C11	2.133(6)
Ni1—C12	2.118(3)	Ni1—C12	2.128(4)
C4—C4'	1.463(3)	C4—C4'	1.470(4)
Ni1—Pn^*_{cent}	1.8300(14)	Ni1—Pn^*_{cent}	1.8505(15)
Ni1—Cp^*_{cent}	1.7687(15)	Ni1—Cp_{cent}	1.8001(19)
Ni1—Ni1'	4.4806(6)	Ni1—Ni1'	4.5495(6)
Angles in 4.3a (°)		**Angles in 4.3b (°)**	
Cp^*_{cent}–Ni1–Pn^*_{cent}	171.27	Cp_{cent}–Ni1–Pn^*_{cent}	175.95
Tilt angle	2.34(18)	Tilt angle	6.5(2)
Hinge angle	2.06	Hinge angle	3.21
$(C4-C4')_{cent}$–C2–C6	173.64	$(C4-C4')_{cent}$–C2–C6	173.99
δ (%)	18.1	δ (%)	19.7

For **4.3a** and **4.3b** the Pn* hinge angles are very small, at 2.06° and 3.21° respectively, and the capping ligand carbon atoms are all coplanar. This contrasts with the complex Cp*Ni(acac), where the bond alternation in the Cp* ring results in significant folding and a large 'hinge angle' of 9.3°.[33]

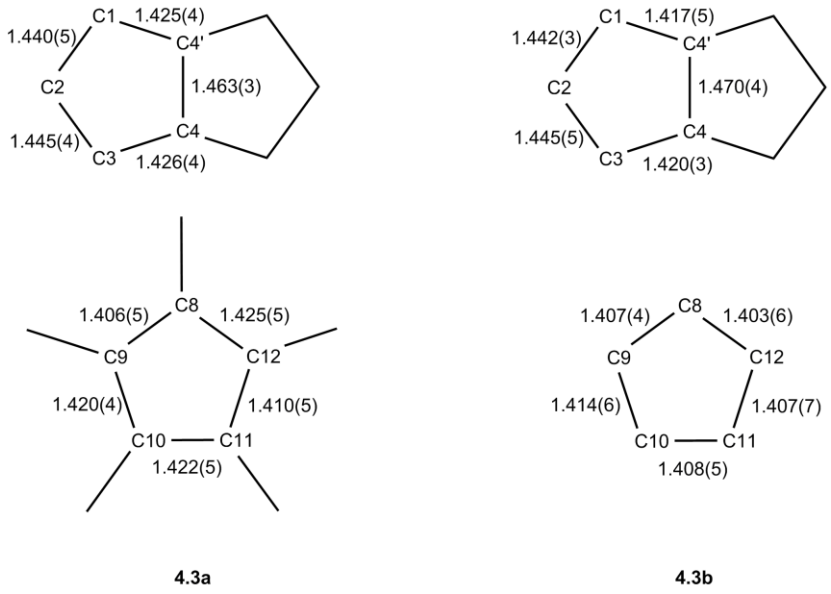

4.3a **4.3b**

Figure 4.7 C—C bond length variation in $(NiCp^*)_2Pn^*$, 4.3a, and $(NiCp)_2Pn^*$, 4.3b.

While the carbon atoms remain essentially coplanar in the two nickel complexes, a bond distortion effect is pronounced in the bridging ligands for both **4.3a** and **4.3b**, and in the Cp* rings but not the Cp ligands (Figure 4.7). In contrast to the Fe and Co complexes, the alternation results in 'single' bonds that are shorter than 'double' bonds. The effect is the inverse of what would be expected for the 'ene-allyl' localisation of allylic and double bonds found in Cp*Ni(acac),[33] but is similar to that seen in the ML_5X complexes $CpMn(CO)_3$.[35]

4.4.3 Comparison of structural and physical properties.

The structures of all five decamethylmetallocenes have C_{2h} symmetry within 3 e.s.d., and contain essentially parallel ligands forming triple decker sandwich compounds. A pronounced variation of the coordination geometry of the bridging ligand occurs across upon changing the metal, resulting in the largest distortions away from η^5-hapticity that have been recorded for *anti*- fused metallocenes with a pentalene bridging ligand. This is clearly depicted in Figures 4.8 and 4.9, where the projection of the metal atom onto the plane of the Pn* ligand moves away from the bridgehead bond.

On moving from Fe, to Co, to Ni, through either series, the distance between the metal atom and the capping group increases. For all complexes, the metal atom is sited closer to the capping group than to the Pn* ligand. The capping groups and Pn* can both contribute five electrons to each ligand-metal bonding interaction *i.e.* both are capable of being L_2X donors. For Pn* however, two of these electrons are shared between the two coordinated metals in a 3c2e bonding interaction, resulting in an overall weaker bonding interaction.

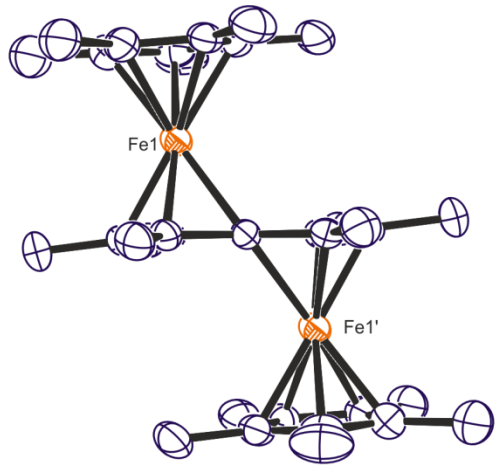

4.1a

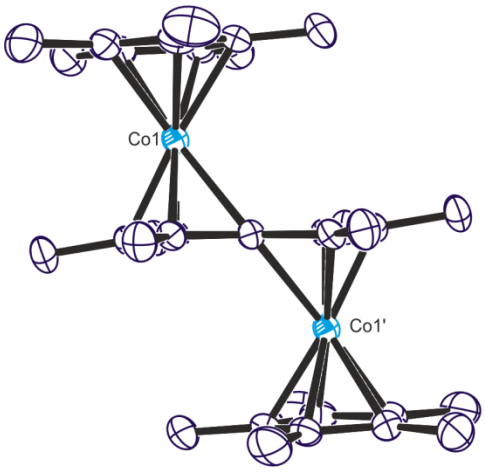

4.2a

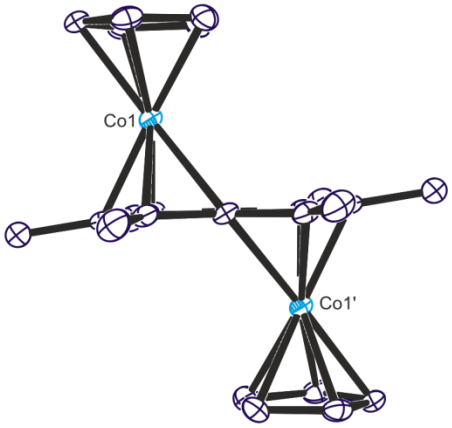

4.2b

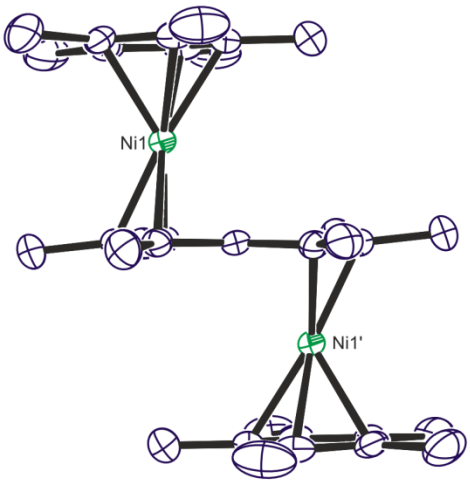

4.3a

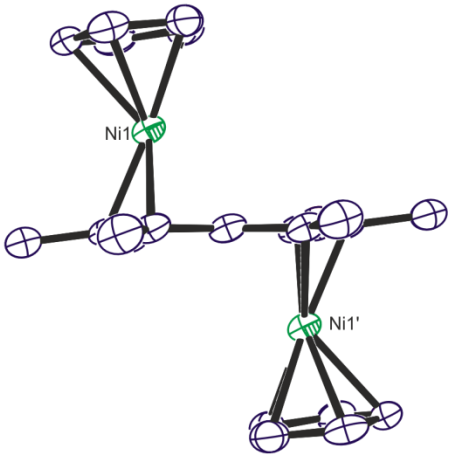

4.3b

Figure 4.8 Side views of the *anti*-bimetallic complexes 4.1a – 4.3b showing the increasing M–bridgehead distances, hinge angles of Pn*, and tilt angles of the capping groups.

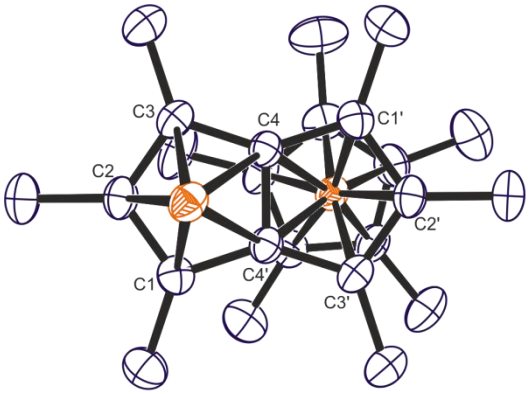

4.1a

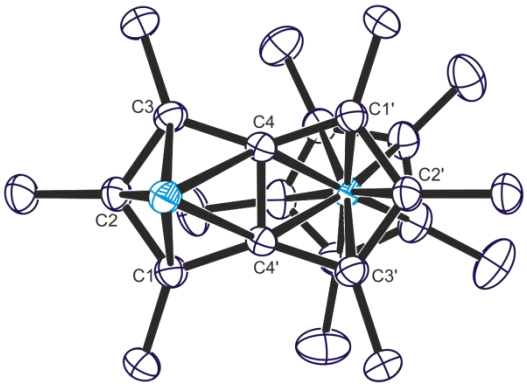

4.2a

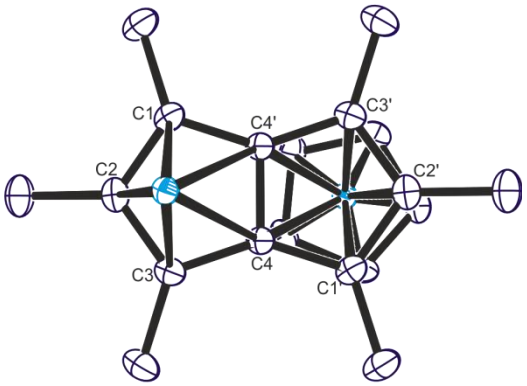

4.2b

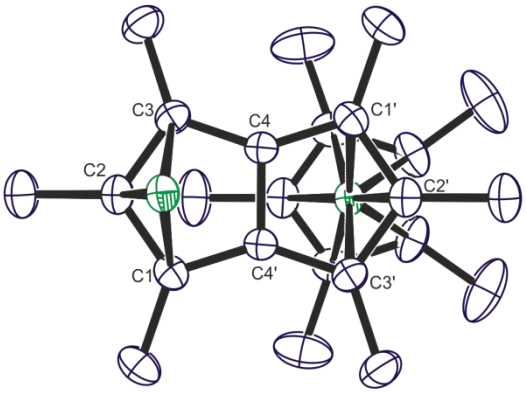

4.3a

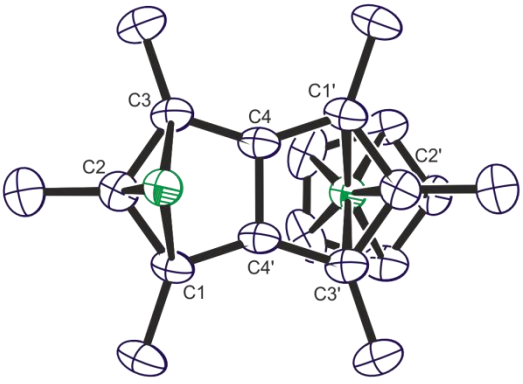

4.3b

Figure 4.9 Plan views of the *anti*-bimetallic complexes 4.1a – 4.3b showing the staggered (4.*n*a) and eclipsing (4.*n*b) capping groups. One capping group has been removed to show the perpendicular projection of the metal atom onto the Pn* plane.

The distorted coordination geometry demonstrated in Figures 4.8 and 4.9 is accompanied by a contraction of the M–WT ring carbon distance and an elongation of the M–bridgehead bond lengths. This can be quantified by the relation $\delta(\%) = \frac{[(M-C4)-(M-C2)]}{(M-C2)} \times 100$, where M—C4 is the metal–bridgehead bond length and M—C2 is the bond length between the metal and the wing-tip ring carbon.[31] The mean results for the compounds described above, and all structurally characterised *anti*-fused transition metal analogues with a pentalene bridge (as well as bis(allylnickel)pentalene) are given in Table 4.4.

Table 4.4 Distortions towards η^3 coordination

Complex	δ(%)	Ref	Complex	δ(%)	Ref
4.1a	8.2	*a*	$(FeCp^*)_2Pn$	5.08	7
4.2a	13.8	*a*	$(CoCp^*)_2Pn$	16.2	8
4.2b	12.1	*a*	(FePnH)Pn(CoCp*)	Fe 4.9 Co 13.05	40
4.3a	18.1	*a*	$[Ni(allyl)]_2Pn$	11.8	39
4.3b	19.7	*a*			

a This work

The distortion, δ, increases with atomic number of the metal, in-keeping with the trend predicted by Garland *et al.*[6] For values of δ in excess of 20%, the bridgehead would be out of bonding distance to the metal, and the coordination mode can be considered allylic.[31] This is almost realised for the dinickel complexes **4.3a** and **4.3b**, which have δ values of 18.1 and 19.7% respectively.

Geometries optimised with quantum mechanical calculations predict greater distortion towards η^3 coordination in the Pn* bridged complexes that contain Cp* capping groups than in those that contain Cp capping groups (*vide infra*). This is found experimentally only for the dicobalt case, while the dinickel complex **4.3b** has greater distortion than **4.3a**. The effect of changing the capping group on the distortion towards η^3 coordination is therefore not clear. For the iron complexes **4.1a** and $(FeCp^*)_2Pn$,

which differ only by alkylation of the bridging ligand, δ is larger for the Pn* complex.[7] For the dicobalt series **4.2a**, **4.2b**, and $(CoCp^*)_2Pn$ however, the distortion is greatest when the bridging ligand is pentalene. For **4.3b**, the largest δ of 19.7%, corresponds to the perpendicular projection of the metal atom onto the Pn* plane being 0.32 Å away from the ring centroid.

Compounds with η^3-cyclopentadienyl and η^3-indenyl rings are known both with and without hinge angles.[1] For Pn*, a large hinge angle would disrupt the conjugation of the aromatic bridging ligand, and very small hinge angles are observed for **4.1a** – **4.3b**, showing the two rings maintain an almost planar geometry despite the shift in coordination of the metal. In combination with the modest C—C bond length localisation (Figure 4.7) seen for the complexes **4.3a** and **4.3b**, which have the highest δ distortion, and it can therefore be inferred that the Pn* π electrons are best considered as delocalised across the bridging ligand, rather than localised.

4.4.4 NMR characterisation

The ^{1}H NMR spectra of the five bimetallic complexes **4.1a** – **4.3b** resolve into three singlets, demonstrating symmetrical coordination of both metal fragments to Pn* in solution. Chemical shifts are listed for comparison in Table 4.5, where non-wing-tip (NWT) denotes the four positions on the Pn* ring adjacent to the bridgehead, and the wing-tip (WT) positions are the remaining two ring positions, each two bonds away from the bridgehead.

For **4.1a** and **4.2b** the ^{13}C NMR resonances could all be assigned using 2D cross coupling experiments, while for **4.2a**, the HMBC coupling is not strong enough to distinguish which of the resonances at 77.1, and 96.4 ppm belongs to the wing-tip (WT) ring carbon and which to the bridgehead. Similarly in spectra of **4.3a** recorded at 223 K, it is not possible to bestow WT or NWT assignments to the two carbon resonances at 70.3, and 92.4 ppm. For **4.3b**, the three ring carbons of Pn* could not be located.

Table 4.5 Summary of ^{1}H and ^{13}C chemical shifts (in ppm) for *anti*-$(MC_5R_5)_2Pn^*$ complexes.

	^{1}H					^{13}C				
	C_5R_5	WT	NWT	NWT^{ring}	WT^{ring}	bh	WT^{Me}	NWT^{Me}	C_5R_5	C_5Me_5
4.1a	1.59	1.46	2.31	64.9	88.9	60.6	10.3	11.5	78.1	9.0
4.2a	1.48	2.12	1.42	59.9	77.1/96.4		11.8	9.8	86.1	9.1
4.2b	4.11	2.08	1.55	99.3	66.1	132.1	12.3	12.0	78.0	-
4.3a	2.75	3.04	2.45	*a*	*a*	*a*	*a*	*a*	*a*	*a*
4.3a*b*	1.93	2.05	2.16	70.3/92.4		101.5	9.6	10.6	91.9	8.8
4.3b	3.17	4.17	2.17	*a*	*a*	*a*	2.9	8.9	95.0	-

4.*n*a R = CH_3, 4.*n*b R = H. *a* ^{13}C resonances could not be detected for paramagnetic complexes 4.3a and 4.3b at room temperature. Chemical shifts measured in benzene-d_6 at 298 K, except for *b* ^{13}C resonances measured in toluene-d_8 at 233 K.

4.4.5 Magnetic studies

The diiron and dicobalt complexes **4.1a**, **4.2a**, and **4.2b**, are diamagnetic, with closed shell configurations, and ^{1}H NMR spectroscopic studies reveal no variation in this behaviour with temperature, in agreement with the finding of Manrìquez for the complexes $(FeCp^*)_2Pn$, $(CoCp^*)_2Pn$, and $(NiCp^*)_2Pn$. In the dinickel complexes **4.3a** and **4.3b** however, the magnetic properties are found to vary with temperature. Due to the *anti*- coordination and large M—M separation (> 4.1 Å) in all cases, any magnetic interactions are expected to be facilitated by the ligand rather than metal—metal overlap.[7,21]

The relationships between chemical shift and inverse temperature (T^{-1}) for $(NiCp^*)_2Pn^*$, **4.3a**, and $(NiCp)_2Pn^*$ **4.3b**, are not linear, and therefore do not conform to the behaviour expected for a simple Curie-Weiss paramagnet. The chemical shifts for both complexes move towards a limiting value (δ_0) with decreasing temperature, corresponding to magnetic resonances in diamagnetic molecules (Figure 4.10 and Figure 4.11). Above ~200 K, the onset of population of a thermally accessible configuration results in the molecules possessing a temperature-dependent magnetisation. The size of the magnetisation, *m(T)*, is proportional to the difference in

population between the ground and excited states. For molecules with a diamagnetic ground state therefore, $(T) \propto \frac{p(T)}{T}$, where $p(T)$ is the Boltzmann population of the excited state, and the factor T^{-1} accounts for the temperature-dependent Curie behaviour of the excited state. Assuming relaxation of electron spin is fast, the nuclei in the molecules will experience a magnetic field proportional to this magnetisation, which augments the field applied inside a spectrometer, causing the chemical shifts to have a temperature-dependent contribution (the isotropic shift). The Boltzmann population, $p(T)$, of a state that differs in energy from the ground state by $\Delta\varepsilon = 2J$, is found by normalising the population of that state ($g_i e^{\Delta\varepsilon/kT}$, where g_i is the multiplicity of state i) by the partition function for the system ($Z = \sum_i g_i e^{-\varepsilon_i/kT}$). For a two level system containing a singlet ground and a triply degenerate triplet excited state, this results in the expression $p(T) = 3e^{2J/kT}/(1 + 3e^{2J/kT})$, which is valid when the Zeeman splitting of the triplet state is small compared to kT.

The temperature-dependence of the chemical shifts of a given nucleus can therefore be modelled using the expression

$$\delta(T) = \delta_0 + \delta_P \cdot m(T) = \delta_0 + \delta_P \cdot \frac{3e^{2J/kT}}{T(1 + 3e^{2J/kT})}$$

where $\delta(T)$ is the position of the chemical shift at temperature T, and δ_p is a constant that relates the temperature-dependence of the high-spin state and hyperfine coupling constant of the described nucleus to the isotropic chemical shift.[41]

The singlet-triplet gap of **4.3a** derived by fitting the Boltzmann description of population of two states to the VT NMR data, yields a *2J* splitting of −1114 cm^{-1} (Figure 4.10). The negative sign of *J* indicates that the ground state is a singlet, and the triplet is higher in energy (see Chapter 3). Solution magnetic susceptibility measured in toluene by the Evans method[42,43] gave a magnetic moment, μ_{eff}, of 1.35 μ_B at 298 K. This intermediate value is lower than expected for an S = 1 species ($\mu_{s.o.}$ = 2.83 μ_B), and consistent with the existence of an $S = 0 \leftrightarrow S = 1$ spin equilibrium. The mole fraction, *x*, of

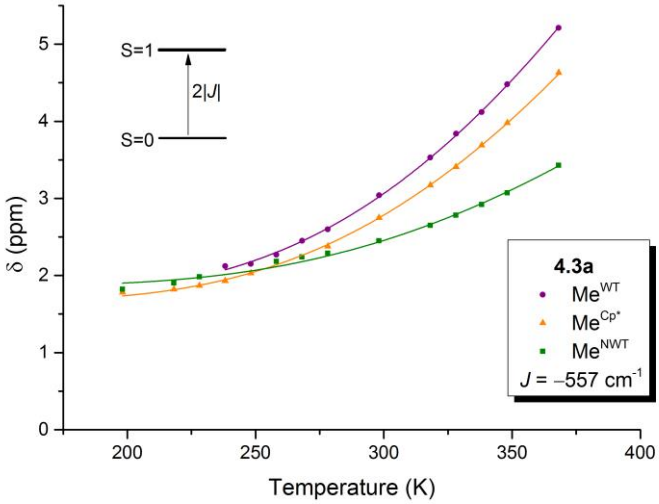

Figure 4.10 Temperature dependence of the ^{1}H chemical shifts of (NiCp*)$_2$Pn*, 4.3a. Me^{WT} = wing-tip methyl protons, Me^{Cp*} = Cp* methyl protons, Me^{NWT} = non-wing-tip methyl protons.

spins in the excited (S = 1) spin state can be calculated using $x = \mu_{eff}^2/\mu_{s.o.}^2$,[15] and is found to be 0.23, *i.e.* 23% of spins populating the triplet state at 298 K.

The fits of the data yield δ_0 values of 1.71, 1.79, and 1.82 ppm for the WT, Cp*, and NWT ^{1}H NMR resonances respectively. A comparison with the values for **4.1a** and **4.2a** reveal there is subtle variation between the diamagnetic shifts of the three Cp* capped complexes. This may be a result of spin polarisation mechanisms, which are discussed in Section 4.4.3.4, and appear to differ in behaviour from the metallocene analogues.

For complex **4.3b**, the Boltzmann fit yields a smaller singlet-triplet gap of −916 cm^{-1} (Figure 4.11). A solution magnetic susceptibility study of **4.3b** in toluene-d$_8$ solution using the Evans' NMR method[43] indicates a solution mass magnetic susceptibility, χ_g, of 6.78 x 10^{-6} dm^3 mol^{-1} at 298 K, which corresponds to an effective magnetic moment, μ_{eff}, of 1.53 μ_B at 298 K, and 29% of spins populating the triplet state at 298 K.

At low temperature, the proton resonances for the WT, NWT and Cp protons are calculated to have δ_0 values of 1.76, 1.88, and 4.79 ppm respectively. As found above,

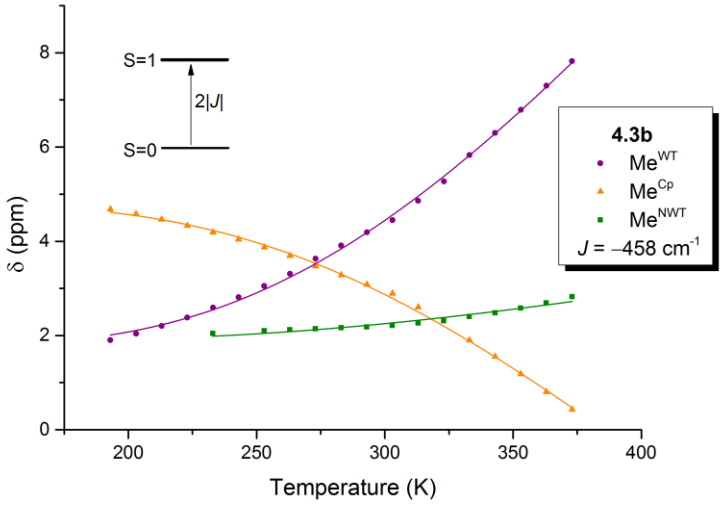

Figure 4.11 Temperature dependence of the ^{1}H chemical shifts of $(NiCp)_2Pn^*$, 4.3b. Me^a = WT methyl protons, Me^b = Cp ring protons, Me^c = NWT methyl protons.

these differ from the diamagnetic values of the isostructural cobalt complex, **4.2b**. The chemical shifts of **4.3a** and **4.3b** are very similar to the monometallic, diamagnetic analogues (η^3-allyl)(η^5-cyclopentadienyl)nickel,[44] and bis(allylnickel)pentalene.[24] These complexes are both NiL_3X_2 species, and by analogy, in **4.3a** and **4.3b**, the bonding may be described as two (ML_3X_2) units at low *T*, *i.e.* the description of Pn* as an allylic, LX donor at low temperatures in these solvated compounds is valid.

4.4.6 DFT studies, electronic structure

Density functional calculations were performed to ascertain information regarding the variation in relative energies and composition of orbitals as a function of the metal, in an attempt to rationalise the observed structural distortions and magnetic properties. Quantum chemical calculations of the optimised geometry for the Cp and Cp* capped complexes of Fe, Co, and Ni, were performed with no symmetry constraints, and resulted in structures with C_i (**4.1a**, **4.2a**) or C_{2h} symmetry (**4.3a**, **4.1b**, **4.2b**, **4.3b**). Selected calculated and observed structural data are shown in Table 4.6. The optimised geometries are in good agreement with the experimental data, with a systematic overestimation of the distortion towards η^3 coordination (δ) observed, as has been

reported for similar calculations on the unmethylated model systems.[31] In particular, the bridgehead bond lengths and hinge angles are reproduced well by the calculations, while the tilt angles are not recreated well; this may be because they are sensitive to the packing of molecules within the crystals. For the dinickel complexes, optimisations were performed for both $S = 0$ and $S = 1$ fixed spin states. The observed δ values are intermediate between the low and high spin states, while the C4—C4' bond length and hinge angles agree better with the $S = 1$ structure for **4.3a**, and the S = 0 for **4.3b**. Overall however, neither calculated structure agrees better than the other with the experimental data.

Table 4.6 Comparison of calculated and observed structural data for 4.1a – 4.3b

	4.1a		**4.2a**		**4.2b**	
	calcd	**obsd**	**calcd**	**obsd**	**calcd**	**obsd**
M—C1/3	2.055	2.050(3)	2.079	2.057	2.064	2.054
M—C2	2.041	2.018(3)	1.968	1.991(3)	1.968	2.008(3)
M—C4/4'	2.175	2.185(3)	2.382	2.266	2.352	2.25
delta (%)	6.6	8.3	21.0	13.8	19.5	12.1
C4—C4'	1.477	1.453(3)	1.435	1.422(4)	1.435	1.425(3)
Tilt angle	5.14	2.39	6.64	1.06	5.04	2.15
Hinge angle	6.81	6.2	8.21	6.84	8.37	7.33

	4.3a			**4.3b**		
	calcd (S = 0)	**calcd** (S = 1)	**obsd**	**calcd** (S = 0)	**calcd** (S = 1)	**obsd**
M—C1/3	2.179	2.192	2.139	2.175	2.157	2.144
M—C2	1.967	2.014	1.996(3)	1.968	1.997	1.998(3)
M—C4/4'	2.551	2.448	2.357	2.531	2.537	2.391
delta (%)	29.7	21.5	18.1	28.6	27.0	19.7
C4—C4'	1.479	1.472	1.463(3)	1.479	1.437	1.470(4)
Tilt angle	10.47	6.25	2.34	10.93	6.75	6.48
Hinge angle	5.47	1.98	2.06	5.24	8.64	3.21

The C—C bond length alternation observed for the diiron and dicobalt complexes, and for **4.3a**, is recreated in the optimised structures. However these effects do not constitute a first order Jahn-Teller distortion, as is seen for the open shell metallocenes

of manganese,[46] cobalt[47] and nickelocene,[48] because the ground states are not degenerate. For complex **4.3a**, both the $S = 0$ and $S = 1$ optimised structures are predicted to exhibit the same alternation; however, for **4.3b** the alternation pattern predicted depends on spin state. The C—C localisation observed in the Pn* ligand of **4.3b** is consistent with the alternation predicted for a singlet structure, in agreement with the observed solution phase magnetic behaviour.

The optimised geometries were used in orbital analysis, and a schematic of the energy levels for **4.1a** – **4.3b** is shown in Figure 4.12. The orbital ordering for $(FeCp)_2Pn^*$, **4.1b**, matches extended Hückel calculations for $(FeCp)_2Pn$ in C_{2h} symmetry, with the non-bonding metal based $22b_u$ – $15b_g$ orbitals (less the $24b_u$) comprising the t_{2g} "block".[6] The HOMO-LUMO gap decreases on crossing from iron to nickel for both series, accounting for the magnetic properties observed in solution, and the Cp* ligands are better π donors than the Cp ligands, raising the energy of orbitals with metal character for the Cp* capped complexes compared to the Cp analogues. The orbital splitting patterns remain essentially unchanged upon changing the capping groups. The exception to this rule is the dinickel complexes, where the LUMO becomes much lower in energy for **4.3b**. DFT calculations confirm the diiron and dicobalt complexes unequivocally adopt closed shell, singlet electronic configurations, as is found experimentally. Complexes **4.1a**, **4.2a**, and **4.2b**, have the same electronic configuration as their literature counterparts where the bridging ligand is unsubstituted.[8]

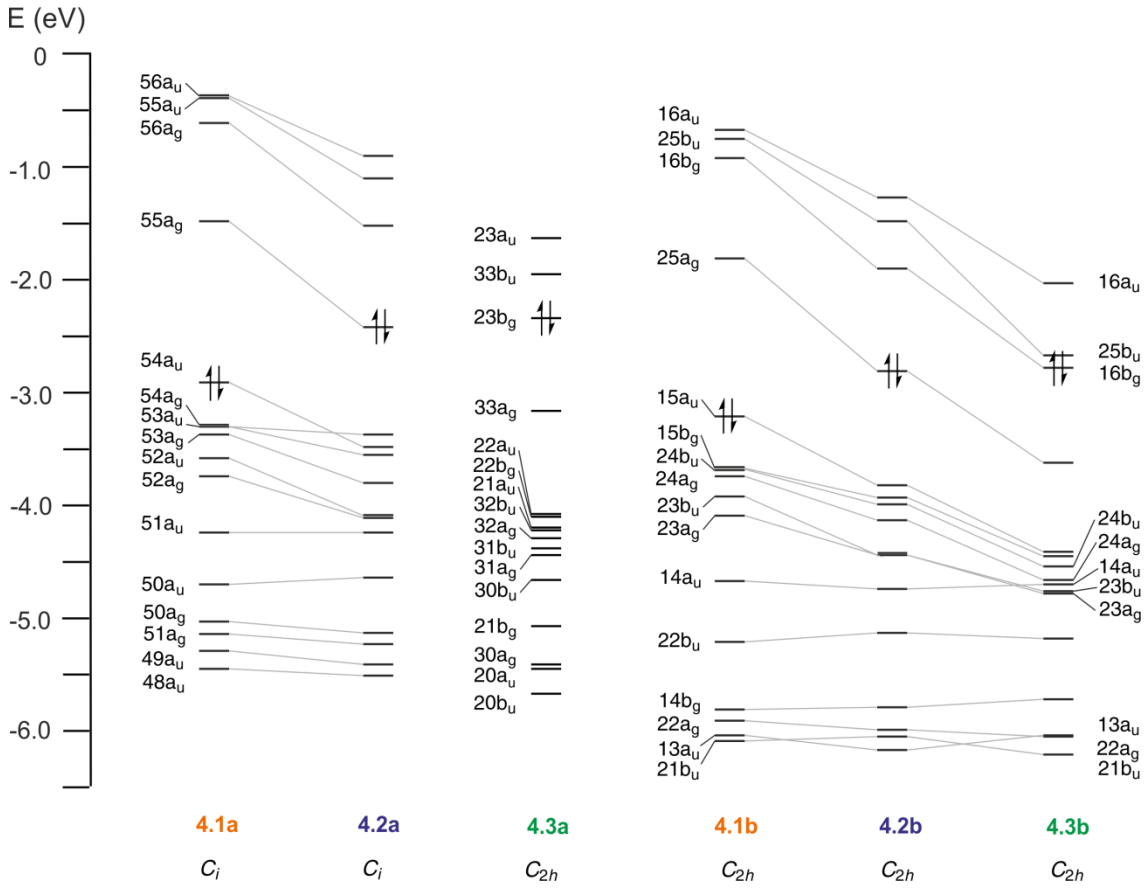

Figure 4.12 Schematic showing calculated energy levels for (MCp*)$_2$Pn*, 4.*n*a, and (MCp)$_2$Pn*, 4.*n*b, complexes (*n* = 1, M = Fe; *n*=2, M = Co; *n* = 3, M = Ni), the HOMO of the ground states are indicated.

The MO diagram has been deconstructed into the Pn* and (Cp*M)···(MCp*) frontier orbitals for **4.2a** (Figure 4.13). Additionally, isosurfaces for the 48a$_u$ – 56a$_u$ orbitals can be found in the Appendix. As can be seen from the Kohn-Sham orbitals, the HOMO of **4.2a** has metal d_{z^2} character and is essentially Co—Pn* non-bonding. The 56a$_g$ LUMO is thermally isolated from the HOMO ($\Delta E \gg kT$), and again has metal character with Co—Pn* antibonding overlap. In the dinickel complexes, this orbital becomes the HOMO in a singlet ground state, and the isosurfaces calculated for 16b$_g$ and 25b$_u$ orbitals of **4.3b** are very similar to the 56a$_g$ and 55a$_u$ depicted for **4.2a**.

The energy of the principle orbitals with M—Pn* bonding overlap ($48a_u$, $49a_u$, $50a_u$, $51a_g$ and $51a_u$) are relatively insensitive to changing the metal (Figure 4.12). The isosurfaces in Figure 4.13 shows how in comparison to **4.1a** where the $54a_u$ HOMO is non-bonding, in the dicobalt and dinickel complexes population of the $55a_g$, and $56a_g$ orbitals (with their appropriate symmetry labels for C_i or C_{2h} symmetry) corresponds to putting electrons into orbitals that have significant M—bridgehead antibonding contributions. Therefore it is the population of these levels that causes the large structural distortions observed in the solid state rather than the stabilisation of orbitals with M—WT bonding character.[31]

For the dinickel complexes **4.3a** and **4.3b**, density functional calculations at the BP level produce optimised structures in which the singlet state lies lower in energy than the triplet, by 0.27 and 0.07 eV respectively. This ordering is consistent with the

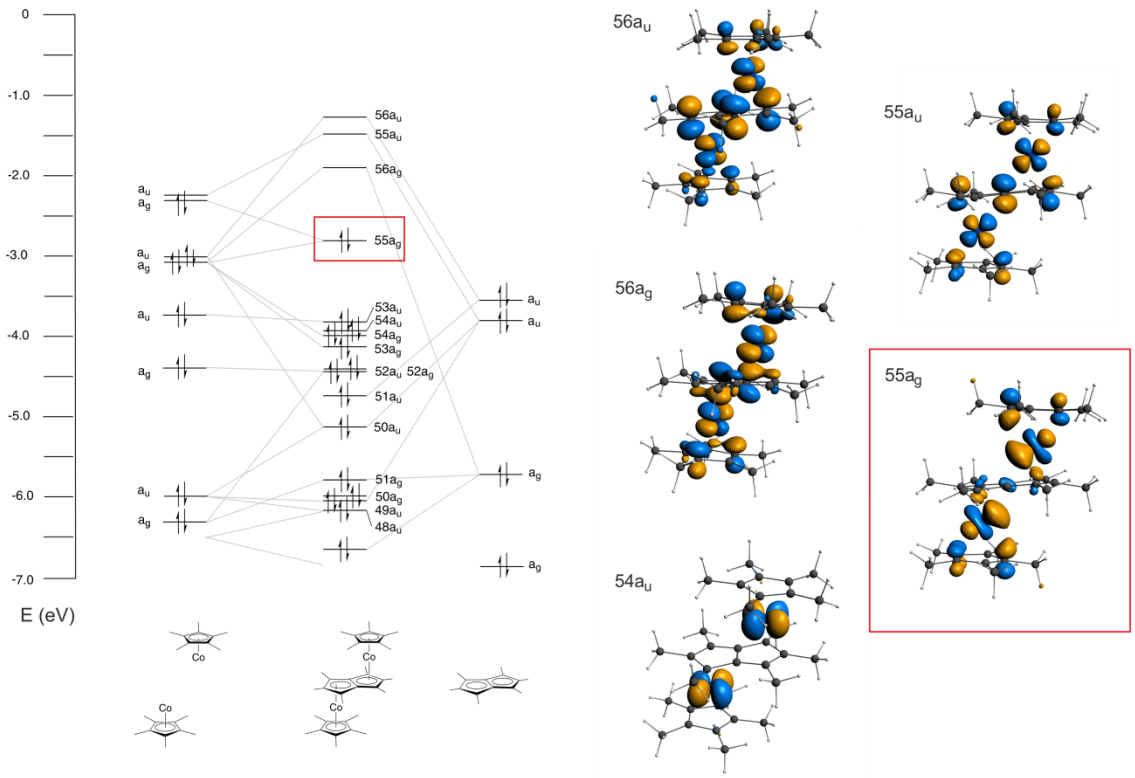

Figure 4.13 MO diagram of $(CoCp^*)_2Pn^*$, 4.2a, with electrons indicating population of the HOMO, showing construction from Pn* and (Cp*Co)···(CoCp*) fragments, with the HOMO highlighted, and selected Kohn-Sham isosurfaces. Isosurface for the other orbitals are collated in the appendix.

solution phase magnetic behaviour observed, and is similar to results calculated for the model system $(NiCp)_2Pn$, where the triplet state was found to lie 0.04 eV higher in energy than the singlet.[31] In calculations at the B3LYP level, the ordering of states inverts, and the triplet is lower in energy, by 0.75 eV for **4.3a**, and 0.81 eV for **4.3b**. By all calculations, a quintet state is not thermally accessible, as it would correspond to promotion of an electron from the next lowest lying $33a_g$ or $25a_g$ orbitals which are well separated in energy from the HOMO. The experimentally observed magnetism indicates that the singlet is lower in energy and the HOMO-LUMO gap of **4.3b** is smaller than that of **4.3a**, consistent with the BP calculations. The observation of diamagnetism in $(NiCp^*)_2Pn$ meanwhile reveals the HOMO-LUMO gap must be larger again when the bridging ligand is unmethylated.[8]

4.4.6.1 Description of the magnetism in *anti*-$(C_5R_5M)_2Pn^*$ complexes

The diamagnetism of the dicobalt complex $(CoCp^*)_2Pn$ was attributed to antiferromagnetic coupling between one unpaired electron per metal site (in analogy with cobaltocene). Making this type of analogy with monometallic metallocenes can work for the bimetallocenes: for example, 38 TNE[31] *anti*-$(CoCp^*)_2$fulvalene exists in a ferromagnetically coupled triplet state,[21] with NMR shifts similar to those in substituted cobaltocenes.[49] However the dicobalt pentalene-bridged *anti*-bimetallics fall into the same 36 TNE class as biferrocene (Figure 4.14), which can be compared to two linked ferrocene moieties. Applying this analogy for the triple-decker complexes $(CoC_5R'_5)_2Pn^{R_6}$ (R, R' = H, Me), these are therefore better described as having closed shell ground configurations, as the electrons are paired in the fully occupied HOMO rather than occupying degenerate SOMOs with antiferromagnetic coupling.[21] This description of the ground state is also applicable to the iron complexes, which are classed as 34 TNE species, as is the biferrocene dication (Figure 4.14). The dinickel complexes

$(NiC_5R'_5)_2Pn^{R_6}$ are 38 TNE species, and therefore it is these for which parallels can be drawn with bicobaltocene (Figure 4.14).

This kind of analogy is limited to isoelectronic bimetallocene complexes that adopt an *anti*-configuration: while *anti*-$(CoCp^*)_2$fulvalene is paramagnetic, isoelectronic *syn*-coordinated 38 TNE bisfulvalene dicobalt has a diamagnetic ground state.[49,50] Similarly, *anti*-$(NiCp^*)_2$fulvalene is paramagnetic, while $[Ni_2(C_{10}H_8)_2]^{2+}$ is diamagnetic.[50]

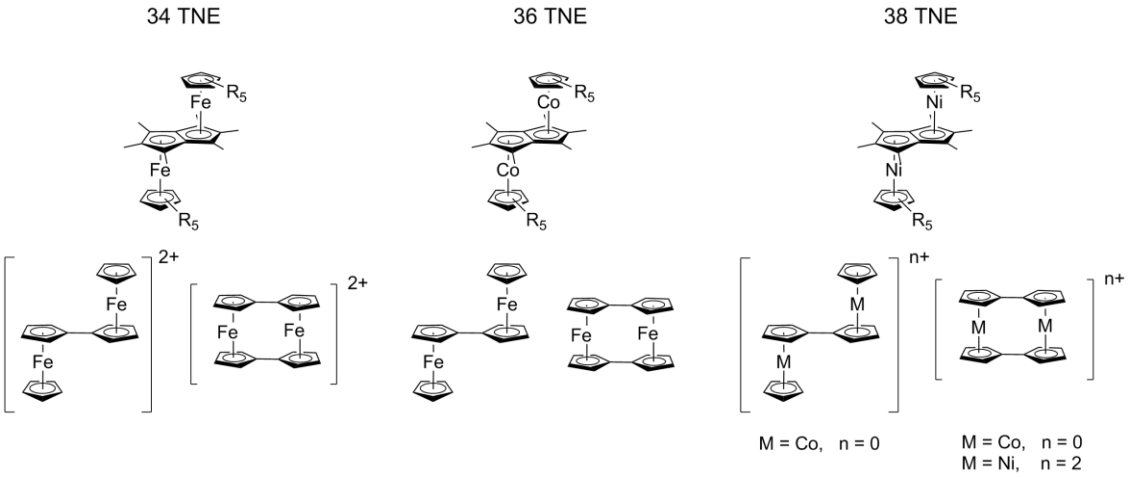

Figure 4.14 Classification of linked and fused bimetallics according to the total number of electrons (TNE) for comparison of magnetic properties.

The ground states of **4.3a** and **4.3b** are diamagnetic and therefore different from that of $(CoCp^*)_2$fulvalene; however, the thermally accessible excited state does have two SOMOs close in energy and similar to $(CoCp^*)_2$fulvalene. The electrons in these can couple through an exchange interaction (see Chapter 3), and antiferromagnetic coupling is observed experimentally. In this way, **4.3a** and **4.3b** behave similarly to the 38 TNE trinuclear hydride bridged nickel complex $K_2[LNi(\mu\text{-}H)_2Ni(\mu\text{-}H)_2NiL]$, where L = *N,N*-(3,5-$C_6H_3{}^iPr_2$)$C_5H_7N_2$.[41]

4.4.6.2 Unusual spin polarisation in **4.3a** and **4.3b**

The isotropic chemical shift of metallocenes and methylmetallocenes can arise from contact or pseudo contact effects. Similar principles should extend to complexes of

Pn*, so it is worth discussing the direction of the paramagnetic NMR shifts in the bimetallic complexes **4.3a** and **4.3b**.

Coupling between electronic and nuclear spin is large, due to the large magnetic moment of an electron. In paramagnetic molecules, this results in two different nuclear states that can be observed by NMR. Electron spin relaxation is fast on the NMR timescale, and uneven population of these nuclear states causes the observed chemical shifts to appear as the weighted average shift of the two states. Contact and pseudo-contact shifts in a molecule operate simultaneously; pseudo-contact shifts arise from interaction of nuclei with the molecules latent magnetic moment, and have both an angular and $\frac{1}{r^3}$ dependence (Figure 4.15 a), while contact shifts are transmitted *via* bonding electrons. Three kinds of contact interactions pertinent to metallocenes are depicted in Figure 4.17 b-d.

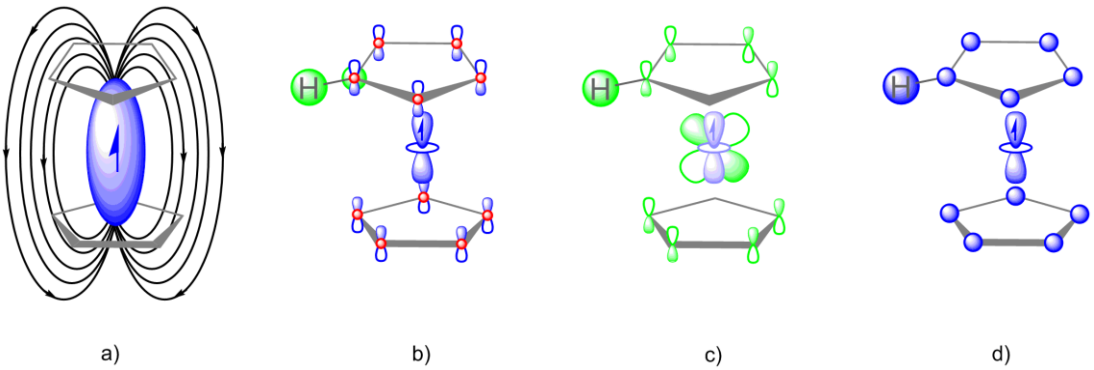

Figure 4.15 Illustrations depicting visualisations of a) the pseudocontact shift mechanism, nuclei interact with a magnetic field generated by the molecules anisotropic spin density; b), c) and d) Fermi contact shift mechanisms: b) electron spin density in mixed Md-Lπ molecular orbitals (depicted blue) results in polarisation of the ring carbon nuclei (depicted red). The spin polarisation mechanism[51] (depicted green) transmits this polarisation to ring substituents through bonds that have electron density at both nuclei; c) electrons in bonding orbitals (green) that overlap with the metal atom are polarised through exchange interactions with the metal-based spin density (blue); d) mixing between the metal based orbital(s) housing the unpaired electron(s) and ligand σ-networks directly causes spin density to reside on the ring protons.

For the paramagnetic 3*d* metallocenes, both Prins[52] and Drago[53] found pseudo-contact interactions to be negligible, and hence the isotropic shift was attributed to a purely Fermi contact processes, later confirmed in quantum approaches.[54,55] The sign of

the hyperfine coupling constant is dependent on whether unpaired electrons occupy ligand based antibonding orbitals, or metal based non-bonding orbitals. For the late metallocenes of cobalt and nickel, the SOMOs are substantially located on the ligands (resembling p_z orbitals, Figure 4.16), resulting in positive spin density (SD) on the ring carbon atoms. This is transmitted to the ring protons by a McConnell type spin-polarisation (SP) mechanism,[51,56] causing ring proton resonances in $Ni(C_5H_4Me)_2$ to move to higher chemical shift, and methyl proton resonances to move to lower chemical shift.[55]

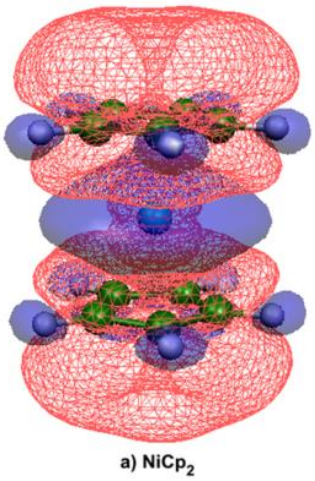

Figure 4.16 Spin-density distribution in nickelocene calculated by Hrobárik *et al.* with DFT methods, +/−0.0001 a.u. isosurfaces; red "chickenwire" indicates positive spin density, blue "transparent" indicates negative spin density.[55]

The sign of the spin density at an atom determines the direction of the isotropic chemical shift in NMR spectra. For each bond across which an SP mechanism operates, the sign of polarisation of the adjacent nucleus is inverted. For methylnickelocene therefore, electron spin density on ring protons is opposite in sign to the carbon to which they are attached.[56–60] The protons in the methyl group have electron density of the same sign as the corresponding ring carbon.[61,62] The proton shifts of the capping ligands in **4.3a** and **4.3b** increase in opposite directions with temperature accordingly. The ring protons on Cp move to lower chemical shift with increasing *T*, while the methyl protons on Cp* move to higher chemical shift (Figure 4.10 and Figure 4.11), thus the sign of the isotropic shifts are the same as those of nickelocene and

dimethylnickelocene.[63,64] Similar behaviour is observed in the trimetallic half-sandwich cobalt complexes $Co_3(\eta^5\text{-}C_5R_5)_3(\mu\text{-}X)_2$ (R=H, X=S; R=Me, X=CO) which exhibit spin equilibria.[65]

Calculations on **4.3a** and **4.3b** reveal the Pn* bridging ligand and C_5R_5 rings bear significant spin density (Figure 4.17), similar to nickelocene and $(CpNi)_2$fulvalene.[21,66] In **4.3a**, positive spin density is spread across the capping ligands, the nickel atoms, and the NWT ring positions of Pn*, with negative spin density at the WT ring carbons (Figure 4.17 a). In **4.3b**, the spin density on MCp fragments are similar to **4.3a**, but on the Pn* rings is different: positive density is concentrated across the bridgehead and WT positions, with negative density at the NWT ring carbons (Figure 4.17 b). This alternation of sign of spin density around the Pn* ligand is different to nickelocene (Figure 4.16), where it is the same at each atom of the Cp rings.

Despite the ring carbons of Pn* having spin densities with opposite sign, both the wing-tip and non-wing-tip methyl protons in **4.3a** and **4.3b** experience positive contact shifts (of the same sign as the methyl groups on Cp* capping groups). A similar effect is seen in the complexes *cis*-$(VCp)_2$COT,[67] and *cis*-$(VCp)_2$Pn,[30] which have two VCp

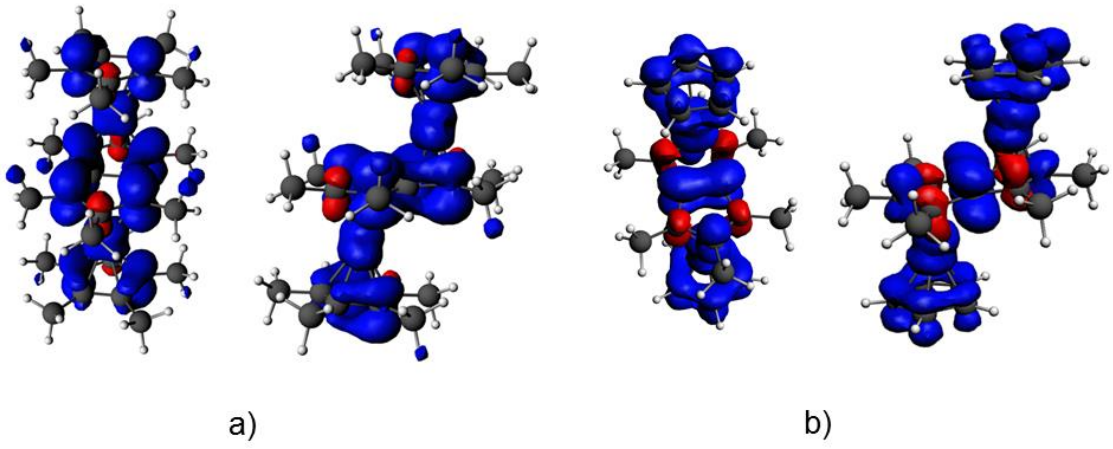

Figure 4.17 Spin density isosurfaces for triplet state of a) $(NiCp^*)_2$Pn*, 4.3a: bh 0.018, NWT, 0.151, WT -0.044; and b) $(NiCp)_2$Pn*, 4.3b: bh 0.174, NWT -0.046, WT 0.078 (two views for each). Positive spin densities are indicated by the colour blue, and negative spin densities by the colour red.

fragments coordinated cofacially to unsubstituted COT and Pn rings respectively: the chemical shifts of both proton resonances of the bridging ligand increase in shift with *T*, while the Cp ring protons decrease in shift.

By analogy with nickelocenes, the contact interactions between the two types of methyl proton in Pn* and the spin density at the ring carbon should result in spin densities with the same sign (Figure 4.18), however this is not observed. Two reasons could explain the fact that the ring carbons have opposite spin densities to each other, but the methyl protons both increase in shift:

1. A pseudo-contact interaction causes the isotropic shift and dominates over the Fermi contact interactions, with a magnetic moment that is highly anisotropic
2. The relative spin distribution and spin polarisation mechanisms contribute differently to the hyperfine coupling constants for substituents at the WT and NWT positions.

In **4.3a** and **4.3b**, the separation of the SOMOs is small, and the similarities in structure and isotropic behaviour of the capping ligands make it likely that the large Fermi contact interactions seen for $NiCp_2$ are not dissimilar in the bimetallics. Therefore

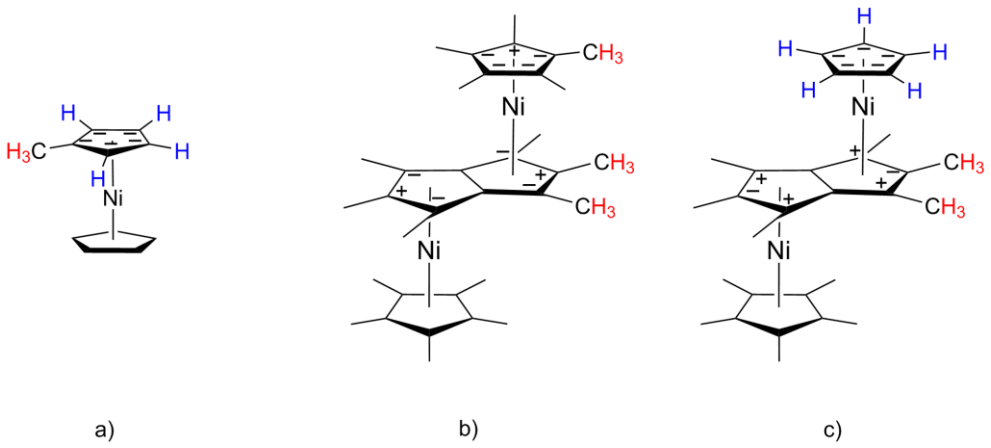

Figure 4.18 Summary of spin densities on ring carbons (indicated by + and − signs) and the corresponding isotropic shift observed for protons in a) 1,1'-dimethylnickelocene, b) $(NiCp^*)_2Pn^*$, 4.3a, and c) $(NiCp)_2Pn^*$, 4.3b. Isotropic shifts to higher chemical shift are indicated by the colour red, and to lower chemical shift by the colour blue.

it is unlikely that the size of a pseudo-contact shift would be much larger than the nickelocenes, where such a shift is negligible.

4.5 Cyclic voltammetry

The bimetallic compounds synthesised in section 4.2 have been subjected to cyclic voltammetry studies. Like the multiferrocenyl linked metallocenes,[68] the bimetallic species **4.1a** – **4.3b** exhibited poor solubilities in acetonitrile, and chemical instability in dichloromethane, precluding these as electrochemical solvents. The solubilities in THF were suitable for all complexes save for **4.3a**, and 0.1 M solutions of an ammonium hexafluorophosphate ($[NBu_4][PF_6]$) electrolyte in THF were used for all CV experiments.

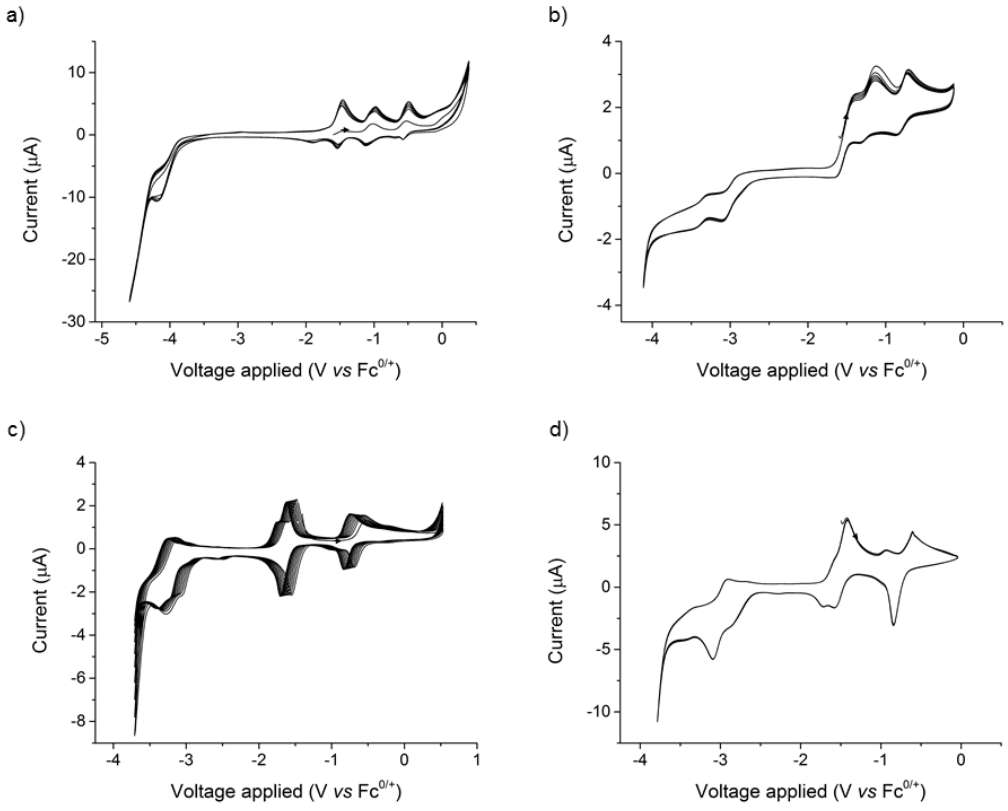

Figure 4.19 Overlaid cyclic voltammograms obtained by scanning 0.1 mM solutions of a) $(FeCp^*)_2Pn^*$, 4.1a (5 cycles), b) $(NiCp)_2Pn^*$, 4.3b (5 cycles), c) $(CoCp^*)_2Pn^*$, 4.2a (10 cycles), and d) $(CoCp)_2Pn^*$, 4.2b (5 cycles), in THF containing 0.1 M $[NBu_4][PF_6]$ at a scan rate of 0.1 V s^{-1}.

Full scans over the accessible solvent window were conducted at a scan rate of 0.1 V s^{-1} for **4.1a**, **4.2a**, **4.2b**, and **4.3b**, with the results shown in Figure 4.19. In accord with the recommendation of Geiger,[69] positive peak currents correspond to oxidative electron transfer (ET) events.

4.5.1.1 Cyclic voltammetry of **4.1a**

The cyclic voltammogram of diiron compound **4.1a** (Figure 4.19 a) exhibits three oxidation events in the region −1.5 to 0 V *vs* $Fc^{0/+}$. In addition to these, one irreversible event occurs at −1.9 V with a very small peak current, and one quasi-reversible reduction at −4 V (*vs* Fc). A similar shaped feature occurs in all voltammograms of pentalene complexes at a similar low potential.[15,70,71] The $E_{½}$ values *vs* Ag and ferrocene (Fc) are recorded in Table 4.7, using the relation $E_{½}=(E_{pa}+E_{pc})/2$ (which is only strictly true for reversible processes).[72]

Table 4.7 Peak potentials of reversible ET events obtained from cyclic voltammograms of 4.1a.

	$E_{½}$	$E_{½}$	$E_{½}$	$(E_{½})$
vs Ag	−2.60 [a]	0.12	0.58	1.05
vs $Fc^{0/+}$	−4.20 [a]	−1.48	−1.02	−0.55

Using $E_{½}= (E_{pa}+E_{pc})/2$ [a] E_{pc}

The $E_{½}$ of −0.55 V *vs* $Fc^{0/+}$ corresponds to the peak potential of $[FeCp^*_2]^{0/+}$ in THF.[73] The small potential separation of the events makes calculation of peak current (i_{pa} or i_{pc}) values difficult. However, a plot of the peak cathodic (E_{pc}) and peak anodic (E_{pa}) potentials shows the voltage for the remaining two events are independent of sweep rate for scan rates of 0.1 to 1 V s^{-1} (Figure 4.20, Figure 21 a), indicating reversible behaviour in this region. This is supported by the difference in peak potentials ($|E_{pc} - E_{pa}|$) for the redox events in the range 0.1 – 1 V s^{-1} (Figure 4.21 b), which fall in the region 57 – 128 mV (for a perfectly reversible couple, $E_{pc} - E_{pa} = -57$ mV).

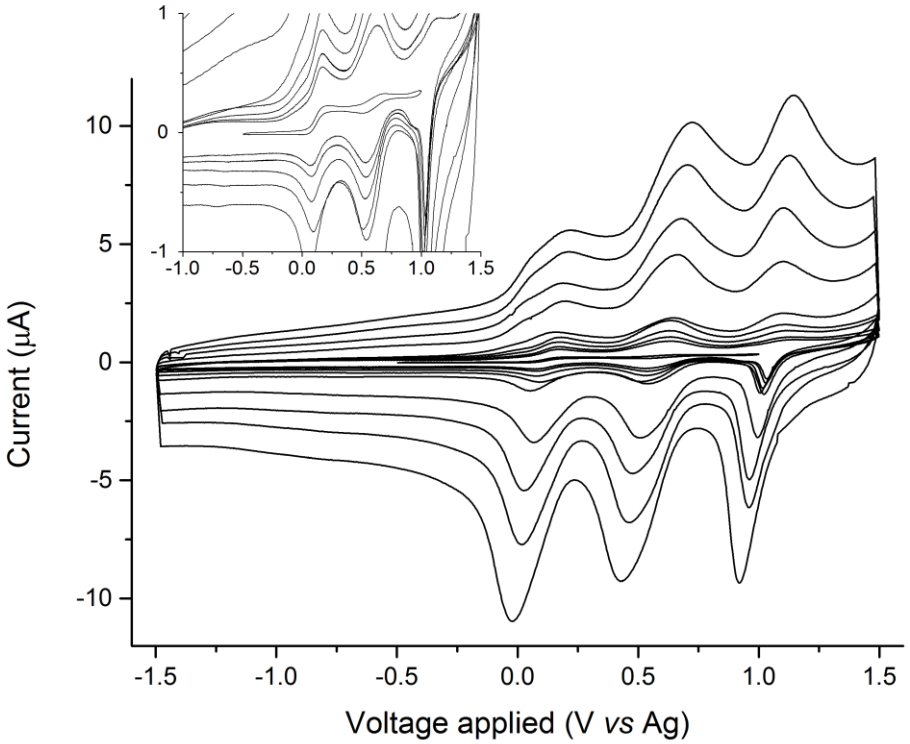

Figure 4.20 Overlaid cyclic voltammograms (1 cycle) obtained by scanning a 0.1 mM solution of 4.1a in THF containing 0.1 M [NBu_4][PF_6] over the region −1.5 to 1.5 V at scan rates ranging from 0.1 to 10 V s^{-1}. The $Fc^{0/+}$ couple comes at 1.60 V.

The two peaks at −1.48 and −1.02 V *vs* $Fc^{0/+}$ are assigned to the [**4.1a**]$^{0/+}$ and [**4.1a**]$^{+/2+}$ couples respectively, and the reduction at −4.20 V to the [**4.1a**]$^{-/0}$ couple. Information regarding the stabilisation of the monocation (conferred by the presence of a second metal atom and facilitated by the bridging ligand) can be inferred from the

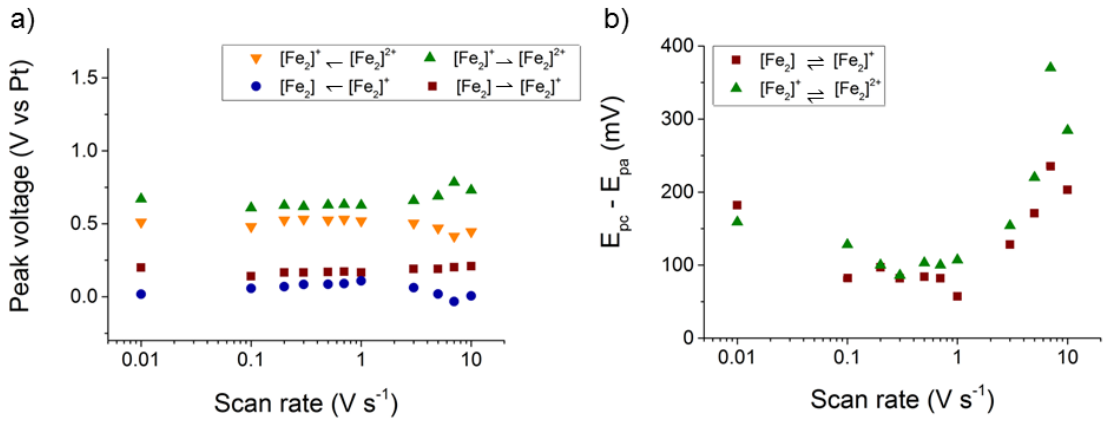

Figure 4.21 Plots of a) peak potentials of ET events versus scan rate for 4.1a, and b) difference in peak potentials, $\Delta E=(E_{pa}-E_{pc})/2$, for the ET events shown in a).

separation of the peak potentials for the 0⇌1+ and 1+⇌2+ events, $\Delta E_{½}^{0/2}$, however it should be noted that the magnitude of K_c is affected by a number of factors in addition to charge delocalisation, including structural reorganisation,[74] electrostatic,[75] inductive, and magnetic factors. The [**4.1a**]$^{0/+}$ and [**4.1a**]$^{+/2+}$ couples are clearly reversible between 0.1 and 1 V s^{-1} (Figure 4.21), and the comproportionation constant, K_c, is 6.02 x 10^7 (using $\Delta E_{½}$ = 0.46 V). Values of K_c >10^6 correspond to extensive delocalisation and complex [**4.1a**]$^+$ can therefore be classified as a Class III mixed-valence species according to the Robin—Day system.[76] This is seven orders of magnitude smaller than the comproportionation constant for the pentalene bridged analogue, $(FeCp^*)_2Pn$, for which the peak separation of the corresponding ET events is 0.85 V.[8]

4.5.1.2 Cyclic voltammetry of **4.3b**

Nickel complex **4.3b** has three quasi-reversible events that occur between 0 and 1 V *vs* Fc$^{0/+}$, and two below −1 V. At scan rates above 1 V s^{-1}, maxima and minima for these events can be distinguished (Figure 4.22). However, at slower scan rates, there is coalescence of the reductive peaks. The five quasi-reversible peaks are listed in Table 4.8.

Table 4.8 Peak potentials of reversible ET events obtained from cyclic voltammograms of 4.3b.

	$E_{½}$(I)	**$E_{½}$(II)**	**$E_{½}$(III)**	**$E_{½}$(IV)**	**$E_{½}$(V)**
vs Ag	−1.86	−1.48 [a]	0.08	0.39	0.87
vs Fc$^{0/+}$	−3.48	−3.10 [a]	−1.54	−1.15	−0.75

The half-cell potentials indicate no nickelocene is present in the sample (for $NiCp_2$ the 1−⇌0, 0⇌1+ and 1+⇌2+ couples are found at −2.3, −0.44, and +0.36 V *vs* Fc$^{0/+}$ respectively in $[NBu_4][PF_6]$/THF[77]), and all five redox events are attributed to **4.3b**. At the slower scan rates of 0.1 and 0.01 V s^{-1}, the i_{pa}/i_{pc} ratios of the two most anodic waves increase, and the reduction events IV and V are diffusion controlled (Figure 4.22).

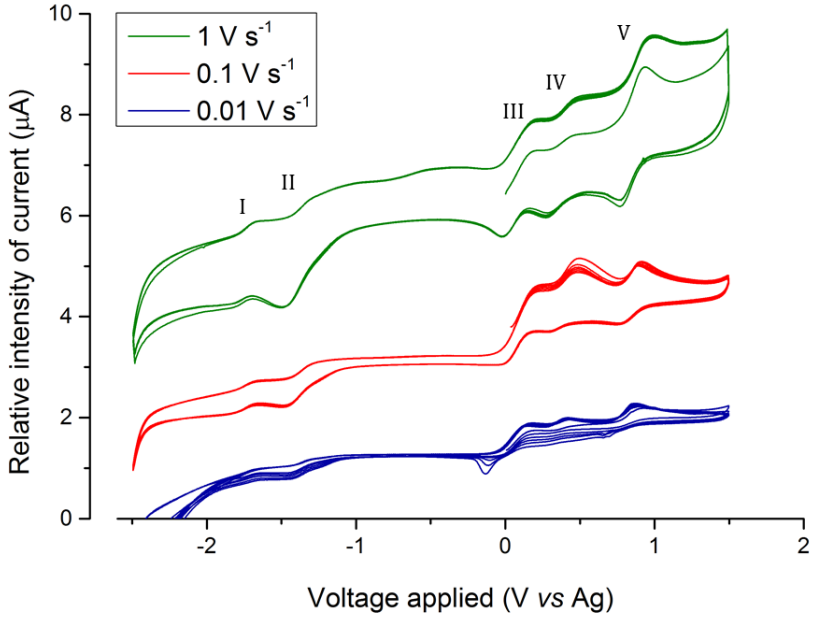

Figure 4.22 Offset plot of overlaid cyclic voltammograms (5 cycles) obtained by scanning a 0.1 mM solution of 4.3b in THF containing 0.1 M [NBu_4][PF_6] over the region −2.5 to 1.5 V at scan rates of 0.01, 0.1, and 1 V s^{-1}. The $Fc^{0/+}$ couple comes at 1.62 V.

Inspection of the MO diagram (Figure 4.14) reveals that oxidation to the monocation of **4.3b** should be accomplished slightly more easily than **4.1a**, and hence peak III at 1.54 V *vs* $Fc^{0/+}$ is attributed to this couple. Events IV and V are hence tentatively assigned to the [**4.3b**]$^{+/2+}$ and [**4.3b**]$^{2+/3+}$ couples respectively. The final events, II and I, then correspond to the [**4.3b**]$^{-/0}$ and [**4.3b**]$^{-2/-}$ couples. The similarity in separation for peaks I and II ($\Delta E_{½}^{-2/0}$) and peaks III and IV ($\Delta E_{½}^{0/2}$) suggest there is very little delocalisation in the mixed valence [**4.3b**]$^-$ anion and [**4.3b**]$^+$ cation. The observation of six accessible oxidation states for 38 TNE **4.3b** contrasts with the reported electrochemistry for 40 TNE fulvalene-bridged binickelocene, for which only [$(CpNi)_2$fulvalene][PF_6]$_n$ n = 0, 1, 2 have been isolated,[50] and with 38 TNE $(CoCp)_2$fulvalene, for which only the 0⇌1+ and 1+⇌2+ couples have been reported.[19,22]

4.5.1.3 Cyclic voltammetry of **4.2a and 4.2b**

The dicobalt complexes **4.2a** and **4.2b** have similar voltammograms, with two main features apparent at 0.1 V s^{-1}, as well as a quasi-reversible event at low potential.

For the overlaid full scan of **4.2a** (Figure 4.21 c), a reference electrode drift is responsible for the cathodic shift of the current responses. After correcting for this drift, all cycles overlap for both **4.2a** and **4.2b**, indicating that there is no decomposition of the redox-active species in solution. For both **4.2a**, and **4.2b**, the scans at 0.1 V s^{-1} contain two overlapping peaks at *circa* −1.5 V (*vs* $Fc^{0/+}$) (Figure 4.21 c,d). The overlapping peaks that occur with $E_{½}$=−1.87 V for **4.2a**, and $E_{½}$=−1.33 V for **4.2b**, can be ascribed to $[CoCp^*_2]^{0/+}$ and $[CoCp_2]^{0/+}$ contaminants respectively.[17,73] The 1−⇌0 couple has not been reported for $CoCp^*_2$, but for $CoCp_2$ in THF it is found at *circa* −2.49 V *vs* $Fc^{0/+}$,[78] and no peak corresponding to this is observed in the full scan of **4.2b**. The remaining two events in the voltammograms of **4.2a** and **4.2b** then have similar peak currents to each other, and can be ascribed to the 0⇌1+ and 1+⇌2+ redox couples.

For **4.2a**, the scan rate was varied from 0.05 to 10 V s^{-1} over the region −1.25 to 1.0 V, and peak voltages were referenced in a fixed relationship to the measured $Fc^{0/+}$ couple to account for a reference electrode drift (Figure 4.23). A plot of the peak currents for each of the two events is shown in Figure 4.24.

The graphs in Figure 4.24 demonstrate that anodic and cathodic peak currents for the two ET events at $E_{½}$ = −1.68 V and −0.79 V (*vs* $Fc^{0/+}$) are very similar. However, the E_{pa} and E_{pc} values are dependent on the scan rate (Figure 4.23), and the peak currents do not vary linearly with the square root of the scan rate (Figure 4.24), thus the two processes are quasi-reversible.

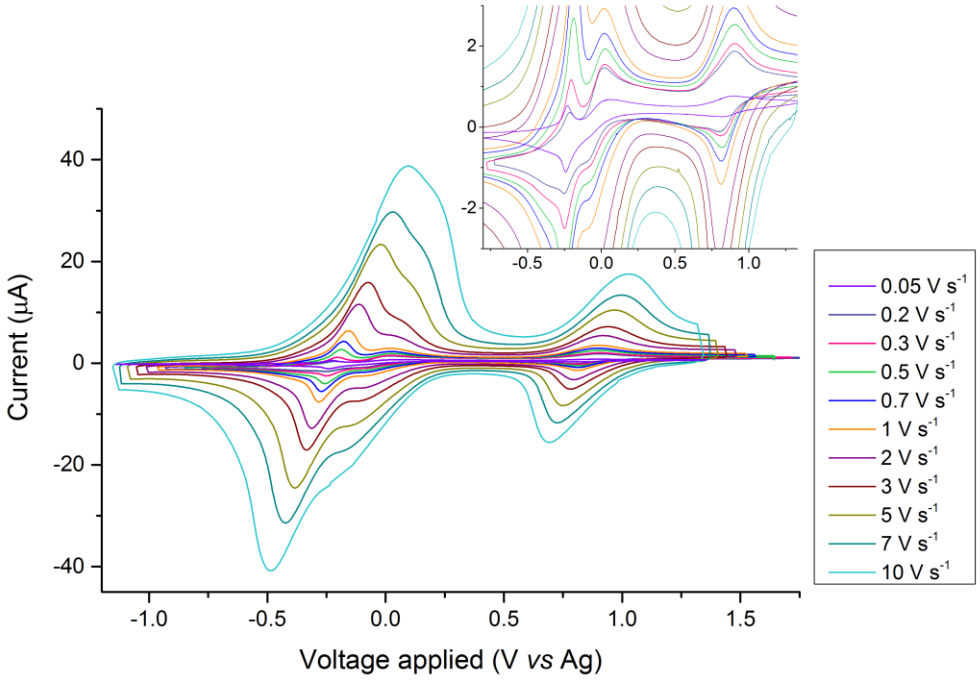

Figure 4.23 Overlaid cyclic voltammograms (1 cycle) obtained by scanning a 0.1 mM solution of 4.2a in THF containing 0.1 M [NBu$_4$][PF$_6$] over the region −1.25 to 1 V at scan rates ranging from 0.05 to 10 V s^{-1}. Drift of the pseudo reference electrode has been corrected by referencing the peak at 0.86 V against the Fc$^{0/+}$ couple, for which E$_{½}$ = 1.65 V.

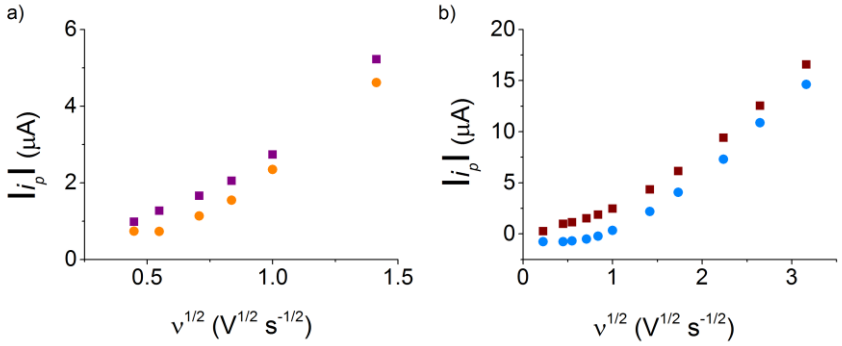

Figure 4.24 Plots of the modulus peak currents *vs* the square root of the scan rate for the two events at a) E$_{½}$=−0.03 V, and b) E$_{½}$=0.86 V, in Figure 4.17. ■ indicates an anodic peak current (i_{pa}), ● indicates the modulus of a cathodic peak current (i_{pc}).

A comparison of the most cathodic features for **4.2a** and **4.2b** with the other scans in Figure 4.21 for isostructural complexes, and with the voltammograms for $Fe_2Pn^*_2$ in Chapter 3, reveals two couples may be coalesced in the voltammograms. This is most apparent for **4.2b**, where increasing the scan rate to 2 V s^{-1} or above confirms the emergence of a quasi-reversible peak (Figure 4.25). One of these events appears Nernstian, while the other is poorly resolved. The first peak can be assigned to a

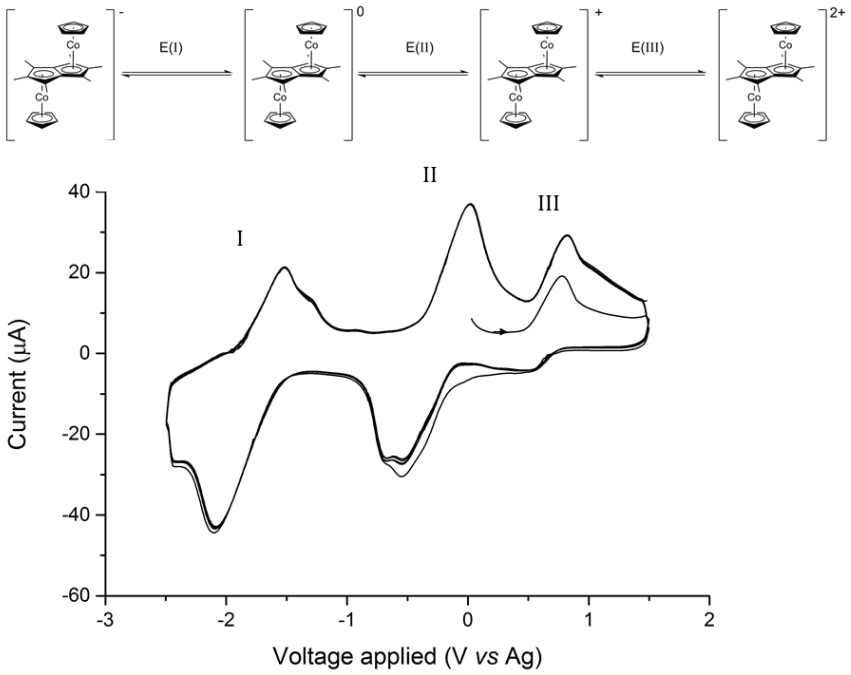

Figure 4.25 Overlaid cyclic voltammograms (5 cycles) obtained by scanning a 0.1 mM solution of 4.2b in THF containing 0.1 M [NBu_4][PF_6] over the region −2.5 to 1.5 V at a scan rate of 5 V s^{-1}, and an inset scheme showing the three ET events corresponding to the peaks observed. The $Fc^{0/+}$ couple comes at 1.54 V.

reversible 1−⇌0 couple for these 36 TNE complexes, while the second peak may correspond to a second reduction. A quasi-reversible 1−⇌0 couple is seen for the 36 TNE $Ni_2Pn^*_2$ compound of O'Hare and coworkers; however, no direduction has been reported for bimetallic pentalene complexes.

An analysis of the three events for **4.2b** reveals that, as above, the peak potentials are all dependent on sweep rate and therefore quasi-reversible. Feature I, centred at $E_{½}$=−3.41 V (*vs* $Fc^{0/+}$), corresponds to the couple [**4.2b**] ⇌ [**4.2b**]$^-$, and the differences in peak potentials for the anodic and cathodic waves ($E_{pc} - E_{pa}$) range from 193 to 233 mV for scan rates of 0.1 to 1 V s^{-1}. Process II has $E_{pa} - E_{pc}$ values ranging from 97 to 830 mV s^{-1}, and process III is assigned as irreversible as the peak shape is non-Nernstian.

The half-cell potentials *vs* $Fc^{0/+}$ have been compiled in Table 4.9, alongside the electrochemical data for the isostructural series of Manrìquez.[8]

Table 4.9 Half-cell potentials for ET events of the triple-decker *anti*-bimetallic fused metallocenes *vs* the $Fc^{0/+}$ couple.

M_2	$[M_2]^{-/0}$	$[M_2]^{0/+}$	$[M_2]^{+/2+}$	$[M_2]^{2+/3+}$	$\Delta E_{½}{}^{0/2}$	$K_c{}^{0/2}$	Ref
4.1a	−4.20 [a]	−1.48	−1.02	-	0.46	6.0×10^7	[b]
$(FeCp^*)_2Pn$	-	−0.84	0.01	-	0.85	2.4×10^{14}	8
4.2a	−3.32 [a]	−1.68	−0.79	-	0.89	1.1×10^{15}	[b]
4.2b	−3.41 [a]	−1.23	−0.84	-	0.39	3.9×10^6	[b]
$(CoCp^*)_2Pn$	-	−1.58	−0.87	-	0.71	1.0×10^{12}	8
4.3b	−3.10 [a]	−1.54	−1.15	−0.75	0.39	3.9×10^6	[b]
$(NiCp^*)_2Pn$	-	−1.37	−0.72	-	0.65	9.8×10^{10}	8

$E_{½} = (E_{pa}+E_{pc})/2$. [a] E_{pc}. [b] This work; measured in 0.1 M $[NBu_4][PF_6]$ in THF and referenced to internal $Fc^{0/+}$. Voltammograms in reference 6 measured in an H-cell in THF, with a 0.1 M $[NBu_4][ClO_4]$/acetonitrile electrolyte *vs* a quasi-reference electrode consisting of Ag/AgCl in 0.1 M $AgNO_3$ solution, reported as 'approximately 0.30 V *vs* SCE', corrected using $Fc^{0/+}$ = 0.53 V *vs* SCE in 0.1 M $[NBu_4][ClO_4]$ in THF.[17]

All the triple-decker *anti*-bimetallic fused metallocenes have K_c values in excess of 10^6, and are therefore Class III species according to the Robin-Day classification scheme,[76] with extensive delocalisation of electrons between metals, through the bridging ligand. A comparison of the novel Pn*-bridged complexes with their Pn-bridged analogues reveals a general trend of greater delocalisation in the Pn compounds by several orders of magnitude. For **4.2a**, the second oxidation is less easy to achieve than expected based on a consideration of the MOs and ionisation potentials, and results in an anomalously large delocalisation value for K_c.

The similar potentials for each couple upon changing the metal reflect the similarity in energy of the HOMOs due to increasing z_{eff} (Figure 4.14). The ease of oxidation, (for example, complex **4.2a** easier to oxidise than **4.1a**), correlates well with the calculated energy levels (Figure 4.14) and gas phase ionisation potentials from DFT calculations. A clear trend is apparent that the complexes with the Pn* bridging ligand are easier to oxidise, and harder to reduce than the isoelectronic Pn bridged series. The same trend is found for MCp^*_2 *vs* MCp_2, and is based on inductive arguments.[4,73]

All four compounds tested exhibited quasi-reversible waves corresponding to the $[\mathbf{M_2}]^{0/+}$ and $[\mathbf{M_2}]^{+/2+}$ couples, consistent with the findings of Manrìquez for the pentalene-bridged analogues.[8] Similarly, only two quasi-reversible oxidations have been reported for the bimetallocenes $(CpM)_2$fulvalene (M = Fe,[79] and Co,[19]) and bisnickelocene has been isolated in neutral, monocationic and dicationic salts.[50] The Pn* bridged complexes all exhibit an additional quasi-reversible reduction to the monoanion, and the voltammogram of **4.3b** has a further quasi-reversible wave, postulated to correspond to formation of a tricationic species.

The *syn*-fused series $M_2Pn^*_2$ (M = V, Cr, Mn, Fe, Co, Ni) have monoreduction potentials ranging from −1.95 to −2.75 V *vs* $Fc^{0/+}$,[15] while the *anti*-fused metallocenes reported above, which are more electron rich and contain only one bridging 3c2e bond, are harder to reduce (−3.22 to −4.20 V). Irreversible one-electron reductions of $[CoCp_2]^-$ and $[NiCp_2]^-$ have been reported at −2.73 V and −2.59 V *vs* $Fc^{0/+}$ respectively in the electrolyte and solvent employed herein, but only at temperatures below −40 °C.[77]

4.6 Conclusions

Anti-homobimetallic complexes of iron, cobalt, and nickel have been prepared and crystallographically characterised, more than doubling the number of first row transition metal complexes with this motif, and including for the first time Pn* bridging ligands. A novel synthetic route has been developed to access Cp capped bimetallics of the late transition metals Co and Ni.

All *anti*-(MC_5R_5)Pn* structures have diamagnetic ground states. Despite varying coordination geometries, bonding is described well by ML_4X (M = Fe, Co), or ML_3X_2 (M = Ni) nomenclature. Application of quantum chemical calculations to determine the electronic structures reveal isolated non-degenerate ground states with closed shell configurations for M = Fe and Co. The dinickel complexes show a thermally accessible excited state, which has not been reported for analogous pentalene bimetallics. A study

of the magnetic properties of the dinickel complexes **4.3a** and **4.3b** reveal Boltzmann population of a Curie triplet state in solution.

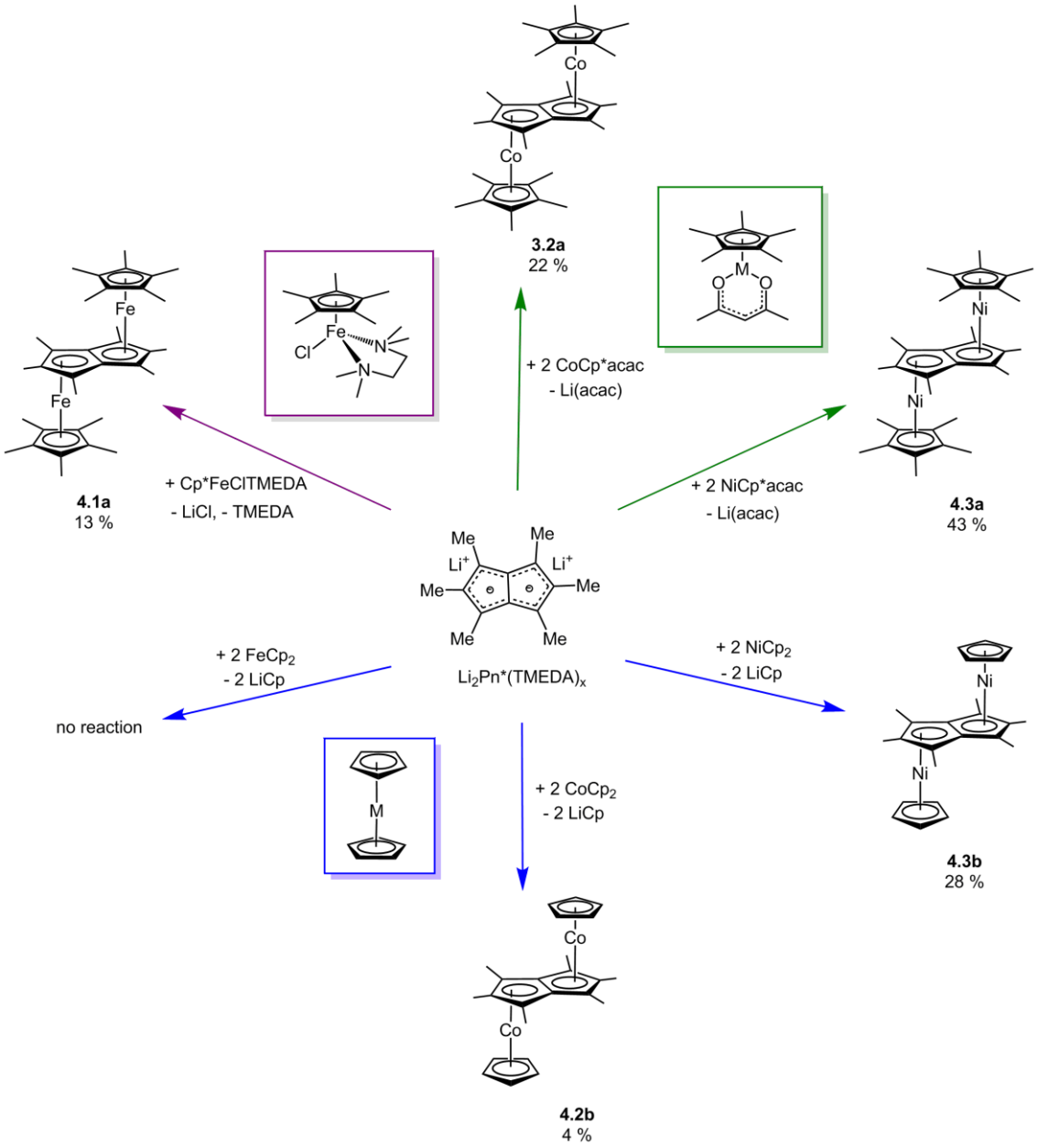

Scheme 4.4 Summary of *anti*-bimetallic compounds synthesised.

Cyclic voltammetry reveals multiple reversible or quasi-reversible redox couples for all the dinuclear complexes. All the bimetallics studied herein exhibit at least two one-electron oxidations and one reduction. In addition, both cobalt complexes exhibit one reduction event, and the dinickel complex **4.3b** is believed to form both [**4.3b**]$^{-}$ and

[**4.3b**]$^{2-}$. The comproportionation constants for the triple-decker Pn* bridged complexes are generally smaller than in the Pn bridged analogues.

4.7 References

(1) O'Connor, J. M.; Casey, C. P. *Chem. Rev.* **1987**, *87*, 307.
(2) Kowaleski, R. M.; Rheingold, A. L.; Trogler, W. C.; Basolo, F. *J. Am. Chem. Soc.* **1986**, *108*, 2460.
(3) Huttner, G.; Brintzinger, H. H.; Bell, L. G.; Friedrich, P.; Bejenke, V.; Neugebauer, D. *J. Organomet. Chem.* **1978**, *145*, 329.
(4) Robbins, J. L.; Edelstein, N.; Spencer, B.; Smart, J. C. *J. Am. Chem. Soc.* **1982**, *104*, 1882.
(5) Burgos, F.; Chávez, I.; Manriquez, J. M.; Valderrama, M.; Lago, E.; Molins, E.; Delpech, F.; Castel, A.; Rivière, P. *Organometallics* **2001**, *20*, 1287.
(6) Garland, M. T.; Saillard, J.-Y.; Chávez, I.; Oëlckers, B.; Manríquez, J.-M. *J. Mol. Struct. THEOCHEM* **1997**, *390*, 199.
(7) Bunel, E. E.; Valle, L.; Jones, N. L.; Carroll, P. J.; Barra, C.; Gonzalez, M.; Munoz, N.; Visconti, G.; Aizman, A.; Manriquez, J. M. *J. Am. Chem. Soc.* **1988**, *110*, 6596.
(8) Manriquez, J. M.; Ward, M. D.; Reiff, W. M.; Calabrese, J. C.; Jones, N. L.; Carroll, P. J.; Bunel, E. E.; Miller, J. S. *J. Am. Chem. Soc.* **1995**, *117*, 6182.
(9) Matsuura, Y.; Matsukawa, K. *Chem. Phys. Lett.* **2008**, *453*, 92.
(10) Matsuura, Y. *Solid State Commun.* **2011**, *151*, 1877.
(11) Ashley, A. E.; Cowley, A. R.; O'Hare, D. *Eur. J. Org. Chem.* **2007**, *2007*, 2239.
(12) Ashley, A. E.; Cowley, A. R.; O'Hare, D. *Chem. Commun.* **2007**, 1512.
(13) Glöckner, A.; Bannenberg, T.; Ibrom, K.; Daniliuc, C. G.; Freytag, M.; Jones, P. G.; Walter, M. D.; Tamm, M. *Organometallics* **2012**, *31*, 4480.
(14) Volbeda, J.; Daniliuc, C. G.; Jones, P. G.; Tamm, M. *Organometallics* **2013**, *32*, 5918.
(15) Ashley, A. E.; Cooper, R. T.; Wildgoose, G. G.; Green, J. C.; O'Hare, D. *J. Am. Chem. Soc.* **2008**, *130*, 15662.
(16) White, A. D.; Hilmey, D. G. In *e-EROS Encyclopedia of Reagents for Organic Synthesis*; John Wiley & Sons, Ltd: Chichester, UK, 2009.
(17) Connelly, N. G.; Geiger, W. E. *Chem. Rev.* **1996**, *96*, 877.
(18) Bochmann, M. In *Organometallics and Catalysis*; Bochmann, M., Ed.; Oxford University Press, 2014; p. 188.
(19) McManis, G. E.; Nielson, R. M.; Weaver, M. J. *Inorg. Chem.* **1988**, *27*, 1827.
(20) Katz, T. J.; Acton, N. *J. Am. Chem. Soc.* **1972**, *94*, 3281.
(21) Hilbig, H.; Hudeczek, P.; Köhler, F. H.; Xie, X.; Bergerat, P.; Kahn, O. *Inorg. Chem.* **1998**, *37*, 4246.
(22) Davison, A.; Smart, J. C. *J. Organomet. Chem.* **1973**, *49*, C43.
(23) Jones, S. C.; Hascall, T.; Norquist, A. J.; O'Hare, D. *Inorg. Chem.* **2003**, *42*, 7707.
(24) Miyake, A.; Kanai, A. *Angew. Chem., Int. Ed.* **1971**, *10*, 801.
(25) Pauson, P. L.; Segal, J. A. *J. Organomet. Chem.* **1973**, *63*, C13.
(26) Pauson, P. L.; Segal, J. A. *J. Chem. Soc. Dalton Trans.* **1975**, 2387.
(27) Wilkinson, G.; Cotton, F. A.; Birmingham, J. M. *J. Inorg. Nucl. Chem.* **1956**, *2*, 95.
(28) Coffield, T. H.; Sandel, V.; Closson, R. D. *J. Am. Chem. Soc.* **1957**, *79*, 5826.
(29) Llinás, G. H.; Mena, M.; Palacios, F.; Royo, P.; Serrano, R. *J. Organomet. Chem.* **1988**, *340*, 37.
(30) Jones, S. C.; O'Hare, D. *Chem. Commun.* **2003**, 2208.
(31) Bendjaballah, S.; Kahlal, S.; Costuas, K.; Bévillon, E.; Saillard, J.-Y. *Chem.—Eur. J.* **2006**, *12*, 2048.
(32) Byers, L. R.; Dahl, L. F. *Inorg. Chem.* **1980**, *19*, 277.

(33) Smith, M. E.; Andersen, R. A. *J. Am. Chem. Soc.* **1996**, *118*, 11119.
(34) Smith, A. E. *Inorg. Chem.* **1972**, *11*, 165.
(35) Fitzpatrick, P. J.; Le Page, Y.; Sedman, J.; Butler, I. S. *Inorg. Chem.* **1981**, *20*, 2852.
(36) Clark, M. M.; Brennessel, W. W.; Holland, P. L. *Acta Crystallogr. Sect. E Struct. Reports Online* **2009**, *65*, m391.
(37) Hadadpour, M.; Liu, Y.; Chadha, P.; Ragogna, P. J. *Macromolecules* **2014**, *47*, 6207.
(38) Green, M. L. H. *J. Organomet. Chem.* **1995**, *500*, 127.
(39) Kitano, Y.; Kashiwagi, M.; Kinoshita, Y. *Bull. Chem. Soc. Jpn.* **1973**, *46*, 723.
(40) Miravitlles, C.; Molins, E.; Maniukiewicz, W.; Mas, M.; Manríquez, J. M.; Chávez, I.; Oelckers, B.; Alvarez-Larena, A.; Briansó, J. L. *Acta Crystallogr. Sect. C Cryst. Struct. Commun.* **1996**, *52*, 3047.
(41) Pfirrmann, S.; Limberg, C.; Herwig, C.; Knispel, C.; Braun, B.; Bill, E.; Stösser, R. *J. Am. Chem. Soc.* **2010**, *132*, 13684.
(42) Evans, D. F. *J. Chem. Soc.* **1959**, 2003.
(43) Schubert, E. M. *J. Chem. Educ.* **1992**, *69*, 62.
(44) Pasynkiewicz, S.; Pietrzykowski, A.; Buchowicz, W.; Poptawska, M. *J. Organomet. Chem.* **1993**, *463*, 235.
(45) Chetcuti, M. J. In *Comprehensive Organometallic Chemistry: A Review of the Literature 1982 - 1994, Volume 9 Nickel, Palladium, and Platinum*; Puddephatt, R. J.; Abel, E. W.; Stone, F. G. A.; Wilkinson, G., Eds.; Pergamon Press, 1995; pp. 107–192.
(46) Freyberg, D. P.; Robbins, J. L.; Raymond, K. N.; Smart, J. C. *J. Am. Chem. Soc.* **1979**, *101*, 892.
(47) Bünder, W.; Weiss, E. *J. Organomet. Chem.* **1975**, *92*, 65.
(48) Hedberg, L. *J. Chem. Phys.* **1970**, *53*, 1228.
(49) Hudeczek, P.; Koehler, F. H. *Organometallics* **1992**, *11*, 1773.
(50) Smart, J. C.; Pinsky, B. L. *J. Am. Chem. Soc.* **1977**, *99*, 956.
(51) McConnell, H. M.; Chesnut, D. B. *J. Chem. Phys.* **1958**, *28*, 107.
(52) Prins, R. *J. Chem. Phys.* **1969**, *50*, 4804.
(53) Anderson, S. E.; Drago, R. S. *J. Am. Chem. Soc.* **1970**, *92*, 4244.
(54) Pennanen, T. O.; Vaara, J. *J. Chem. Phys.* **2005**, *123*, 174102.
(55) Hrobárik, P.; Reviakine, R.; Arbuznikov, A. V; Malkina, O. L.; Malkin, V. G.; Köhler, F. H.; Kaupp, M. *J. Chem. Phys.* **2007**, *126*, 024107.
(56) McConnell, H. M. *J. Chem. Phys.* **1956**, *24*, 764.
(57) Jarrett, H. S. *J. Chem. Phys.* **1956**, *25*, 1289.
(58) Williams, G. A.; Gutowsky, H. S. *J. Chem. Phys.* **1956**, *25*, 1288.
(59) Weissman, S. I. *J. Chem. Phys.* **1956**, *25*, 890.
(60) Bersohn, R. *J. Chem. Phys.* **1956**, *24*, 1066.
(61) McLachlan, A. D. *Mol. Phys.* **1958**, *1*, 233.
(62) Forman, A.; Murrell, J. N.; Orgel, L. E. *J. Chem. Phys.* **1959**, *31*, 1129.
(63) Rettig, M. F. In *NMR of Paramagnetic Molecules: Principles and Applications*; La Mar, G. N.; Horrocks Jr., W. D.; Holm, R. H., Eds.; Academic Press Inc., 1973; pp. 218–241.
(64) Hebendanz, N.; Köhler, F. H.; Scherbaum, F.; Schlesinger, B. *Magn. Reson. Chem.* **1989**, *27*, 798.
(65) Olson, W. L.; Stacy, A. M.; Dahl, L. F. *J. Am. Chem. Soc.* **1986**, *108*, 7646.
(66) Fantucci, P.; Balzarini, P.; Valenti, V. *Inorganica Chim. Acta* **1977**, *25*, 113.
(67) Bachmann, B.; Hahn, F.; Heck, J.; Wuensch, M. *Organometallics* **1989**, *8*, 2523.
(68) Camire, N.; Mueller-Westerhoff, U. T.; Geiger, W. E. *J. Organomet. Chem.* **2001**, *637-639*, 823.
(69) Geiger, W. E. *Organometallics* **2007**, *26*, 5738.
(70) Chadwick, F. M.; Ashley, A.; Wildgoose, G.; Goicoechea, J. M.; Randall, S.; O'Hare, D. *Dalton Trans.* **2010**, *39*, 6789.

(71) Kilpatrick, A. F. R. Bimetallic Complexes of d- and f-Block Metals with Pentalene Ligands, PhD Thesis, University of Sussex, 2014.
(72) Heinze, J. *Angew. Chem., Int. Ed.* **1984**, *23*, 831.
(73) Aranzaes, J. R.; Daniel, M.-C.; Astruc, D. *Can. J. Chem.* **2006**, *84*, 288.
(74) Brunschwig, B. S.; Sutin, N. *Coord. Chem. Rev.* **1999**, *187*, 233.
(75) Palaniappan, V.; Singru, R. M.; Agarwala, U. C. *Inorg. Chem.* **1988**, *27*, 181.
(76) Robin, M. B.; Day, P. *Adv. Inorg. Chem. Radiochem.* **1968**, *10*, 247.
(77) Bard, A. J.; Garcia, E.; Kukharenko, S.; Strelets, V. V. *Inorg. Chem.* **1993**, *32*, 3528.
(78) Sanello, P. *Inorganic Electrochemistry: Theory, Practice and Applications*; Royal Society of Chemistry, 2003.
(79) Morrison, W. H.; Krogsrud, S.; Hendrickson, D. N. *Inorg. Chem.* **1973**, *12*, 1998.

Chapter 5 MONOMETALLIC COMPLEXES WITH PERMETHYLPENTALENE DERIVATIVES

5.1 Introduction

During the course of the syntheses described previously in this thesis, it was discovered that protonation of the permethylpentalenyl dianion would sometimes occur. The route employed to make permethylpentalene[1] allows isolation of the permethylhydropentalenyl synthon $[Pn^*H]^-$.[1] Li(Pn*H) provides a direct entry point to monometallic complexes containing the Pn*H ligand, as Turner *et al.* have demonstrated with the synthesis of group IV complexes that catalyse lactide polymerisation.[2] Hydropentalenyl (PnH) complexes of iron and ruthenium are also precursors to *anti*-bimetallic complexes bridged by pentalene ligands,[3–8] of the type presented in Chapter 4.

The Pn*H ligand is facially diastereotopic, and in compounds the sp^3 methyl group can be on the same face as the coordinated metal, or on the opposite face. Complexes containing a single Pn*H ligand and a non-chiral ancilliary ligand therefore contain both central chirality (at the sp^3 ring atom) and planar chirality. When there are two Pn*H ligands however, there are 2^4 possible isomers (Figure 5.1). Schlögl adapted the planar chirality notation of Cahn-Ingold-Prelog[9] to ferrocenes containing an unsymmetrically substituted Cp ring.[10] The planar chirality descriptor is distinguished from the central chirality of the sp^3 carbon by the subscript '*p*'. Using these descriptors, it becomes clear that some of the combinations $M(Pn^*H)_2$ can adopt are actually identical, and in total there are only 10 unique stereochemistries.

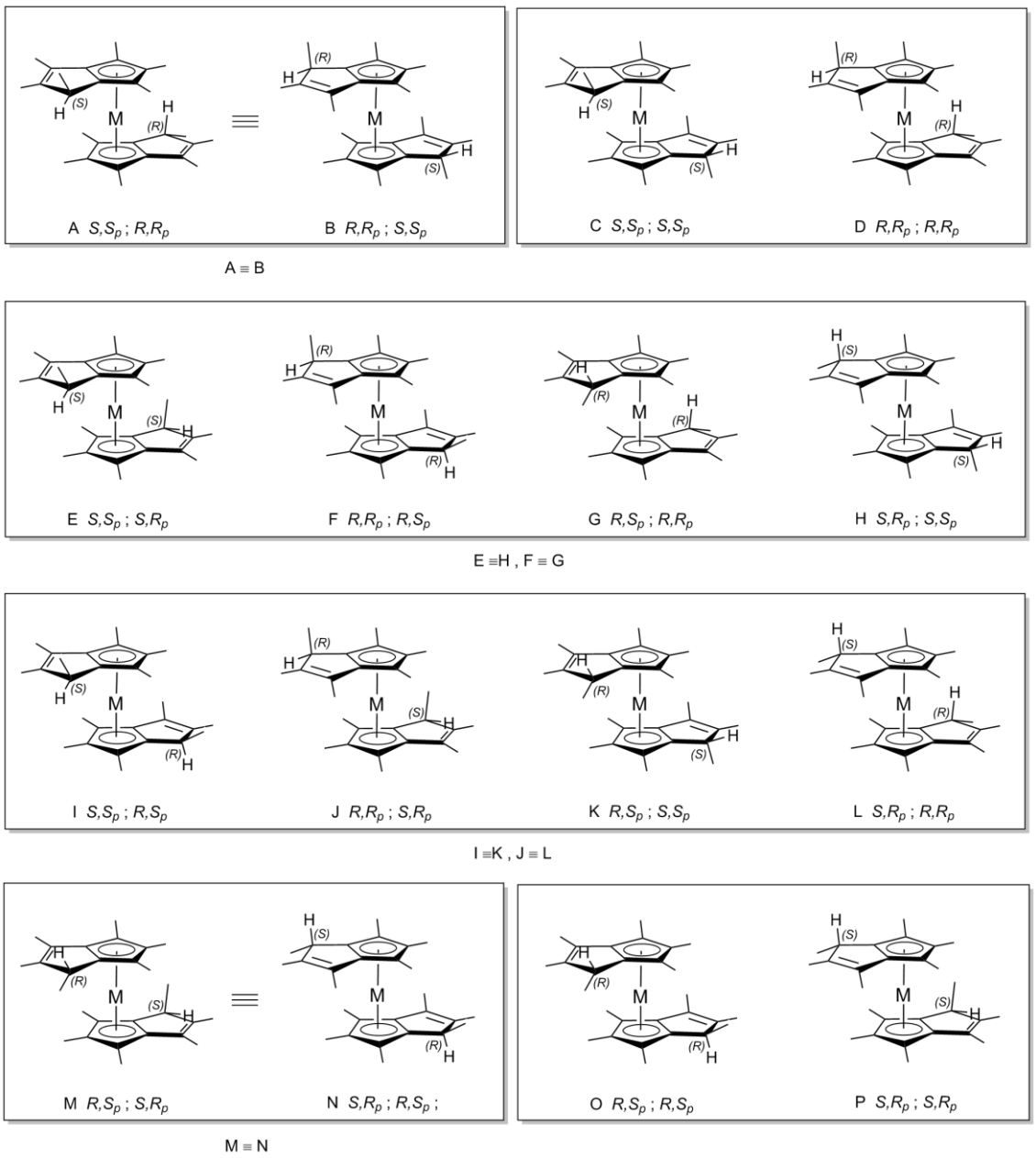

Figure 5.1 Chirality in complexes of Pn*H. In a perfectly staggered conformation, the isomers indicated can be transformed by a rotation, and are therefore no longer enantiomeric.

The first metal hydropentalenyl complex to be structurally characterised was $Fe(PnH)_2$, which has only planar chirality, and crystallises with eclipsing ligands in a disordered mixture of $R_p;R_p$, $S_p;S_p$, $R_p;S_p$ and $S_p;R_p$ isomers.[11] The $Ti(Pn^*H)X_nY_m$ (X = Cl, Y = ArO, x,y = 0–3) species form only diastereomers with the alkyl group *anti*- with respect to the coordinated titanium fragment,[2] as does the rhodium complex (2,4,7,8-tetrakistrimethylsilyl-8-endo-H-C_8H_2)RhCOD (COD = 1,5-cyclooctadiene).

Meanwhile, (8,8-Me,H-6-NMe_2-Pn)$ZrCpCl_2$ (using the numbering scheme set out in Chapter 1) has been reported with two different methyl environments, assigned to diastereomers with methyl groups pointing towards and away from the coordinated zirconium.[12]

This chapter sets out to describe the synthesis and characterisation of monometallic complexes containing the Pn*H ligand. Reaction conditions employed are such that no enantiomeric enrichment is expected. Therefore, where structures are discussed or drawn showing one enantiomer, they represent a racemic mixture of enantiomers, and are used interchangeably. However, the different diastereomeric product distributions will be discussed.

5.2 Syntheses

5.2.1 Synthesis of $Fe(Pn^*H)_2$, **5.1**

Reaction of freshly sublimed $Fe(acac)_2$ with two equivalents of Li(Pn*H) at −78 °C, followed by extraction into pentane and recrystallisation at −78 °C yielded $Fe(Pn^*H)_2$, **5.1**, as an orange-tan powder (42%) (Scheme 5.1).

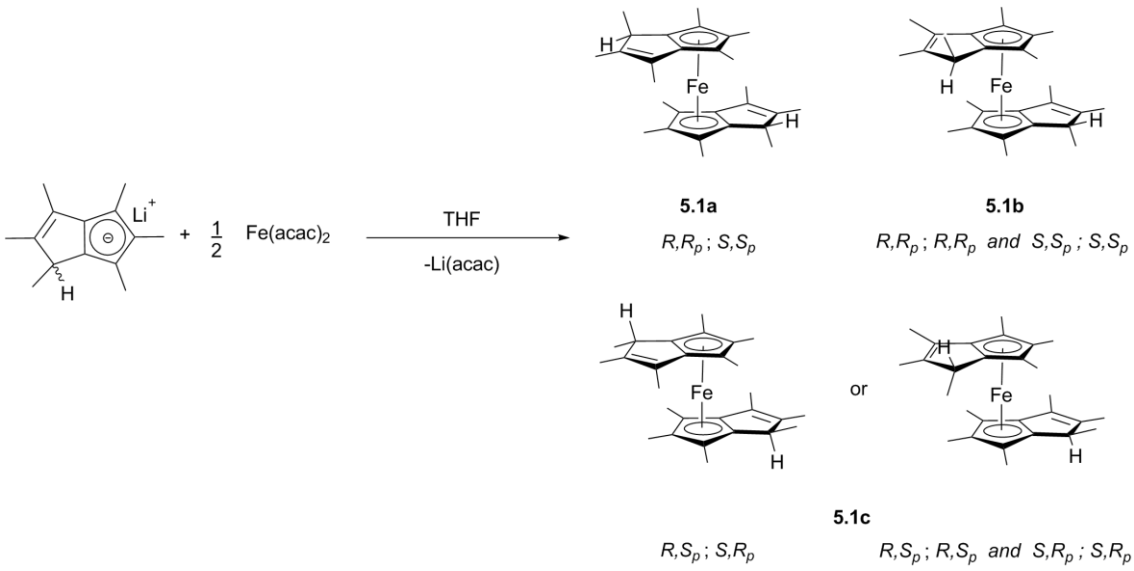

Scheme 5.1 Synthesis of three isomers of $Fe(Pn^*H)_2$, 5.1a, 5.1b, and 5.1c.

^{1}H NMR spectroscopy revealed six sharp and four broadened singlets all of equal intensity, consistent with formation of two major isomers in a 1:1 ratio, both containing chemically equivalent Pn*H ligands. The doublet and quartet resonances for each of these two isomers occur at coincident chemical shifts of 1.14 and 2.74 ppm respectively, indicating both isomers are chemically similar, and hence they are formulated as *S,S*$_p$;*R,R*$_p$ **5.1a**, and as *S,S*$_p$;*S,S*$_p$ and *R,R*$_p$;*R,R*$_p$ **5.1b** (Scheme 5.1). In addition, a third isomer, **5.1c**, was indicated by a well-defined quartet and doublet at 0.87 and 2.06 ppm, with one fifth of the intensity of the (combined) **5.1a** and **5.1b** resonances. Two further isomers were indicated by weak quartets at 2.81 and 3.08 ppm (combined integration 0.07 compared to quartet at 2.84 ppm). The methyl singlets for these three isomers are obscured by the intense resonances of **5.1a** and **5.1b**. The observation of only one doublet for **5.1c** requires that the two ligands are chemically equivalent and therefore the structure must be one of those indicated in Scheme 5.1 (*i.e.* M – P in Figure 5.1). On conducting the same reaction at room temperature, the isomer distribution shifts slightly, favouring a 3:2:1 ratio of **5.1a** to **5.1b** to **5.1c**, and allowing the full assignment of ^{13}C NMR spectra for **5.1a** and **5.1b**, using 2D correlation spectroscopy and the 2:1 integral ratio of ^{13}C resonances. Overall the observation of two major stereoisomers is consistent with the regioselectivity reported in the literature.[2,12]

Although efforts to separate the isomers proved of limited success, single crystals of **5.1a** were grown from a slowly evaporated benzene-d$_6$ solution, and solved in the triclinic space group *P*-1 (Figure 5.2). Each molecule has an inversion centre at the iron atom, such that the two Pn*H ligands are identical and perfectly staggered, and the molecules have C_i symmetry. This contrasts with solid state structure of unmethylated Fe(PnH)$_2$, in which the eclipsing ligands have disorder of the ring double bond, and of the iron atom site.[11]

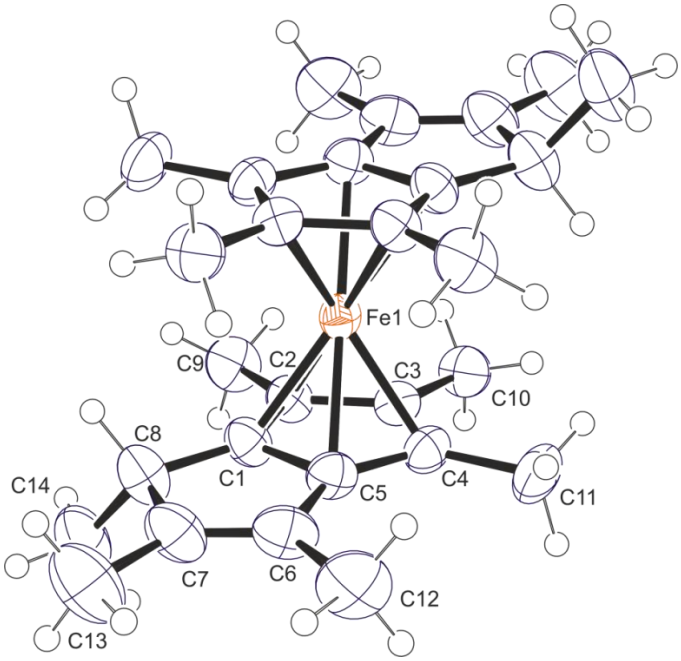

Figure 5.2 Molecular structure of Fe(Pn*H)$_2$, 5.1a. Ellipsoids are shown at 50% probability. Carbon atoms are shown in blue, the iron atom in orange, and hydrogen atoms in black. Selected bond lengths and distances (in Å): C1—C2 1.421(3), C2—C3 1.444(4), C3—C4 1.446(4), C4—C5 1.426(4), C5—C1 1.415(4), C5—C6 1.477(3), C6—C7 1.347(5), C7—C8 1.518(4), C8—C1 1.509(4), Fe1—centroid 1.657.

The molecular structure reveals that the protonated C8 positions are sp^3 hybridised, with methyl groups pointing away from the coordinated iron atoms, which are coordinated to the C_5 rings with Fe—C distances ranging from 2.048 to 2.059 Å. These are the same within e.s.d. to the corresponding distances in Fe(PnH)$_2$ (2.035(2)—2.068(2) Å),[11] and FeCp*$_2$ (2.05 Å),[13,14] which may be explained by steric repulsion between permethylated pentalene ligands counterbalancing the expected strengthening of M—C bonds due to a more electron rich aromatic ligand. The mean aromatic C—C bond lengths is 1.430 Å, almost identical to the 1.42 Å in FeCp*$_2$, and 1.422(3) Å in Fe(PnH)$_2$. The C6—C7 bond, at 1.347(5) Å is clearly an unconjugated double bond, flanked by single bonds.

5.2.2 Synthesis of FeCp*(Pn*H), **5.2**

FeCp*(Pn*H), **5.2**, was made through the reaction of Cp*FeCl·TMEDA with Li(Pn*H), and isolated as a tan powder in 46% yield (Scheme 5.2). ^{1}H NMR spectral

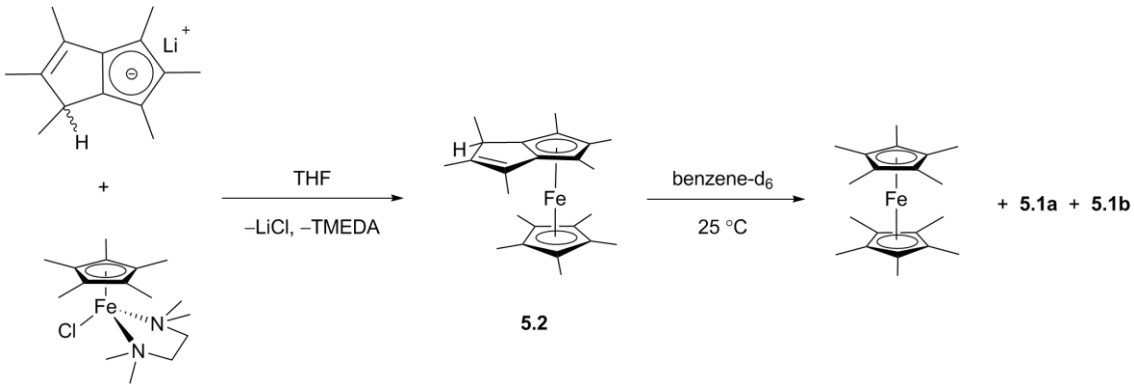

Scheme 5.2 Synthesis of FeCp*(Pn*H), 5.2, and ligand redistribution.

resonances attributed to **5.2** indicate the formation of only one isomer which exhibits a doublet and quartet at 1.15 and 2.84 ppm respectively. The similarity of these shifts to the corresponding protons in **5.1a** and **5.1b** indicate the favoured structure of **5.2** is that shown in Scheme 5.2, with the methyl group pointing away from the coordinated iron atom. As noted previously, no reason for enantioenrichment exists, and therefore both enantiomers will exhibit identical NMR spectra. Additional resonances develop in ^{1}H NMR spectra over a few hours, and can be assigned to FeCp*$_2$, **5.1a**, and **5.1b**, indicating the mixed sandwich compound is unstable with respect to ligand rearrangement at 25 °C.

5.2.3 Synthesis of Mn(Pn*H)$_2$, **5.3**

Reactions between two equivalents of Mn(acac)$_2$ or MnCl$_2$ and LiCp* with one equivalent of Li$_2$Pn* did not result in the anticipated bimetallic species (MnCp*)$_2$Pn*, but invariably in the monometallic sandwich complex Mn(Pn*H)$_2$, **5.3**.

A rational synthesis of **5.3** was achieved by reaction of Li(Pn*H) with Mn(acac)$_2$ at −78 °C in THF, with isolation of **5.3** in high yield (62%) as cherry red crystals (Scheme 5.3). EA and MS were consistent with the proposed formulation of Mn(Pn*H)$_2$, while ^{1}H NMR spectra contain resonances at shifts ranging from −19.55 to 16.58 ppm,

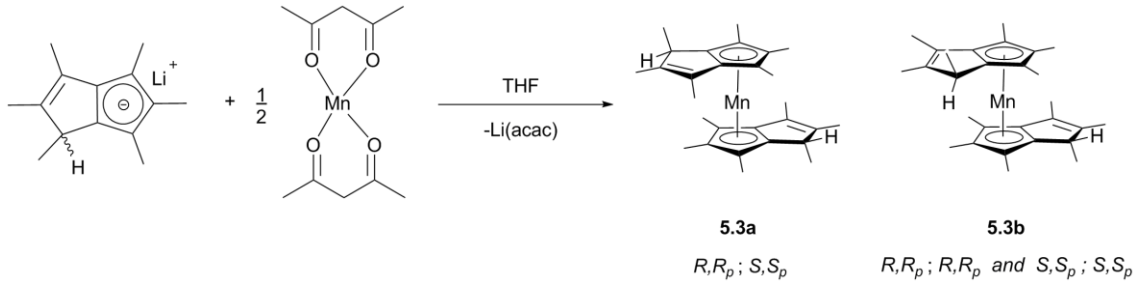

Scheme 5.3 Synthesis of two isomers of Mn(Pn*H)$_2$, 5.3a and 5.3b.

attesting to the open-shell configuration of the products, and the presence of a variety of isomers.

Initially isolated as a mixture of isomers, recrystallisation from pentane at −78 °C afforded good separation of the two major isomers, **5.3a** and **5.3b**. Triclinic single crystals of isomer **5.3a** show it is monometallic, and isostructural with **5.1a** in the solid state, with very similar unit cell parameters and an inversion centre at the manganese atom (Figure 5.3). The C—C bond lengths in the Pn*H ligands are the same as **5.1a** within one e.s.d., while M—C bond lengths are slightly elongated, (mean length 2.115 Å), in excellent agreement with the 2.11 Å in MnCp*$_2$.[13] The slightly larger range of M—C

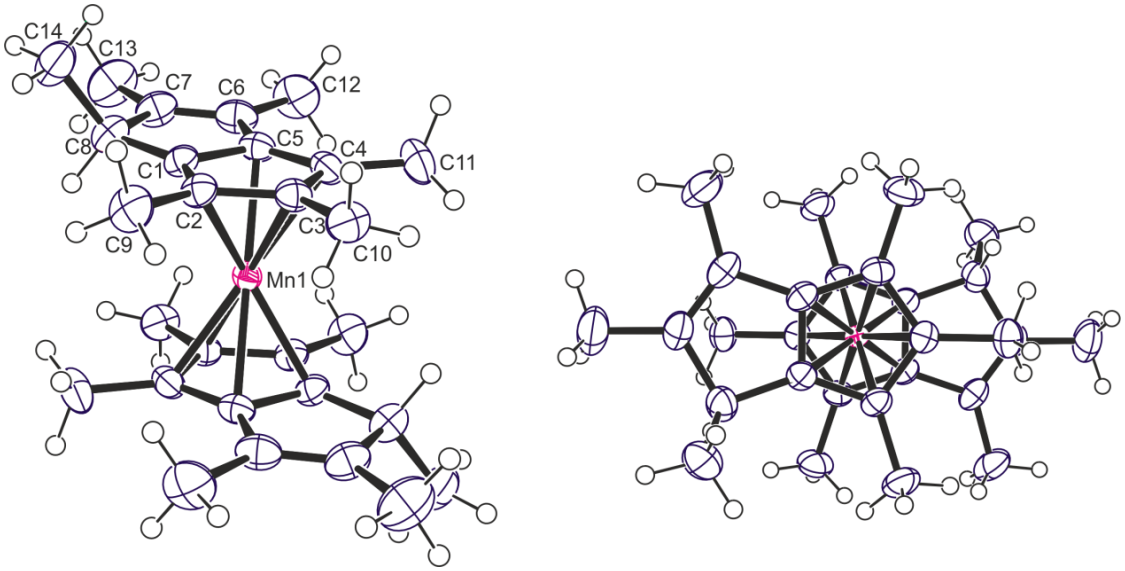

Figure 5.3 Molecular structure of Mn(Pn*H)$_2$, 5.3a, perspective and plan views. Ellipsoids shown at 50% probability. Carbon atoms are shown in blue, manganese atoms in pink, and hydrogen atoms in black. Selected bond lengths and distances (in Å): C1—C2 1.421(2), C2—C3 1.443(3), C3—C4 1.437(2), C4—C5 1.418(3), C5—C1 1.410(3), C5—C6 1.474(2), C6—C7 1.348(3), C7—C8 1.516(2), C8—C1 1.509(3), Mn1—centroid 1.733.

bond lengths in **5.3a** compared to **5.1a**, from 2.099 to 2.145 Å, is consistent with a Jahn-Teller distortion, more exaggerated than in decamethylmanganocene, where bond lengths range from 2.105(2) to 2.118(2) Å. This effect relieves the degeneracy of a $^2E_{2g}$ ground state in decamethylmanganocene,[13] and the observation of the effect in **5.3** in the solid state at 150 K suggests that $Mn(Pn^*H)_2$ may also have an electronically degenerate ground state.

5.3 Magnetic studies on **5.3**

Compared to the other first row transition metals, sandwich complexes of manganese are rare.[21] Work by Hanusa,[17] Walter,[18] and Arnold *et al.*,[20] has only recently offered advances in the field, with a range of bis(indenyl)manganese complexes containing annulated Cp ligands.

A study of the solution phase magnetic susceptibility using the Evans' NMR method[15,16] on a 22 mM toluene solution containing **5.3a** indicated an effective magnetic moment of 2.79 μ_B at 298 K, which is intermediate between the spin-only predicted 1.73 μ_B of a singlet and 5.82 μ_B of a sextet. A linear dependence of the chemical shifts in solution on reciprocal temperature indicates Curie behaviour between 198 and 378 K (Figure 5.4), and is not typical behaviour of manganocenes.[17–20]

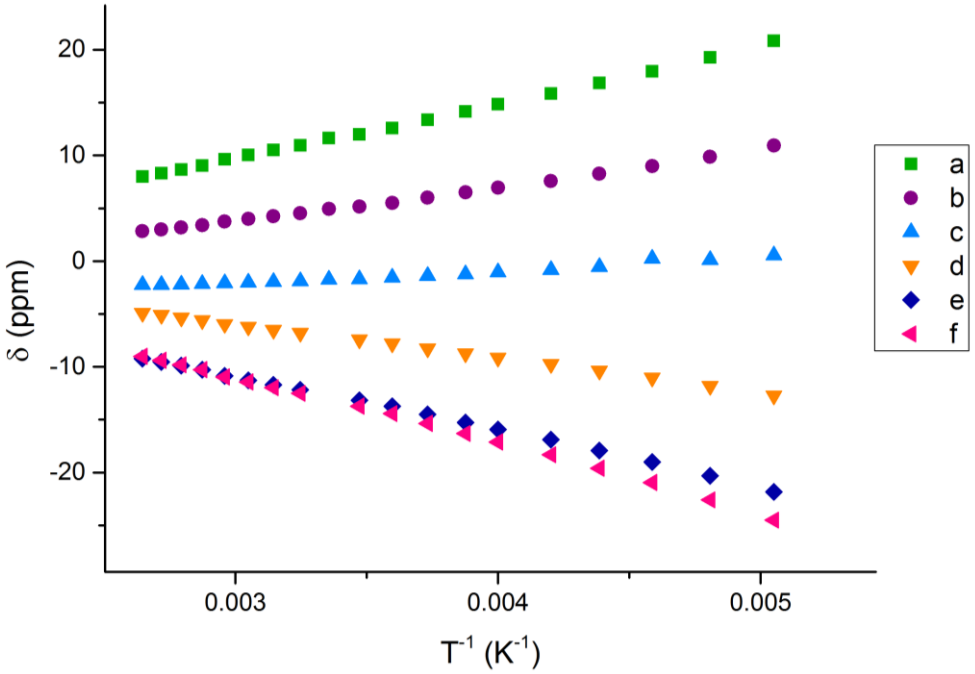

Figure 5.4 Variation of methyl chemical shifts with reciprocal temperature for a single isomer of Mn(Pn*H)$_2$, 5.3a.

Solid state magnetic susceptibility measurements were recorded on **5.3a** in the solid state between 5 and 300 K, and the results are displayed in Figure 5.5. A plot of the inverse magnetic susceptibility for **5.3a** exhibits a linear variation with temperature between 5 and 36 K, and above 100 K (consistent with the paramagnetic behaviour observed in solution), with a smooth transition appearing between the two in the region 36 to 100 K. A least squares fit these data to the Curie-Weiss Law gives effective magnetic moments of 3.68 μ_B in the low temperature and 3.63 μ_B in the high temperature regions respectively (average values for zfc and fc fitted data), both of which are intermediate between the spin-only predicted values for singlet and sextet species. The Weiss constants obtained for each region are −13.9 and −50.8 K at low and high temperature respectively. Taken together, these results suggest the spin state of **5.3a** is invariant over the region 5 — 300 K. At this time, it is not clear what is occurring between 36 and 100 K. For example, it could be a structural phase transition.

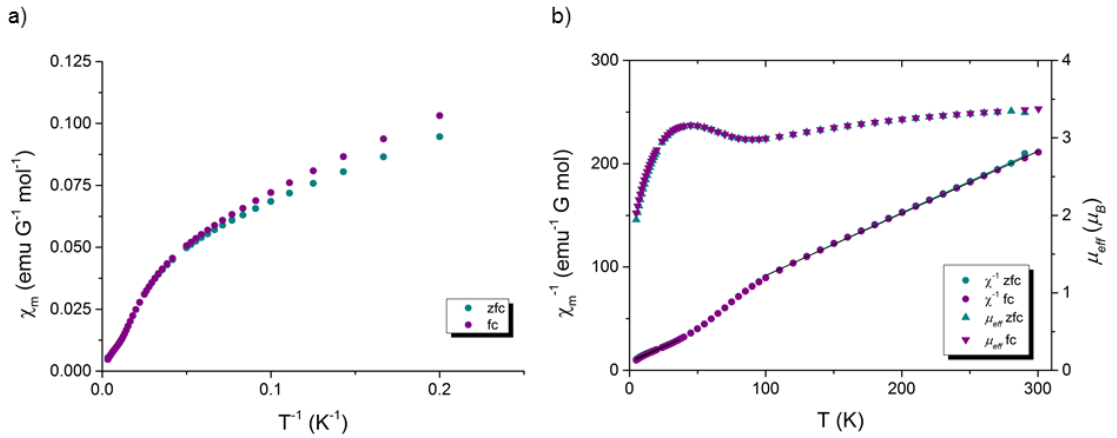

Figure 5.5 Plots of a) magnetic susceptibility of Mn(Pn*H)$_2$, 5.3a, with reciprocal temperature, and b) inverse magnetic susceptibility and effective magnetic moment of 5.3a with temperature, for zero-field-cooled and field cooled samples.

In the highly symmetrical extremes of D_{5h} (eclipsing) or D_{5d} (staggered) structures, manganocenes have two accessible spin states, and tuning of the cyclopentadienyl substituents can cause manganocenes to adopt high spin, low spin, or intermediate spin configurations.[22–25] However the degeneracy present in D_{5h} (eclipsing) or D_{5d} complexes is broken on employing the Pn*H or indenyl ligands. Bis(alkylindenyl)chromium complexes have low spin configurations at low temperature, and spin crossover to high spin states as temperature is raised.[26] For Cr(Ind')$_2$ (Ind' = 2,4,7-trimethylindene), the accessibility of a high spin state was found to differ between molecules with eclipsing and staggered geometries.[26] In contrast, no spin cross over behaviour is exhibited by **5.3a** either in solution or in the solid state. The effective magnetic moment of Mn(Pn*H)$_2$ is intermediate between the spin-only values predicted for the high and low spin extremes of manganocenes, and can be interpreted as the existence of an intermediate spin state. The value of μ_{eff} in solution is 2.79 μ_B, close to the spin-only prediction of 2.88 μ_B for a species with two unpaired electrons, while the solid state μ_{eff} of 3.6 μ_B is much closer to the 3.88 μ_B predicted for an S = 3/2 state.

The linear, Curie dependence of susceptibility above 100 K for **5.3a** is similar to bis(permethylindenyl)manganese, Mn(Ind*)$_2$, between 50 and 200 K.[20] This contrasts

with all less symmetrically substituted bis(indenyl)manganese derivatives, $Mn(Ind')_2$ (where Ind' = 2-methylindene, 2-trimethylsilylindene, 1,3-bis(trimethylsilyl)indene, 1,3-diisopropylindene, 1,3-ditertbutylindene), for which room temperature effective magnetic moments of 5.25 to 5.92 μ_B in solution are observed. In the solid state, $Mn(Ind')_2$ (Ind' =1,3-tetraisopropylindene and 1,3-ditertbutylindene) have been reported to maintain a high-spin $S = 5/2$ configuration down to 4 and 2 K respectively.[17,18] $Mn(Pn^*H)_2$ is therefore one of the first examples of a manganocene with annulated ligands to display an intermediate spin state.

Finally, in contrast to the $Mn(Ind')_2$ complexes of Hanusa (Ind' = 2-methylindene, 2-trimethylsilylindene, 1,3-bis(trimethylsilyl)indene, 1,3-diisopropylindene),[17] and Maekawa (Ind' = 1,3-ditertbutylindene,),[18] the synthesis of the permethylated hydropentalenyl manganocene **5.3** can be achieved from both $Mn(acac)_2$ and $MnCl_2$ starting materials without excessive pre-drying of reagents. The monometallic products are soluble in aliphatic, ethereal, and aromatic solvents, and air-sensitive but relatively easy to manipulate, with the stringent exclusion of air employed for indenyl sandwich complexes unnecessary.[17] The bulky permethylated Pn*H ligand provides sufficient steric bulk to favour the formation of monomeric species, whereas the bisindenylmanganocenes with fewer substituents on the 'Cp' ring (e.g. bis(2-methylindenyl)manganese) form oligomeric structures.[17]

5.4 Conclusions

Three monometallic iron and one monometallic manganese metallocene have been successfully synthesised and characterised. It is found that the major isomers of $Fe(Pn^*H)_2$ (**5.1a** and **5.1b**) and $Mn(Pn^*H)_2$ (**5.3a** and **5.3b**), with C_i and C_2 symmetry respectively, form in a 1:1 ratio from reaction between metal(II) acetylacetonates and Li(Pn*H). The sole isomer (**5.2**) of FeCp*(Pn*H) that forms from reaction of Li(Pn*H) with FeCp*Cl·TMEDA has been characterised, and is prone to undergo ligand

redistribution in solution with formation of $FeCp^*_2$ and $Fe(Pn^*H)_2$. In **5.1** – **5.3** the major isomers formed are all believed to have methyl groups *anti*- to the coordinated metal.

Complex **5.3** is an unusual example of a manganese sandwich complex with sterically bulky ligands, and has been elucidated crystallographically to have a perfectly staggered conformation in the solid state, identical to the iron derivative **5.1a**. The magnetic moment in solution and in the solid state is intermediate between spin-only predictions for high and low-spin species. It therefore differs from the invariably high-spin electronic structures found for all literature $Mn(Ind')_2$ analogues. Magnetic character of **5.3** is similar to the behaviour displayed by alkylated bisindenylchromium complexes.

5.5 References

(1) Ashley, A. E.; Cowley, A. R.; O'Hare, D. *Chem. Commun.* **2007**, 1512.
(2) Turner, Z. R.; Buffet, J.-C.; O'Hare, D. *Organometallics* **2014**, *33*, 3891.
(3) Oelckers, B.; Chavez, I.; Manriquez, J. M.; Roman, E. *Organometallics* **1993**, *12*, 3396.
(4) Miravitlles, C.; Molins, E.; Maniukiewicz, W.; Mas, M.; Manríquez, J. M.; Chávez, I.; Oelckers, B.; Alvarez-Larena, A.; Briansó, J. L. *Acta Crystallogr. Sect. C Cryst. Struct. Commun.* **1996**, *52*, 3047.
(5) Manriquez, J. M.; Ward, M. D.; Reiff, W. M.; Calabrese, J. C.; Jones, N. L.; Carroll, P. J.; Bunel, E. E.; Miller, J. S. *J. Am. Chem. Soc.* **1995**, *117*, 6182.
(6) Burgos, F.; Chávez, I.; Manriquez, J. M.; Valderrama, M.; Lago, E.; Molins, E.; Delpech, F.; Castel, A.; Rivière, P. *Organometallics* **2001**, *20*, 1287.
(7) Burgos, F.; Arancibia, V.; Manriquez, J. M.; Chavez, I. *Bol. Soc. Chil. Quim.* **2000**, *45*, 621.
(8) Kilpatrick, A. F. R. Bimetallic Complexes of d- and f-Block Metals with Pentalene Ligands, PhD Thesis, University of Sussex, 2014.
(9) Cahn, R. S.; Ingold, C.; Prelog, V. *Angew. Chem. Int. Ed. English* **1966**, *5*, 385.
(10) Schlögl, K. In *Topics in Stereochemistry*; Allinger, N. L.; Eliel, E. L., Eds.; Topics in Stereochemistry; John Wiley & Sons, Inc.: Hoboken, NJ, USA, 1967; Vol. 1, pp. 39–91.
(11) Molins, E.; Maniukiewicz, W.; Miravitlles, C.; Mas, M.; Manriquez, J. M.; Chávez, I.; Oelckers, B.; Farran, J.; Briansó, J. L. *Acta Crystallogr. Sect. C Cryst. Struct. Commun.* **1996**, *52*, 2414.
(12) Xu, B.-H.; Kehr, G.; Fröhlich, R.; Nauha, E.; Erker, G. *Dalton Trans.* **2010**, *39*, 9973.
(13) Freyberg, D. P.; Robbins, J. L.; Raymond, K. N.; Smart, J. C. *J. Am. Chem. Soc.* **1979**, *101*, 892.
(14) Struchkov, Y. T.; Andrianov, V. G.; Sal'nikova, T. N.; Lyatifov, I. R.; Materikova, R. B. *J. Organomet. Chem.* **1978**, *145*, 213.
(15) Evans, D. F. *J. Chem. Soc.* **1959**, 2003.
(16) Schubert, E. M. *J. Chem. Educ.* **1992**, *69*, 62.

(17) Crisp, J. A.; Meier, R. M.; Overby, J. S.; Hanusa, T. P.; Rheingold, A. L.; Brennessel, W. W. *Organometallics* **2010**, *29*, 2322.
(18) Maekawa, M.; Daniliuc, C. G.; Freytag, M.; Jones, P. G.; Walter, M. D. *Dalton Trans.* **2012**, *41*, 10317.
(19) Smart, J. C.; Robbins, J. L. *J. Am. Chem. Soc.* **1978**, *100*, 3936.
(20) Arnold, T. A. Q.; Ransom, P.; Binding, S. C.; Myers, W. K.; Turner, Z. R.; Buffet, J.-C.; O'Hare, D. *Synthesis, Characterisation, and Magnetic Properties of a Permethylated Manganocene*; p. in preparation.
(21) Layfield, R. A. *Chem. Soc. Rev.* **2008**, *37*, 1098.
(22) Köhler, F. H.; Hebendanz, N.; Thewalt, U.; Kanellakopulos, B.; Klenze, R. *Angew. Chem., Int. Ed.* **1984**, *23*, 721.
(23) Pauson, P. L.; Segal, J. A. *J. Chem. Soc. Dalton Trans.* **1975**, 2387.
(24) Hemond, R. C.; Hughes, R. P.; Rheingold, A. L. *Organometallics* **1989**, *8*, 1261.
(25) Coffield, T. H.; Sandel, V.; Closson, R. D. *J. Am. Chem. Soc.* **1957**, *79*, 5826.
(26) Meredith, M. B.; Crisp, J. A.; Brady, E. D.; Hanusa, T. P.; Yee, G. T.; Pink, M.; Brennessel, W. W.; Young, V. G. *Organometallics* **2008**, *27*, 5464.

Chapter 6 EXPERIMENTAL DETAILS

6.1 General methods and materials

Air and moisture sensitive reactions were performed on a dual-manifold vacuum/N_2 line using standard Schlenk techniques, or in a N_2 filled MBraun Unilab glovebox. All glassware was heated in an oven at 170 °C for at least 1 hour prior to use. Hexane, pentane, dichloromethane (DCM), benzene, and toluene were dried using a Braun SPS-800 solvent purification system. Diethyl ether was distilled from potassium, and tetrahydrofuran was dried over Na/benzophenone until purple, and distilled under N_2. Dry solvents were stored under N_2 in oven dried ampoules with a Rotaflo cap containing K mirrors (pentane, hexane, benzene, toluene, ether) or 3 Å molecular sieves dried for 12 hours at 160 °C (THF, DCM). Deuterated NMR solvents were purchased from Goss Scientific or Cambridge Isotopes Laboratories and stored in the glovebox after drying. Benzene-d_6 and toluene-d_8 were either stirred over NaK for at least 3 days then distilled, or dried over a potassium mirror and freeze–thaw–degassed three times. THF-d_8, pyridine-d_5, chloroform-d_1, and DCM-d_2 were stirred over powdered calcium hydride for at least three days and then distilled. All solvents were degassed prior to use.

Reagents were purchased from Sigma Aldrich or Alfa Aesar and were used without further purification unless otherwise stated. Metal(II) acetylacetonates were dried at 10^{-2} mbar overnight and stored in the glovebox and freshly sublimed prior to use. 2,4,6,8-tetramethoxycarbonxyl-bicyclo[3.3.0]octa-1,5-dione,[1] $Li_2Pn^*TMEDA_x$,[2] $(SnMe_3)_2Pn^*$,[2] Cp*FeCl·TMEDA,[3] Cp*Fe(acac),[4,5] Cp*Co(acac),[5] Cp*Ni(acac),[5] and $(Pn^*TiCl_2)_2$[6] were prepared according to literature methods. CO gas (99.99%) from ARGO International Ltd was passed directly into a dual manifold Schlenk line. H_2 gas was passed through a drying column containing activated 3 Å molecular sieves, and ethylene

from BOC through a drying column containing 3 Å molecular sieves, before being passed into a Schlenk line.

6.2 Physical techniques

6.2.1 NMR spectroscopy

^{1}H and $^{13}C\{^{1}H\}$ NMR spectra were obtained either on a Agilent Mercury VX-Works 300 MHz spectrometer running Varian software, or on a Bruker AVIII 400 MHz running ICON automation of TOPSPIN software. Air sensitive NMR samples were prepared in a glovebox under a nitrogen atmosphere and sealed in 5 mm tubes with Young's type concentric stopcocks. ^{1}H and ^{13}C shifts (in parts per million, ppm) are referenced internally to residual protio-solvent relative to TMS ($\delta = 0$); *J* values are given in Hz.

^{1}H, $^{13}C\{^{1}H\}$, and 2D spectra of paramagnetic molecules, variable temperature, and Evans NMR studies were conducted on a Bruker AVIII 500 MHz running TOPSPIN software.

For Evans' NMR measurements, a concentrated toluene-d_8 solution of a paramagnetic complex and a sealed glass capilliary containing pure toluene-d_8 were placed in an NMR tube sealed with a Young's concentric stopcock. The samples were heated as required to ensure full solvation of the complex.

6.2.2 Mass spectroscopy and elemental analysis

Electrospray ionisation (ES-API) spectra of air and moisture stable samples diluted in methanol or acetonitrile were collected in positive and negative modes on an Agilent Technologies 6120 Quadrupole LCMS spectrometer. Electron ionisation (EI) mass spectra of air and moisture sensitive samples were recorded by Colin Sparrow of the Chemistry Research Laboratory, University of Oxford, using a Bruker μTOF spectrometer. Elemental analyses were carried out by Stephen Boyer of London Metropolitan University.

6.2.3 Electronic absorption spectra

UV-vis spectra were recorded on a PG Instruments T60U Spectrometer. Samples were diluted in volumetric flasks in a glovebox, and sealed in a quartz cell fitted with a Young's concentric stopcock. IR spectra were recorded on a Nicolet iS5 ThermoScientific spectrometer (range 4000 – 400 cm^{-1}, resolution cm^{-1}) as KBr disks, thin films deposited on KBr windows, or neat oils. Air and moisture sensitive samples were prepared in the glovebox, ground with anhydrous KBr, and then pressed into disks using an in-house purpose-built press and holder, the spectra were then recorded immediately.

6.2.4 Single crystal X-ray crystallography

A typical crystal was mounted on a MiTeGen Micromounts using perfluoropolyether oil and cooled rapidly to 150 K in a stream of nitrogen gas using an Oxford Cryosystems Cryostream unit.[7] Data were collected with an Enraf-Nonius KappaCCD diffractometer (using graphite-monochromated Mo K_α radiation, λ = 0.71073 Å) or on an Agilent SuperNova A diffractomenter (Cu K_α radiation, λ = 1.54180 Å). Raw frame data were reduced using the DENZO-SMN package or using CrysAlisPro.[8,9] Intensity data were corrected using multi-scan method with SCALEPACK (within DENZO-SMN). The structure was solved using direct methods with SIR92[10] or a charge-flipping algorithm with Superflip,[11] and refined using full-matrix least squares refinement on all F^2 data using the CRYSTALS program suite.[12–14] In general, distances and angles were calculated using the full variance–covariance matrix. Centroids, planes, and dihedral angles were calculated using PLATON,[15] and Ortep-3 was used to render molecular structures.[16]

6.2.5 DFT Calculations

Ab-initio calculations for chapter 2 were performed with the ChemBio3D Ultra 14.0 package from PerkinElmer. Geometry optimisation and calculation of steric parameters was performed with MM2 force field calculation methods.[17] Beginning from

these optimised structures, heats of formation were calculated using the ab-initio methods AM1 and PM3 and 6-21G basis sets using the GAMESS interface.[18–20] Calculations performed with 3-21G, 6-21G and STO-6G basis sets were found to be in excellent agreement to within 0.1 kcal mol^{-1}.[21,22]

Density functional calculations for chapters 3 and 4 were performed by Professor Jennifer Green with the ADF program package.[23,24] Geometry optimisation calculations were carried out at BP,[25,26] B3LYP,[25,27–29] and MO6L[30] levels of DFT. The hybrid functional B3LYP often gives better results for transition metal compounds than pure gradient-corrected functionals, especially with regard to metal–ligand covalency. For geometry optimisations the triple-zeta[31] Slater type basis sets were used. Orbitals were generated with the program Chimera. Molecular graphics and analyses were performed with the UCSF Chimera package. Chimera is developed by the Resource for Biocomputing, Visualization, and Informatics at the University of California, San Francisco (supported by NIGMS P41-GM103311).

6.2.6 Electrochemical measurements

Cyclic voltammetry measurements were carried out in a three-electrode configuration, with a silver pseudo-reference electrode, a glassy-carbon working electrode and a platinum auxiliary electrode, all sourced from Bioanalytical Systems®, within a Saffron Omega Scientific glovebox under anhydrous nitrogen on a PARAMETEK® VersaSTAT 3 potentiostat. The supporting electrolyte (0.1 M $[N^nBu_4][PF_6]$ in THF) was prepared from recrystallized salt with freshly distilled THF, thoroughly degassed, and scanned prior to use. The electrodes were immersed in 10 mL of a 1 mM solution of the analyte, prepared in the glovebox. Voltammograms were collected, typically scanning a potential range between −2.5 V and 1.5 V *vs* Ag at scan rates ranging from 0.1 V s^{-1} to 10 V s^{-1}. All potentials were referenced to the internal

ferrocene/ferrocenium ($Fc^{0/+}$) couple by addition of ferrocene to each sample and recording its potential under identical conditions.

6.2.7 SQUID magnetic susceptibility measurements

The magnetic susceptibilities were measured on powdered samples with a Quantum Design MPMS-5 SQUID magnetometer. The accurately weighed samples were placed in a gelatine capsule and loaded into a non-magnetic plastic straw before being lowered into the cryostat. Experimental susceptibility data were collected over a temperature range of 5 – 300 K under an applied field of 1000 G (**5.3a**), or 3000 G (**3.1**), and corrected for underlying diamagnetism using Pascal's constants unless specified otherwise.[32] The mass magnetic susceptibility, χ_g, of bimetallic molecules is expressed *per mole of molecules* unless explicitly stated otherwise.

6.3 Synthesis

6.3.1 Chapter 2

6.3.1.1 Synthesis and separation of **2.1** – **2.3**

A 500 mL round bottomed flask containing 2,4,6,8-tetramethoxycarbonxyl-bicyclo[3.3.0]octa-1,5-dione (colloquial name $WeissH_4$, 6.93 g, 18 mmol, 1 eq.) and potassium carbonate (23.22 g, 168 mmol, 9 eq.) in 100 mL acetone was fitted with a reflux condenser and heated to 40 °C with vigorous stirring. Ethyl iodide (52.5 g, 26.9 mL, 336 mmol) was added portionwise to the yellow solution *via* the condenser, resulting in formation of a white precipitate. The temperature was increased to 56 °C and the reaction was held at this temperature and stirred for 48 hours. On cooling, a cream coloured KI precipitate settled from a yellow solution. Filtration to remove excess K_2CO_3 and KI, followed by removal of the solvent from the filtrate left an oil which was redissolved in 100 mL DCM. Filtration through Celite and removal of the solvent left *ca.* 12 g of a thick yellow oil. Attempts to triterate the oil by adding MeOH and pentane

failed. The oil had good solubility in DCM, some solubility in MeOH, and was completely insoluble in pentane. The oil was solvated in 5 mL DCM and mixed with 5 g Celite, then left to stand in a beaker overnight to dry. The product-loaded Celite was spread atop 1 kg silica and eluted with a 2:1 mixture of Et_2O/hexanes. Fractions were tested by thin layer chromatography (TLC), combined, and the solvent removed *in vacuo* to yield **2.1** (716 mg, 1.48 mmol, 7.9%), **2.2** (400 mg, 0.829 mmol, 4.4%), and **2.3** (2.15 g, 4.46 mmol, 24%). A mixed fraction containing mostly **2.3** with some **2.1** yielded a further 3.227 g (6.68 mmol, 36%). Total (combined) yield of tetraethylated products 72%.

6.3.1.2 Synthesis and separation of **2.4** – **2.10**

2,4,6,8-tetramethoxycarbonxyl-bicyclo[3.3.0]octa-1,5-dione (6.93 g, 18 mmol) was dissolved in 100 mL acetone in a 500 mL 2-necked round bottomed flask. Nine equivalents of K_2CO_3 (23.22 g, 168 mmol) were added, rinsing glassware with 75 mL acetone. The mixture was stirred vigorously and refluxed at 57 °C. A pressure-equalising dropping funnel fitted to a side arm of the rbf was used to add a 4.5-fold excess of 2-iodopropane (30.77 mL, 52.4 g, 336 mmol) dropwise. The reaction was refluxed at 60 °C for 6 days. The reaction was allowed to cool and the solution tested each day until no change in the NMR spectrum of products was observed. On cooling, a cream KI precipitate settles out of a yellow solution. The cooled reaction mixture was filtered, washing the KI precipitate with acetone. Acetone was removed from the cloudy yellow filtrate *in vacuo* to leave a yellow oil, which was redissolved in DCM and filtered through Celite. Removal of the DCM *in vacuo* afforded 2.78 g of a yellow oil. The oil was suspended in 5 mL DCM and absorbed onto 5 g of Celite. Chromatographic separation was performed by elution of the product with Et_2O/hexanes (1:1) through a static phase of 700 g silica. Fractions were combined and solvent removed, to yield **2.5** (132 mg, 0.245 mmol, 1.4%), **2.6** (550 mg, 1.11 mmol, 6.2%). **2.4** eluted in a mixed fraction

containing **2.5**; **2.7** and **2.10** eluted together in a fraction containing **2.6**; **2.8** and **2.9** eluted together in a 2:1 ratio. Attempts to separate products further by chromatograpy, or fractional crystallisation from MeOH, EtOH, THF, pentanes, hexanes, toluene, DCM, and chloroform, failed.

6.3.1.3 Synthesis of **2.11**

A 25 mL round bottom flask containing **2.3** (200 mg, 0.414 mmol) in 2.5 mL glacial acetic acid and 2.5 mL hydrochloric acid (1 M) was refluxed at 100 °C for 24 hours. After cooling to room temperature, the mixture was diluted with 4 mL distilled water, and the product extracted with 3 x 8 mL DCM. The combined organics were washed with saturated aqueous $NaHCO_3$ and dried over $MgSO_4$. Removal of the solvent left the product as a yellow oil which was assessed to be free of impurities by ^1H NMR spectroscopy. Yield 127 mg, 0.3204 mmol, 98%.

6.3.1.4 Synthesis of **2.12**

A 25 mL round bottom flask charged with **2.6** (200 mg, 0.403 mmol) in 2.5 mL glacial acetic acid and 2.5 mL hydrochloric acid (1 M) was refluxed at 100 °C for 24 hours. The solution was cooled to room temperature, diluted with 4 mL distilled water, and the product extracted with 3 x 8 mL DCM. The combined organics were washed with saturated aqueous $NaHCO_3$ and dried over $MgSO_4$. Removal of the solvent left the product as a yellow oil which was assessed to be free of impurities by NMR. Yield 74 mg, 0.311 mmol, 77%.

6.3.1.5 Synthesis of **2.13**

2.11 (127 mg, 0.3204 mmol) was dispersed in 2 mL concentrated hydrochloric acid in a round bottomed flask, and heated at reflux 12 days, turning into a pink solution with a dark brown sticky residue. An additional 5 mL HCl was added *via* the condenser as necessary. After cooling to room temperature, the mixture was diluted with 10 mL

H_2O and extracted with 2 x 5 mL DCM. Combined organics were washed with 4 mL $NaHCO_3$ and dried over $MgSO_4$. Approximately 2 g of activated carbon was added and filtered through Celite to give a colourless filtrate. Removal of solvent *in vacuo* left **2.13** as a colourless oil that smelled of toffee, which was dried on the rotary evaporator at 40 °C for 1 hour. Yield 14 mg, 0.063 mmol, 20%.

6.3.2 Chapter 3

6.3.2.1 Synthesis of $Fe_2Pn^*_2$ **3.1**

A red orange solution of $Fe(acac)_2$ (321.7 mg, 1.27 mmol) in 5 mL THF was added to a slurry of $Li_2Pn^*TMEDA_{0.102}$ (272.8 mg, 1.29 mmol) in 10 mL THF at room temperature with vigorous stirring, and glassware rinsed with 2 mL THF. The mixture instantly darkened, and was stirred at room temperature overnight. THF was removed *in vacuo* and the black residue dried at 10^{-2} mbar for 2 hours. Benzene (200 mL) was used to extract an initially brown solution using a filter cannula, the solution turning purple as it became more dilute. The benzene solution was reduced past minimum volume to 10 mL, transferred to a mini-Schlenk flask, and stored at 9 °C for 2 days. After decanting the solution and drying at 30 °C for 1 hour, a 57 mg crop of microcrystalline **3.1** was isolated as a purple-black powder. A second recrystallisation from the concentrated supernatant yielded a further 13.4 mg. Yield 70.4 mg, 0.145 mmol, 23%.

6.3.2.2 Synthesis of $Fe_2Pn^*_2(CO)_2$ **3.2**

A solution of $Fe_2Pn^*_2$ (57 mg, 0.12 mmol) in 5 mL of benzene was subjected to three freeze-pump-thaw-degas cycles, then backfilled at room temperature with 1 atm carbon monoxide. A rapid reaction turned the solution orange. Removal of the solvent left **3.2** as an orange residue, which was washed with pentane at 0 °C (2 x 2 mL) and dried at 10^{-3} mbar for 1 hour. Yield 32 mg, 0.059 mmol, 49%.

6.3.3 Chapter 4

6.3.3.1 Synthesis of $(FeCp^*)_2Pn^*$ **4.1a**

A bright green solution of Cp*FeCl·TMEDA (441.6 mg, 1.29 mmol) in 10 mL THF was cooled to −78 °C. A slurry of $Li_2Pn^*TMEDA_{0.102}$ (136.6 mg, 0.64 mmol) in 15 mL THF at −78 °C was added quickly *via* cannula with vigorous stirring. The dark brown mixture was stirred at −78 °C for 20 minutes then allowed to warm to room temperature and stirred for a further 1 hour. Above −10 °C, the mixture became an intensely dark black-yellow solution. The solvent was removed *in vacuo*, and a dark brown solution was extracted with hexanes (16 x 25 mL) until the washings contained no colour, to leave a grey-brown chalky residue. The hexane solution was concentrated to 15 mL, transferred without filtration to a mini-Schlenk flask, and stored at −78 °C overnight, where a black microcrystalline precipitate formed. The brown supernatant was decanted and the black crystals of **4.1a** were washed with 3 x 5 mL of cold (−78 °C) pentane, then dried at 1.6 x 10^{-2} mbar for 3 hours. The supernatant was concentrated and yielded a second crop of crystals. Yield 49.5 mg, 0.0869 mmol, 13%.

6.3.3.2 Synthesis of $(CoCp^*)_2Pn^*$ **4.2a**

A slurry of $Li_2Pn^*TMEDA_{0.102}$ (227 mg, 1.07 mmol, 1 eq.) in 10 mL THF at −78 °C was added quickly to a very dark yellow solution of Cp*Co(acac) (629 mg, 2.14 mmol, 2 eq.) in 15 mL THF at −78 °C, and stirred at this temperature for 1 hour. The yellow mixture was warmed to room temperature, resulting in a colour change to dark brown-black above −10 °C. After stirring for 1 hour at room temperature, the solvent was stripped and the brown-black residue was dried at 2 x 10^{-2} mbar for 2 hours. A brown solution was extracted with hexanes (10 x 20 mL), reduced in volume to 20 mL before transferring to a new flask and storing at −78 °C for 2 days. After 2 days, decanting the supernatant and washing crystals with −78 °C pentanes yielded **4.2a** as black crystals. Total yield 187.1 mg, 0.326 mmol, 31%.

6.3.3.3 Synthesis of $(CoCp)_2Pn^*$ **4.2b**

A solution of cobaltocene (1026 mg, 5.43 mmol, 1.9 eq.) in 10 mL THF was added to a vigorously stirred slurry of $Li_2Pn^*TMEDA_{0.102}$ (606 mg, 2.86 mmol, 1 eq.) in 10 mL THF at −78 °C. The resulting dark mixture was allowed to warm to room temperature over the course of an hour, then stirred at room temperature overnight. Removal of the solvent left a black residue, which was dried at 10^{-2} mbar overnight, with the sublimation of black crystals of unreacted $CoCp_2$. The black residue was isolated from the sublimed crystals by redissolving in THF and transferred *via* cannula to a new Schlenk flask. The THF was removed *in vacuo*, and a brown solution extracted into 200 mL boiling hexane with the aid of sonication. Following filtration, the hexane solution was reduced in 75 mL and stored at −78 °C. After 18 hours, a brown solution was decanted from a 276 mg crop of black crystals, which were washed with −78 °C pentane and dried for 4 hours at 10^{-2} mbar. The crystals were redissolved in THF with $Li_2Pn^*TMEDA_{0.102}$ (50 mg, 0.24 mmol) and stirred overnight. Removal of the solvent left a black residue, from which a brown solution was extracted with benzene. Reduction of the benzene to minmum volume and storage at 9 °C for 1 month yielded analytically pure black microcrystals of **4.2b**. Yield 49.5 mg, 0.114 mmol, 4.0%.

6.3.3.4 Synthesis of $(NiCp^*)_2Pn^*$ **4.3a**

A red solution of Cp*Ni(acac) (98.4 mg, 0.336 mmol) in 10 mL toluene was added to a slurry of $Li_2Pn^*TMEDA_{0.102}$ (35.6 mg, 0.168 mmol) in 10 mL toluene at 25 °C. The solution immediately darkened and was stirred for 4 hours, during which the colour turned from red to orange-red. The solution was transferred *via* filter cannula to a new Schlenk, and the chalky grey residue was washed with toluene (4 x 10 mL). The filtrate was concentrated to 10 mL and stored in the −78 °C freezer. After 13 days, black crystals of $(NiCp^*)_2Pn^*$ had precipitated. The supernatant was decanted and the crystals washed with 1 x 5 mL −78 °C toluene then dried at 2 x 10^{-2} mbar for 2 hours to yield a sample

that gave a satisfactory elemental analysis. Concentration of the supernatant and returning it to the −78 °C freezer yielded a second crop of crystalline **4.3a**. Yield 41.1 mg, 0.0715 mmol, 43%.

6.3.3.5 Synthesis of $(NiCp)_2Pn^*$ **4.3b**

Green nickelocene (562.5 mg, 2.98 mmol, 1.97 eq.) solvated in 15 mL benzene in an ampoule was added to $Li_2Pn^*TMEDA_{0.102}$ (321 mg, 1.51 mmol, 1 eq.) at 25 °C with stirring, resulting in an immediate dark brown colour, and the reaction stirred for 24 hours. After sonicating for 30 minutes, the dark brown benzene solution was transferred *via* filter cannula to a new Schlenk, and the grey LiCp residue washed with benzene (3 x 10 mL). The solution was concentrated to 10 mL, and stored at 9 °C for 50 days. Following removal of the solvent and washing with 10 mL 9 °C benzene, the black crystals of **4.3b** were dried at 2×10^{-2} mbar for 3 hours. Yield 184.6 mg, 0.425 mmol, 29%.

6.3.4 Chapter 5

6.3.4.1 Synthesis of $Fe(Pn^*H)_2$ **5.1**

A slurry of Li(Pn*H) (2.11 g, 10.8 mmol) in 10 mL THF was added to a vigorously stirred solution of $Fe(acac)_2$ (1.317 g, 5.18 mmol) in 10 mL THF at −78 °C. The reaction was allowed to warm to room temperature over an hour, then stirred for 2 hours. Solvent was removed *in vacuo* to leave a brown residue. A tan solution was extracted in boiling pentane (150 mL), reduced to minimum volume, and transferred *via* filter cannula to a new flask. After storage at −78 °C for 24 hours, **5.1** was isolated as a mixture of tan powder and red crystals, containing a 1:1 mixture of two major isomers, and trace amounts of a third isomer. Yield 0.941 g, 2.18 mmol, 42%.

6.3.4.2 Synthesis of FeCp*(Pn*H) **5.2**

A green solution of FeCp*Cl·TMEDA (246.6 mg, 0.720 mmol) in 5 mL THF was added to a slurry of Li(Pn*H) (141.5 mg, 0.720 mmol) in 5 mL THF at 0 °C with stirring. After warming to room temperature, the solution was stirred at this temperature overnight. The solvent was removed *in vacuo* to leave a sticky, oily looking grey-yellow residue. Extraction of a yellow solution with 15 mL benzene left behind a residue that appeared grey-black when wet, and dried to leave a chalky grey solid. Removal of the benzene left a sticky oil, from which a white precipitate (presumably LiCl) developed overnight. Pentane (10 mL) was used to extract an orange solution, which after filtering and stripping of the solvent, was dried for 2 hours at 10^{-2} mbar. This extraction step was repeated a second time, after which **5.2** was isolated as a tan coloured residue. The NMR spectrum revealed this to contain only one isomer. Yield 125 mg, 0.330 mmol, 46%.

6.3.4.3 Synthesis of $Mn(Pn^*H)_2$ **5.3**

To a Schlenk containing Li(Pn*H) (500 mg, 2.57 mmol) and $Mn(acac)_2$ (325 mg, 1.28 mmol), 10 mL THF was added at −78 °C, with vigorous stirring. The solution was warmed to room temperature, and the solvent removed *in vacuo*. A red solution was extracted with pentane, and the filtrate reduced to minimum volume. After storing at −78 °C for 1 day, the supernatent was decanted and the large crystals were washed with 5 x 5 mL pentane at −78 °C. After drying at 1.2 x 10^{-2} mbar for three hours, 172.4 mg of dark red crystals of **5.3** were isolated. Concentration of the supernatant and storage at −78 °C for 3 days yielded a further 172.2 mg. Total yield 344.6 mg, 0.802 mmol, 62%.

6.4 References

(1) Bertz, S. H.; Cook, J. M.; Gawish, A.; Weiss, U.; Jones, T. K.; Denmark, S. E.; Govindan, S. V; Coates, R. M. *Org. Synth.* **1986**, *64*, 27.
(2) Ashley, A. E.; Cowley, A. R.; O'Hare, D. *Chem. Commun.* **2007**, 1512.
(3) Jonas, K.; Klusmann, P.; Goddard, R. *Z. Naturforsch., B: Chem. Sci.* **1995**, *50*, 394.
(4) Manriquez, J. M.; Bunel, E. E.; Oelckers, B.; Vasquez, C.; Miller, J. S. In *Inorganic Syntheses*; Cowley, A. H., Ed.; John Wiley & Sons, Inc., 1997; Vol. 31, p. 215.

(5) Bunel, E. E.; Valle, L.; Manriquez, J. M. *Organometallics* **1985**, *4*, 1680.
(6) Cooper, R. T.; Chadwick, F. M.; Ashley, A. E.; O'Hare, D. *Organometallics* **2013**, *32*, 2228.
(7) Cosier, J.; Glazer, A. M. *J. Appl. Cryst.* **1986**, *19*, 105.
(8) Otwinowski, Z.; Minor, W. In *Methods in Enzymol.*; Carter, C. W.; Sweet, R. M., Eds.; Academic Press, 1997; p. 276.
(9) Oxford Diffraction Ltd. CrysAlisPro, 2011.
(10) Altomare, A.; Cascarano, G.; Giacovazzo, C.; Guagliardi, A.; Burla, M. C.; Polidori, G.; Camalli, M. *J. Appl. Cryst.* **1994**, *27*, 435.
(11) Palatinus, L.; Chapuis, G. *J. Appl. Cryst.* **2007**, *40*, 786.
(12) Betteridge, P. W.; Carruthers, J. R.; Cooper, R. I.; Prout, K.; Watkin, D. J. *J. Appl. Cryst.* **2003**, *36*, 1487.
(13) Cooper, R. I.; Thompson, A. L.; Watkin, D. J. *J. Appl. Cryst.* **2010**, *43*, 1100.
(14) Carruthers, J. R.; Watkin, D. J. *Acta Crystallogr. Sect. A* **1979**, *35*, 698.
(15) Spek, A. L. *J. Appl. Cryst.* **2003**, *36*, 7.
(16) Farrugia, L. J. *J. Appl. Cryst* **1997**, *30*, 565.
(17) Allinger, N. L. *J. Am. Chem. Soc.* **1977**, *99*, 8127.
(18) Dewar, M. J. S.; Zoebisch, E. G.; Healy, E. F.; Stewart, J. J. P. *J. Am. Chem. Soc.* **1985**, *107*, 3902.
(19) Stewart, J. J. P. *J. Comput. Chem.* **1989**, *10*, 209.
(20) Stewart, J. J. P. *J. Comput. Chem.* **1989**, *10*, 221.
(21) Binkley, J. S.; Pople, J. A.; Hehre, W. J. *J. Am. Chem. Soc.* **1980**, *102*, 939.
(22) Hehre, W. J. *J. Chem. Phys.* **1969**, *51*, 2657.
(23) ADF, 2010.
(24) Te Velde, G.; Bickelhaupt, F. M.; van Gisbergen, S. J. A.; Foneseca Guerra, C.; Baerends, E. J.; Snijders, J. G.; Ziegler, T. *J. Comput. Chem.* **2001**, *11*, 931.
(25) Becke, A. D. *Phys. Rev. A* **1988**, *38*, 3098.
(26) Perdew, J. P.; Yue, W. *Phys. Rev. B* **1986**, *33*, 8800.
(27) Vosko, S. H.; Wilk, L.; Nusair, M. *Can. J. Phys.* **1980**, *58*, 1200.
(28) Lee, C.; Yang, W.; Parr, R. G. *Phys. Rev. B* **1988**, *37*, 785.
(29) Miehlich, B.; Savin, A.; Stoll, H.; Preuss, H. *Chem. Phys. Lett.* **1989**, *157*, 200.
(30) Zhao, Y.; Truhlar, D. G. *Theor. Chem. Acc.* **2007**, *120*, 215.
(31) Kendall, R. A.; Dunning, T. H.; Harrison, R. J. *J. Chem. Phys.* **1992**, *96*, 6796.
(32) Bain, G. A.; Berry, J. F. *J. Chem. Educ.* **2008**, *85*, 532.

Chapter 7 CHARACTERISING DATA

7.1 2,4,6,8-tetramethylcarboxylate-3,7-diethoxy-2,6-exo-diethyl-bicyclo[3.3.0]octa-3,7-diene (**2.1**)

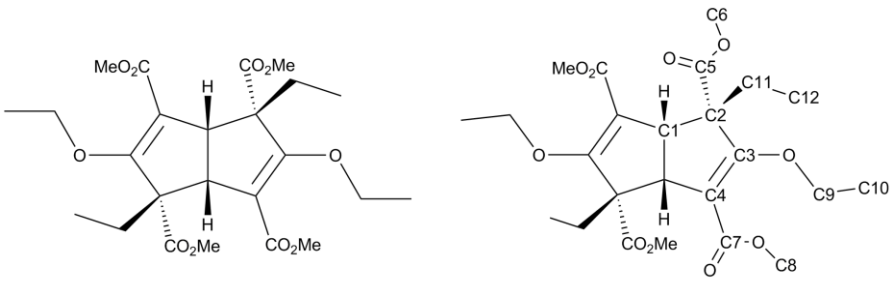

Numbering scheme for NMR

General properties: Colourless blocky crystals or yellow oil.

Elemental analysis found (calculated) for $C_{24}H_{34}O_{10}$ (MW = 482.52) (%): C 59.86 (59.74), H 6.91 (7.10).

HRMS (ESI) *m/z* 505.20441 (predicted 505.20442) $[M+Na]^+$.

Mass spec (ES-API) *m/z* 505.2 $[M+Na]^+$, 483.2 $[M+H]^+$.

IR (solid, cm^{-1}) 624 (w), 700 (w, alkane C–H rock); 768, 780, 790, 807, 854, 890, 924, 956 (w); 1004, 1015 (m, ester C–O–C stretches); 1044, 1088, 1104 (w); 1129 (m); 1203 (s), 1231, 1250 (m, ester C–O–C stretches and vinyl ether C–O–C asymm stretch); 1316 (w), 1332 (w), 1369 (w), 1391 (w), 1434 1434 (m, aliphatic CH_3 symm and asymm deformation); 1613, 1622 (m, vinyl ether C=C stretches); 1708, 1716, 1734 (m, ester C=O stretches); 2948, 2975 (br, CH_3 and CH_2 asymm and symm C–H stretches).

^{1}H NMR (400 MHz, $CDCl_3$, 298 K) δ (ppm) 0.84 (6H, t, $^3J_{HH}$ = 7.4 Hz, H12), 1.22 (6H, t, $^3J_{HH}$ = 7.0 Hz, H10), 1.95 (4H, two overlapping q, $^3J_{HH}$ = 7.3 Hz, $^4J_{HH}$ = 1.1 Hz, H11, H11'), 3.52 (2H, s, H1), 3.59 (6H, s, H6), 3.66 (6H, s, H8), 4.18 (2H, dq, $^2J_{HH}$ = 9.9 Hz, $^3J_{HH}$ = 7.0 Hz, H9), 4.32 (2H, dq, $^2J_{HH}$ = 9.9 Hz, $^3J_{HH}$ = 7.0 Hz, H9').

^{13}C NMR (400 MHz, $CDCl_3$, 298 K) δ (ppm) 8.6 (C12), 15.7 (C10), 28.5 (C11), 48.5 (C1), 51.0 (C8), 51.6 (C6), 65.1 (C2), 71.7 (C9), 109.4 (C4), 164.4 (C7), 168.3 (C3), 172.8 (C5).

Structure determined by single crystal X–ray diffraction 056scb14

7.2 2,4,6,8-tetramethylcarboxylate-3,7-diethoxy-2,8-*exo*-diethyl-bicyclo[3.3.0]octa-3,6-diene (**2.2**)

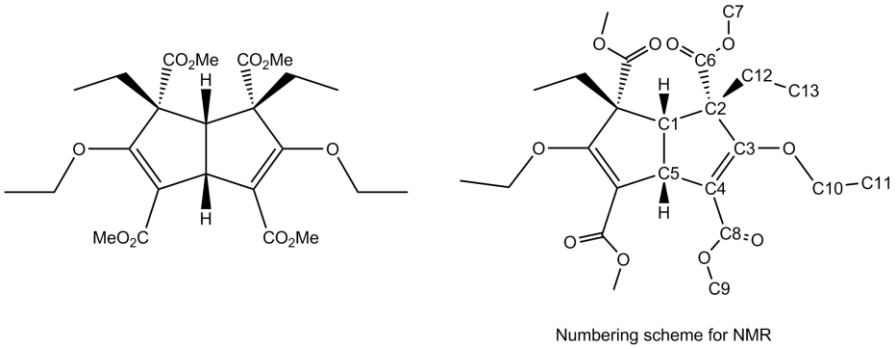

Numbering scheme for NMR

General properties: Colourless blocky crystals or yellow oil.

HRMS (ESI) *m/z* 505.20443 (predicted 505.20442) $[M+Na]^+$.

Mass spec (ES-API) *m/z* 505.2 $[M+Na]^+$, 483.2 $[M+H]^+$.

IR (neat, cm^{-1}) 807, 1020, 1126, 1157 (m, ring 'breathing'); 1206, 1241 (strong with shoulders, ester C–O–C stretches and vinyl ether C–O–C asymm stretch); 1308, 1338 (m, CH_2 scissors); 1371, 1434 (m, aliphatic CH_3 symm and asymm deformation); 1627 (vinyl ether C=C stretch); 1650, 1721 (s, two ester C=O stretches); 2841, 2882, 2902, 2951, 2979 (br, CH_3 and CH_2 asymm and symm C–H stretches).

^{1}H NMR (400 MHz, $CDCl_3$, 298 K) δ (ppm) 0.85 (6H, t, $^3J_{HH}$ = 7.5 Hz, H13), 1.23 (6H, t, $^3J_{HH}$ = 7.0 Hz, H11), 1.82 (2H, dq, $^2J_{HH}$ = −14.0 Hz, $^3J_{HH}$ = 7.5 Hz, H12), 1.96 (2H, dq, $^2J_{HH}$ = −15.0 Hz, $^3J_{HH}$ = 7.5 Hz, H12'), 2.74 (1H, d, $^3J_{HH}$ = 7.7 Hz, H1), 3.56 (6H, s, H7), 3.67 (6H, s, H9), 4.12 (4H, dq, $^2J_{HH}$ = −8.26 Hz, $^3J_{HH}$ = 7.0 Hz, H10), 4.15 (1H, d, $^3J_{HH}$ = 7.0 Hz, H5).

^{13}C NMR (400 MHz, $CDCl_3$, 298 K) δ (ppm) 9.0 (C13), 15.5 (C11), 30.1 (C12), 48.8 (C5), 49.3 (C1), 51.3 (C9), 51.6 (C7), 61.6 (C2), 69.9 (C10), 109.5 (C4), 165.0 (C3), 166.1 (C8), 171.8 (C6).

7.3 2,4,6,8-tetramethylcarboxylate-7-ethoxy-2,4,6-*exo*-triethyl-3-keto-bicyclo[3.3.0]oct-7-ene (**2.3**)

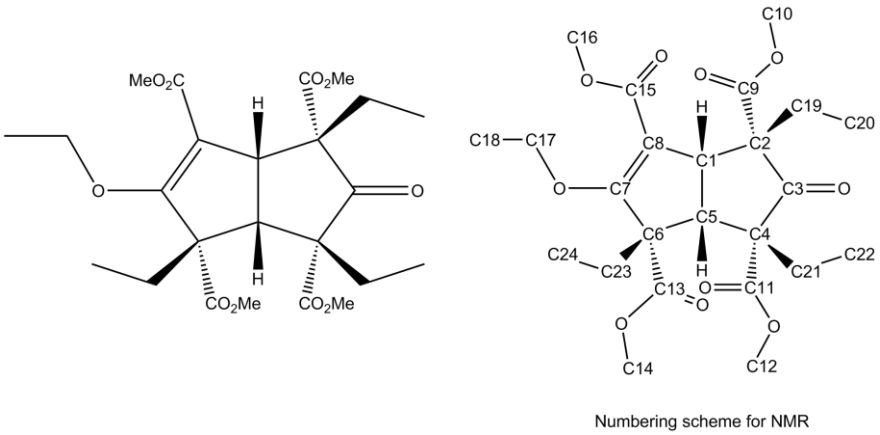

Numbering scheme for NMR

General properties: Colourless blocky crystals or yellow oil.

Elemental analysis found (calculated) for $C_{24}H_{34}O_{10}$ (MW = 482.52) (%): C 59.84 (59.74), H 7.09 (7.10).

HRMS (ESI) *m/z* 505.20442 (predicted 505.20442) $[M+Na]^+$.

Mass spec (ES-API) *m/z* 505.2 $[M+Na]^+$, 483.2 $[M+H]^+$.

IR (solid, cm^{-1}) 800 (m); 906, 931, 996, 1007, 1032, 1050, 1076, 1087, 1128, 1157 (m, ring 'breathing'); 1216, 1244 (strong with shoulders, ester C–O–C stretches and vinyl ether C–O–C asymm stretch); 1315, 1329, 1350 (m, CH_2 scissors); 1374, 1386, 1436 (m, aliphatic CH_3 symm and asymm deformation); 1633 (vinyl ether C=C stretch); 1693, 1722 (br), 1738, 1765 (s, four ester C=O stretches and one ketone stretch); 2881, 2954 (br, CH_3 and CH_2 asymm and symm C–H stretches).

^{1}H NMR (400 MHz, $CDCl_3$, 298 K) δ (ppm) 0.82 (3H, t, $^3J_{HH}$ = 7.5 Hz, H22), 0.86 (3H, t, $^3J_{HH}$ = 7.4 Hz, H24), 0.96 (3H, t, $^3J_{HH}$ = 7.4 Hz, H20), 1.19 (3H, t, $^3J_{HH}$ = 7.0 Hz, H18), 1.83 (1H, dq, $^2J_{HH}$ = −13.9 Hz, $^3J_{HH}$ = 7.4 Hz, H19), 1.88 (2H, dq, overlapping, H23, H23'), 1.89 (1H, dq, overlapping, H21), 2.22 (1H, dq, $^2J_{HH}$ = −13.9 Hz, $^3J_{HH}$ = 7.4 Hz, H19'), 2.25 (1H, dq, $^2J_{HH}$ = −12.3 Hz, $^3J_{HH}$ = 7.5 Hz, H21'), 2.89 (1H, d, $^3J_{HH}$ = 9.4 Hz, H5), 3.42 (3H, s, H12), 3.57 (3H, s, H10), 3.62 (3H, s, H14), 3.68 (1H, d, $^3J_{HH}$ = 9.4 Hz, H1), 3.73 (3H, s, H16), 4.09 (1H, dq, $^2J_{HH}$ = 9.8 Hz, $^3J_{HH}$ = 7.0 Hz, H17), 4.26 (1H, dq, $^2J_{HH}$ = 9.8 Hz, $^3J_{HH}$ = 7.0 Hz, H17').

^{13}C NMR (400 MHz, $CDCl_3$, 298 K) δ (ppm) 8.5 (C22), 9.4 (C24), 9.8 (C20), 15.6 (C18), 26.3 (C21), 33.7 (C23), 35.6 (C19), 47.2 (C5), 49.4 (C1), 51.2 (H16), 51.3 (C12), 51.7 (C14), 51.8 (C10), 62.6 (C6), 62.8 (C4), 63.3 (C2), 71.8 (C17), 112.9 (C8), 164.4 (C15), 165.9 (C7), 169.4 (C13), 169.7 (C9), 172.0 (C11), 205.5 (C3).

Structure determined by single crystal X–ray diffraction 057scb14

7.4 2,4,6,8-tetramethylcarboxylate-3,7-diisopropoxy-2,6-exo-diisopropyl-bicyclo[3.3.0]octa-3,7-diene (**2.4**)

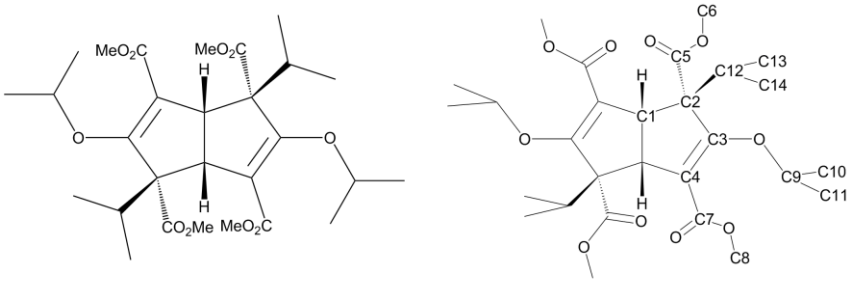

Numbering scheme for NMR

General properties: Colourless, clear oil. Inseparable from **2.5**.

HRMS (ESI) *m/z* 561.26697 (predicted 561.26702) $[M+Na]^+$.

Mass spec (ES-API) *m/z* 561.3 $[M+Na]^+$.

IR of mixture see **2.5**.

^{1}H NMR (400 MHz, $CDCl_3$, 298 K) δ (ppm) 0.92 (6H, d, $^3J_{HH}$ = 6.9 Hz, H13), 1.04 (6H, d, $^3J_{HH}$ = 6.9 Hz, H14), 1.19 (6H, d, $^3J_{HH}$ = 6.1 Hz, H10 or H11), 1.28 (6H, d, $^3J_{HH}$ = 6.1 Hz, H10 or H11), 2.41 (2H, sept, $^3J_{HH}$ = 6.9 Hz, H12), 3.50 (2H, s, H1), 3.57 (6H, s, H6 or H8), 3.61 (6H, s, H6 or H8), 5.21 (2H, sept, $^3J_{HH}$ = 6.1 Hz, H9).

^{13}C NMR (400 MHz, $CDCl_3$, 298 K) δ (ppm) 18.0 (C14), 19.0 (C13), 22.2 (C10 or C11), 23.2 (C10 or C11), 34.1 (C12), 48.3 (C1), 50.8 (C6 or C8), 51.3 (C6 or C8), 68.4 (C2), 77.0 (C9), 107.4 (C4), 164.9 (C5 or C7), 165.7 (C3), 172.2 (C5 or C7).

7.5 2,4,6,8-tetramethylcarboxylate-3,7-diisopropoxy-2,8-exo-diisopropoxy-bicyclo[3.3.0]octa-3,6-diene (**2.5**)

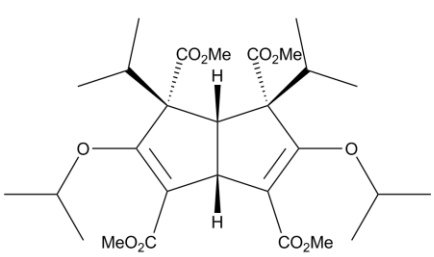

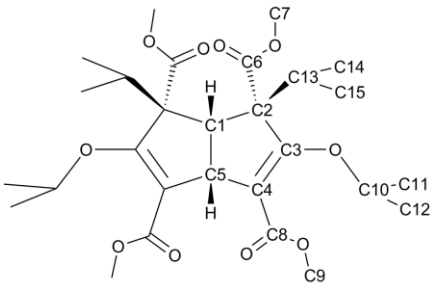

Numbering scheme for NMR

General properties: Colourless, clear oil.

HRMS (ESI) *m/z* 561.26706 (predicted 561.26702) $[M+Na]^+$.

Mass spec (ES-API) *m/z* 561.3 $[M+Na]^+$.

Elemental Analysis found (calculated) for $C_{28}H_{42}O_{10}$ (MW = 538.63) (%): C 69.37 (62.44), H 7.99 (7.86).

IR (neat, cm^{-1}) 904, 921, 940, 985, 1017, 1045, 1060 (w, carbon ring 'breathing'); 1203 (s, C–O–C vinyl ether asymm stretch); 1254, 1296 (s, C–O–C ester stretches); 1374, 1386 (m, isopropyl group CH_3 deformations); 1433 (s), 1466 (m); 1621, 1657 (doublet, vinyl ether C=C stretch); 1724 (s, unsaturated ester C=O stretch), 1742 (s, ester C=O stretch); 2879, 2950, 2966 (br, CH_3 and CH_2 asymm and symm C–H stretches).

^{1}H NMR (400 MHz, $CDCl_3$, 298 K) δ (ppm) 0.88 (6H, d, $^3J_{HH}$ = 6.9 Hz, H14), 1.06 (6H, d, $^3J_{HH}$ = 6.9 Hz, H15), 1.19 (6H, d, $^3J_{HH}$ = 6.0 Hz, H11), 1.22 (6H, d, $^3J_{HH}$ = 6.0 Hz, H12), 2.37 (2H, 2 overlapping q, $^3J_{HH}$ = 6.9 Hz, H13), 2.65 (1H, d, $^3J_{HH}$ = 8.35 Hz, H1), 3.52 (6H, s, H7), 3.66 (6H, s, H9), 4.20 (1H, d, $^3J_{HH}$ = 8.35 Hz, H5), 4.91 (1H, sept, $^3J_{HH}$ = 6.0 Hz, H10).

^{13}C NMR (400 MHz, $CDCl_3$, 298 K) δ (ppm) 18.2 (C14), 19.3 (C15), 21.8 (C11), 22.9 (C12), 36.3 (C13), 45.2 (C1), 50.7 (C7), 51.3 (C9), 53.4 (C5), 66.3 (C2), 74.6 (C10), 107.0 (C4), 160.8 (C3), 166.8 (C8), 171.4 (C6).

7.6 2,4,6,7-tetramethylcarboxylate-3,7-diisopropyl-2-exo-isopropyl-bicyclo[3.3.0]octa-3,7-diene (**2.6**)

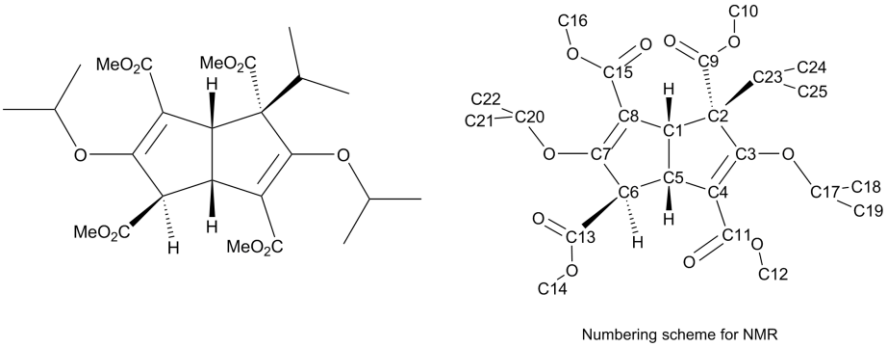

General properties: Colourless, clear oil or amorphous solid.

Elemental Analysis found (calculated) for $C_{25}H_{36}O_{10}$ (MW = 496.55) (%): C 60.63 (60.47), H 7.40 (7.31).

HRMS (ESI) *m/z* 497.23831 (predicted 497.23812) $[M+H]^+$.

Mass spec (ES-API) *m/z* 519.2 $[M+Na]^+$.

IR (Nüjol, cm^{-1}) 916, 988, 1101, 1136, 1152, (w, carbon ring 'breathing'); 1209 (s, C–O–C vinyl ether asymm stretch); 1236, 1248, 1266 (s, C–O–C ester stretches); 1368 (m, isopropyl group CH_3 deformations); 1437, 1463, 1613, 1638 (doublet, vinyl ether C=C stretch); 1743, 1712, 1726 (br, four ester C=O stretches, one ketone C=O stretch); 2853, 2924, 2953 (br, CH_3 and CH_2 asymm and symm C–H stretches).

^{1}H NMR (400 MHz, $CDCl_3$, 298 K) δ (ppm) 0.97 (3H, d, $^3J_{HH}$ = 6.8 Hz, H24), 1.05 (3H, d, $^3J_{HH}$ = 6.8 Hz, H25), 1.15 (3H, d, $^3J_{HH}$ = 6.1 Hz, H18), 1.21 (3H, d, $^3J_{HH}$ = 6.1 Hz, H21), 1.26 (3H, d, overlapping, H22), 1.27 (3H, d, overlapping, H19), 2.42 (1H, sept, $^3J_{HH}$ = 6.8 Hz, H23), 3.54 (3H, s, H10), 3.61 (1H, dd, $^3J_{HH}$ = 9.2 Hz, $^4J_{HH}$ = 2.6 Hz, H1), 3.64 (3H, s, H12), 3.65 (3H, s, H16), 3.72 (1H, dd, $^3J_{HH}$ = 5.5 Hz, $^4J_{HH}$ = 2.6 Hz, H6), 3.74 (3H, s, H14), 3.84 (1H, dd, $^3J_{HH}$ = 9.2 Hz, $^3J_{HH}$ = 5.5 Hz, H5), 4.61 (1H, sept, $^3J_{HH}$ = 6.1 Hz, H20), 5.29 (1H, sept, $^3J_{HH}$ = 6.1 Hz, H17).

^{13}C NMR (400 MHz, $CDCl_3$, 298 K) δ (ppm) 17.9 (C25), 19.3 (C24), 21.6 (C18), 22.4 (C21), 22.8 (C22), 23.1 (C19), 33.4 (C23), 46.7 (C1), 48.6 (C5), 50.9 (C16), 51.2 (C12), 51.5 (C10), 52.4 (C14), 58.8 (C6), 69.3 (C2), 74.8 (C20), 76.4 (C17), 106.2 (C4), 113.5 (C8), 163.5 (C7), 164.5 (C15), 164.7 (C11), 166.6 (C3), 172.5 (C9), 172.8 (C13).

7.7 2,4,6,8-tetramethylcarboxylate-3,7-diisopropoxy-2-*exo*-isopropoxy-bicyclo[3.3.0]octa-3,6-diene (**2.7**)

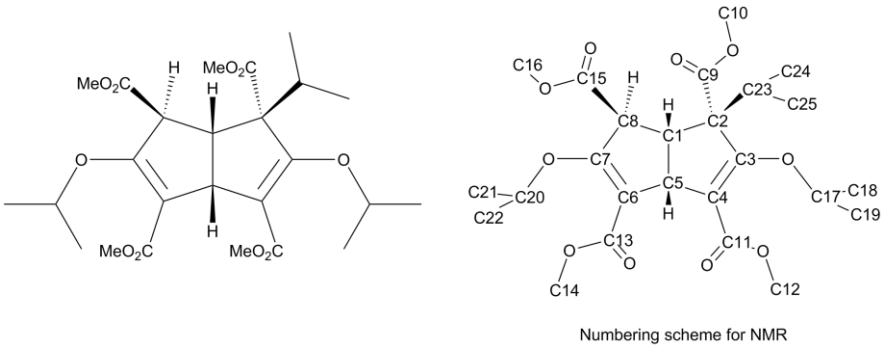

General properties: Colourless, clear oil. Inseparable from **2.6** and **2.10**.

HRMS (ESI) *m/z* 519.2195 (predicted 561.26702) $[M+Na]^+$.

Mass spec (ES-API) *m/z* 519.2 $[M+Na]^+$.

^{1}H NMR (400 MHz, $CDCl_3$, 298 K) δ (ppm) 0.92 (3H, d, $^3J_{HH}$ = 6.9 Hz, H24), 0.99 (3H, d, $^3J_{HH}$ = 6.9 Hz, H25), 1.16 (3H, d, $^3J_{HH}$ = 6.0 Hz, H21), 1.18 (6H, d, $^3J_{HH}$ obscured, H18 and H19), 1.21 (3H, d, $^3J_{HH}$ = 6.0 Hz, H22), 2.28 (1H, sept, $^3J_{HH}$ = 6.9 Hz, H23), 3.02 (1H, dd, $^3J_{HH}$ = 7.8 Hz, $^3J_{HH}$ = 5.4 Hz, H1), 3.61 (3H, s, H16), 3.64 (3H, s, H14), 3.65 (3H, s, H10), 3.66 (obscured, cross–peak observed in 2D spectra, H8), 3.70 (3H, s, H12), 4.25 (1H, dd, $^3J_{HH}$ = 7.8 Hz, $^4J_{HH}$ = 1.7 Hz, H5), 4.60 (1H, sept, $^3J_{HH}$ = 6.0 Hz, H20), 4.86 (1H, sept, $^3J_{HH}$ = 6.0 Hz, H17).

^{13}C NMR (400 MHz, $CDCl_3$, 298 K) δ (ppm) 17.5 (C25), 19.3 (C24), 22.1, 22.3, 22.65, 22.7 (C18,19,21,22), 35.0 (C23), 45.6 (C1), 51.3 (C16), 51.3 (C14), 51.6 (C5), 54.2 (C5), 54.2 (C10), 58.7 (C12), 66.1 (C2), 74.4 (C17), 74.8 (C20), 107.7 (C4), 111.8 (C6), 158.3 (C3), 160.8 (C7), 165.3 (C13), 167.0 (C9), 172.2 (C11), 172.9 (C15).

7.8 2,4,6,8-tetramethylcarboxylate-3-keto-7-isopropoxy-2,4-exo-diisopropyl-bicyclo[3.3.0]oct-6-ene (**2.8**)

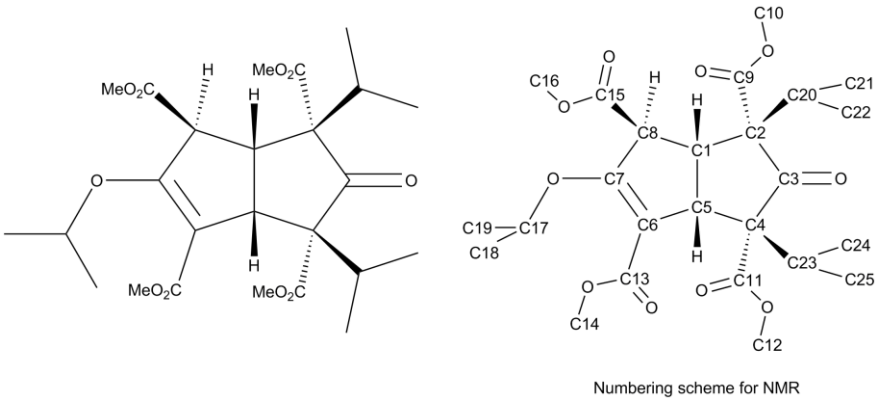

General properties: Colourless, clear oil. Inseparable from **2.9**.

HRMS (ESI) *m/z* 519.21963 (predicted 561.26702) $[M+Na]^+$.

Mass spec (ES-API) *m/z* 519.2 $[M+Na]^+$.

IR of mixture (neat, cm^{-1}) 984, 1034, 1047, 1064 (w, carbon ring 'breathing'); 1099 (s, C–O–C ester stretch); 1212 (s, C–O–C vinyl ether asymm stretch); 1250 (s, C–O–C ester stretch); 1374, 1385 (s, isopropyl group CH_3 deformations); 1435 (s), 1465 (m); 1619 (s, vinyl ether C=C stretch); 1728 (br, four ester C=O stretches, one ketone C=O stretch); 2881, 2954 (br, CH_3 and CH_2 asymm and symm C–H stretches).

^{1}H NMR (400 MHz, $CDCl_3$, 298 K) δ (ppm) 0.89 (3H, d, $^3J_{HH}$ = 6.8 Hz, H21), 0.92 (3H, d, $^3J_{HH}$ = 6.8 Hz, H22), 1.01 (3H, d, $^3J_{HH}$ = 6.9 Hz, H24), 1.09 (3H, d, $^3J_{HH}$ = 6.9 Hz, H25), 1.21 (3H, d, $^3J_{HH}$ = 6.1 Hz, H18), 1.26 (3H, d, $^3J_{HH}$ = 6.1 Hz, H19), 2.41 (1H, sept, $^3J_{HH}$ = 6.8 Hz, H20), 2.47 (1H, sept, $^3J_{HH}$ = 6.9 Hz, H23), 3.43 (1H, dd, $^3J_{HH}$ = 9.1 Hz, $^3J_{HH}$ = 9.1 Hz, H1), 3.58 (3H, s, H14), 3.66 (3H, s, H10), 3.66 (obscured, cross–peak observed in 2D spectra, H5), 3.69 (3H, s, H16), 3.77 (3H, s, H14), 4.10 (1H, dd, $^3J_{HH}$ = 8.9 Hz, $^4J_{HH}$ = 1.8 Hz, H8), 4.77 (1H, sept, $^3J_{HH}$ = 6.1 Hz, H17).

^{13}C NMR (400 MHz, $CDCl_3$, 298 K) δ (ppm) 17.3 (C24), 18.47 (C21), 18.50 (C22), 18.9 (C25), 22.4 (C18), 23.0 (C19), 32.2 (C23), 36.2 (C20), 43.2 (C1), 47.4 (C5), 51.1 (C16), 52.0 (C14), 52.3 (C10), 52.5 (C12), 54.7 (C8), 66.2 (C2), 68.2 (C4), 76.5 (C17), 111.0 (C6), 164.4 (C15), 164.7 (C7), 169.7 (C9), 171.8 (C13), 172.1 (C11), 208.7 (3).

7.9 2,4,6-trimethylcarboxylate-7-keto-3-isopropoxyl-2-*exo*-isopropyl-bicyclo[3.3.0]oct-3-ene (**2.9**)

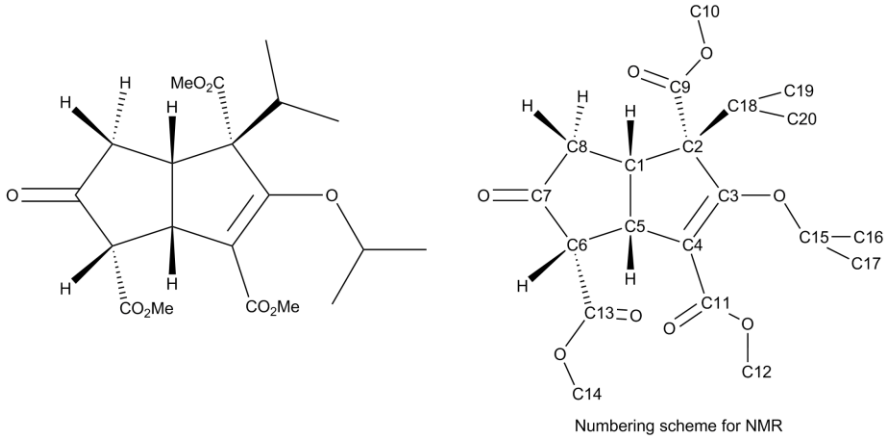

General properties: Colourless, clear oil. Inseparable from **2.8**.

HRMS (ESI) *m/z* 419.16774 (predicted 419.16874) $[M+Na]^+$.

Mass spec (ES-API) *m/z* 419.2 $[M+Na]^+$.

IR see **2.8**.

^{1}H NMR (400 MHz, $CDCl_3$, 298 K) δ (ppm) 0.84 (3H, d, $^3J_{HH}$ = 6.9 Hz, H19), 0.91 (3H, d, $^3J_{HH}$ = 6.5 Hz, H20), 1.02 (3H, d, $^3J_{HH}$ = 6.0 Hz, H16), 1.26 (3H, d, $^3J_{HH}$ = 6.1 Hz, H17), 2.14 (1H, d, $^2J_{HH}$ = −19.2 Hz, H8), 2.57 (1H, sept, $^3J_{HH}$ = 6.8 Hz, H18), 2.64 (1H, dd, $^2J_{HH}$ = −19.2 Hz, $^3J_{HH}$ = 10 Hz, H8'), 2.93 (1H, tdd, $^3J_{HH}$ = 10.0 Hz, $^3J_{HH}$ = 9.7 Hz, $^4J_{HH}$ = 1.3 Hz, H1), 3.38 (1H, dd, $^3J_{HH}$ = 7.7 Hz, $^4J_{HH}$ = 1.3 Hz, H6), 3.62 (3H, s, H10), 3.62 (3H, s, H12), 3.76 (3H, s, H14), 4.04 (1H, dd, $^3J_{HH}$ = 9.7 Hz, $^3J_{HH}$ = 7.7 Hz, H5), 5.21 (1H, sept, $^3J_{HH}$ = 6.0 Hz, H15).

^{13}C NMR (400 MHz, $CDCl_3$, 298 K) δ (ppm) 17.4 (C19), 18.2 (C20), 21.4 (C16), 22.8 (C17), 30.3 (C18), 34.1 (C1), 42.7 (C8), 49.5 (C5), 51.36 (C12), 51.44 (C10), 52.6 (C14), 61.3 (C6), 69.1 (C2), 75.9 (C15), 108.7 (C4), 166.2 (C3), 164.7 (C11), 170.4 (C13), 172.0 (C9), 211.4 (C7).

7.10 Partial assignment of **2.10** 2,4,6-trimethylcarboxylate-7-keto-3-isopropoxyl-6-*exo*-isopropyl-bicyclo[3.3.0]oct-2-ene

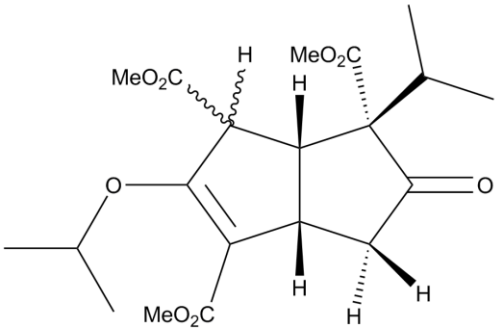

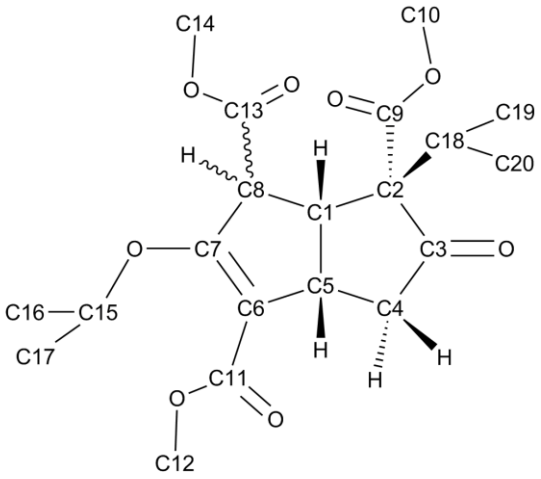

Numbering scheme for NMR

General properties: Inseparable from **2.6** and **2.7**.

^{1}H NMR (400 MHz, CDCl3, 298 K) δ (ppm) 2.24 (1H, sept, $^{3}J_{HH}$ = 6.9 Hz, H18), 2.45 (1H, dd, $^{2}J_{HH}$ = −19.7 Hz, $^{3}J_{HH}$ = 7.0 Hz, H4), 2.67 (1H, dd, $^{2}J_{HH}$ = −19.7 Hz, $^{3}J_{HH}$ = 9.3 Hz, H4'), 3.26 (1H, dd, $^{3}J_{HH}$ = 8.5 Hz, $^{3}J_{HH}$ = 5.7 Hz, H1), 3.59 (obscured, H5), 3.86 (1H, dd, $^{3}J_{HH}$ = 5.7 Hz, $^{4}J_{HH}$ = 1.8 Hz, H8).

^{13}C NMR (400 MHz, CDCl3, 298 K) δ (ppm) 18.4 (C19), 34.1 (C18), 44.6 (C4), 46.7 (C5), 47.0 (C1), 65.5 (C2), 168.0 (C7), 170.6 (C9), 171.6 (C13), 213.4 (C3).

7.11 2,4,6-trimethylcarboxylate-2,4,6-triethyl-bicyclo[3.3.0]octa-3,7-dione (**2.11**)

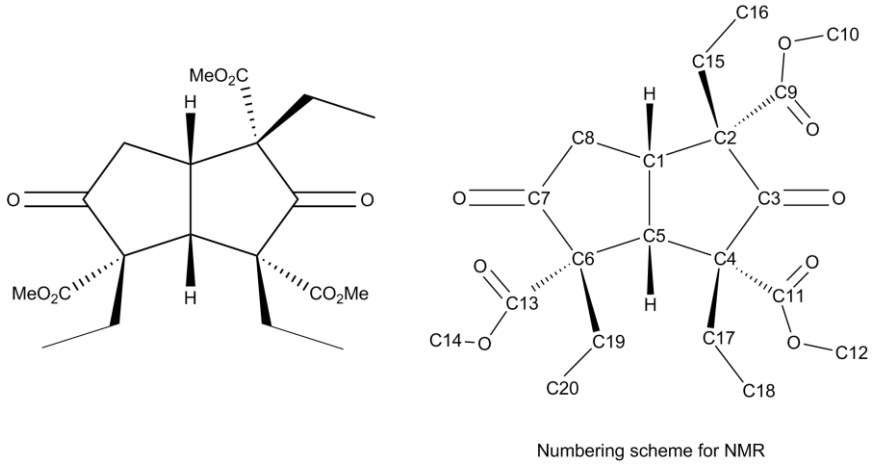

Numbering scheme for NMR

General properties: Dark yellow, clear oil.

HRMS (ESI) *m/z* 419.16769 (predicted 419.16764) $[M+Na]^+$.

Mass spec (ES-API) 419.2 $[M+Na]^+$, 397.2 $[M+H]^+$, 361.2 $[M+H-CO_2Me]^+$.

IR (neat, cm^{-1}) 803 (m); 998, 1015, 1032 (m), 1218, 1239, 1259 (s, C–O–C ester symm and asymm stretches); 1386 (w), 1434 (m, aliphatic CH_3 symm and asymm deformations); 1459 (m, CH_2 scissors); 1633 (m), 1730 (br, s), 1764 (s, three ester C=O stretches and 2 ketone C=O stretches); 2882, 2954 (br, CH_3 and CH_2 asymm and symm C–H stretches).

^{1}H NMR (400 MHz, $CDCl_3$, 298 K) δ (ppm) 0.91 (3H, t, overlapping, H16), 0.93 (6H, t, overlapping, H18 and H20), 1.83 (1H, dd, $^2J_{HH}$ = −14.0 Hz, $^3J_{HH}$ = 7.0 Hz, H19), 1.90 (2H, q, $^3J_{HH}$ = 7.7 Hz, H17), 1.98 (1H, dd, $^2J_{HH}$ = −14.0 Hz, $^3J_{HH}$ = 7.0 Hz, H15), 2.09 (1H, dd, $^2J_{HH}$ = −14.4 Hz, $^3J_{HH}$ = 7.4 Hz, H19'), 2.32 (1H, dd, $^2J_{HH}$ = −14.4 Hz, $^3J_{HH}$ = 7.4 Hz, H15'), 2.57 (2H, dd, $^2J_{HH}$ = 11.4 Hz, $^3J_{HH}$ = 9.3 Hz, H8), 2.92 (1H, q, $^2J_{HH}$ = 9.3 Hz, $^3J_{HH}$ = 9.3 Hz, H1), 3.05 (1H, d, $^3J_{HH}$ = 8.2 Hz, H5), 3.53 (3H, s, H10), 3.67 (3H, s, H12), 3.71 (3H, s, H14).

^{13}C NMR (400 MHz, $CDCl_3$, 298 K) δ (ppm) 9.2 (C18, C20), 9.7 (C16), 29.8 (C15), 30.1 (C19), 31.2 (C17), 39.7 (C8), 42.6 (C1), 49.8 (C5), 52.0 (C12), 52.2 (C10), 52.5 (C14), 63.1 (C4), 64.0 (C6), 64.8 (C2), 169.2 (C9), 169.4 (C11), 170.2 (C13), 207.9 (C3), 208.4 (C7).

7.12 2-methylcarboxylate-2-isopropyl-bicyclo[3.3.0]octa-3,7-dione (**2.12**)

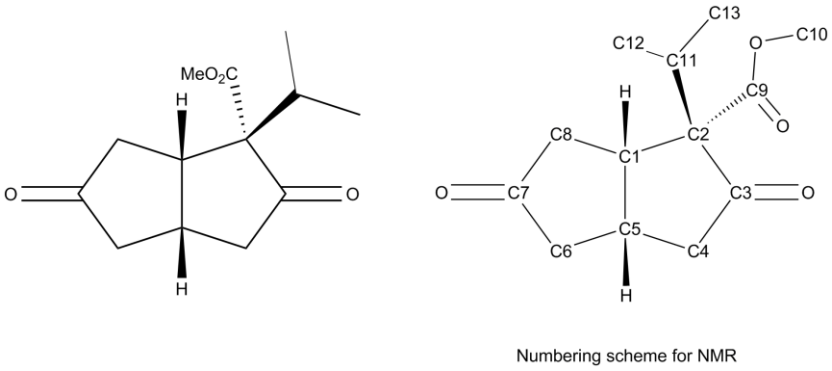

Numbering scheme for NMR

General properties: Pale, slightly orange solid.

HRMS (ESI) *m/z* 261.10977 (predicted 261.10973) $[M+Na]^+$.

Mass spec (ES-API) 261.1 $[M+Na]^+$.

Elemental Analysis found (calculated) for $C_{13}H_{18}O_4$ (MW = 238.28) (%): C 65.72 (65.53), H 7.31 (7.61).

IR (Nüjol, cm^{-1}) 632, 866 (w); 916, 944, 978, 1025, 1069, 1114 (m); 1167 (m), 1218 (s, C–O–C ester stretches); 1374, 1406, 1430 (m, aliphatic CH_3 symm and asymm deformation); 1458 (m, CH_2 scissors); 1722 (s), 1735 (br, s, three ester C=O stretches and 2 ketone C=O stretches); 2852, 2921, 2959 (br, CH_3 and CH_2 asymm and symm C–H stretches).

^{1}H NMR (400 MHz, $CDCl_3$, 298 K) δ (ppm) 0.87 (3H, d, $^3J_{HH}$ = 6.8 Hz, H12), 0.92 (3H, d, $^3J_{HH}$ = 6.8 Hz, H13), 2.10 (1H, ddd, $^2J_{HH}$ = −18.8 Hz, $^3J_{HH}$ = 5.1 Hz, $^4J_{HH}$ = 1.5 Hz, H4 or H6), 2.17 (1H, ddd, $^2J_{HH}$ = −19.1 Hz, $^3J_{HH}$ = 6.7 Hz, $^4J_{HH}$ = 1.6 Hz, H4 or H6), 2.33 (1H, dd, $^2J_{HH}$ = −19.3 Hz, $^3J_{HH}$ = 5.4 Hz, H8), 2.37 (1H, sept, $^3J_{HH}$ = 6.8 Hz, H11), 2.49 (1H, m, H4' or H6'), 2.44 (2H, m, H4' or H6'), 2.56 (1H, dd, $^2J_{HH}$ = −19.3 Hz, $^3J_{HH}$ = 9.2 Hz, H8'), 2.96 (1H, m, H1), 3.06 (1H, m, H5), 3.54 (3H, s, H10).

^{13}C NMR (400 MHz, $CDCl_3$, 298 K) δ (ppm) 18.2 (C12), 18.3 (C13), 33.2 (C11), 33.6 (C1), 42.3 (C 4 or 6), 45.6 (C5), 43.5 (C4 or C6), 45.3 (C8), 51.8 (C10), 67.9 (C2), 170.2 (C9), 214.0 (C3 or C7), 217.0 (C3 or C7).

7.13 2,4,6-triethyl-*cis*-bicyclo[3.3.0]octa-3,7-dione (**2.13**)

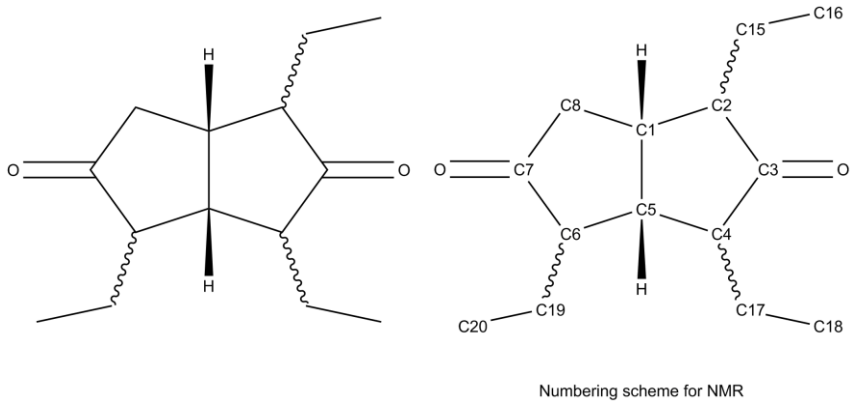

Numbering scheme for NMR

General properties: Colourless, clear oil.

HRMS (ESI) *m/z* 245.15146 (predicted 245.15120) $[M+Na]^+$.

Mass spec (ES-API) *m/z* 245.2 $[M+Na]^+$.

IR (neat, cm^{-1}) 798, 1040, 1074, 1109, 1162 (m, ring 'breathing'); 1259, 1381 (m, CH_2 scissors); 1407, 1459 (m, aliphatic CH_3 symm and asymm deformation); 1646, 1734 (br, s, C=O stretches); 2876, 2933, 2962 (br, CH_3 and CH_2 asymm and symm C–H stretches).

^{1}H NMR (400 MHz, $CDCl_3$, 298 K) δ (ppm) 0.94, 0.97, 1.01(9H total, three overlapping triplets, H16, H18, H20), 1.49 – 1.53 (6H total, three overlapping quartets, H15, H17, H19), 1.91 (2H, m, two of H2, H4, or H6), 2.15 (1H, m, H2, H4, or H6), 2.31 (H8), 2.36 (H1 or H5), 2.55 (H8'), 2.59 (H1 or H5).

^{13}C NMR (400 MHz, $CDCl_3$, 298 K) δ (ppm) 11.7, 11.7, 12.1 (C16, C18, and C20), 22.9, 22.9, 23.8 (C15, C17, and C19), 38.4 (C1 or C5), 44.0 (C8), 45.9 (C1 or C5), 54.7 (C2, C4, or C6), 55.0 (C2, C4, or C6), 55.5 (C2, C4, or C6), 219.8 (C3 or C7), 221.4 (C3 or C7).

7.14 $Fe_2Pn^*_2$ (**3.1**)

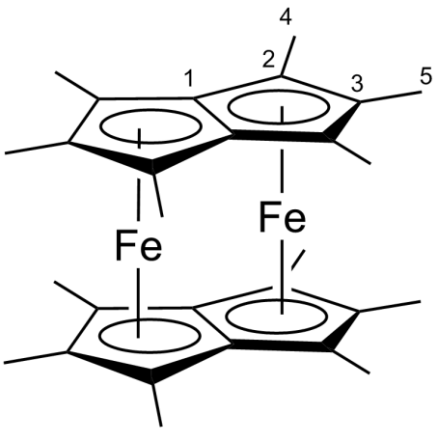

Numbering scheme for NMR

General properties: Black purple or black red crystals, forms purple solutions.

HRMS (EI) *m/z* 484.1552 (predicted 484.1517) $[M]^+$, 428 $[M–Fe]^+$, 413 $[M–Fe–CH_3]^+$, 398 $[M^+–Fe–2CH_3]^+$, 185 $[Pn^*–H]^+$.

Elemental Analysis found (calculated) for $C_{28}H_{36}Fe_2$ (MW = 484.28) (%): C 69.31 (69.44), H 7.34 (7.49).

IR (KBr, cm^{-1}) 801 (m, methyl C–H rocking), 1027 (m), 1091 (m), 1206 (w), 1261 (m), 1375 (w, methyl C–H rocking), 1450 (m, aromatic C–C stretch or methyl C–H bend); 1604 (w, aromatic C–C stretch); 2855, 2905, 2933, 2959 (m, CH_3 asymm and symm C–H stretches).

UV–Vis (toluene) λ_{max} (nm) (ε): 618 (552), 516 (2453), 338 (4581), 288 (15147).

^{1}H NMR (500 MHz, C_7D_8, 298 K) δ (ppm) 12.04 (24H, br s, H4), –89.10 (12H, br s,H5).

^{1}H NMR (400 MHz, C_6D_6, 298 K) δ (ppm) 11.92 (24H, br s, H4), –88.88 (12H, br s, H5).

^{13}C NMR (500 MHz, C_7D_8, 298 K) δ (ppm) only –199.69 observed. Unassigned.

Structure determined by single crystal X–ray diffraction 014TAQA14

7.15 $Fe_2Pn^*_2(CO)_2$ (**3.2**)

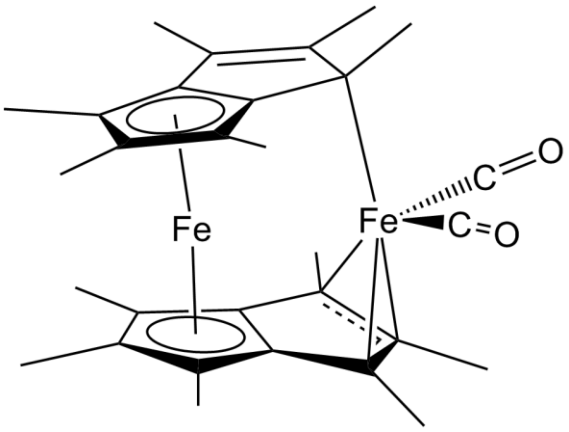

General properties: Black orange crystals, forms orange solutions.

HRMS (EI) *m/z* 540.1923 (predicted 540.1415) $[M]^+$, 484.1559 $[M-2(CO)]^+$, 428 $[M-Fe(CO)_2]^+$.

Elemental Analysis found (calculated) for $C_{30}H_{36}Fe_2O_2$ (MW = 540.30) (%): C 66.50 (66.69), H 6.86 (6.72).

IR (KBr, cm^{-1}) 668 (m), 802 (m), 859 (m, shoulder), 1023 (m), 1094 (m), 1180 (vw), 1261 (m), 1430 (m, aromatic C–C stretch), 1544 (m, C=C stretch); 1888, 1942 (m, C=O symm and asymm stretches); 2854, 2924, 2962 (m, CH_3 asymm and symm C–H stretches).

UV–Vis (toluene) λ_{max} (nm) (ε): 667 (387), 455 (2005), 359 (4739), 289 (15380).

^{1}H NMR (500 MHz, C_7D_8, 243 K) δ (ppm) 0.34, 0.88, 1.11, 1.18, 1.48, 1.58, 1.96, 2.05, 2.11, 2.14, 2.24, 2.58.

^{13}C NMR (500 MHz, C_7D_8, 243 K) δ (ppm) 8.7, 9.1, 9.3, 9.4, 9.5, 10.2, 10.6, 11.4, 11.9, 12.1, 12.3 (11 sp^2 CH_3); 24.4 (1 sp^3 CH_3); 38.0 (1 sp^3 ring C); 56.8, 63.0, 63.9, 65.8, 76.0, 83.8 (6 NWT ring C); 78.4, 82.0, 85.0, 86.4 (4 bridgehead C); 89.5, 94.2, 101.7, (3 WT ring C); 113.2, 145.6 (2 vinylic ring C).

^{1}H NMR (500 MHz, C_6D_6, 298 K) δ (ppm) 0.93, 1.21, 1.90, 1.91, 2.06, 2.15.

^{13}C NMR (500 MHz, C_6D_6, 298 K) δ (ppm), 9.14, 11.7, 11.9, 12.2, 14.5, 15.5, 18.0, 47.6, 67.6, 116.6, 125.7, 146.2, 146.7, 150.9, 213.7 (CO), 226.2 (CO).

Structure determined by single crystal X–ray diffraction 059scb14

7.16 $(FeCp^*)_2Pn^*$ (**4.1a**)

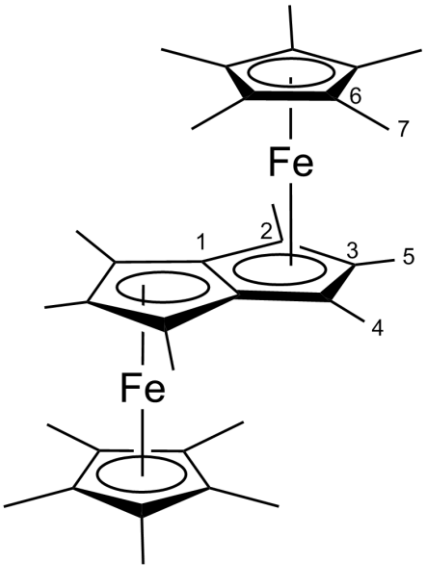

Numbering scheme for NMR

General properties : Black microcrystalline powder, forms brown solutions.

HRMS (EI) *m/z* 568.2523 (predicted 538.2456) $[M]^+$, 378 $[M+H-FeCp^*]^+$, 363 $[M+H-FeCp^*CH_3]^+$, 348 $[M+H-FeCp^*-2CH_3]^+$, 186 $[M-2FeCp^*]^+$.

Satisfactory elemental microanalysis could not be achieved despite testing multiple samples.

IR (KBr, cm^{-1}) 668 (m), 801 (m), 851 (m, shoulder), 1026 (m), 1070 (w, shoulder), 1092 (m), 1180 (w), 1261 (m), 1374 (m), 1418 (m, shoulder), 1447 (m), 1471 (m, shoulder, aromatic C–C stretch); 1568 (m); 2854, 2899, 2939, 2962 (m, CH_3 asymm and symm C–H stretches).

UV–Vis (toluene) λ_{max} (nm) (ε): 498 (908), 400 (3654), 317 (17594), 288 (14926).

^{1}H NMR (400 MHz, C_6D_6, 298 K) δ (ppm) 1.46 (6H, s, H5), 1.59 (30H, s, H7), 2.31 (12H, s, H4).

^{13}C NMR (400 MHz, C_6D_6, 298 K) δ (ppm) 9.0 (C7), 10.3 (C5), 11.5 (C4), 60.6 (C1), 64.9 (C2), 78.1 (C6), 88.9 (C3).

Structure determined by single crystal X–ray diffraction 048scb14

7.17 $(CoCp^*)_2Pn^*$ (**4.2a**)

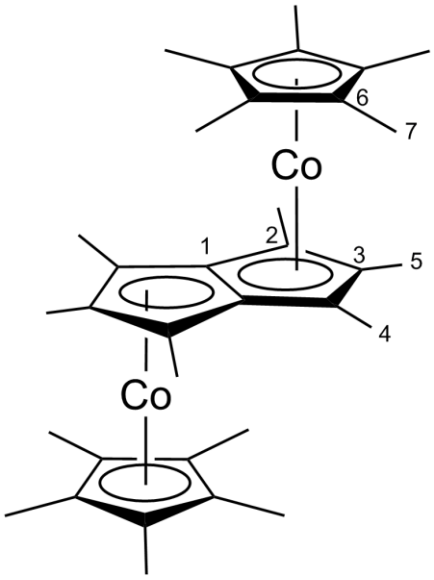

Numbering scheme for NMR

General properties: Black crystals, forms brown solutions.

HRMS (EI) *m/z* 574.2281 (predicted 574.2420) $[M]^+$, 380 $[M-CoCp^*]^+$, 365 $[M-CoCp-CH_3]^+$.

Satisfactory elemental microanalysis could not be achieved despite testing multiple samples.

IR (KBr, cm^{-1}) 801 (m), 874 (w), 1025 (m), 1092 (m), 1179 (w), 1261 (m), 1376 (m), 1448 (m, aromatic C–C stretch); 1548 (w), 1617 (m), 2853, 2899, 2939, 2962 (m, CH_3 asymm and symm C–H stretches); 3442 (br).

UV–Vis (toluene) λ_{max} (nm) (ε): 596 (2458), 464 (5158), 381 (26024), 289 (6478).

^1H NMR (300 MHz, C_6D_6, 298 K) δ 1.42 (12H, s, H4), 1.48 (30H, s, H7), 2.12 (6H, s, H5).

^1H NMR (300 MHz. C_7D_8, 298 K) δ 1.41 (12H, s, H4), 1.45 (30H, s, H7), 2.13 (6H, s, H5).

^{13}C NMR (300 MHz, C_6D_6, 298 K) δ 9.1 (C7), 9.8 (C4), 11.8 (C5), 59.9 (C2), 77.1 (C1 or C3). 86.1 (C6), 96.4 (C1 or C3).

Structure determined by single crystal X–ray diffraction 035scb13

7.18 $(CoCp)_2Pn^*$ (**4.2b**)

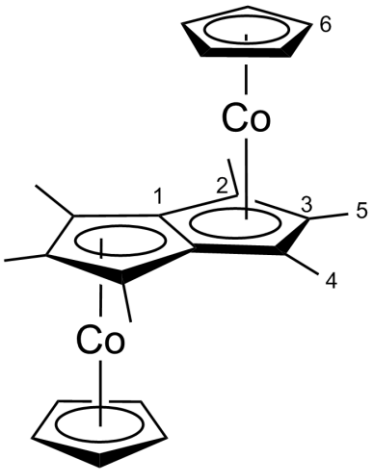

Numbering scheme for NMR

General properties: Black needles, forms brown solutions.

HRMS (EI) *m/z* 434.0858 (predicted 434.0855) $[M]^+$, 309 $[M-CoCpH]^+$, 295 $[M-CoCp-CH_3]^+$.

Elemental Analysis found (calculated) for $C_{24}H_{28}Co_2$ (MW = 434.35) (%): C 66.15 (66.37), H 6.37 (6.50).

IR (solvent/KBr, cm^{-1}) 782 (m, Cp C–H "oop"); 801, 874 (w), 1018, 1104, 1179, 1261, 1374, 1407 (m); 1438 (m, aromatic C–C stretch); 1617 (w); 2854, 2903, 2941, 2963 (m, CH_3 asymm and symm C–H stretches); 3098 (w, Cp C–H stretch).

UV–Vis (toluene) λ_{max} (nm) (ε): 600 (2578), 468 (7805), 365 (33781), 285 (12196).

^1H NMR (300 MHz, C_6D_6, 298 K) δ (ppm) 1.55 (12H, s, H4), 2.08 (6H, s, H5), 4.11 (10H, s, H6).

^{13}C NMR (300 MHz, C_6D_6, 298 K) δ (ppm) 12.0 (C4), 12.3 (C5), 66.1 (C3), 78.0 (C6), 99.3 (C2), 132.1 (C1).

Structure determined by single crystal X–ray diffraction 062scb15

7.19 $(NiCp^*)_2Pn^*$ (**4.3a**)

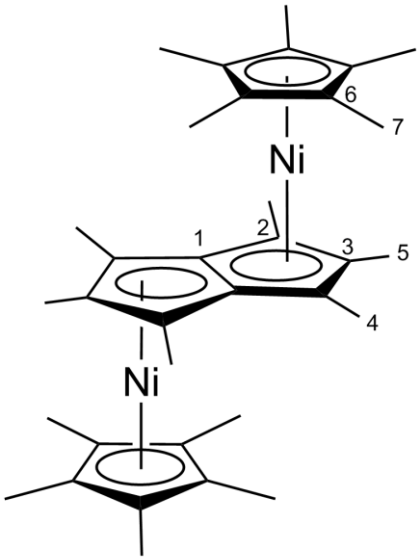

Numbering scheme for NMR

General properties: Black crystals, forms intensely yellow brown solutions.

HRMS (EI) *m/z* 572.2354 (predicted 572.2463) $[M]^+$, 436 $[M-Cp^*H]^+$, 378 $[M-NiCp^*H]^+$, 364 $[M-NiCp^*H-CH_3]^+$.

Elemental Analysis found (calculated) for $C_{34}H_{48}Ni_2$ (MW = 574.13) (%): C 70.89 (71.13), H 8.29 (8.43).

IR (KBr, cm^{-1}) 800 (m), 877 (w), 1022, 1094, 1261, 1376, 1444 (m, aromatic C–C stretch); 1607 (w); 2854, 2906, 2962 (m, CH_3 asymm and symm C–H stretches); 3451 (br).

UV–Vis (toluene) λ_{max} (nm) (ε): 671 (1116), 495 (9700), 454 (6316), 373 (4232).

^1H NMR (300 MHz, C_6D_6, 298 K) δ (ppm) 2.45 (12H, s, H4), 2.75 (30H, s, H7), 3.04 (6H, s, H5).

^1H NMR (500 MHz, C_7D_8, 223 K) δ (ppm) 1.93 (30H, s, H7), 2.05 (6H, s, H5), 2.16 (12H, s, H4).

^{13}C NMR (500 MHz, C_7D_8, 223 K) δ (ppm) 8.75 (C7), 9.57 (C5), 10.57 (C4), 70.27 (C2 or C3), 91.86 (C6), 92.43 (C2 or C3), 101.45 (C1).

Structure determined by single crystal X–ray diffraction 033scb13

7.20 $(NiCp)_2Pn^*$ (**4.3b**)

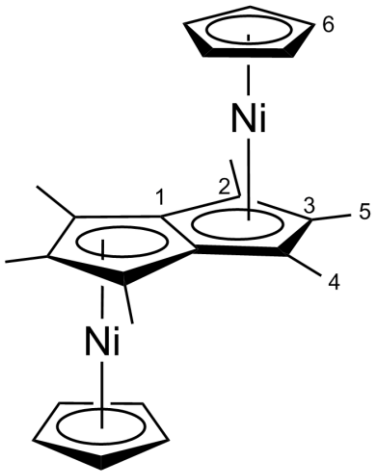

Numbering scheme for NMR

General properties: Black, microcrystalline powder, forms intensely dark, yellow solutions.

HRMS (EI) *m/z* 432.0900 (predicted 432.0898) $[M]^+$, 366 $[M-CpH]^+$, 308 $[M-NiCpH]^+$, 186 $[Pn^*]^+$, 123 $[NiCp]^+$.

Elemental Analysis found (calculated) for $C_{24}H_{28}Ni_2$ (MW = 433.87) (%): C 66.25 (66.44), H 6.60 (6.50).

IR (KBr, cm^{-1}) 767 (m, Cp C–H "oop"); 800, 1021, 1094, 1261, 1375 (m), 1443 (m, aromatic C–C stretch); 1618 (w); 2856, 2903, 2932, 2963 (m, CH_3 asymm and symm C–H stretches); 3098 (w, Cp C–H stretch).

UV–Vis (toluene) λ_{max} (nm): 602 (720), 478 (3104), 436 (4852), 352 (2248).

^1H NMR (300 MHz, C_6D_6, 298 K) δ (ppm) 2.17 (12H, s, H4), 3.17 (10H, s, H6), 4.17 (6H, s, H5).

^{13}C NMR (300 MHz, C_6D_6, 298 K) δ (ppm) 2.9 (C5), 8.9 (C4), 95.0 (C6), C1, C2, and C3 not observed.

Structure determined by single crystal X–ray diffraction 044scb14

7.22 $Fe(Pn^*H)_2$ (**5.1**)

General properties: Orange crystals to tan powder, major isomers **5.1a** and **5.1b**.

HRMS (EI) *m/z* 430.2311 (predicted 430.2323) $[M]^+$, 415 $[M-CH_3]^+$, 400 $[M-2CH_3]^+$.

Elemental Analysis found (calculated) for $C_{28}H_{38}Fe$ (MW = 430.45) (%): C 78.14 (78.13), H 8.81 (8.90).

IR (KBr, cm^{-1}) 668 (m), 720 (w), 802 (m), 854 (m, shoulder), 1027 (m), 1095 (m), 1143 (w), 1261 (m), 1369 (m), 1379 (m, C–H rocking), 1411 (m), 1446 (m, aromatic C–C stretches), 1543 (m, C=C stretch); 2859, 2909, 2957 (m, CH_3 asymm and symm C–H stretches).

UV–Vis (toluene) λ_{max} (nm) (ε): 459 (3220), 360 (7245), 309 (20181).

5.1a **5.1b**

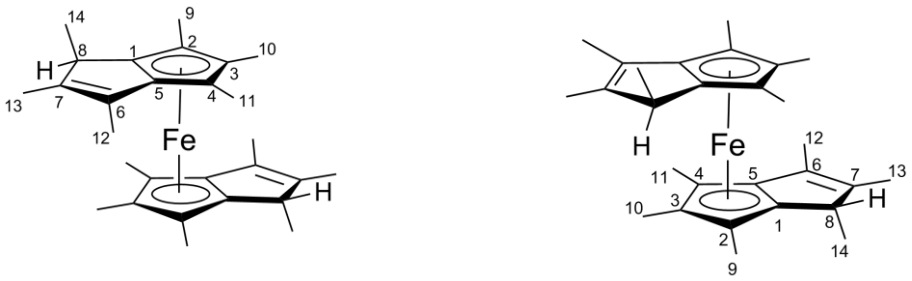

5.1a

^1H NMR (400 MHz, C_6D_6, 298 K) δ (ppm) 1.15 (6H, d, $^3J_{HH}$ = 7.0 Hz, H14), 1.69 (6H, s, H10), 1.73 (6H, s, H13), 1.82 (6H, s, H9), 1.88 (6H, s, H11), 1.93 (6H, s, H12), 2.74 (1H, q, $^3J_{HH}$ = 7.0 Hz, H8).

^{13}C NMR (400 MHz, C_6D_6, 298 K) δ (ppm) 9.65 (C10), 10.13 (C11), 10.59 (C9), 12.39 (C13), 12.41 (C12), 16.65 (C14), 41.22 (C8), 71.93 (C4), 74.75 (C2), 81.77 (C3), 92.68 (C1), 94.26 (C5), 129.29 (C6), 140.00 (C7).

Structure determined by single crystal X–ray diffraction 053scb14

5.1b

^1H NMR (400 MHz, C_6D_6, 298 K) δ (ppm) 1.15 (6H, d, $^3J_{HH}$ = 7.0 Hz, H14), 1.67 (6H, s, H10), 1.76 (6H, s, H13), 1.79 (6H, s, H9), 1.84 (6H, s, H11), 1.94 (6H, s, H12), 2.74 (1H, q, $^3J_{HH}$ = 7.0 Hz, H8).

^{13}C NMR (400 MHz, C_6D_6, 298 K) δ (ppm) 9.65 (C10), 10.10 (C11), 10.50 (C9), 12.32 (C13), 12.49 (C12), 16.55 (C14), 41.06 (C8), 71.88 (C4), 74.69 (C2), 81.85 (C3), 94.38 (C1), 129.01 (C6), 140.41 (C7).

7.23 FeCp*(Pn*H) (**5.2**)

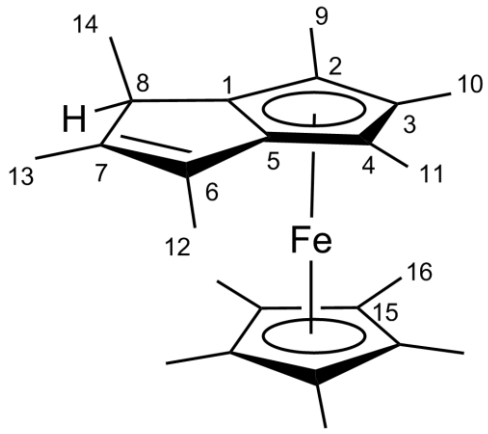

General properties: Tan powder, 1:0.85 mixture of isomers.

HRMS (EI) *m/z* 378.1756 (predicted 378.2010) $[M]^+$, 363 $[M-CH_3]^+$, 348 $[M-2CH_3]^+$, 187 $[C_{14}H_{19}]^+$.

Satisfactory elemental microanalysis could not be achieved despite testing numerous samples.

IR (KBr, cm^{-1}) 668 (m), 720 (w), 802 (m), 854 (m, shoulder), 1027 (m), 1095 (m), 1143 (w), 1261 (m), 1369 (m), 1379 (m, C–H rocking), 1411 (m); 1446 (m, aromatic C–C stretches); 1543 (m, C=C stretch); 2859, 2909, 2957 (m, CH_3 asymm and symm C–H stretches).

UV–Vis (toluene) λ_{max} (nm) (ε): 448 (980), 360 (1756), 289 (19550).

^{1}H NMR (400 MHz, C_6D_6, 298 K) δ (ppm) 1.14 (3H, d, $^3J_{HH}$ = 7.0 Hz, H14), 1.67, (15H, s, H16), 1.71 (3H, s, H10), 1.76 (3H, br s, H13), 1.84 (3H, s, H9), 1.86 (3H, s, H11), 1.94 (3H, br s, H12), 2.84 (1H, q, $^3J_{HH}$ = 7.0 Hz, H8).

^{13}C NMR (400 MHz, C_6D_6, 298 K) δ (ppm) 9.8 (C16), 9.9 (C10), 10.2 (C11), 10.5 (C9), 12.4 (C13 or C14), 12.35 (C13 or C14), 16.8 (C14), 41.6 (C8), 71.5 (C3), 74.3 (C3), 78.5 (C15), 81.2 (C4), 92.2 (C1), 94.0 (C5), 128.2 (C6), 140.0 (C7).

7.24 $Mn(Pn^*H)_2$ (**5.3**)

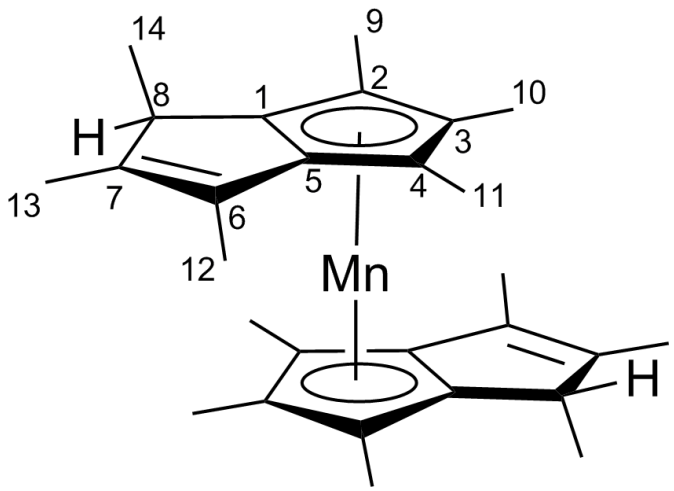

General properties: Dark red crystalline solid, forms deep cherry red solutions.

HRMS (EI) *m/z* 429.2257 (predicted 429.2354) $[M]^+$, 414 $[M-CH_3]^+$, 399 $[M-2CH_3]^+$, 187 $[C_{14}H_{19}]^+$.

Elemental Analysis found (calculated) for $C_{28}H_{39}Mn$ (MW = 429.54) (%): C 78.38 (78.29), H 8.86 (8.92).

IR (KBr, cm^{-1}) 801 (m), 1024 (m), 1094 (m), 1261 (m), 1379 (w, C–H rocking), 1443 (m, aromatic C–C stretches); 1654 (w, C=C stretch); 2854, 2916, 2958 (m, CH_3 asymm and symm C–H stretches).

UV–Vis (toluene) λ_{max} (nm) (ε) 530 (3458), 484 (3500), 360 (10856), 291 (36280).

^1H NMR (500 MHz, C_7D_8, 298 K) δ (ppm) −13.29 (6H, br, s, a), −12.80 (6H, br, s, b), −7.20 (6H, s, c), −1.74 (6H, br, s, d), 2.79 (6H, s, e), 4.93 (6H, s, H14), 11.65 (2H, br, s, H8).

^{13}C NMR (500 MHz, C_7D_8, 298 K) δ (ppm) −139.6 (C^b), −136.5, −126.3 (C^d), −71.2 (C^a), −6.7 (C14), 16.6 (C^c), 34.4, 42.1, 51.6, 58.2, 68.1, 121.7 (C^e), 229.0 (C1), 241.6.

Structure determined by single crystal X–ray diffraction 050scb14

CONCLUSIONS

Bimetallic Pn* bridged compounds developed herein have been extensively characterised, revealing new and interesting properties compared to the small range of literature analogues. These compounds may be considered the simplest building blocks for multimetallic, polymer-like structures with bridging pentalene ligands, and the knowledge of their properties should set the groundwork for studies on extended, chain-type structures.

The development of a range of monometallic permethylhydropentalenyl complexes has created a range of precursors to heterobimetallic species, which may show further interesting properties. In a world where heterobimetallic catalysis is being rapidly revealed to offer enhanced rates and selectivities for chemical transformations, understanding how a bridging ligand can facilitate or block the transmission of an effect at one site to another active site is key to developing more efficient systems.

Finally, it has been demonstrated that the permethylation route developed in the group of O'Hare can incorporate alternative alkyl groups at the non-wing-tip positions of the pentalene framework, and can produce alkylpentalene precursors of low symmetry. Further developments in this field should allow for alkylpentalene ligands with electronic and steric tailoring of the substituents, which may be relevant in subsequent reactivity. In addition, these results may have implications in the development on non-natural polyquinane species with previously unencountered substitution patterns.

APPENDIX

Curie-Weiss fitting of SQUID data for Fe2Pn*2, 3.1, between 100 – 300 K

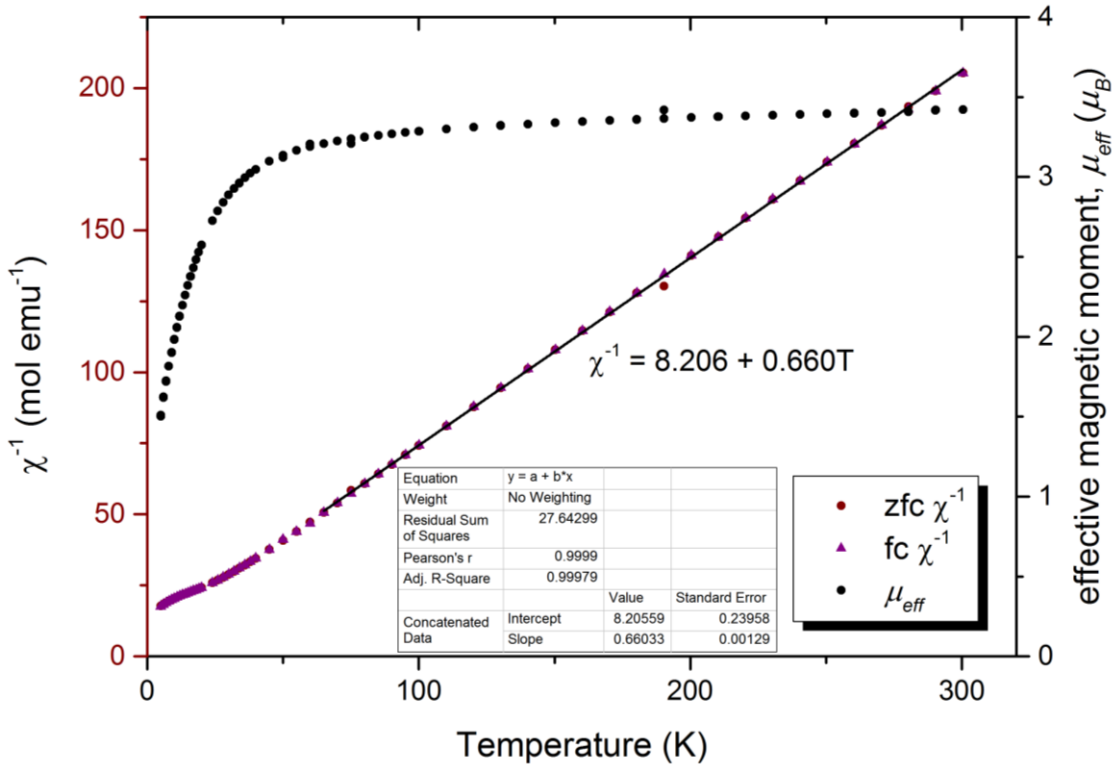

Linear fitting of VT NMR data for $Fe_2Pn^*_2$, **3.1**

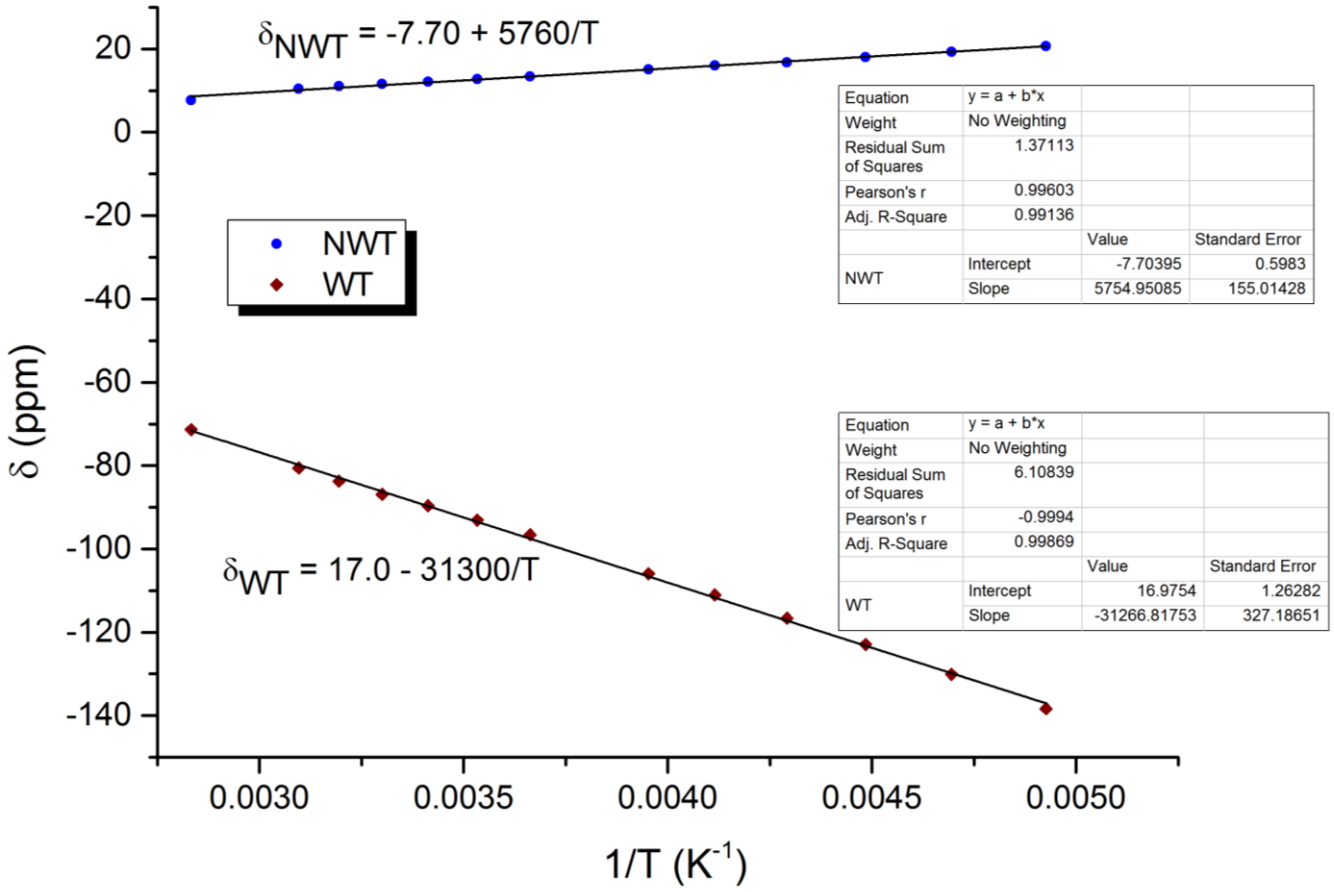

Equation	y = a + b*x		
Weight	No Weighting		
Residual Sum of Squares	1.37113		
Pearson's r	0.99603		
Adj. R-Square	0.99136		
		Value	Standard Error
NWT	Intercept	-7.70395	0.5983
	Slope	5754.95085	155.01428

Equation	y = a + b*x		
Weight	No Weighting		
Residual Sum of Squares	6.10839		
Pearson's r	-0.9994		
Adj. R-Square	0.99869		
		Value	Standard Error
WT	Intercept	16.9754	1.26282
	Slope	-31266.81753	327.18651

Boltzmann fitting of VT NMR data for $(NiCp^*)_2Pn^*$, **4.3a**

Model	singlet_to_triplet_Boltzmann (User)			
Equation	d0 + dp * (exp(2*J/(k*T))/(1+3*exp(2*J/(k*T))))			
Reduced Chi-Sqr				9.84254E-4
Adj. R-Square				0.9988
		Value	Standard Error	
D	J*	-557.27239	9.91685	
	d0	1.74028	0.03007	
	dp	281.62607	20.28185	
	E	-21.87517	0.38928	
E	J*	-557.27239	9.91685	
	d0	1.66268	0.02013	
	dp	238.68882	17.99112	
	E	-21.87517	0.38928	
F	J*	-557.27239	9.91685	
	d0	1.86298	0.01686	
	dp	126.20857	9.66711	
	E	-21.87517	0.38928	

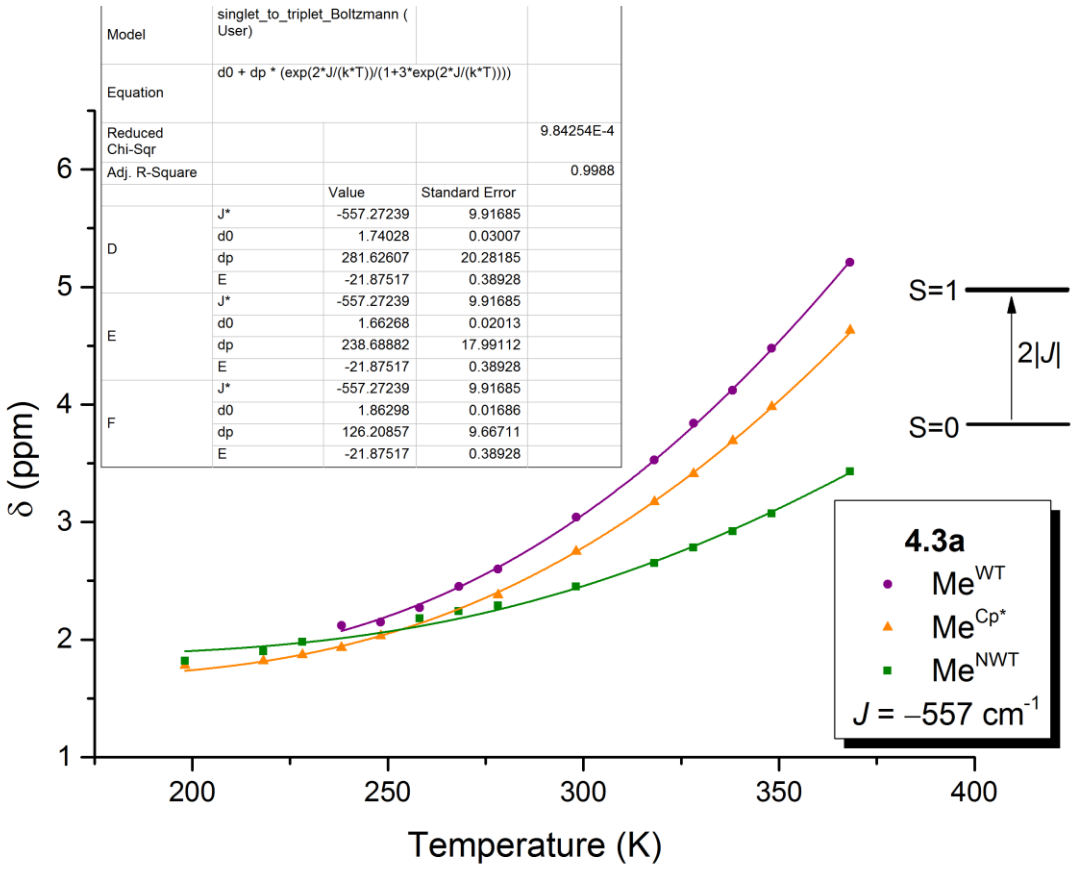

Boltzmann fitting of VT NMR data for $(NiCp)_2Pn^*$, **4.3b**

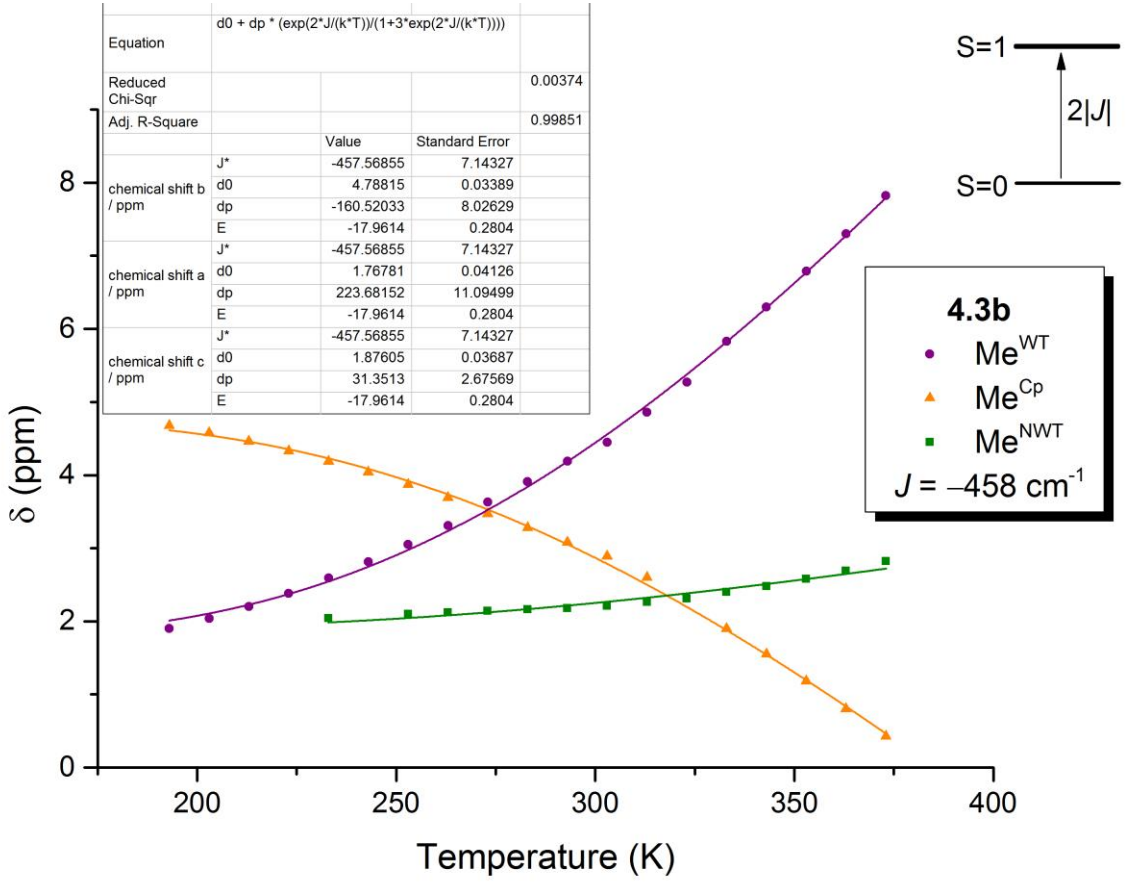

Curie-Weiss fitting of SQUID data for $Mn(Pn^*H)_2$ between 100 – 300 K (zfc and fc)

Equation	y = a + b*x		
Weight	No Weighting	zfc	
Residual Sum of Squares	14.92065	12.38557	
Pearson's r	0.9997	0.99976	
Adj. R-Square	0.99937	0.99949	
		Value	Standard Error
1/CHI	Intercept	30.49295	0.71814
	Slope	0.61041	0.00353
	Intercept	31.53353	0.64093
	Slope	0.6018	0.00313

Equation	y = a + b*x		
Weight	No Weighting	fc	
Residual Sum of Squares	2.09407	2.44114	
Pearson's r	0.99837	0.99826	
Adj. R-Square	0.99659	0.99637	
		Value	Standard Error
1/CHI	Intercept	8.61513	0.14364
	Slope	0.57408	0.00716
	Intercept	7.64653	0.15508
	Slope	0.60067	0.00773